

Summary of the Bulletin of the International Seismological Centre

2014

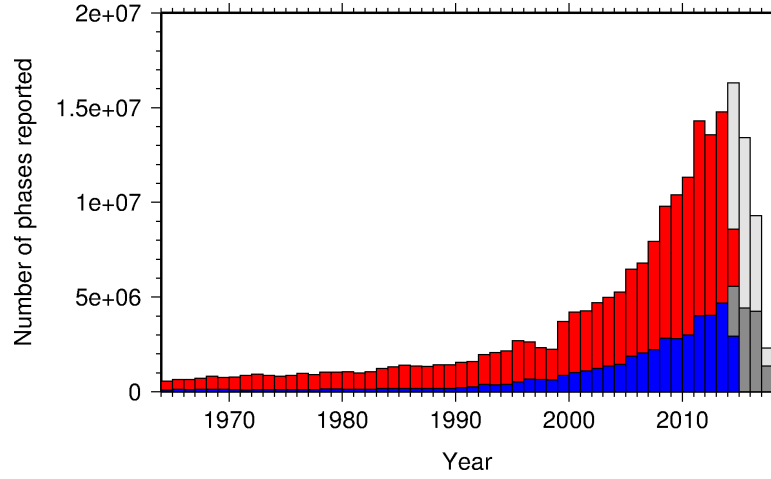
January – June

Volume 51 Issue I

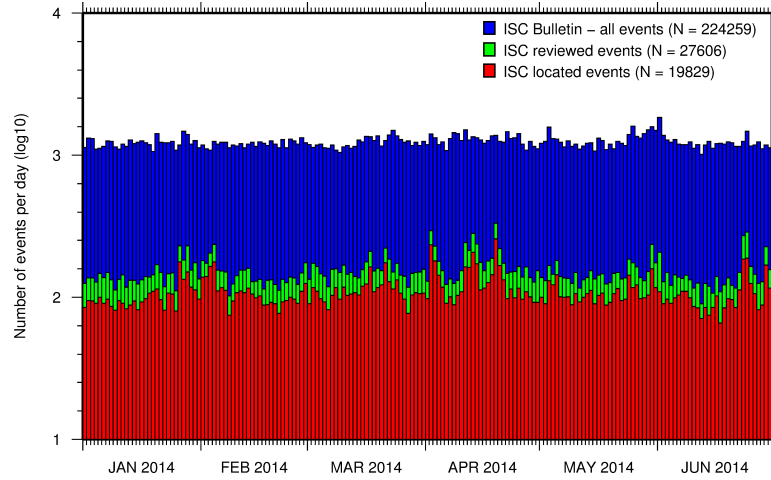
www.isc.ac.uk

isc-mirror.iris.washington.edu

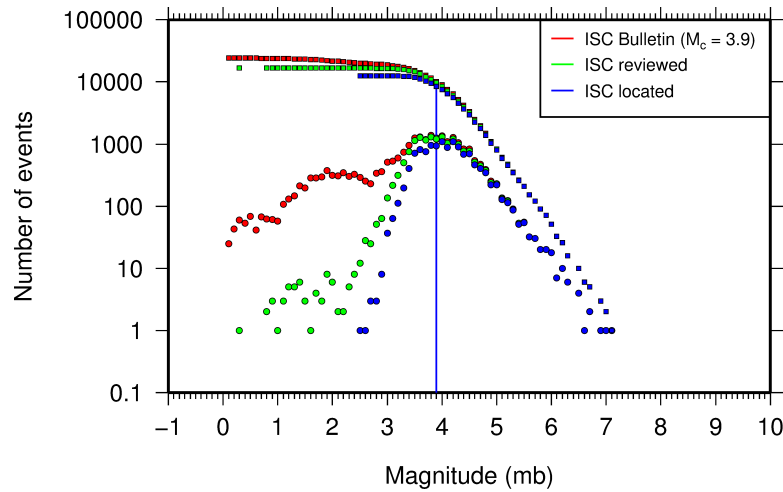
ISSN 2309-236X



The number of phases (red) and number of amplitudes (blue) collected by the ISC for events each year since 1964. The data in grey covers the current period where data are still being collected before the ISC review takes place and are accurate at the time of publication. See Section 7.3.



The number of events within the Bulletin for the current summary period. The vertical scale is logarithmic. See Section 8.1.



Frequency and cumulative frequency magnitude distribution for all events in the ISC Bulletin, ISC reviewed events and events located by the ISC. The magnitude of completeness (M_C) is shown for the ISC Bulletin. Note: only events with values of m_b are represented in the figure. See Section 8.4.

Summary of the Bulletin of the International Seismological Centre

2014

January – June

Volume 51 Issue I

Produced and edited by:

Kathrin Lieser, James Harris and Dmitry Storchak

Published by
International Seismological Centre



Copyright © 2017 by International Seismological Centre

Permission granted to reproduce for personal and educational use only. Commercial copying, hiring, lending is prohibited.

International Seismological Centre

Pipers Lane

Thatcham

RG19 4NS

United Kingdom

www.isc.ac.uk

ISSN 2309-236X

Printed and bound in Wales by Cambrian Printers.

Contents

1	Preface	1
2	The International Seismological Centre	2
2.1	The ISC Mandate	2
2.2	Brief History of the ISC	3
2.3	Former Directors of the ISC and its U.K. Predecessors	4
2.4	Member Institutions of the ISC	5
2.5	Sponsoring Organisations	11
2.6	Data Contributing Agencies	13
2.7	ISC Staff	23
3	Availability of the ISC Bulletin	29
4	Citing the International Seismological Centre	30
5	Operational Procedures of Contributing Agencies	32
5.1	Collm Geophysical Observatory	32
5.1.1	History and Present Status	32
5.1.2	Data Analysis	35
5.1.3	Local Network	37
5.1.4	Acknowledgements	44
5.1.5	References	44
5.2	Seismological Observatory Berggießhübel	45
5.2.1	History	45
5.2.2	Present Observatory Status	47
5.2.3	Data Analysis	54
5.2.4	References	58
6	Summary of Seismicity, January - June 2014	59
7	Statistics of Collected Data	65
7.1	Introduction	65
7.2	Summary of Agency Reports to the ISC	65
7.3	Arrival Observations	70
7.4	Hypocentres Collected	77

7.5	Collection of Network Magnitude Data	79
7.6	Moment Tensor Solutions	85
7.7	Timing of Data Collection	87
8	Overview of the ISC Bulletin	90
8.1	Events	90
8.2	Seismic Phases and Travel-Time Residuals	99
8.3	Seismic Wave Amplitudes and Periods	105
8.4	Completeness of the ISC Bulletin	108
8.5	Magnitude Comparisons	109
9	The Leading Data Contributors	114
9.1	The Largest Data Contributors	114
9.2	Contributors Reporting the Most Valuable Parameters	116
9.3	The Most Consistent and Punctual Contributors	120
10	Appendix	122
10.1	ISC Operational Procedures	122
10.1.1	Introduction	122
10.1.2	Data Collection	122
10.1.3	ISC Automatic Procedures	123
10.1.4	ISC Location Algorithm	127
10.1.5	Review Process	137
10.1.6	History of Operational Changes	138
10.2	IASPEI Standards	139
10.2.1	Standard Nomenclature of Seismic Phases	139
10.2.2	Flinn-Engdahl Regions	146
10.2.3	IASPEI Magnitudes	153
10.2.4	The IASPEI Seismic Format (ISF)	157
10.2.5	Ground Truth (GT) Events	159
10.2.6	Nomenclature of Event Types	161
10.3	Tables	162
11	Glossary of ISC Terminology	182
12	Acknowledgements	186
	References	187

1

Preface

Dear Colleague,

This is the first 2014 issue of the Summary of the ISC Bulletin which remains the most fundamental purpose for the continued operations at the ISC. This issue covers seismic events that occurred during the period from January to June 2014. The full annual DVD-ROM will be attached to the second 2014 issue. In the mean time, the monthly files for January to June period are available from the ISC ftp site. For instructions, please see the www.isc.ac.uk/iscbulletin/.

This publication contains information on the ISC, its staff, Members, Sponsors and Data providers. It offers analysis of the data contributed to the ISC by many seismological agencies worldwide as well as analysis of the data in the ISC Bulletin itself. The Appendix includes the IASPEI seismological standards and procedures used by the ISC in its operations.

We continue publishing invited articles describing the history, current status and operational procedures at those networks that contribute data to the ISC. This time it is the turn for two of the most long-serving observatories in Germany, Collm and Berggießhübel, to be described.

We hope that you find this relatively new publication useful in your work. If your home-institution or company is unable, for one reason or another, to support the long-term international operations of the ISC in full by becoming a Member, then, please, consider subscribing to this publication by contacting us at admin@isc.ac.uk.

With kind regards to our Data Contributors, Members, Sponsors and users,

Dr Dmitry A. Storchak

Director

International Seismological Centre (ISC)

2

The International Seismological Centre

2.1 The ISC Mandate

The International Seismological Centre (ISC) was set up in 1964 with the assistance of UNESCO as a successor to the International Seismological Summary (ISS) to carry forward the pioneering work of Prof. John Milne, Sir Harold Jeffreys and other British scientists in collecting, archiving and processing seismic station and network bulletins and preparing and distributing the definitive summary of world seismicity.

Under the umbrella of the International Association of Seismology and Physics of the Earth Interior (IASPEI/IUGG), the ISC has played an important role in setting international standards such as the International Seismic Bulletin Format (ISF), the IASPEI Standard Seismic Phase List (SSPL) and both the old and New IASPEI Manual of the Seismological Observatory Practice (NMSOP-2) (www.iaspei.org/projects/NMSOP.html).

The ISC has contributed to scientific research and prominent scientists such as John Hodgson, Eugene Herrin, Hal Thirlaway, Jack Oliver, Anton Hales, Ola Dahlman, Shigeji Suehiro, Nadia Kondorskaya, Vit Karnik, Stephan Müller, David Denham, Bob Engdahl, Adam Dziewonski, John Woodhouse and Guy Masters all considered it an important duty to serve on the ISC Executive Committee and the Governing Council.

The current mission of the ISC is to maintain:

- the ISC **Bulletin** – the longest continuous definitive summary of World seismicity (collaborating with 130 seismic networks and data centres around the world). (www.isc.ac.uk/iscbulletin/)
- the International Seismographic Station Registry (**IR**, jointly with the World Data Center for Seismology, Denver). (www.isc.ac.uk/registries/)
- the IASPEI Reference Event List (Ground Truth, **GT**, jointly with IASPEI). (www.isc.ac.uk/gtevents/)

These are fundamentally important tasks. Bulletin data produced, archived and distributed by the ISC for almost 50 years are the definitive source of such information and are used by thousands of seismologists worldwide for seismic hazard estimation, for tectonic studies and for regional and global imaging of the Earth's structure. Key information in global tomographic imaging is derived from the analysis of ISC data. The ISC Bulletin served as a major source of data for such well known products as the ak135 global 1-D velocity model and the EHB (*Engdahl et al.*, 1998) and Centennial (*Engdahl and Villaseñor*, 2002) catalogues. It presents an important quality-control benchmark for the Comprehensive Nuclear-Test-Ban Treaty Organization (CTBTO). Hypocentre parameters from the ISC Bulletin are used

by the Data Management Center of the Incorporated Research Institutions for Seismology (IRIS DMC) to serve event-oriented user-requests for waveform data. The ISC-GEM Bulletin is a cornerstone of the ISC-GEM Global Instrumental Reference Earthquake Catalogue for Global Earthquake risk Model (GEM).

The ISC Bulletin contains over 6 million seismic events: earthquakes, chemical and nuclear explosions, mine blasts and mining induced events. At least 1.7 million of them are regional and teleseismically recorded events that have been reviewed by the ISC analysts. The ISC Bulletin contains approximately 200 million individual seismic station readings of arrival times, amplitudes, periods, SNR, slowness and azimuth, reported by approximately 17,000 seismic stations currently registered in the IR. Over 6,000 stations have contributed to the ISC Bulletin in recent years. This number includes the numerous sites of the USArray. The IASPEI GT List currently contains 8816 events for which latitude, longitude and depth of origin are known with high confidence (to 5 km or better) and seismic signals were recorded at regional and/or teleseismic distances.

2.2 Brief History of the ISC

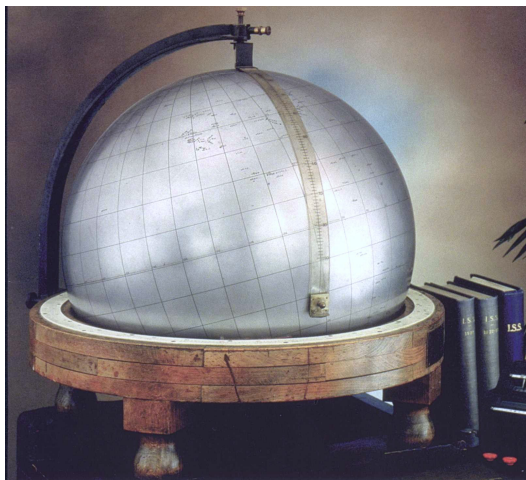


Figure 2.1: The steel globe bearing positions of early seismic stations was used for locating positions of earthquakes for the *International Seismological Summaries*.

(BCIS).

Earthquake effects have been noted and documented from the earliest times, but it is only since the development of earthquake recording instruments in the latter half of the 19th century that a proper study of their occurrence has been possible. After the first teleseismic observation of an earthquake in 1889, the need for international exchange of readings was recognised in 1895 by Prof. John Milne and by Ernst von Rebeur Paschwitz together with Georg Gerland, resulting in the publication of the first international seismic bulletins. Milne's "Slide Circulars" were issued under the auspices of the Seismological Committee of the British Association for the Advancement of Science (BAAS), while co-workers of Gerland at the Central Bureau of the International Association of Seismology worked independently in Strasbourg

Following Milne's death in 1913, Seismological Bulletins of the BAAS were continued under Prof. H.H. Turner, later based at Oxford University. Upon formal post-war dissolution of the International Association of Seismology in 1922 the newly founded Seismological Section of the International Union of Geodesy and Geophysics (IUGG) set up the International Seismological Summary (ISS) to continue at Oxford under Turner, to produce the definitive global catalogues from the 1918 data-year onwards, under the auspices of IUGG and with the support of the BAAS.

ISS production, led by several professors at Oxford University, and Sir Harold Jeffreys at Cambridge

University, continued until it was superseded by the ISC Bulletin, after the ISC was formed in Edinburgh in 1964 with Dr P.L. Willmore as its first director.

During the period 1964 to 1970, with the help of UNESCO and other international scientific bodies, the ISC was reconstituted as an international non-governmental body, funded by interested institutions from various countries. Initially there were supporting members from seven countries, now there are almost 60, and member institutions include national academies, research foundations, government departments and research institutes, national observatories and universities. Each member, contributing a minimum unit of subscription or more, appoints a representative to the ISC's Governing Council, which meets every two years to decide the ISC's policy and operational programme. Representatives from the International Association of Seismology and Physics of the Earth's Interior also attend these meetings. The Governing Council appoints the Director and a small Executive Committee to oversee the ISC's operations.



Figure 2.2: *ISC building in Thatcham, Berkshire, UK.*

In 1975, the ISC moved to Newbury in southern England to make use of better computing facilities there. The ISC subsequently acquired its own computer and in 1986 moved to its own building at Pipers Lane, Thatcham, near Newbury. The internal layout of the new premises was designed for the ISC and includes not only office space but provision for the storage of extensive stocks of ISS and ISC publications and a library of seismological observatory bulletins, journals and books collected over many tens of years.

In 1997 the first set of the ISC Bulletin CD-ROMs was produced (not counting an earlier effort at USGS). The first ISC website appeared in 1998 and the first ISC database was put in day-to-day operations from 2001.

Throughout 2009-2011 a major internal reconstruction of the ISC building was undertaken to allow for more members of staff working in mainstream ISC operations as well as major development projects such as the CTBTO Link, ISC-GEM Catalogue and the ISC Bulletin Rebuild.

2.3 Former Directors of the ISC and its U.K. Predecessors



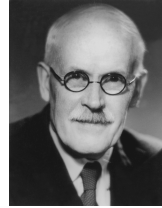
John Milne
Publisher of the Shide Circular Reports on Earthquakes
1899-1913



Herbert Hall Turner
Seismological Bulletins of the BAAS
1913-1922
Director of the ISS
1922-1930



Harry Hemley Plaskett
Director of the ISS
1931-1946



Harold Jeffreys
Director of the ISS
1946-1957



Robert Stoneley
Director of the ISS
1957-1963



P.L. (Pat) Willmore
Director of the ISS
1963-1970
Director of the ISC
1964-1970



Edouard P. Arnold
Director of the ISC
1970-1977



Anthony A. Hughes
Director of the ISC
1977-1997



Raymond J. Willemann
Director of the ISC
1998-2003



Avi Shapira
Director of the ISC
2004-2007

2.4 Member Institutions of the ISC

Article IV(a-b) of the ISC Working Statutes stipulates that any national academy, agency, scientific institution or other non-profit organisation may become a Member of the ISC on payment to the ISC of a sum equal to at least one unit of subscription and the nomination of a voting representative to serve on the ISC's governing body. Membership shall be effective for one year from the date of receipt at the ISC of the annual contribution of the Member and is thereafter renewable for periods of one year.

The ISC is currently supported with funding from its 62 Member Institutions and a four-year Grant Award EAR-1417970 from the US National Science Foundation.

Figures 2.3 and 2.4 show major sectors to which the ISC Member Institutions belong and proportional

financial contributions that each of these sectors make towards the ISC's annual budget.

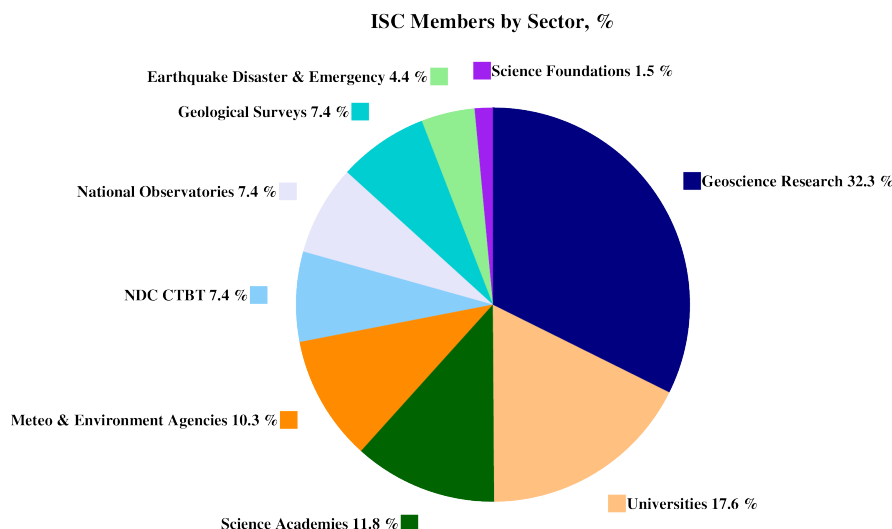


Figure 2.3: Distribution of the ISC Member Institutions by sector in year 2013 as a percentage of total number of Members.

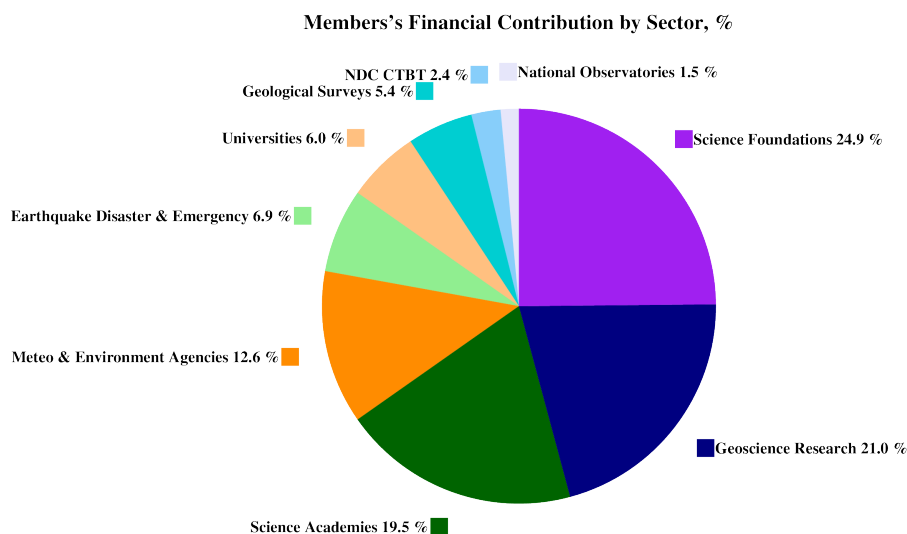


Figure 2.4: Distribution of Member's financial contributions to the ISC by sector in year 2013 as a percentage of total annual Member contributions.

There follows a list of all current Member Institutions with a category (1 through 9) assigned according to the ISC Working Statutes. Each category relates to the number of membership units contributed.



Centre de Recherche en Astronomie, Astrophysique et Géophysique (CRAAG)
Algeria
www.craag.dz
Category: 1



Instituto Nacional de Prevención Sísmica (INPRES)
Argentina
www.inpres.gov.ar
Category: 1



The University of Melbourne
Australia
www.unimelb.edu.au
Category: 1



Geoscience Australia
Australia
www.ga.gov.au
Category: 3



Bundesministerium für Wis-
senschaft, Forschung und
Wirtschaft (BMFWF)
Austria
www.bmbwk.gv.at
Category: 2



Centre of Geophysical Moni-
toring (CGM) of the National
Academy of Sciences of Belarus
Belarus
www.cgm.org.by
Category: 1



Belgian Science Policy Office
(BELSPO)
Belgium

Category: 1



Universidade de São Paulo, Cen-
tro de Sismologia
Brazil
www.sismo.iag.usp.br
Category: 1



Seismological Observatory, Insti-
tute of Geosciences, University of
Brasilia
Brazil
www.obsis.unb.br
Category: 1



The Geological Survey of Canada
Canada
gsc.nrcan.gc.ca
Category: 4



Centro Sismologico Nacional,
Universidad de Chile
Chile
ingenieria.uchile.cl
Category: 1



China Earthquake Administra-
tion
China
www.gov.cn
Category: 5



Institute of Earth Sciences,
Academia Sinica
Chinese Taipei
www.earth.sinica.edu.tw
Category: 1



Geological Survey Department
Cyprus
www.moa.gov.cy
Category: 1



Insitute of Geophysics, Academy
of Sciences of the Czech Republic
Czech Republic
www.avcr.cz
Category: 2



Geological Survey of Denmark
and Greenland (GEUS)
Denmark
www.geus.dk
Category: 2

Korea Earthquake Administra-
tion
DPR Korea

Category: 1



National Research Institute
for Astronomy and Geophysics
(NRIAG), Cairo
Egypt
www.nriag.sci.eg
Category: 1



The University of Helsinki
Finland
www.helsinki.fi
Category: 2



Laboratoire de Détection et de
Géophysique/CEA
France
www-dase.cea.fr
Category: 2



Institute National des Sciences de
l'Univers
France
www.insu.cnrs.fr
Category: 4



Bundesanstalt für Geowis-
senschaften und Rohstoffe
Germany
www.bgr.bund.de
Category: 4



GeoForschungsZentrum Potsdam
Germany
www.gfz-potsdam.de
Category: 2



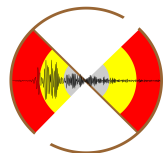
The Seismological Institute, Na-
tional Observatory of Athens
Greece
www.noa.gr
Category: 1



The Hungarian Academy of Sci-
ences
Hungary
www.mta.hu
Category: 1



The Icelandic Meteorological Of-
fice
Iceland
www.vedur.is
Category: 1



National Centre for Seismology,
Ministry of Earth Sciences of In-
dia
India
www.moes.gov.in
Category: 4



Iraqi Seismic Network
Iraq
www.imos-tm.com
Category: 1



The Geophysical Institute of Is-
rael
Israel
www.gii.co.il
Category: 1



Soreq Nuclear Research Centre
(SNRC)
Israel
www.soreq.gov.il
Category: 1



Istituto Nazionale di Geofisica e
Vulcanologia
Italy
www.ingv.it
Category: 3



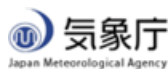
Istituto Nazionale di
Oceanografia e di Geofisica
Sperimentale
Italy
www.ogs.trieste.it
Category: 1



University of the West Indies at
Mona
Jamaica
www.mona.uwi.edu
Category: 1



National Institute of Polar Re-
search (NIPR)
Japan
www.nipr.ac.jp
Category: 1



The Japan Meteorological
Agency (JMA)
Japan
www.jma.go.jp
Category: 5



Japan Agency for Marine-Earth
Science and Technology (JAM-
STEC)
Japan
www.jamstec.go.jp
Category: 3



Earthquake Research Institute,
University of Tokyo
Japan
www.eri.u-tokyo.ac.jp
Category: 3



Natural Resources Authority,
Amman
Jordan
www.nra.gov.jo
Category: 1



Centro de Investigación Cientí-
fica y de Educación Superior de
Ensenada (CICESE)
Mexico
resnom.cicese.mx
Category: 1



Institute of Geophysics, National
University of Mexico
Mexico
www.igeofcu.unam.mx
Category: 1



The Royal Netherlands Meteoro-
logical Institute (KNMI)
Netherlands
www.knmi.nl
Category: 2



Institute of Geological and Nu-
clear Sciences
New Zealand
www.gns.cri.nz
Category: 3



Stiftelsen NORSAR
Norway
www.norsar.no
Category: 2



The University of Bergen
Norway
www.uib.no
Category: 2



Institute of Geophysics, Polish
Academy of Sciences
Poland
www.igf.edu.pl
Category: 1



Instituto Português do Mar e da
Atmosfera
Portugal
www.ipma.pt
Category: 2



Red Sísmica de Puerto Rico
Puerto Rico
redsismica.uprm.edu
Category: 1



Korean Meteorological Adminis-
tration
Republic of Korea
www.kma.go.kr
Category: 1



National Institute for Earth
Physics
Romania
www.infp.ro
Category: 1



Russian Academy of Sciences
Russia
www.ras.ru
Category: 5



Earth Observatory of Singapore
(EOS), an autonomous Institute
of Nanyang Technological Uni-
versity
Singapore
www.earthobservatory.sg
Category: 1



Environmental Agency of Slove-
nia
Slovenia
www.arso.gov.si
Category: 1



Council for Geoscience
South Africa
www.geoscience.org.za
Category: 1



Institut Cartogràfic i Geològic de
Catalunya (ICGC)
Spain
www.igc.cat
Category: 1



Institute of Earth Sciences
Jaume Almera
Spain
www.ictja.csic.es
Category: 1



National Defence Research Es-
tablishment (FOI)
Sweden
www.foi.se
Category: 1



Uppsala Universitet
Sweden
www.uu.se
Category: 2



The Swiss Academy of Sciences
Switzerland
www.scnat.ch
Category: 2



The Seismic Research Centre,
University of the West Indies at
St. Augustine
Trinidad and Tobago
www.uwiseismic.com
Category: 1



Disaster and Emergency Man-
agement Authority (AFAD)
Turkey
www.deprem.gov.tr
Category: 2



Kandilli Observatory and Earth-
quake Research Institute
Turkey
www.koeri.boun.edu.tr
Category: 1



AWE Blacknest
United Kingdom
www.blacknest.gov.uk
Category: 1



British Geological Survey
United Kingdom
www.bgs.ac.uk
Category: 2



The Royal Society of London
United Kingdom
www.royalsociety.org
Category: 6



National Earthquake Informa-
tion Center, U.S. Geological Sur-
vey
U.S.A.
www.neic.usgs.gov
Category: 2



University of Texas at Austin
U.S.A.
www.utexas.edu
Category: 1



Incorporated Research Institu-
tions for Seismology
U.S.A.
www.iris.edu
Category: 1



The National Science Foundation
of the United States. (Grant No.
EAR-1417970)
U.S.A.
www.nsf.gov
Category: 9

In addition the ISC is currently in receipt of grants from the International Data Centre (IDC) of the Preparatory Commission of the Comprehensive Nuclear-Test-Ban Treaty Organization (CTBTO), FM Global, Lighthill risk Network, OYO, USGS (Award G15AC00202), Aspen Re and BGR.



2.5 Sponsoring Organisations

Article IV(c) of the ISC Working Statutes stipulates any commercial organisation with an interest in the objectives and/or output of the ISC may become an Associate Member of the ISC on payment of an Associate membership fee, but without entitlement to representation with a vote on the ISC's governing body.



www.reftek.com

REF TEK designs and manufactures application specific, high-performance, battery-operated, field-portable geophysical data acquisition devices for the global market. With over 35 years of experience, REF TEK provides customers with complete turnkey solutions that include high resolution recorders, broadband sensors, state-of-the-art communications (V-SAT, GPRS, etc), installation, training, and continued customer support. Over 7,000 REF TEK instruments are currently being used globally for multiple applications. From portable earthquake monitoring to telemetry earthquake monitoring, earthquake aftershock recording to structural monitoring and more, REF TEK equipment is suitable for a wide variety of application needs.

<http://www.geosig.com/>

GeoSIG provides earthquake, seismic, structural, dynamic and static monitoring and measuring solutions. As an ISO Certified company, GeoSIG is a world leader in design and manufacture of a diverse range of high quality, precision instruments for vibration and earthquake monitoring. GeoSIG instruments are at work today in more than 100 countries around the world with well-known projects such as the NetQuakes installation with USGS and Oresund Bridge in Denmark. GeoSIG offers off-the-shelf solutions as well as highly customised solutions to fulfil the challenging requirements in many vertical markets including the following:

- Earthquake Early Warning and Rapid Response (EEWRR)
- Seismic and Earthquake Monitoring and Measuring
- Industrial Facility Seismic Monitoring and Shutdown
- Structural Analysis and Ambient Vibration Testing
- Induced Vibration Monitoring
- Research and Scientific Applications

<http://www.guralp.com/>

Güralp has been developing revolutionary force-feedback broadband seismic instrumentation for more than thirty years. Our sensors record seismic signals of all kinds, from teleseismic events occurring on the other side of the planet, to microseisms induced by unconventional hydrocarbon extraction. Our sophisticated digitisers record these signals with the highest resolution and accurate timing.

We supply individual instruments or complete seismic systems. Our services include field support such as installation and maintenance, to complete network and data management.

We design our instruments to meet increasingly complex requirements for deployment in the most challenging circumstances. As a result, you will find Güralp instruments gathering seismic data in the harshest of environments, from the Antarctic ice sheet; to boreholes 100s of metres deep; to the world's most active volcanoes and deepest ocean trenches.

SEISMOLOGY
RESEARCH
CENTRE<http://src.com.au/>

The Seismology Research Centre is an Australian earthquake observatory that began developing their own seismic recorders and data processing software in the late 1970s when digital recorders were un-

common. The Gecko is the SRC's 7th generation of seismic recorder, now available with a variety of integrated sensors to meet every monitoring requirement, including:

- Strong Motion Accelerographs
- 2Hz and 4.5Hz Blast Vibration Monitors
- Short Period 1Hz Seismographs
- Broadband 200s-1500Hz Optical Seismographs

Visit src.com.au/downloads/waves to grab a free copy of the SRC's MiniSEED waveform viewing and analysis software application, Waves.

2.6 Data Contributing Agencies

In addition to its Members and Sponsors, the ISC owes its existence and successful long-term operations to its 142 seismic bulletin data contributors. These include government agencies responsible for national seismic networks, geoscience research institutions, geological surveys, meteorological agencies, universities, national data centres for monitoring the CTBT and individual observatories. There would be no ISC Bulletin available without the regular stream of data that are unselfishly and generously contributed to the ISC on a free basis.



The Institute of Seismology,
Academy of Sciences of Albania
Albania
TIR



Centre de Recherche en As-
tronomie, Astrophysique et Géo-
physique
Algeria
CRAAG



Universidad Nacional de La Plata
Argentina
LPA



Instituto Nacional de Prevención
Sísmica
Argentina
SJA



National Survey of Seismic Pro-
tection
Armenia
NSSP



Geoscience Australia
Australia
AUST



International Data Centre,
CTBTO
Austria
IDC



Zentralanstalt für Meteorologie
und Geodynamik (ZAMG)
Austria
VIE



Republic Center of Seismic Sur-
vey
Azerbaijan
AZER



Royal Observatory of Belgium
Belgium
UCC



Observatorio San Calixto
Bolivia
SCB

Republic Hydrometeorological
Service, Seismological Observa-
tory, Banja Luka
Bosnia-Herzegovina
RHSSO



Instituto Astronomico e Ge-
ofisico
Brazil
VAO



Geophysical Institute, Bulgarian
Academy of Sciences
Bulgaria
SOF



Canadian Hazards Information
Service, Natural Resources
Canada
Canada
OTT



Centro Sismológico Nacional,
Universidad de Chile
Chile
GUC



China Earthquake Networks
Center
China
BJI



Institute of Earth Sciences,
Academia Sinica
Chinese Taipei
ASIES



Red Sismológica Nacional de
Colombia
Colombia
RSNC



Sección de Sismología, Vul-
canología y Exploración Ge-
ofísica
Costa Rica
UCR



Seismological Survey of the Re-
public of Croatia
Croatia
ZAG



Servicio Sismológico Nacional
Cubano
Cuba
SSNC



Cyprus Geological Survey De-
partment
Cyprus
NIC



Geophysical Institute, Academy
of Sciences of the Czech Republic
Czech Republic
PRU



West Bohemia Seismic Network
Czech Republic
WBNET



The Institute of Physics of the
Earth (IPEC)
Czech Republic
IPEC

Korea Earthquake Administra-
tion
DPR Korea
KEA



Geological Survey of Denmark
and Greenland
Denmark
DNK

Observatorio Sismologico Po-
litecnico Loyola
Dominican Republic
OSPL



Servicio Nacional de Sismología y
Vulcanología
Ecuador
IGQ



National Research Institute of
Astronomy and Geophysics
Egypt
HLW



Servicio Nacional de Estudios
Territoriales
El Salvador
SNET



University of Addis Ababa
Ethiopia
AAE



Institute of Seismology, Univer-
sity of Helsinki
Finland
HEL



Institut de Physique du Globe
France
STR



Laboratoire de Détection et de
Géophysique/CEA
France
LDG

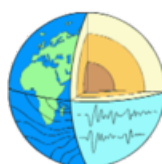
Laboratoire de Géo-
physique/CEA
French Polynesia
PPT



Seismological Observatory
Skopje
FYR Macedonia
SKO



Institute of Earth Sciences/ Na-
tional Seismic Monitoring Center
Georgia
TIF



Geophysikalisches Observato-
rium Collm
Germany
CLL



Alfred Wegener Institute for Polar and Marine Research
Germany
AWI



Bundesanstalt für Geowissenschaften und Rohstoffe
Germany
BGR



Seismological Observatory Berggießhübel, TU Bergakademie Freiberg
Germany
BRG



National Observatory of Athens
Greece
ATH



Department of Geophysics, Aristotle University of Thessaloniki
Greece
THE



INSIVUMEH
Guatemala
GCG



Hong Kong Observatory
Hong Kong
HKC



Geodetic and Geophysical Research Institute
Hungary
BUD

Geodetic and Geophysical Research Institute, Hungarian Academy of Sciences
Hungary
KRSZO



Icelandic Meteorological Office
Iceland
REY



National Geophysical Research Institute
India
HYB



National Centre for Seismology of the Ministry of Earth Sciences of India
India
NDI



Badan Meteorologi, Klimatologi dan Geofisika
Indonesia
DJA



Tehran University
Iran
TEH



International Institute of Earthquake Engineering and Seismology (IIEES)
Iran
THR



Iraqi Meteorological and Seismology Organisation
Iraq
ISN



The Geophysical Institute of Israel
Israel
GII



Dipartimento per lo Studio del
Territorio e delle sue Risorse
(RSNI)
Italy
GEN



MedNet Regional Centroid - Mo-
ment Tensors
Italy
MED_RCMT



Osservatorio Sismologico Univer-
sità di Bari
Italy
OSUB



Laboratory of Research on Ex-
perimental and Computational
Seimology
Italy
RISSC



Istituto Nazionale di Geofisica e
Vulcanologia
Italy
ROM

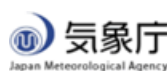


Istituto Nazionale di
Oceanografia e di Geofisica
Sperimentale (OGS)
Italy
TRI

Station Géophysique de Lamto
Ivory Coast
LIC



Jamaica Seismic Network
Jamaica
JSN



Japan Meteorological Agency
Japan
JMA



National Institute of Polar Re-
search
Japan
SYO



The Matsushiro Seismological
Observatory
Japan
MAT



National Research Institute for
Earth Science and Disaster Pre-
vention
Japan
NIED



Jordan Seismological Observa-
tory
Jordan
JSO



National Nuclear Center
Kazakhstan
NNC

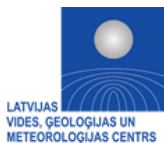


Seismological Experimental
Methodological Expedition
Kazakhstan
SOME



Kyrgyz Seismic Network
Kyrgyzstan
KNET

Institute of Seismology, Academy
of Sciences of Kyrgyz Republic
Kyrgyzstan
KNET



Latvian Seismic Network
Latvia
LVSN



National Council for Scientific
Research
Lebanon
GRAL



Geological Survey of Lithuania
Lithuania
LIT



Macao Meteorological and Geo-
physical Bureau
Macao, China
MCO



Geological Survey Department
Malawi
Malawi
GSDM

Malaysian Meteorological Service
Malaysia
KLM



Instituto de Geofísica de la
UNAM
Mexico
MEX



Centro de Investigación Cientí-
fica y de Educación Superior de
Ensenada
Mexico
ECX



Institute of Geophysics and Ge-
ology
Moldova
MOLD



Seismological Institute of Mon-
tenegro
Montenegro
PDG



Centre National de Recherche
Morocco
CNRM



The Geological Survey of
Namibia
Namibia
NAM



National Seismological Centre,
Nepal
Nepal
DMN



Institute of Geological and Nu-
clear Sciences
New Zealand
WEL



Instituto Nicaragüense de Estu-
dios Territoriales
Nicaragua
INET



Stiftelsen NORSAR
Norway
NAO



University of Bergen
Norway
BER



Sultan Qaboos University
Oman
OMAN



Micro Seismic Studies Pro-
gramme, PINSTECH
Pakistan
MSSP



Universidad de Panama
Panama
UPA



Philippine Institute of Volcanol-
ogy and Seismology
Philippines
MAN



Manila Observatory
Philippines
QCP



Institute of Geophysics, Polish
Academy of Sciences
Poland
WAR



Instituto Português do Mar e da
Atmosfera, I.P.
Portugal
INMG

Sistema de Vigilância Sismológ-
ica dos Açores
Portugal
SVSA



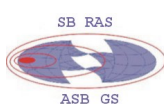
Instituto Geofísico do Infante
Dom Luiz
Portugal
IGIL



Centre of Geophysical Monitoring of the National Academy of Sciences of Belarus
Republic of Belarus
BELR



National Institute for Earth Physics
Romania
BUC



Altai-Sayan Seismological Centre, GS SB RAS
Russia
ASRS



North Eastern Regional Seismological Centre, GS RAS
Russia
NERS



Institute of Environmental Problems of the North, Russian Academy of Sciences
Russia
IEPN



Yakutiya Regional Seismological Center, GS SB RAS
Russia
YARS



Geophysical Survey of Russian Academy of Sciences
Russia
MOS

Sakhalin Experimental and Methodological Seismological Expedition, GS RAS
Russia
SKHL



Mining Institute of the Ural Branch of the Russian Academy of Sciences
Russia
MIRAS



Baykal Regional Seismological Centre, GS SB RAS
Russia
BYKL



Kamchatkan Experimental and Methodical Seismological Department, GS RAS
Russia
KRSC



Kola Regional Seismic Centre, GS RAS
Russia
KOLA



Saudi Geological Survey
Saudi Arabia
SGS



Seismological Survey of Serbia
Serbia
BEO



Geophysical Institute, Slovak Academy of Sciences
Slovakia
BRA



Slovenian Environment Agency
Slovenia
LJU



Ministry of Mines, Energy and
Rural Electrification
Solomon Islands
HNR



Council for Geoscience
South Africa
PRE



Instituto Geográfico Nacional
Spain
MDD



Institut Cartogràfic i Geològic de
Catalunya
Spain
MRB

Real Instituto y Observatorio de
la Armada
Spain
SFS



University of Uppsala
Sweden
UPP



Swiss Seismological Service
(SED)
Switzerland
ZUR



Thai Meteorological Department
Thailand
BKK



The Seismic Research Centre
Trinidad and Tobago
TRN



Institut National de la
Météorologie
Tunisia
TUN



Disaster and Emergency Man-
agement Presidency
Turkey
DDA

The Earthquake Research Center
Ataturk University
Turkey
ATA



Kandilli Observatory and Re-
search Institute
Turkey
ISK



Subbotin Institute of Geophysics,
National Academy of Sciences
Ukraine
SIGU



Dubai Seismic Network
United Arab Emirates
DSN



British Geological Survey
United Kingdom
BGS



IRIS Data Management Center
U.S.A.
IRIS



National Earthquake Informa-
tion Center
U.S.A.
NEIC



The Global CMT Project
U.S.A.
GCMT



Red Sísmica de Puerto Rico
U.S.A.
RSPR

Institute of Seismology, Academy
of Sciences, Republic of Uzbek-
istan
Uzbekistan
ISU



Fundación Venezolana de Investi-
gaciones Sismológicas
Venezuela
FUNV

Geological Survey Department of
Zambia
Zambia
LSZ



Goetz Observatory
Zimbabwe
BUL

East African Network

EAF



CWB
Chinese Taipei
TAP

2.7 ISC Staff

Listed below are the staff (and their country of origin) who were employed at the ISC at the time of this ISC Bulletin Summary.

- Dmitry Storchak
- Director
- Russia/United Kingdom



- Lynn Elms
- Administration Officer
- United Kingdom



- James Harris
- Senior System and
Database Administrator
- United Kingdom



- Przemek Ozgo
- System Administrator
- Poland



- Alfie James Barber
- System Administrator
- United Kingdom



- Gergely Csontos
- Web Developer
- Hungary



- John Eve
- Data Collection Officer
- United Kingdom



- Edith Korger
- Data Collection Seismologist
- Austria



- Domenico Di Giacomo
- Seismologist
- Italy



- Konstantinos Lentas
- Seismologist/Developer
- Greece



- Rosemary Hulin (née Wylie)
- Analyst/Administrator
- United Kingdom



- Blessing Shumba
- Seismologist/Analyst
- Zimbabwe



- Rebecca Verney
- Analyst
- United Kingdom



- Jennifer Weston
- Seismologist/Analyst
- United Kingdom



- Elizabeth Entwistle
- Seismologist/Analyst
- United Kingdom



- Elizabeth Ayres (née Ball)
- Analyst/Historical Data Entry Officer
- United Kingdom



- Kathrin Lieser
- Seismologist/Analyst
- Germany



- Lonn Brown
- Seismologist/Analyst
- Canada



- Daniela Olaru
- Historical Data Entry Officer
- Romania



3

Availability of the ISC Bulletin

The ISC Bulletin is available from the following sources:

- Web searches

The entire ISC Bulletin is available directly from the ISC website via tailored searches.

(www.isc.ac.uk/iscbulletin/search)

(isc-mirror.iris.washington.edu/iscbulletin/search)

- Bulletin search - provides the most verbose output of the ISC Bulletin in ISF or QuakeML.
- Event catalogue - only outputs the prime hypocentre for each event, producing a simple list of events, locations and magnitudes.
- Arrivals - search for arrivals in the ISC Bulletin. Users can search for specific phases for selected stations and events.

- CD-ROMs/DVD-ROMs

CDs/DVDs can be ordered from the ISC for any published volume (one per year), or for all back issues of the Bulletin (not including the latest volume). The data discs contain the Bulletin as a PDF, in IASPEI Seismic Format (ISF), and in Fixed Format Bulletin (FFB) format. An event catalogue is also included, together with the International Registry of seismic station codes.

- FTP site

The ISC Bulletin is also available to download from the ISC ftp site, which contains the Bulletin in PDF, ISF and FFB formats. (<ftp://www.isc.ac.uk>)

(<ftp://isc-mirror.iris.washington.edu>)

Mirror service

A mirror of the ISC database, website and ftp site is available at IRIS DMC (isc-mirror.iris.washington.edu), which benefits from their high-speed internet connection, providing an alternative method of accessing the ISC Bulletin.

4

Citing the International Seismological Centre

Data from the ISC should always be cited. This includes use by academic or commercial organisations, as well as individuals. A citation should show how the data were retrieved and may be in one of these suggested forms:

Data retrieved from the ISC web site:

- International Seismological Centre, On-line Bulletin, <http://www.isc.ac.uk>, Internatl. Seismol. Cent., Thatcham, United Kingdom, 2017.

Data transcribed from the IASPEI reference event bulletin:

- International Seismological Centre, Reference Event Bulletin, <http://www.isc.ac.uk>, Internatl. Seismol. Cent., Thatcham, United Kingdom, 2017.

Data transcribed from the EHB bulletin:

- International Seismological Centre, EHB Bulletin, <http://www.isc.ac.uk>, Internatl. Seismol. Cent., Thatcham, United Kingdom, 2017.

Data copied from ISC CD-ROMs/DVD-ROMs:

- International Seismological Centre, Bulletin Disks 1-25 [CD-ROM], Internatl. Seismol. Cent., Thatcham, United Kingdom, 2017.

Data transcribed from the printed Bulletin:

- International Seismological Centre, Bull. Internatl. Seismol. Cent., 50(I), Thatcham, United Kingdom, 2017.

Data transcribed from the printed Summary of the Bulletin:

- International Seismological Centre, Summ. Bull. Internatl. Seismol. Cent., January - June 2014, 50(I), Thatcham, United Kingdom, 2017.

The ISC is named as a valid data centre for citations within American Geophysical Union (AGU) publications. As such, please follow the AGU guidelines when referencing ISC data in one of their journals. The ISC may be cited as both the institutional author of the Bulletin and the source from which the data were retrieved.

BibTex entry example:

```
@manual{ISCcitation2017,  
author = "International Seismological Centre",  
title = "On-line Bulletin",  
organization = "Internatl. Seismol. Cent.",  
note = "http://www.isc.ac.uk",  
address = "Thatcham, United Kingdom",  
year = "2017"  
}
```

5

Operational Procedures of Contributing Agencies

5.1 Collm Geophysical Observatory

S. Wendt, P. Buchholz, Institute for Geophysics and Geology, University of Leipzig, Germany



Siegfried Wendt and Petra Buchholz

In this article we will give a short overview of recording and evaluating earthquakes at the Geophysical Observatory in Collm, Germany.

5.1.1 History and Present Status

In the 1920's conditions in Leipzig were more and more disturbed by increasing industrialization and traffic. Ludwig Weickmann, head of the Geophysics Institute since 1923, was looking for a better place for the Wiechert horizontal seismograph, which had been working in Leipzig since 1902, but also for other branches of geophysical research like magnetism, gravity and meteorology. The observatory was built on the slopes of Collm hill near the city of Oschatz and about 50 km east of Leipzig (Fig. 5.1). The main building (Fig. 5.2) was opened in 1932 and the seismometer hut in 1934. Since 1935 station CLL has been working continuously, including during the Second World War. Since 1993 station CLL has been part of the German Regional Seismological Network (GRSN) and is equipped with a STS-2 broadband seismometer with digital data logging and online data transmission. Some generations of analogue seismometers used at CLL, for instance short-period Benioff seismometers, Wood-Anderson torsion instrument, short-period SSJ-2 and long-period SSJ-1 seismometers, developed in Jena, demonstrate technical progress and can be visited. Our Wiechert seismograph with a mass of 1100 kg is still working today (Fig. 5.3). In 2007 the STS-2 seismometer was moved to a new underground vault. Our

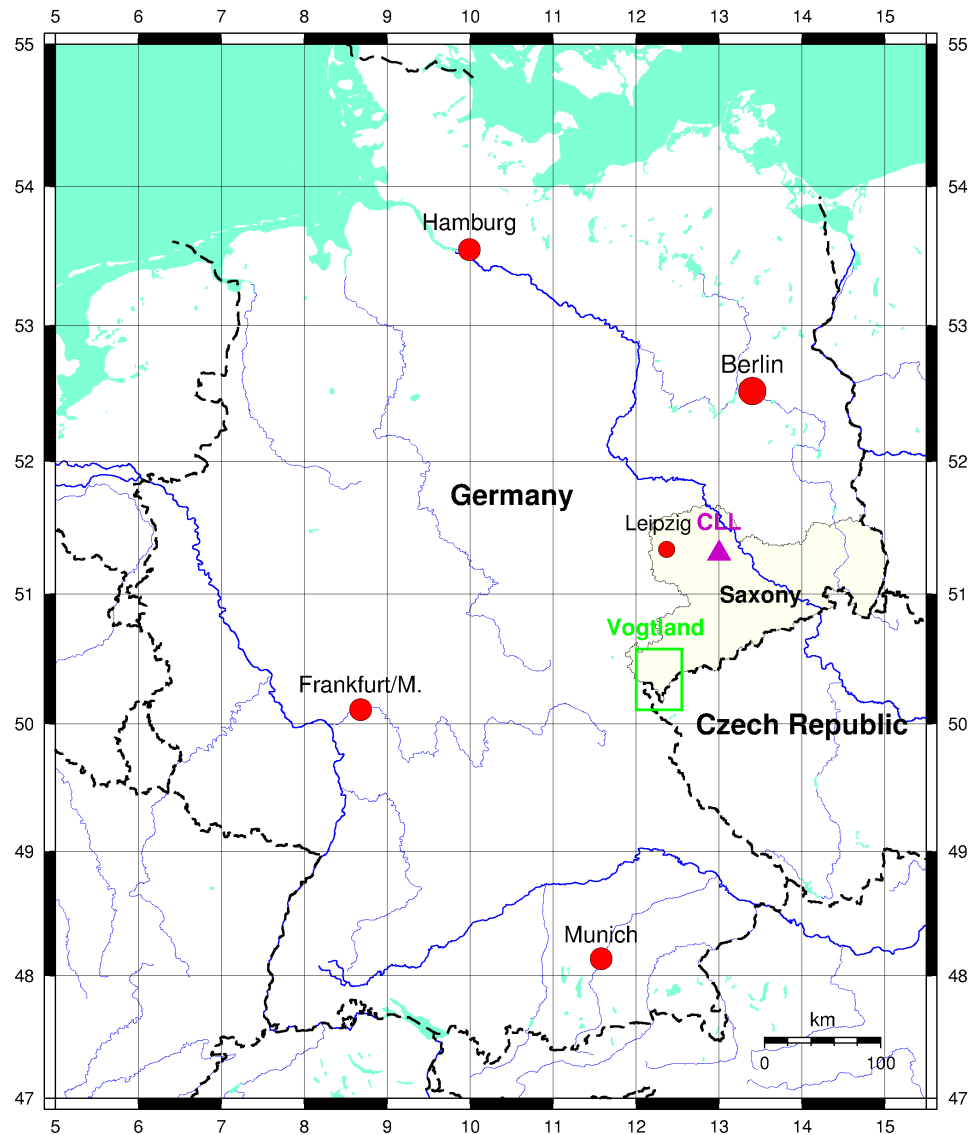


Figure 5.1: Map of Germany with Saxony, CLL and Vogtland region (see Fig. 5.12).

analogue archives contain an enormous number of earthquake records, which can be used for processing old events with new methods. Since 1993 wave form data from broadband station CLL is available via the Federal Institute for Geosciences and Natural Resources (BGR) in Hanover:

http://www.bgr.bund.de/DE/Themen/Erdbeben-Gefaehrdungsanalysen/Seismologie/Seismologie/Datenzentrum/waveform_request/waveform_request_node.html.

The observatory also accommodates equipment for other geophysical research. Ludwig Weickmann was a meteorologist interested in microclimatic investigations. In 1956 Rudolf Schminder began with LF measurements, which use low-frequency radio waves, of the wind in the ionosphere. Magnetic measurements (variation of magnetic field of the earth) completed ionospheric investigations. A VHF (very high frequency) meteor radar was installed at Collm in 2004 to replace the LF measurements. Both methods were used until LF measurements were stopped in 2007.

The geographical co-ordinates of station Collm (CLL) are: Latitude 51.3077°N, Longitude: 13.0026°E, Elevation: 230 m.



Figure 5.2: Main building of Collm Geophysical Observatory (Petra Buchholz, 2017).



Figure 5.3: Wiechert seismograph still working in seismometer hut (Petra Buchholz, 2017).

Year	Number of events	Events with source parameters
2006	5329	4113
2007	5398	4341
2008	5802	4694
2009	4992	3434
2010	4981	3996
2011	8026	6372
2012	5611	4826
2013	5658	4614
2014	6720	5501
2015	5214	4395
Sum	57731	46286

Table 5.1: Number of earthquakes evaluated in CLL per year.

5.1.2 Data Analysis

In general we use CLL broadband data for seismogram interpretation which includes manual phase picking, identification of phases, and magnitude estimation. The data is analysed with Seismic Handler (*Stammler, 1993*). We use GRSN stations to help interpret complicated seismograms with superposition of two events where estimating the slowness is helpful. We calculate many magnitudes and study the various relations between them: beside mb, mB, Ms_20 and Ms_BB also magnitudes for P, PP (short- and long-periodic, on vertical and horizontal components), S and surface waves (also for periods outside the 18 to 22 s window). For local events we estimate Ml and MSgV.

Twice per week we send the results of our seismogram readings to the data centre GSR in Moscow and to our neighbouring stations. One year behind real-time we send our interpretation in a final version to the ISC. This data is completed by source parameters from NEIC or CSEM yielding to our bulletin, which is the basis for some of the figures in this article.

CLL station recorded about 4500 earthquakes per year on average over the last 10 years. Table 5.1 contains numbers of events per year and Figure 5.4 shows a histogram of events per month subdivided into magnitude classes. The maximum amount of recorded events was reached in March 2011 when the Tohoku earthquake with its large aftershocks sequence occurred. In 2008, 2011, and 2014 we recorded a lot of events in NW Czech Republic, less than 10km away from the German-Czech border.

Figure 5.5 represents the global seismicity with more than 46000 earthquakes recorded by CLL during ten years. Blue isolines represent the travel times of the primary longitudinal waves in 2-minute steps. Magnitude mb over epicentral distance and histograms of events over epicentral distance are shown in Figure 5.6. Most of the recorded events are teleseismic events with two peaks between 75° to 85° (the very active regions Japan, Kurile, and Kamchatka) and 145° to 155° (SW Pacific region with Fiji, Tonga, and Kermadec Islands). Recording conditions mainly depend on epicentral distance but also on focal depth. The large number of local events is caused by seismic activity in the German-Czech border region. About 80 percent are swarms and series of quakes in the NW part of Czech Republic.

Figure 5.7 shows histograms of magnitudes mb and MSZ (=Ms_20) and the correlation mb-MSZ for

Earthquakes recorded in CLL

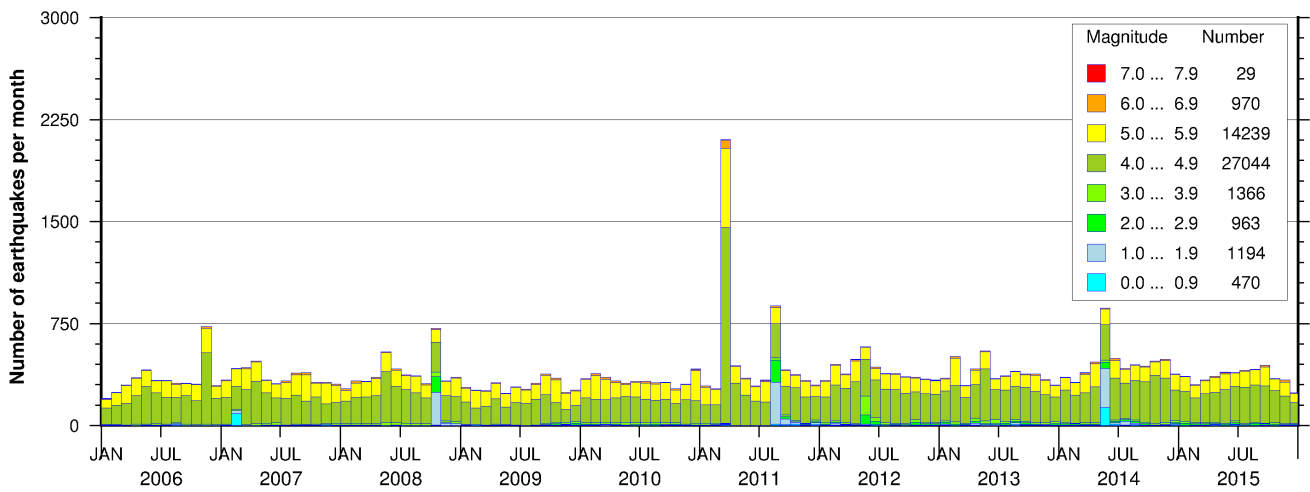


Figure 5.4: Histogram with earthquakes per month evaluated at CLL.

Seismicity of the Earth 2006 – 2015

46276 in CLL recorded earthquakes (Source: NEIC, EDR)

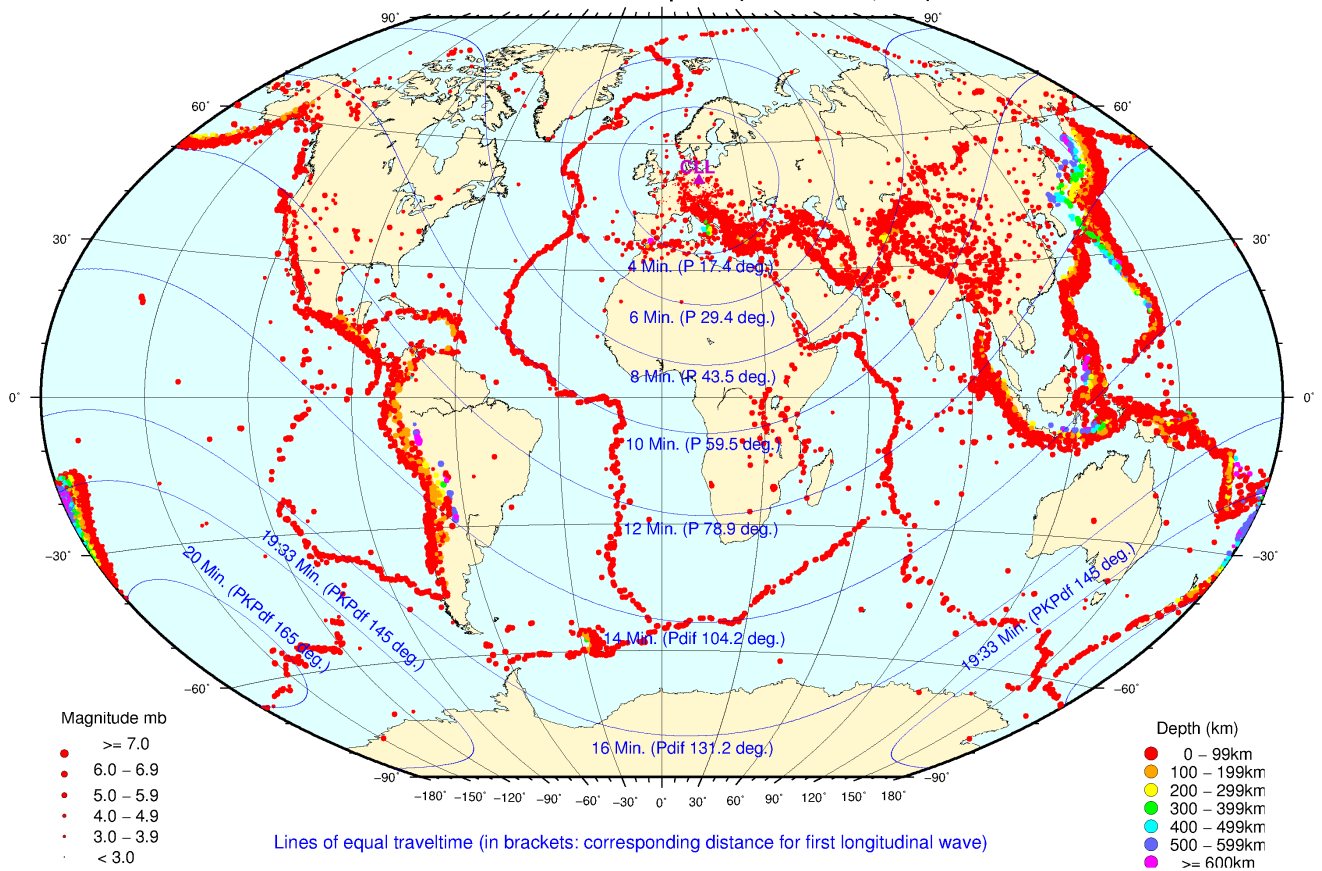


Figure 5.5: Map of global seismicity with more than 46000 epicenters of earthquakes recorded at CLL. (Earthquake data retrieved from NEIC, <ftp://hazards.cr.usgs.gov/NEICPDE/isf2.0/>)

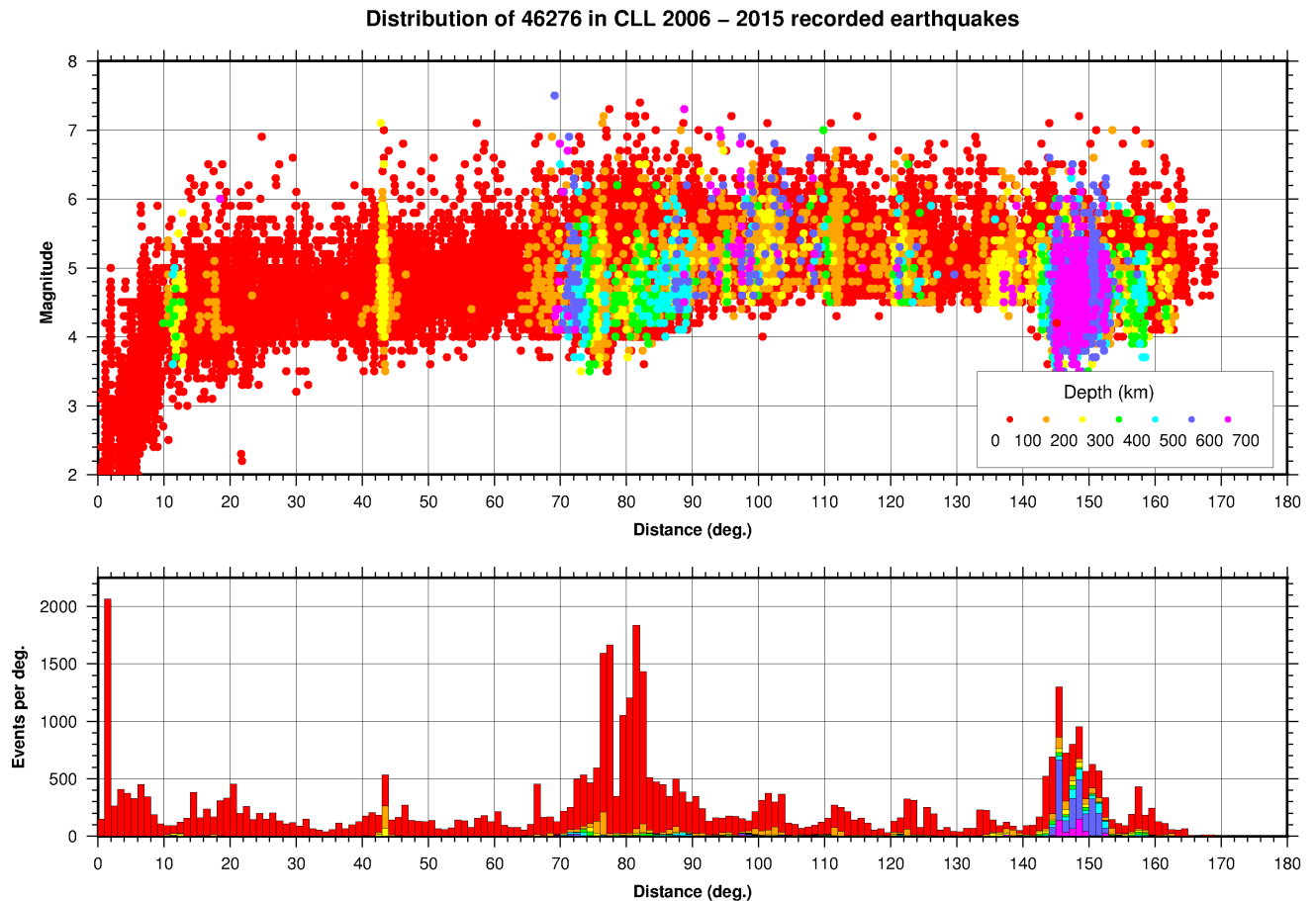


Figure 5.6: Top: Distribution of m_b (M_l for local events) versus epicentral distance colour coded by depth. Bottom: Histogram of events with magnitude m_b over epicentral distance colour coded by depth.

recorded events at CLL. For large quakes with $m_b \geq 6.0$, around where m_b saturates, the surface wave magnitude MSZ is greater than body wave magnitude m_b . For small quakes m_b dominates. In Figure 5.8 we compare three source regions with quite different recording conditions: (1) Kurile Islands (centre) with very good recording conditions at CLL. The first onsets are pure mantle P-waves from an average distance of 77° . (2) Our station has very bad recording conditions for earthquakes in Chile and the Sunda Arc (left) because they nucleate close to the P-wave shadow zone. P_{diff} in a distance of about 110° can only be observed for strong earthquakes. The first detectable phase in a seismogram often is PP and in many cases we recorded only surface waves. (3) We have very good recording conditions for PKP waves from source regions in Fiji, Tonga, and Kermadec (right). The histogram of Fiji shows that we record nearly all events with magnitudes larger than $m_b=5.0$. The good propagation conditions for PKP waves can result in the recording of late and very late core phases ($P'N$, $PNKP$). Figure 5.9 shows travel times of such phases and Figure 5.10 the corresponding ray paths in the Earth. Misinterpretation of late and very late core phases as P phases can yield to the creation of bogus earthquakes. We appreciate the interpretation of complicated seismograms with many phases (Fig. 5.11).

5.1.3 Local Network

In 2000 the installation of a local network (SXNET) in Vogtland region began (network administrator: Sigward Funke, University of Leipzig). A map of station distribution and epicenters for the years 2009

Magnitudes of events recorded in CLL 2006 – 2015

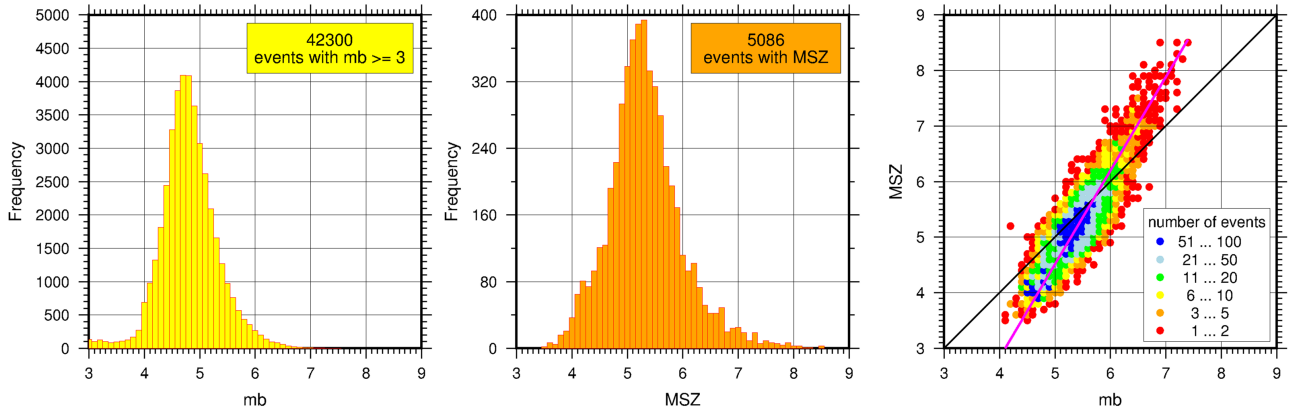


Figure 5.7: Histograms of distribution of mb and MSZ and correlation mb-MSZ.

Different Ray Paths and Recording Conditions

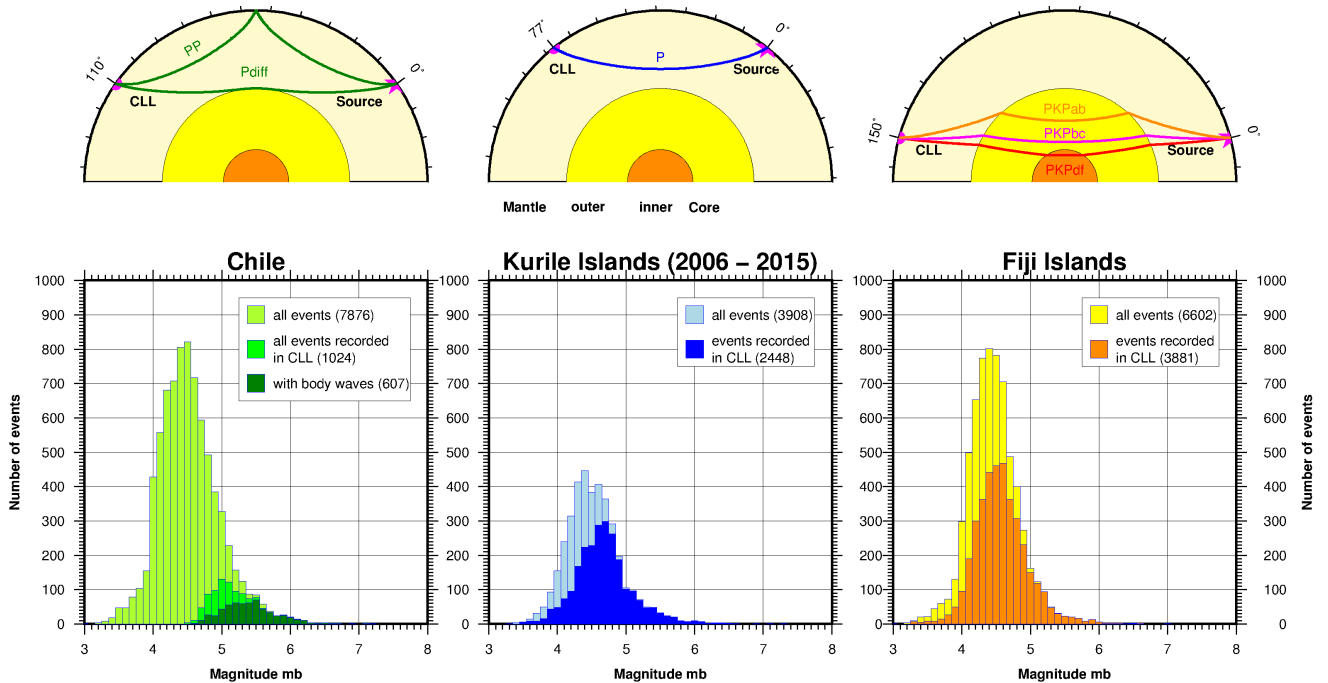


Figure 5.8: Different recording conditions for three source regions: Chile, Kuril Islands, and Fiji Islands and the corresponding ray paths in the Earth. Light coloured histograms in the back are magnitude distributions of all events given by NEIC in Earthquake Data Report (EDR), whereas dark coloured histograms in the front are events recorded at CLL.

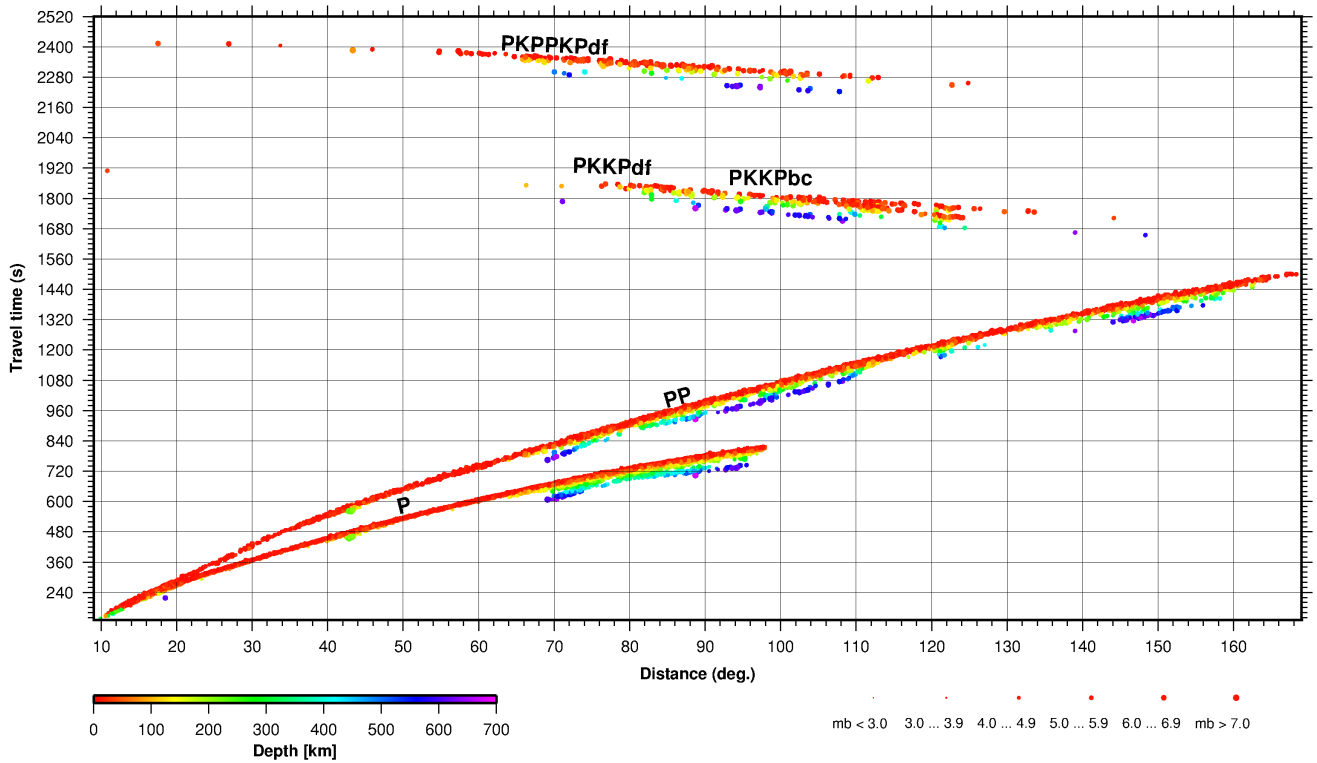


Figure 5.9: Travel times of P, PP, PKKPdf, PKKPbc, and PKPPKPdf colour coded by depth.

to 2016 is shown in Figure 5.12 while Figure 5.13 shows the time distribution of local magnitudes.

At Collm Observatory we detect and manually pick regional events recorded by the network on a daily basis. The picks and hypocenters of local events larger than M_l 2.0 are also included in our reports to the ISC. We use Seisan (*Havskov and Ottemöller, 1999*) for manual phase picking and amplitude measurements. 100-Hz waveform data for more than 30 stations is available from several networks, generally: SXNET (network, Saxony), TSN (network, Thuringia), NKC (Station, Czech Republic), VIEL (Station, Bavaria). The distance between stations in Upper Vogtland region is 10 to 15 km. We evaluate on an average 1200 local earthquakes per year of which about 80 percent are events located in the NW part of the Czech Republic less than 10 km away from the German-Czech border. Our data base contains more than 13000 local events with magnitudes ranging from -1.2 to 4.2. Even standard seismogram evaluation yields to good results with respect to the quality of epicenter location and depth. Location and magnitude estimates can be substantially improved by applying station corrections. To account for variations in seismic velocity we use different velocity models for different geographical epicentral regions. When only a small amount of data is available we search for the best velocity model with the lowest RMS by stepwise changing the velocity and depth of a layer. Events large enough for macroseismic observation are reliably detected and located by automatic systems as SeisComP3 (<http://www.seiscomp3.org>) and RTQUAKE (*Utheim et al., 2014*).

To characterize the quality of a hypocentre location we follow the criteria given in the Seisan manual (*Havskov and Ottemöller, 1999*). Distributive criteria (Fig. 5.14) describe the network configuration as number of stations used, distance to nearest station, or azimuthal gap, whereas statistical criteria (Fig. 5.15) show location errors mainly caused by the quality of picked arrival times and the applied velocity model. Table 5.2 shows the codes for the different quality classes used in Figures 5.14 and 5.15.

Wavepropagation in the Earth

Distance = 96.0 deg.

Depth = 0 km

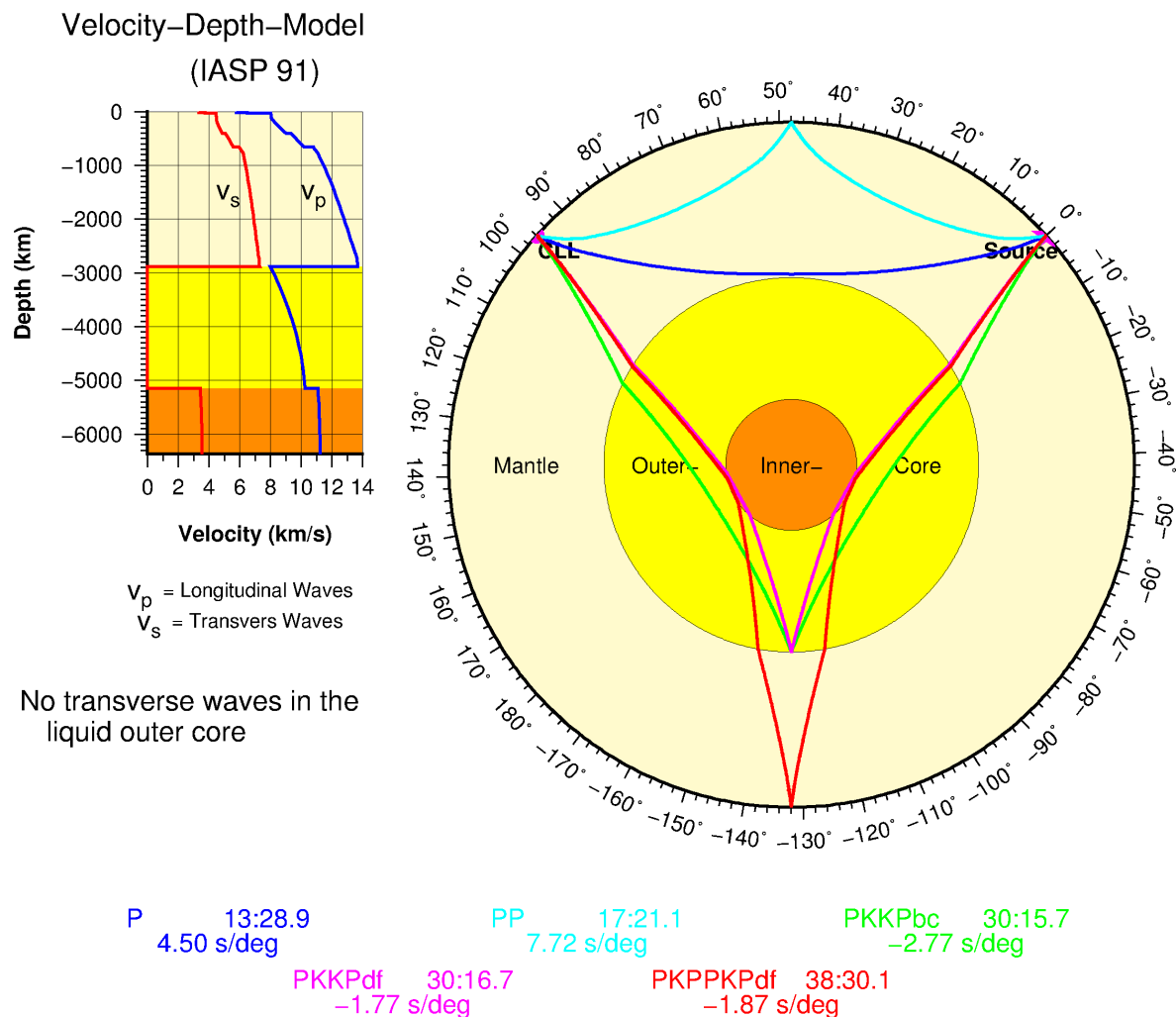


Figure 5.10: Ray paths in the inner Earth for P, PP, PKKPdf, PKKPbc, and PKPPKpdf. On the right side of the phase names are travel times, below slowness.

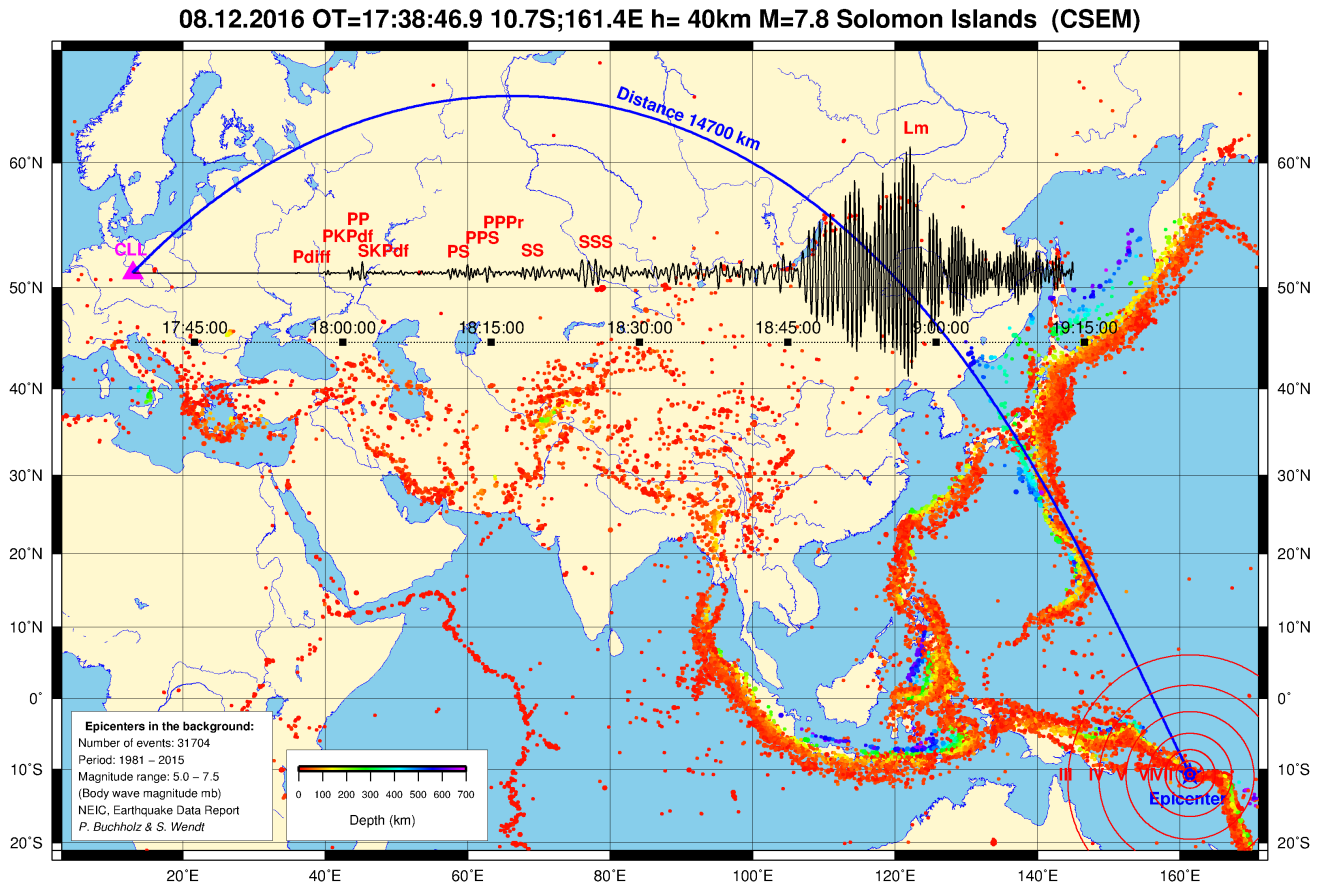


Figure 5.11: Map with background seismicity and example of a seismogram with many phases from a 7.8 event in the Solomon Islands recorded by CLL.

Quality	Distributive	Statistical
Excellent	a / Circle	A / Red
Good	b / Pentagon	B / Yellow
Fair	c / Diamond	C / Green
Poor	d / Triangle	D / Blue

Table 5.2: Codes for different quality classes (Fig. 5.14 and 5.15).

In some histograms the horizontal axis is colour coded by quality, e.g. a azimuthal gap between 0° and 90° is considered “excellent” and marked in red in the upper left image of Figure 5.14. The longitudinal location errors show higher values than the latitudinal errors (Fig. 5.15, top left and middle) which is due to the network being elongated predominantly in NS direction. The RMS errors (Fig. 5.15, bottom left) almost all fall in the highest quality class confirming the high quality of the velocity models. The combination of all single qualities give the total quality of a location. The matrix in Figure 5.15 (bottom middle) shows the number of events by quality classes Aa to Dd, e.g. 58 events are of the highest quality Aa which is reflected by a red circle. Depicting the quality classes with coloured shapes makes it easy to identify the quality of an event location in maps.

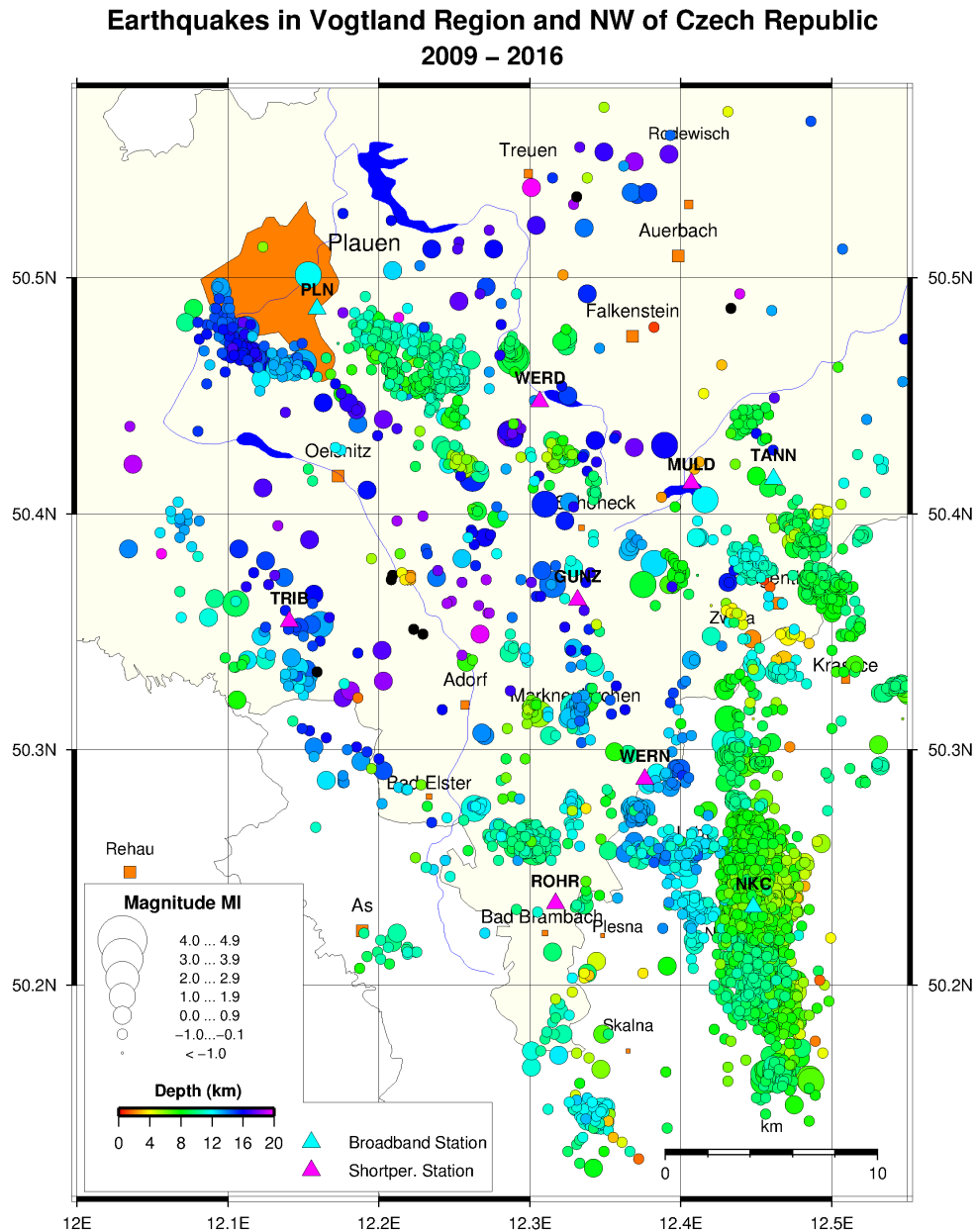


Figure 5.12: Epicenters of Vogtland region and NW part of Czech Republic (see green box in Fig. 5.1).

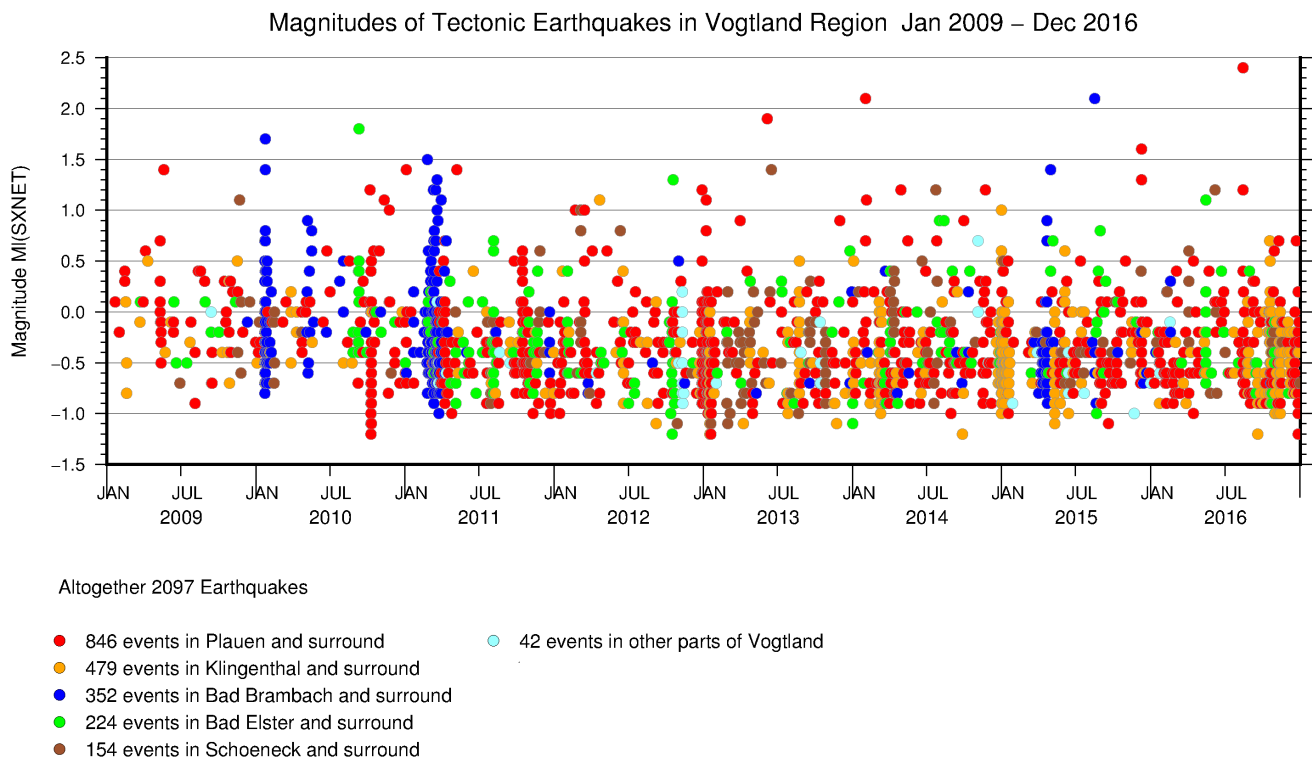


Figure 5.13: Local Magnitude M_l versus time (only for Vogtland region).

Distributive Quality – Vogtland Region

Jan. 2009 – Dec. 2016

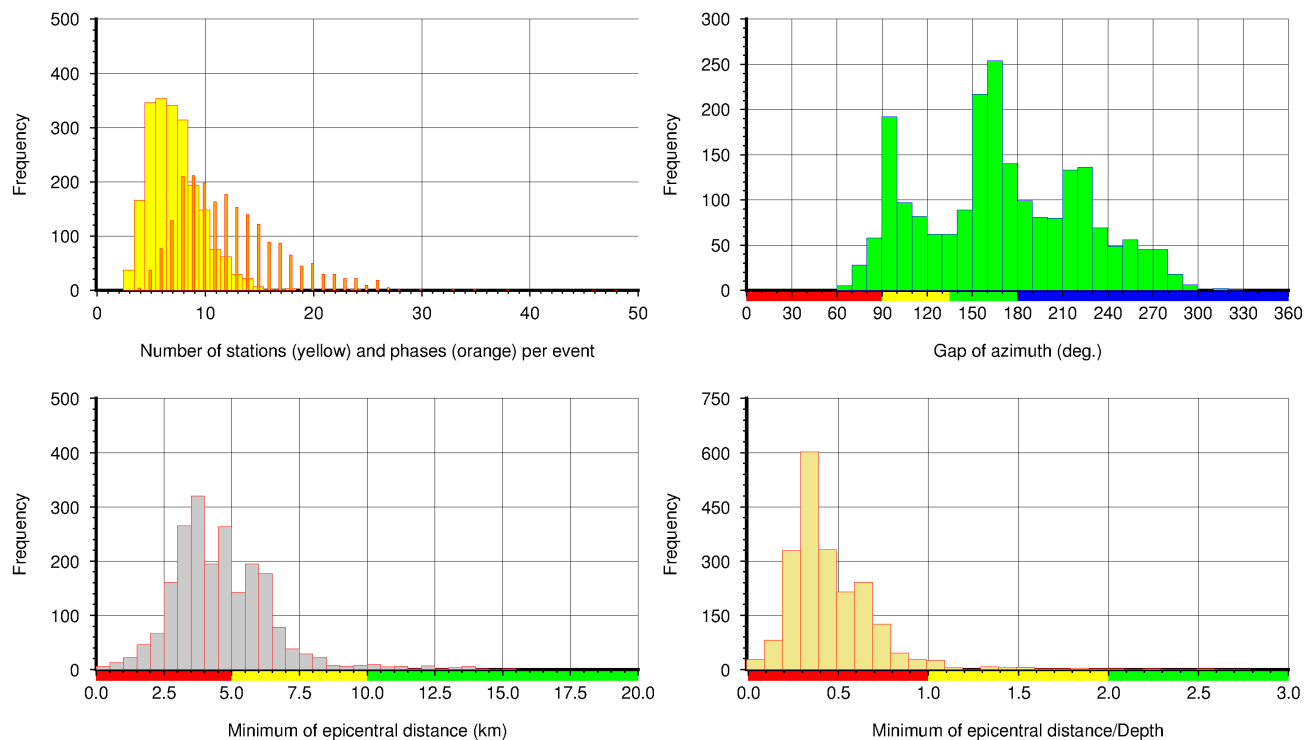


Figure 5.14: Distributive quality for Vogtland region. Colours on horizontal axis represent quality class, where red=excellent, yellow=good, green=fair, and blue=poor. See text for more information.

Statistical Quality – Vogtland Region

Jan. 2009 – Dec. 2016

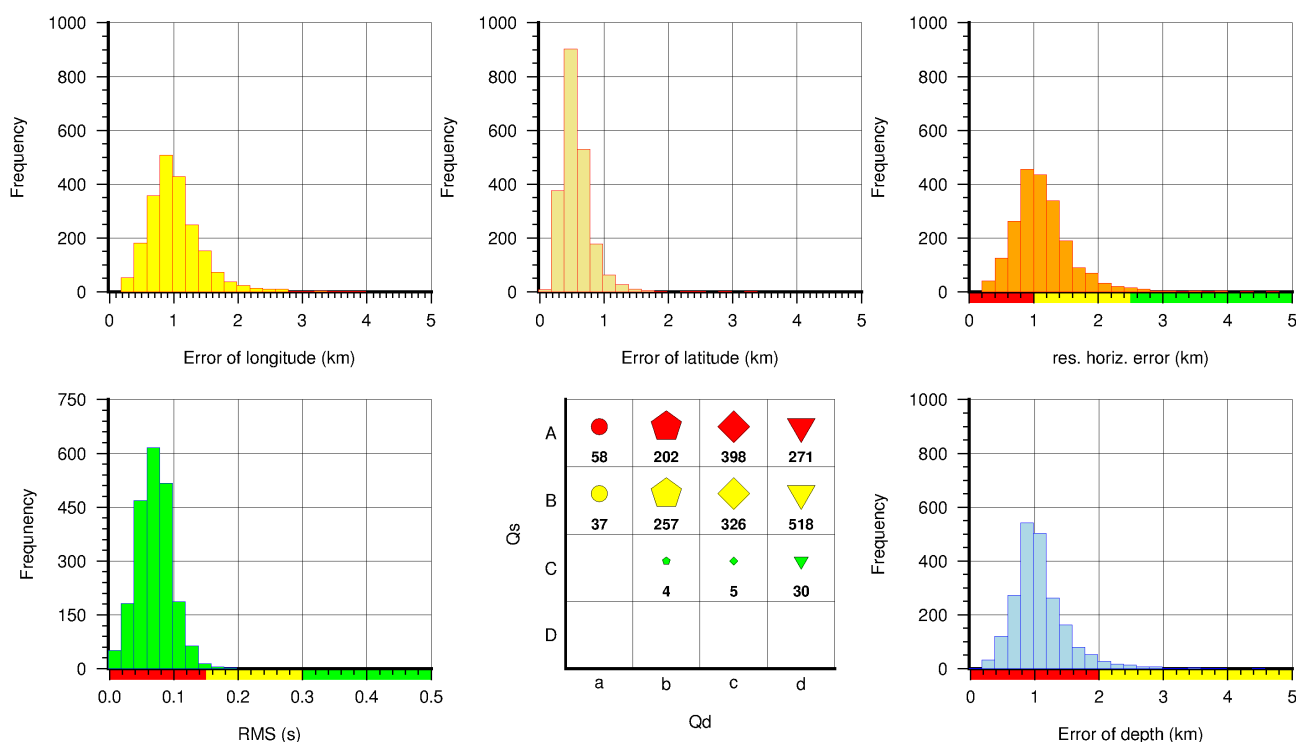


Figure 5.15: Statistical quality for Vogtland region. Bottom middle: Matrix showing distribution of location qualities. Colours represent quality class, where red=excellent, yellow=good, green=fair, and blue=poor. See text for more information.

5.1.4 Acknowledgements

The authors are grateful to editor Kathrin Lieser for her enormous help in designing this manuscript and for her very helpful suggestions. We thank the developers of Generic Mapping Tool (GMT) Paul Wessel and Walter H.F. Smith for powerful software which we have used for producing some of the figures.

5.1.5 References

- Havskov, J. and L. Ottemöller (1999), SeisAn Earthquake analysis software, *Seismological Research Letters*, 70(5), 532–534.
- Stammler, K. (1993), Seismic Handler – Programmable multichannel data handler for interactive and automatic processing of seismological analyses, *Computers & Geosciences*, 19(2), 135–140, <http://www.seismic-handler.org>, DOI:10.1016/0098-3004(93)90110-Q.
- Utheim, T., J. Havskov, M. Ozyazicioglu, J. Rodriguez, E. Talavera (2014), RTQUAKE, A Real-Time Earthquake Detection System Integrated with SEISAN, *Seismological Research Letters*, 85(3), 735–742, DOI:10.1785/0220130175.

5.2 Seismological Observatory Berggießhübel

R. Mittag, Institute for Geophysics and Geoinformatics, TU Bergakademie Freiberg, Germany



*Reinhard Mittag,
Observatory manager since 1977, from 1995 – 1997 seismologist at the ISC.*

The Seismological Observatory Berggießhübel was founded by the Freiberg University of Mining and Technology (TU Bergakademie Freiberg) in 1957 as an initiative of the project “International Geophysical Year”. The Observatory belongs to the Institute for Geophysics and Geoinformatics and is situated about 60 km south-east of Freiberg at the edge of the Saxonian Ore Mountains (Fig. 5.16). The remoteness of the location and the underground installation of measurement devices within an old mine provides excellent conditions for seismological measurements, which have been done continuously since 1966.

5.2.1 History

The idea to establish a seismic station close to Freiberg mines came along after the 1st International Seismological Conference in Strasbourg in 1901, but for political reasons it took a while to set up a seismic station. The first who took action at the beginning of the 1950’s was Prof. Wolfgang Buchheim, director of the Institute for Theoretical Physics and Geophysics of Bergakademie Freiberg and a former student of Werner von Heissenberg. He looked for an alternative, quieter site for seismological measurements in the environment of noisy Freiberg town and found it in Berggießhübel, where the instruments could be installed within a tunnel of an abandoned mine. Based on the intention to measure a broad spectrum of Earth’s oscillations, the observatory was established as a so-called “Earth tide station” first. A seismic test recording was set up on 1st May 1960, just 22 days before the strongest earthquake ever recorded by seismographs occurred with a magnitude of Mw 9.5 in Chile. This was good timing and a stroke of luck because this strong event showed that the amplification of the horizontal components (Fig. 5.17) was very low (only ten times real ground motion) while the vertical component was completely locked and station operators would have waited, unsuccessfully, for a long time for any visible deflection of the seismic record.

The continuous seismic record began in October 1966, two years after the International Seismological Centre (ISC) was established. Equipped with 3-component short and long periodic seismometers, seismic station Berggießhübel was integrated under code BRG into the World-Wide Standard Seismographic

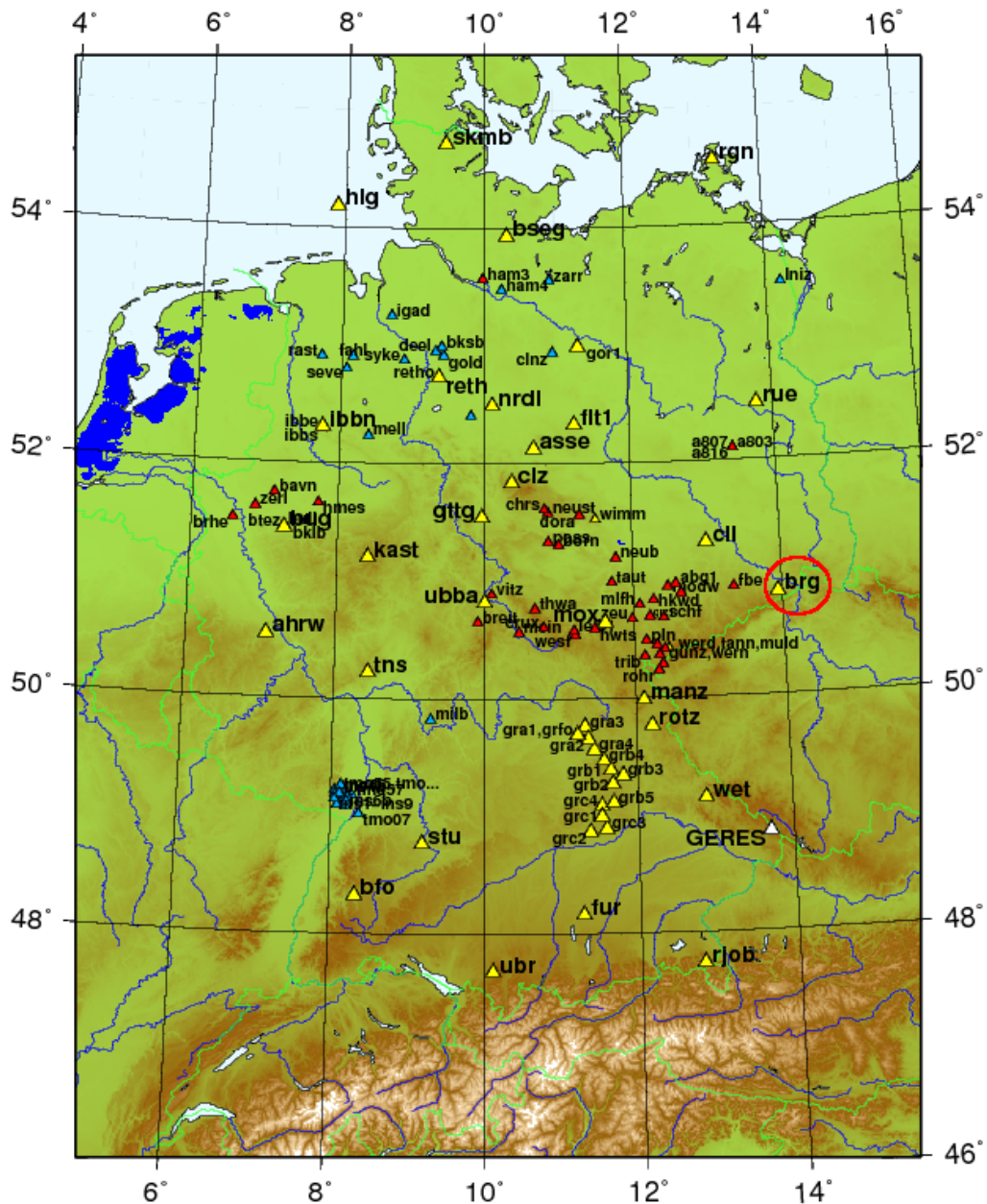


Figure 5.16: GRSN (German Regional Seismic Network) seismic station network with station BRG (red circle). Yellow triangles are GRSN stations and GRF array, red triangles are stations from institutions other than Federal Institute for Geosciences and Natural Resources (BGR) and blue triangles are temporary BGR deployments. © BGR (http://www.bgr.bund.de/EN/Themen/Seismologie/Seismologie/Seismometer_Stationen/Stationsnetze/d_stationsnetz_node.html)

Network WWSSN. From 1974 the observatory BRG began to send seismo reports to the ISC and became a consistent data contributor.

In 1993 the observatory was equipped with a Streckeisen triaxial broadband seismometer of type STS-2 (Fig. 5.18) with digital data acquisition. Via the German Regional Seismic Network GRSN seismic station BRG was also integrated into the Global Digital Seismographic Network GDSN. In 2001 a LaCoste earth tide gravimeter of type G 701 and an in-house made tiltmeter were set up to extend measurements to low frequencies.

A short description of the development of the observatory is given below.

1951	First visit to the abandoned mine in Berggießhübel and planning of installation of a seismic station.
1953	First tide measurements with horizontal pendulums.
1957	Establishment of the observatory building and reconstruction of mining tunnel with vaults. In September 1957 official opening of the Observatory as “Earth tides station” under the umbrella of the Institute for Theoretical Physics and Geophysics of the TU Bergakademie Freiberg.
1960	Beginning of continuous earth tide and geomagnetic measurements. First seismic test measurements.
1964	First gravimetric measurements.
1966	Beginning of continuous seismic measurements with 3-component short- and long-period seismometer and permanent analogue drum recording.
1970	Takeover of the observatory by the Central Institute for Physics of the Earth ZIPE in Potsdam.
1974	Beginning of routine interpretation of seismic records and exchange of seismological data with data centres (ISC, NEIS, WDC-B (Moscow)).
1980-82	Operation of a seismic array for monitoring of induced seismicity in the environment of a nearby reservoir.
1981-92	Transmission of vertical short-periodic components of the seismic record for digital archiving to ZIPE in Potsdam.
1992	Takeover of the observatory by the German Research Center for Geosciences GFZ in Potsdam.
1993	Permanent installation of broadband seismometer STS-2 with digital data acquisition, transfer and archiving at the national data centre for German Regional Seismic Network GRSN in Hanover. Temporary installation of 3 gravimeters for device adjustment.
1994	Repatriation of the observatory into the hands of the Institute for Geophysics within TU Bergakademie Freiberg.
2001	Installation of a LaCoste gravimeter G 701 and home made tiltmeter.

5.2.2 Present Observatory Status

The observatory site includes a station building (Fig. 5.19) with office and facilities for the staff (Fig. 5.20) and a 200 m long mining tunnel system (Figs. 5.21 and 5.22) with vaults, that host measurement devices

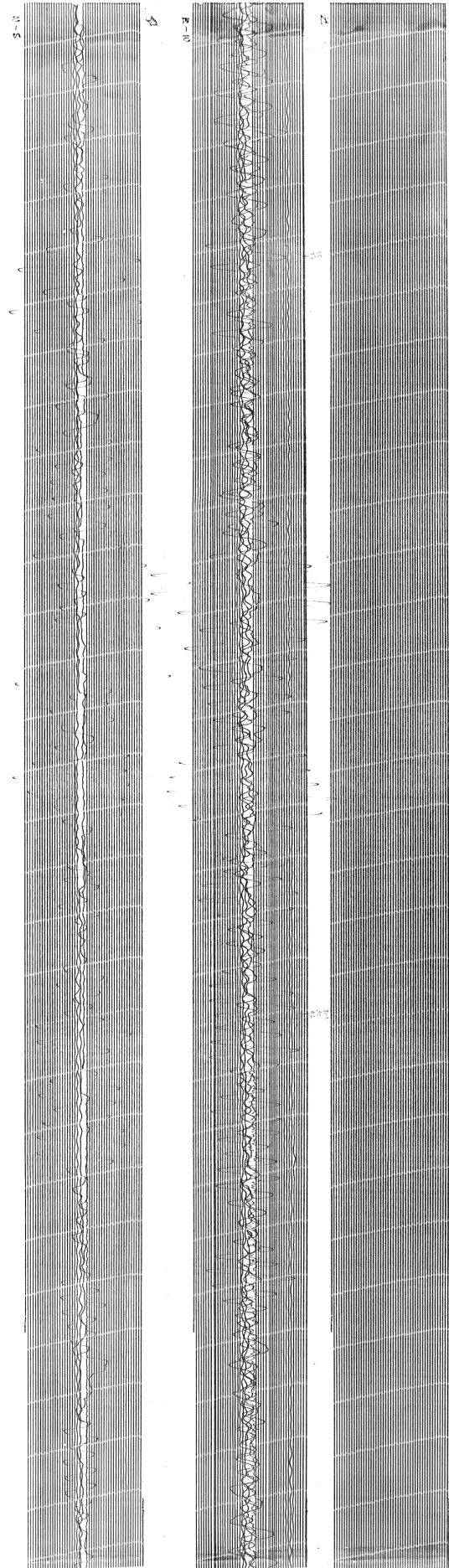


Figure 5.17: Record on BRG of the M 9.5 1960 Chile event, the strongest earthquake ever recorded by seismographs. Left: N-S component, middle:, E-W component, and right: Z component, which unfortunately was locked.



Figure 5.18: STS-2 seismometer and Quantera data logger.

(Fig. 5.18) and a collection of historical instruments (Figs. 5.23 and 5.24). The tunnel system is air conditioned. The broadband triaxial seismometer STS-2 as well as the gravimeter G 701 are installed in an isolated measurement chamber in a depth of 36 meters and coupled with the hard bedrock directly. The annual seismic noise spectra of station BRG is given in comparison to High and Low Noise Models for 2016 in Figure 5.25 showing that the noise level at the BRG site is at the lower end.

Digital data acquisition of the broadband seismometer is carried out by a 24 bit Quanterra digitizer, which generates data in miniSEED format. The time signal is provided by a GPS receiver. Data exchange is organized using a SEEDlink server that works as a ring buffer and can hold data on site for up to half a year.

Waveform data is transmitted online to the data centre of the GRSN, hosted by the Federal Institute for Geosciences and Natural Resources (BGR) in Hanover. Digital waveform data is stored and archived at this site and can be requested within suitable formats via the following website:

http://www.bgr.bund.de/DE/Themen/Erdbeben-Gefaehrdungsanalysen/Seismologie/Seismologie/Datenzentrum/waveform_request/waveform_request_node.html

The archiving of seismic drum records from 1966 to 1995 was taken out of the observatory to TU Bergakademie Freiberg (Fig. 5.26). Seismogram copies can be requested via email (brg@geophysik.tu-freiberg.de).

Data acquisition and storage of SG G 701 accelerometer data is done offline with a sampling frequency of 1 sample per minute. Data archiving is organized by an internal format on site.



Figure 5.19: Observatory building.

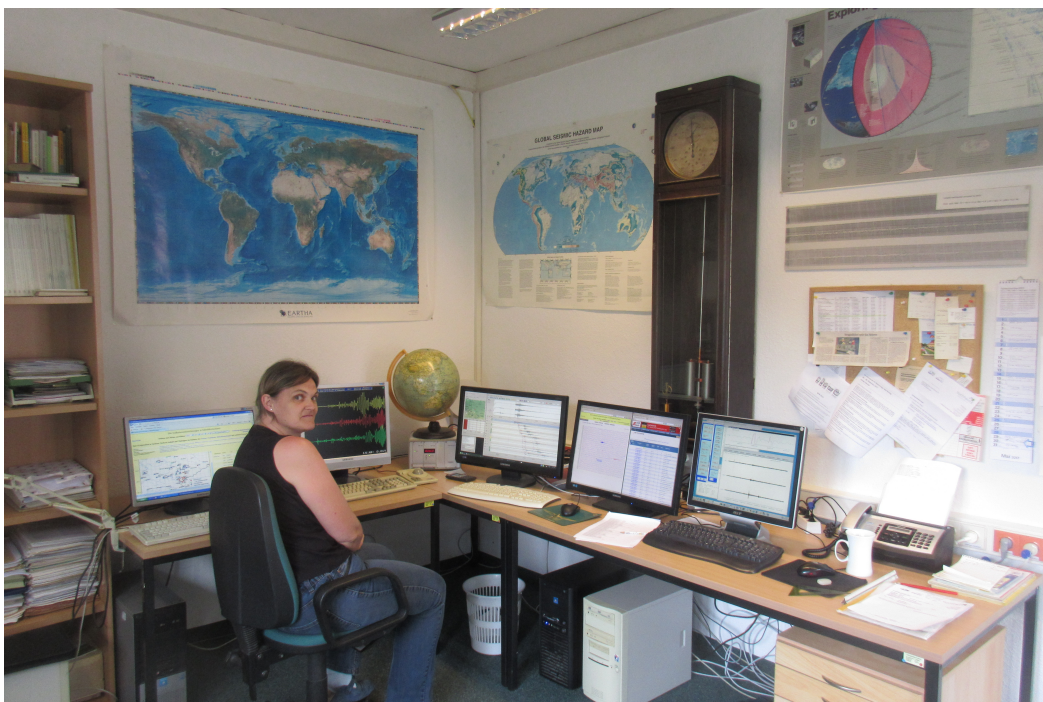


Figure 5.20: Observatory office with seismologist Anja Zeibig.



Figure 5.21: Entry to mining tunnel.



Figure 5.22: Mining tunnel.



Figure 5.23: Reconstruction of the Bina vertical pendulum seismoscope.



Figure 5.24: Historical instruments including Kirnos and SSJ-1,2 seismometers.

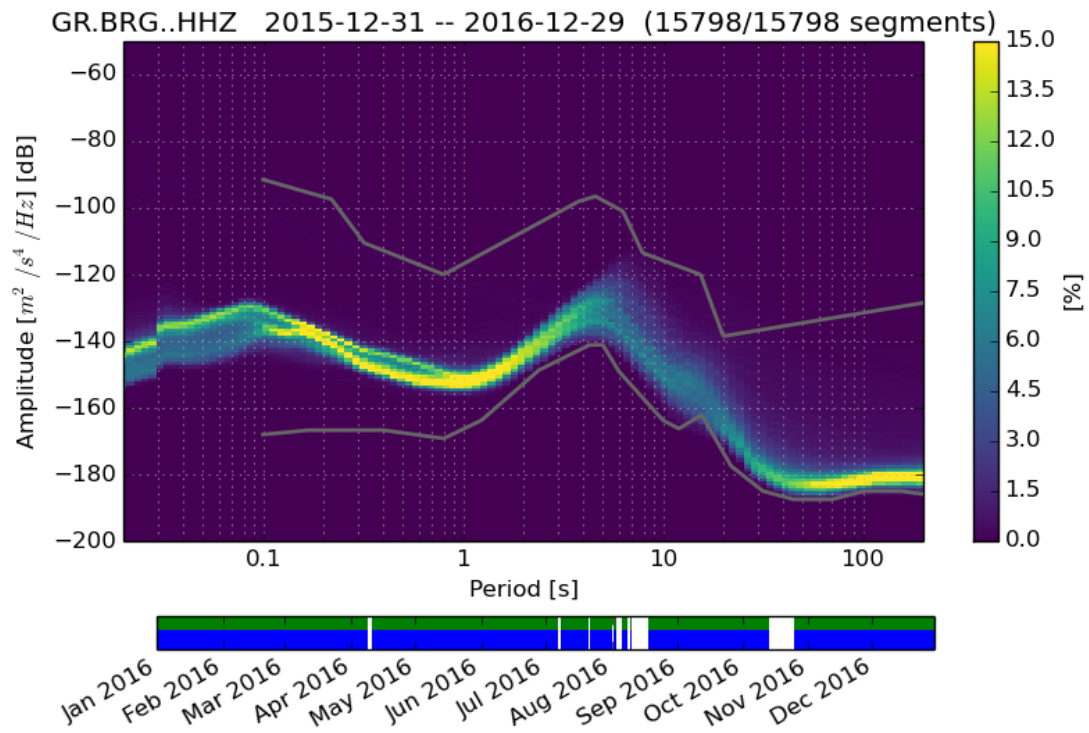


Figure 5.25: Power spectral density of noise for station BRG, determined over one year period for 2016. Upper grey line is High Noise Model, lower grey line is Low Noise Model. White areas in time line below represent time periods with no data. © K.Stammler, BGR.



Figure 5.26: Archive of drum records.

5.2.3 Data Analysis

For seismic waveform analysis the software packages Seismic Handler SH (*Stammler, 1993*) and Seis89 (*Baumbach, 1990*) are used. Data analysis is done in the tradition of observatory practice and must provide data for the monitoring of local, regional and global seismicity simultaneously. For that purpose, digital data of STS-2 broadband seismometer are processed by high pass (1 Hz), low pass (10 Hz) and bandpass filtering (0.588 Hz – 2.5 Hz) to simulate streams, equivalent to the WWSSN short- and long-period characteristics. The high pass and bandpass streams are processed by a STA/LTA detector to detect both crustal phases of local seismic events as well as body wave phases of teleseismic events. Phase and amplitude picking is done manually. Therefore, accuracy of onset time determination is limited by the sampling frequency and can be picked up to hundredths of seconds at the best. Figure 5.27 shows an example for the data analysis with Seismic Handler. For determination of amplitudes an Auto Peak procedure within Seismic Handler is mostly used and values are given to a tenth of nanometers. For seismic reports amplitude values are rounded and are given with three decimal place accuracy.

For event and phase type determination in routine station analysis data is compared with the hypocenter determination results of the local seismic network SXNET and the European data center EMSC. Because seismic station BRG is integrated into the real time information and seismic event notification services of both seismic monitoring systems, an appropriate association of event and phase type of the station records can be done. The local seismic network SXNET was set up in 2001 to monitor the local seismicity in Saxony. The seismic waveform data of the local network is processed using SeisComp (<http://www.seiscomp3.org>), a seismological software developed for data acquisition, processing, distribution and interactive analysis by the GEOFON Program (<http://geofon.gfz-potsdam.de>) at Helmholtz Centre Potsdam, GFZ German Research Centre for Geosciences. For detecting regional and teleseismic earthquakes at station BRG, a review of event data provided by the European data centre EMSC is used to ensure a proper phase association. Based on sophisticated manual routine analysis observatory BRG can provide the ISC with most accurate and relevant data of extensively exploited waveform data. As a result, observatory BRG is one of the leading single stations data providers for ISC with regard to teleseismic and secondary phase arrivals as well as amplitudes and period data for determination of magnitudes. Statistical investigations of the last ten years reveal that 7000 to 11000 seismic events are recorded by observatory BRG every year. Detected events colour coded by different event types are shown for the last 10 years in Figure 5.28. Figure 5.29 shows the percentage of each event type for 2016 in more detail. Nearly one third of the 7288 events are earthquakes, whereof 1495 (20%) are recorded from distances greater than 1000 km and 961 (13%) from distances less than 1000 km. 1138 events (16%) are associated with mining induced seismic events, mainly from Lubin Copper mine in Poland. Because station BRG is situated in a very dense region of explosion sites, nearly half of the detected events (3433, or 47%) are explosions. The rest (less than 3%) are unassociated detections.

The station's capability for detecting small magnitude events in relation to epicentral distance is shown in Figure 5.30 where all events in the ISC database for 2013, that had been recorded at station BRG, are plotted with magnitude M_w versus epicentral distance. According to the figure, from about 3 to 10 degrees epicentral distance the lowest detectable magnitude increases from $\sim M_w$ 3.3 to $\sim M_w$ 4. From epicentral distance of 10 to about 25 degrees the lowest magnitude threshold increases to $\sim M_w$ 4.5 with a few smaller magnitude events around 20 degree distance. From epicentral distance 25 degrees

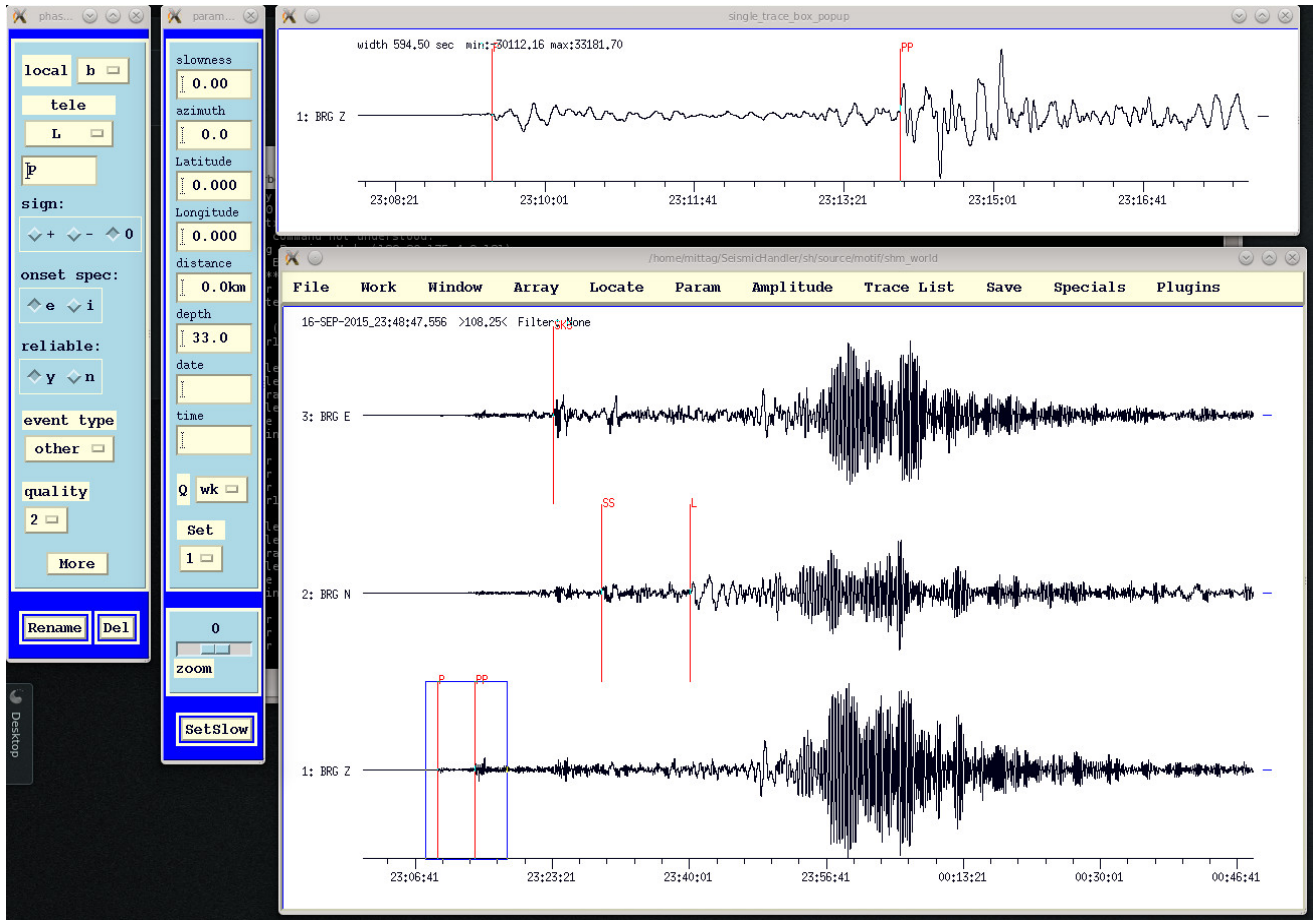


Figure 5.27: Example for data analysis with Seismic Handler for the Mw 8.2 Illapel earthquake in Chile on 16th September 2016.

onwards the lower magnitude limit shows a slight increase up to magnitudes of \sim Mw 5. For epicentral distances ranging around 80 degrees, that cover the Kuril Islands earthquake region, also smaller events with magnitude \sim Mw 4 are detected by BRG. From the linear part of cumulative magnitude-frequency distribution of all events (Fig. 5.31) recorded at station BRG in 2013 the Gutenberg-Richter-Relation can be determined to $\lg N = -0.91 Mw + 7.61$. Furthermore, a magnitude threshold of Mw \sim 5.2 for complete detection of global seismicity can be derived for BRG and other single stations located in Central Europe, which have similar recording conditions to BRG.

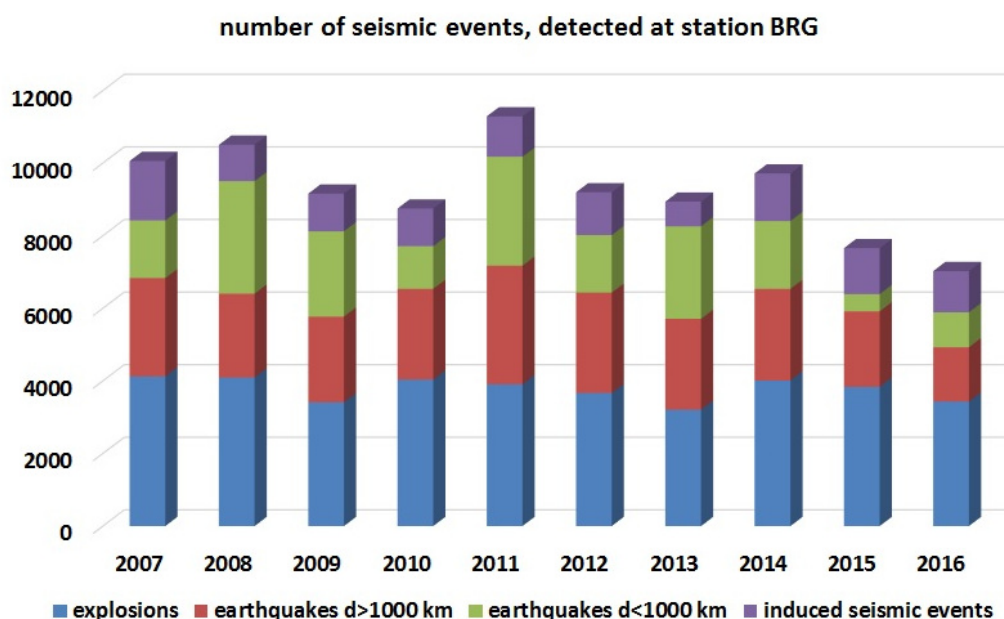


Figure 5.28: Annual number of seismic events detected at station BRG.

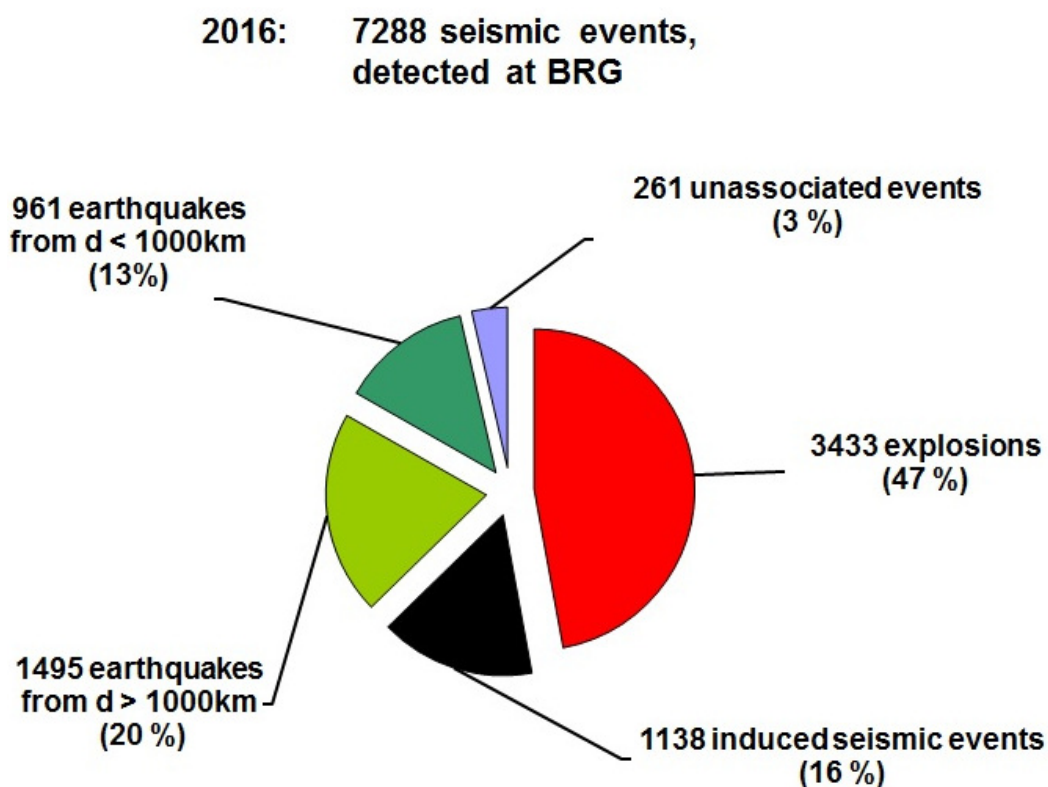


Figure 5.29: Percentages of seismic event types detected at station BRG in 2016.

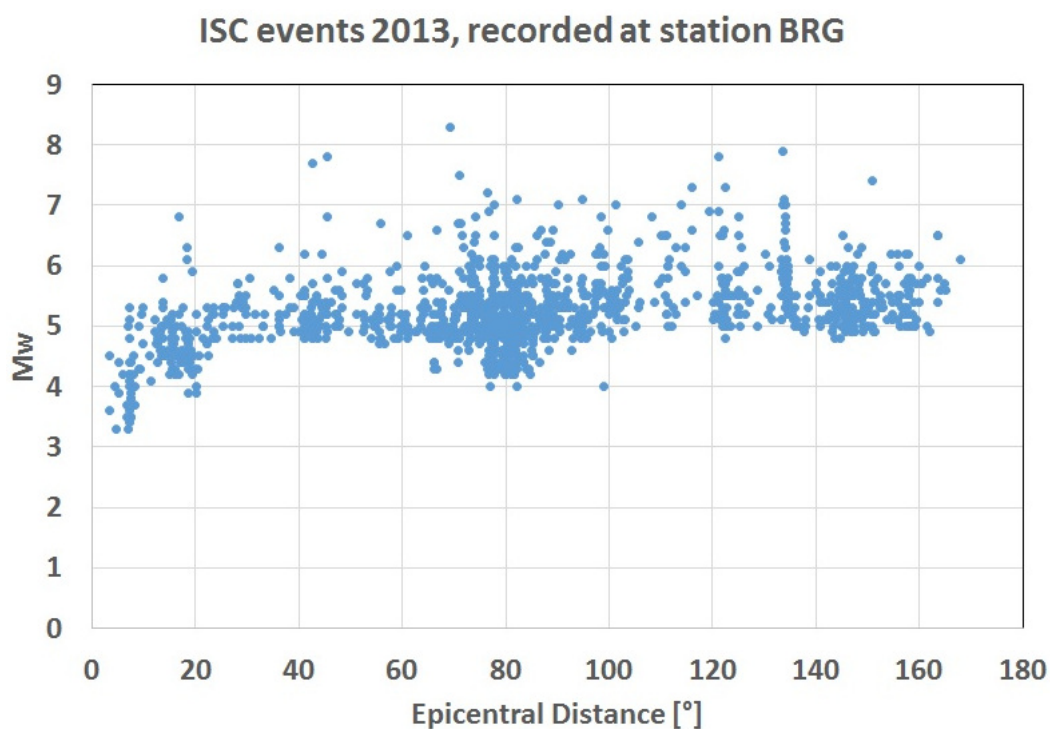


Figure 5.30: ISC events in 2013, recorded at station BRG according to ISC bulletin.

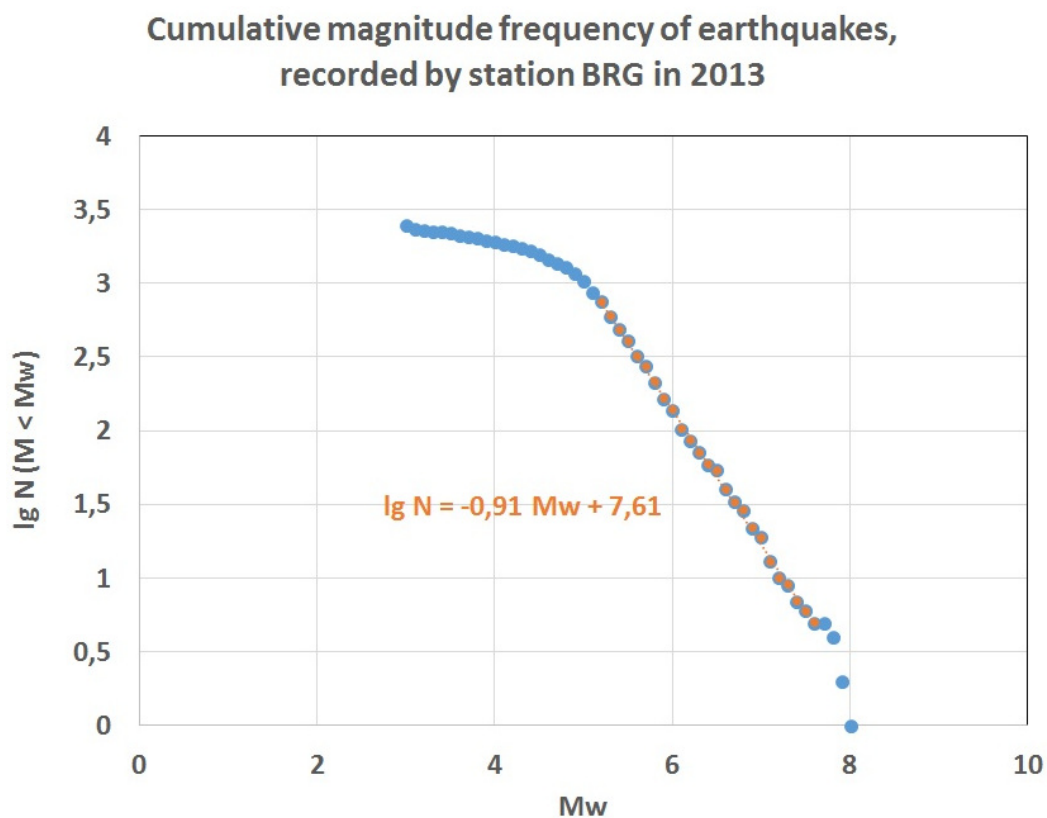


Figure 5.31: Cumulative magnitude frequency of earthquakes, recorded at station BRG in 2013 according to ISC bulletin.

5.2.4 References

- Baumbach, M. (1992), SEIS89 – A PC application for interactive seismogram analysis and processing. *XXII General Assembly European Seismological Commission*, Barcelona, 17-22 September 1990.
- Stammler, K. (1993), Seismic Handler – Programmable multichannel data handler for interactive and automatic processing of seismological analyses, *Computers & Geosciences*, 19(2), 135–140, <http://www.seismic-handler.org>, DOI:10.1016/0098-3004(93)90110-Q.

6

Summary of Seismicity, January - June 2014

April 2014 was, seismologically speaking, a very busy month with 8 out of 9 earthquakes showing magnitudes larger than Mw 7 during the first half of 2014 occurring within only 19 days (Tab.6.2). On 1st April the largest earthquake that occurred during the first six months of 2014, the Mw 8.1 Iquique event, nucleated near the coast of northern Chile where the Nazca Plate subducts beneath the South American Plate (23:46:47 UTC, 19.6193°S, 70.7877°W, 17.1 km, 2285 stations (ISC)). With 55 entries in the ISC Event Bibliography so far (*Di Giacomo et al.*, 2014; *International Seismological Centre*, 2016) it is also the event that raised most interest in the scientific community during this time period. The intraplate thrust event broke a central fraction of the Northern Chile seismic gap (*Schurr et al.*, 2014), a segment of the continental margin that was ruptured last in 1877 by a large megathrust event. About 200 km of the segment to the north and south of the rupture area was left unbroken and remains locked, posing a significant risk of another large megathrust event in this area (*e.g.* *Schurr et al.*, 2014). The largest aftershock followed two days later on 3rd April with a magnitude of Mw 7.7. A striking feature of the Iquique sequence was the increasing foreshock seismicity that started a month before the main shock occurred and raised discussions about what potential triggering role the foreshocks played and whether they were accompanied by aseismic slow slip processes (*e.g.* *Ruiz et al.*, 2016; *Bürgmann*, 2014; *Cesca et al.*, 2016; *Schurr et al.*, 2014).

Most of the other large earthquakes of April 2014 were located in the Bougainville-Solomon Islands region (Tab.6.2) where four events larger than Mw 7 occurred between 11th and 19th April. However, the four events do not belong to the same sequence. The Mw 7.5 (19th April) and Mw 7.1 (11th April) events are thrust events within the subduction zone where the Australian Plate subducts beneath the Pacific Plate (*USGS*, 2014a; *USGS*, 2014b). They belong to a sequence of seismicity that started on 11th April. Until the end of June 2014 over 300 events with magnitudes larger than 4.5 can be found in the ISC Bulletin in this region. The Mw 7.6 event of 12th April on the other hand was caused by nearly pure transform faulting where the plate boundary between the Australia and Pacific plate transitions from thrust to transform tectonics about 950 km away from the seismic sequence. This event was followed by a Mw 7.4 thrust faulting aftershock a day later on 13th April (*USGS*, 2014c).

The number of events in this Bulletin Summary categorised by type are given in Table 6.1.

The period between January and June 2014 produced 9 earthquakes with $M_W \geq 7$; these are listed in Table 6.2.

Figure 6.1 shows the number of moderate and large earthquakes in the first half of 2014. The distribution of the number of earthquakes should follow the Gutenberg-Richter law.

Figures 6.2 to 6.6 show the geographical distribution of moderate and large earthquakes in various magnitude ranges.

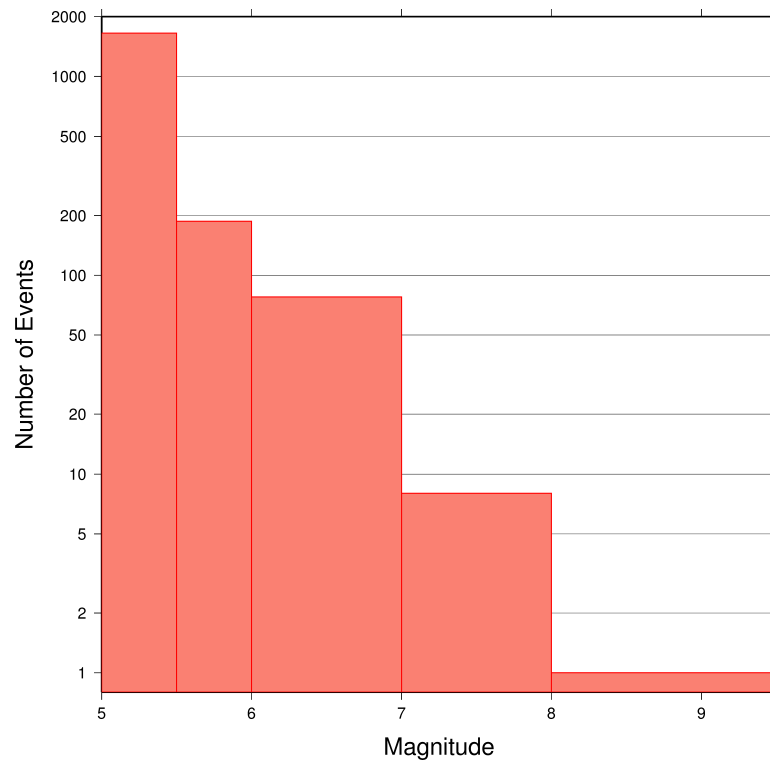


Figure 6.1: Number of moderate and large earthquakes between January and June 2014. The non-uniform magnitude bias here correspond with the magnitude intervals used in Figures 6.2 to 6.6.

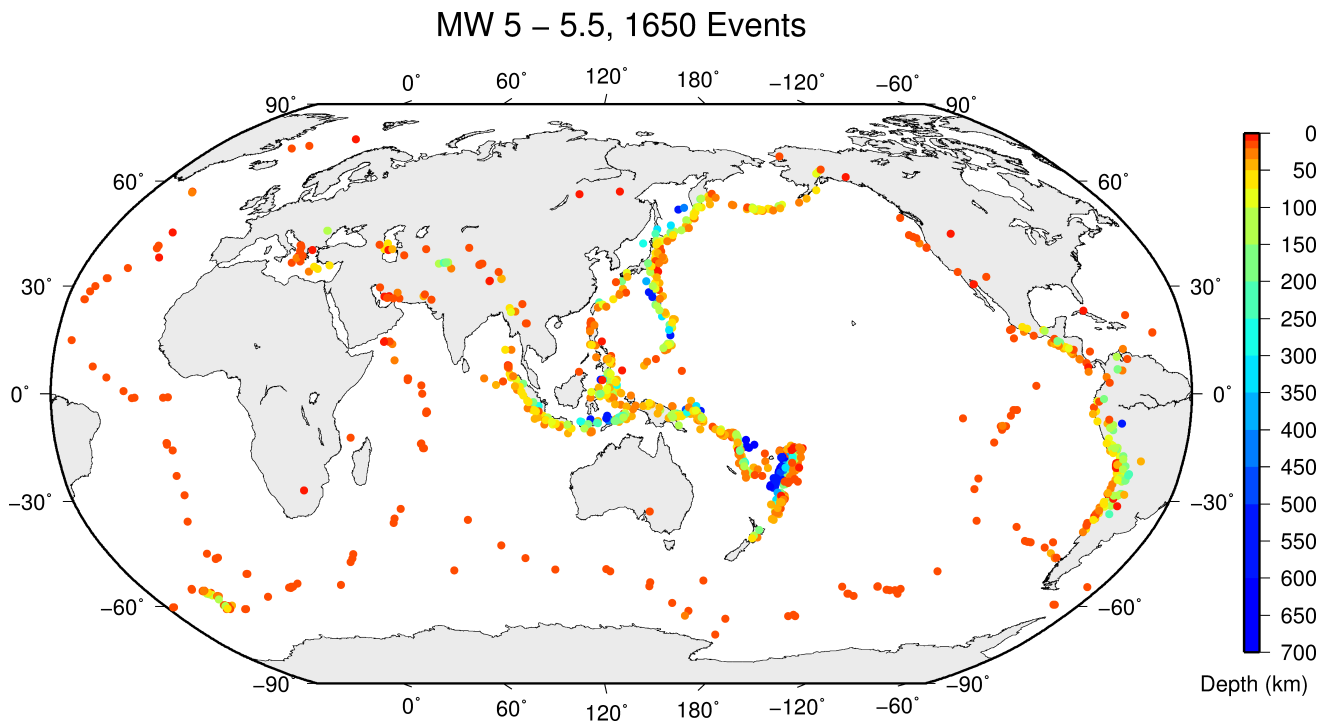


Figure 6.2: Geographic distribution of magnitude 5-5.5 earthquakes between January and June 2014.

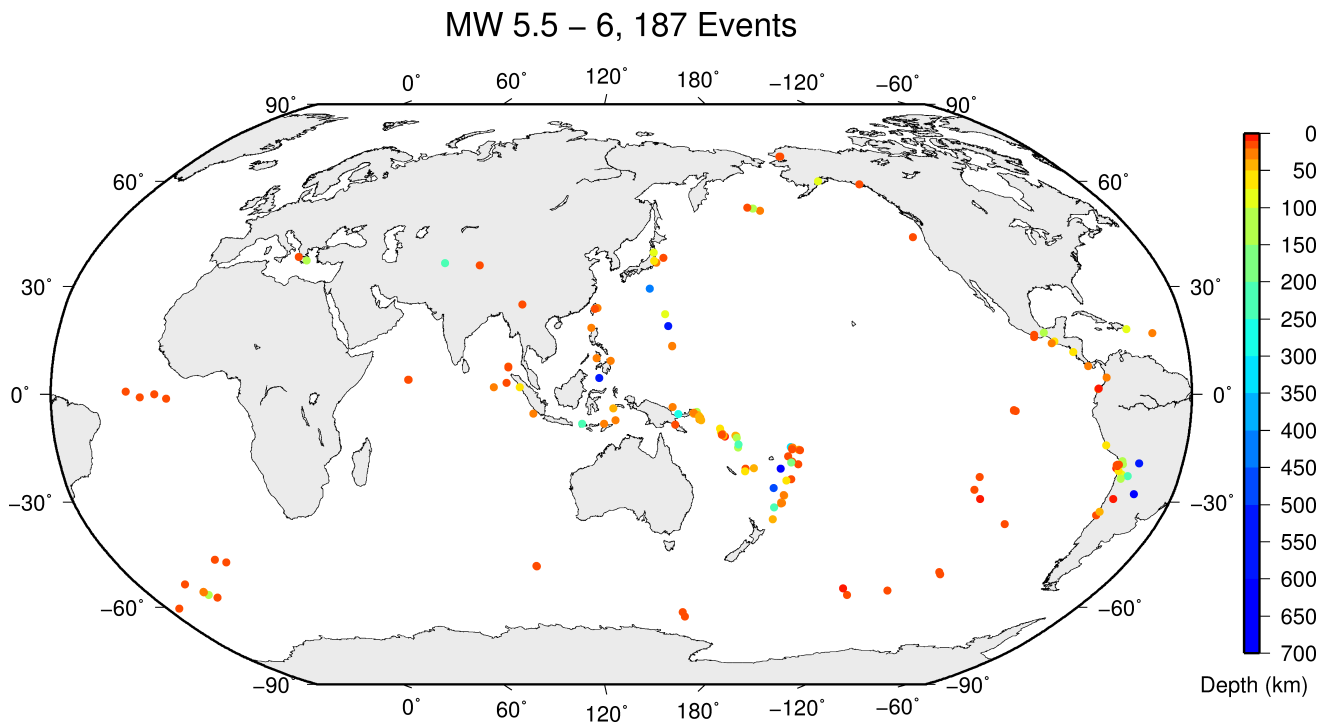


Figure 6.3: Geographic distribution of magnitude 5.5-6 earthquakes between January and June 2014.

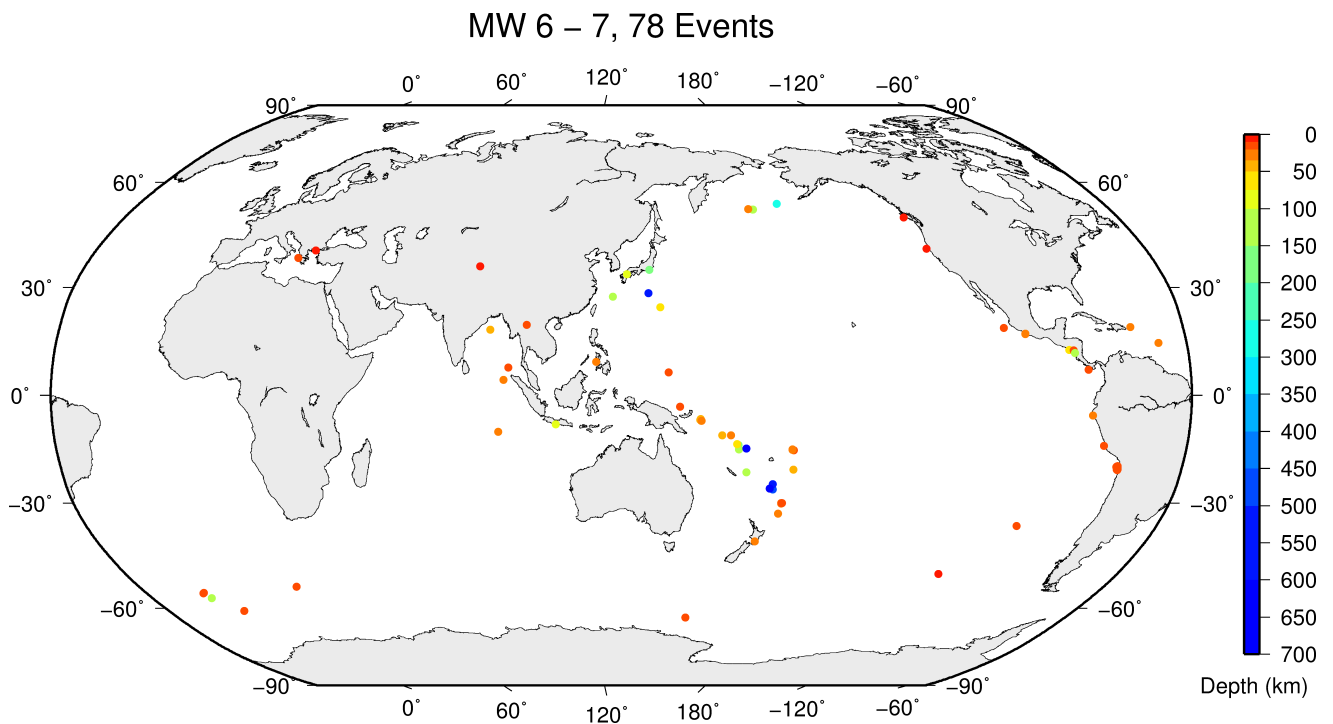


Figure 6.4: Geographic distribution of magnitude 6-7 earthquakes between January and June 2014.

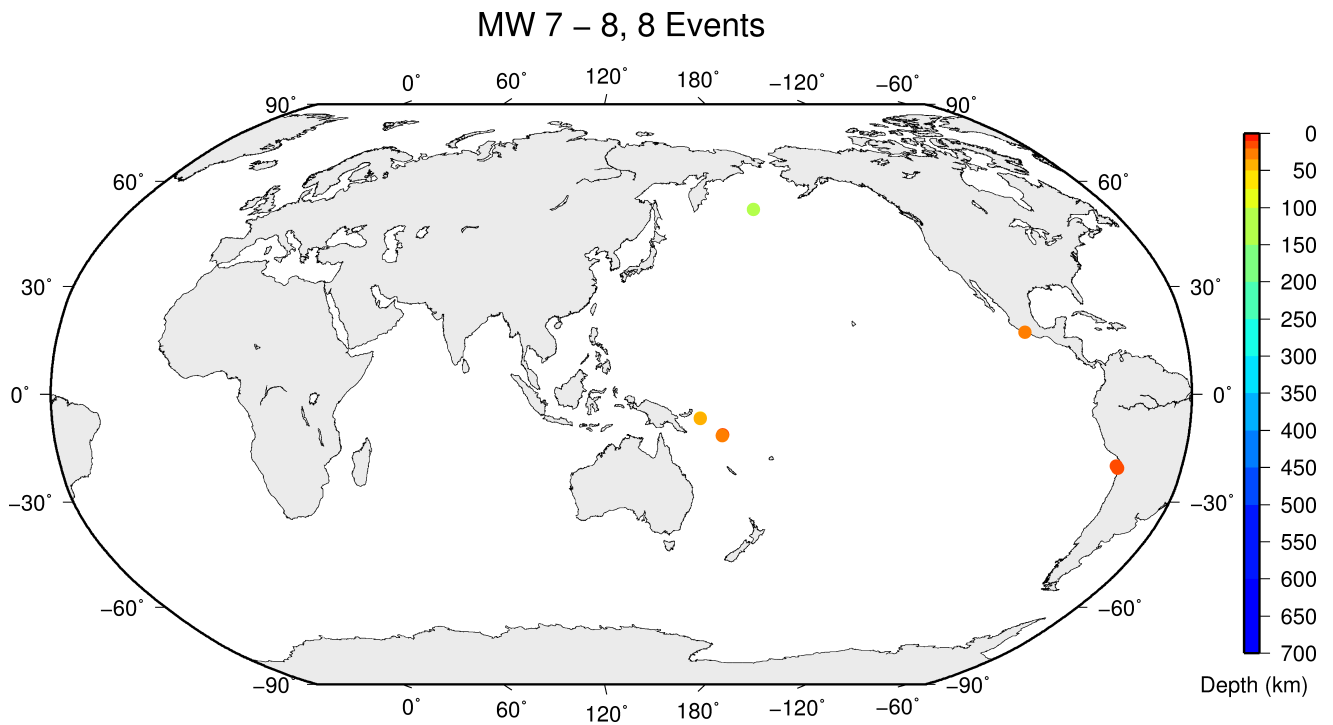


Figure 6.5: Geographic distribution of magnitude 7-8 earthquakes between January and June 2014.

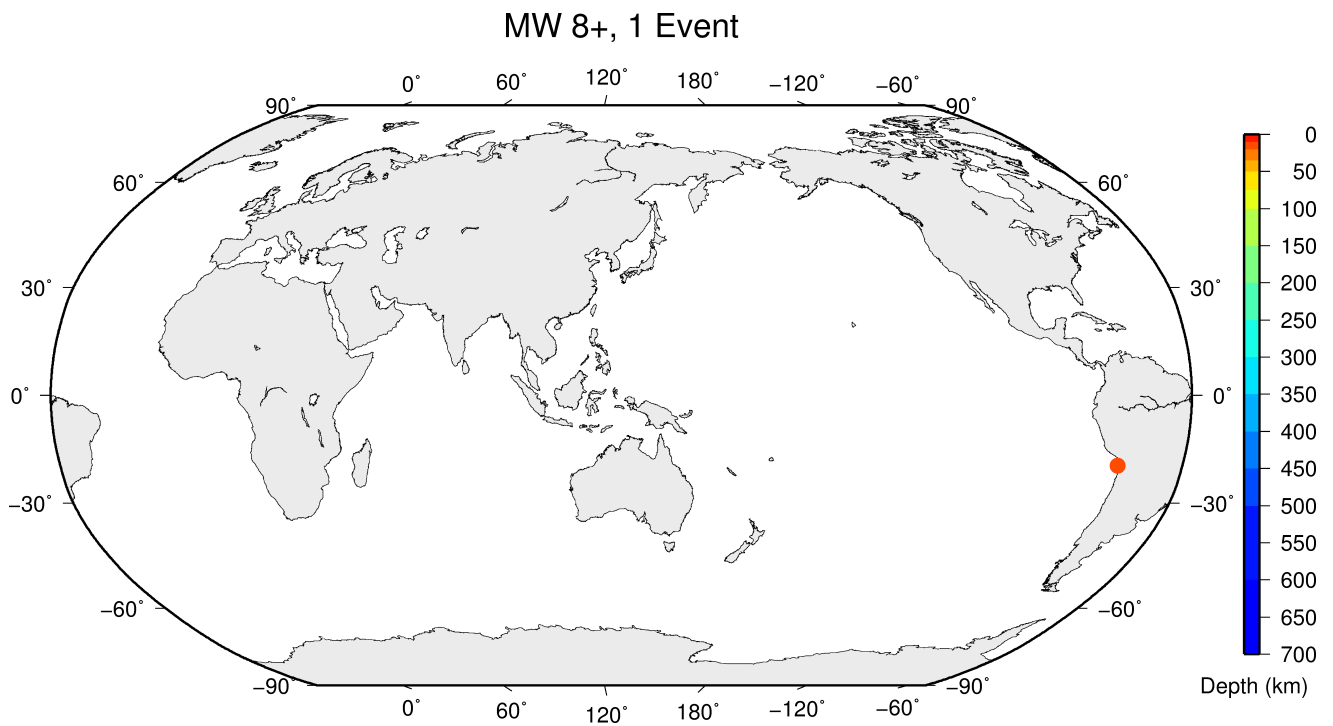


Figure 6.6: Geographic distribution of magnitude 8 and above earthquakes between January and June 2014.

Table 6.1: Summary of events by type between January and June 2014.

felt earthquake	746
known earthquake	181566
known chemical explosion	7755
known induced event	3454
known mine explosion	771
known rockburst	20
known experimental explosion	46
suspected earthquake	23923
suspected chemical explosion	341
suspected induced event	103
suspected mine explosion	3834
suspected rockburst	799
suspected experimental explosion	18
unknown	932
total	224308

Table 6.2: Summary of the earthquakes of magnitude $M_w \geq 7$ between January and June 2014.

Date	lat	lon	depth	M_w	Flinn-Engdahl Region
2014-04-01 23:46:47	-19.62	-70.79	17	8.1	Near coast of northern Chile
2014-06-23 20:53:09	51.70	178.64	102	7.9	Rat Islands
2014-04-03 02:43:14	-20.59	-70.49	11	7.7	Near coast of northern Chile
2014-04-12 20:14:38	-11.26	162.14	15	7.6	Bougainville-Solomon Islands region
2014-04-19 13:28:00	-6.71	154.99	39	7.5	Bougainville-Solomon Islands region
2014-04-13 12:36:19	-11.47	161.96	34	7.4	Bougainville-Solomon Islands region
2014-04-18 14:27:24	17.32	-100.99	24	7.3	Guerrero
2014-04-11 07:07:22	-6.61	155.03	57	7.1	Bougainville-Solomon Islands region
2014-04-01 23:57:56	-19.96	-71.02	10	7.0	Off coast of northern Chile

References

- Bürgmann, R. (2014), Warning signs of the Iquique earthquake, *Nature*, 512(7514), 258, DOI:10.1038/nature13655.
- Cesca, S., F. Grigoli, S. Heimann, T. Dahm, M. Kriegerowski, M. Sobiesiak, C. Tassara and M. Olcay (2016), The M_w 8.1 2014 Iquique, Chile, seismic sequence: a tale of foreshocks and aftershocks, *Geophysical Journal International*, 204(3), 1766–1780, DOI:10.1093/gji/ggv544.
- Di Giacomo, D., D.A. Storchak, N. Safronova, P. Ozgo, J. Harris, R. Verney and I. Bondár (2014), A New ISC Service: The Bibliography of Seismic Events, *Seismol. Res. Lett.*, 85(2), 354–360, DOI:10.1785/0220130143.
- International Seismological Centre, On-line Event Bibliography, www.isc.ac.uk/event_bibliography, Internatl. Seis. Cent., Thatcham, United Kingdom, 2016.
- Ruiz, S., M. Metois, A. Fuenzalida, J. Ruiz, F. Leyton, R. Grandin, C. Vigny, R. Madariaga, J. Campos (2014), Intense foreshocks and a slow slip event preceded the 2014 Iquique M_w 8.1 earthquake, *Science*,

345(6201), 1165–1169, DOI:10.1126/science.1256074.

Schurr, B., G. Asch, S. Hainzl, J. Bedford, A. Hoechner, M. Palo, R. Wang, M. Moreno, M. Bartsch, Y. Zhang and O. Oncken (2014), Gradual unlocking of plate boundary controlled initiation of the 2014 Iquique earthquake, *Nature*, 512(7514), p.299, DOI:10.1038/nature13681.

USGS (2014a), Earthquake Summary Poster, <https://earthquake.usgs.gov/archive/product/poster/20140419/us/1480722326516/poster.jpg> (visited on 14 August 2017).

USGS (2014b), Earthquake Summary Poster, <https://earthquake.usgs.gov/archive/product/poster/20140411/us/1480722784387/poster.jpg> (visited on 14 August 2017).

USGS (2014c), Earthquake Summary Poster, <https://earthquake.usgs.gov/archive/product/poster/20140412/us/1480722582481/poster.jpg> (visited on 14 August 2017).

7

Statistics of Collected Data

7.1 Introduction

The ISC Bulletin is based on the parametric data reports received from seismological agencies around the world. With rare exceptions, these reports include the results of waveform review done by analysts at network data centres and observatories. These reports include combinations of various bulletin elements such as event hypocentre estimates, moment tensors, magnitudes, event type and felt and damaging data as well as observations of the various seismic waves recorded at seismic stations.

Data reports are received in different formats that are often agency specific. Once an authorship is recognised, the data are automatically parsed into the ISC database and the original reports filed away to be accessed when necessary. Any reports not recognised or processed automatically are manually checked, corrected and re-processed. This chapter describes the data that are received at the ISC before the production of the reviewed Bulletin.

Notably, the ISC integrates all newly received data reports into the automatic ISC Bulletin (available on-line) soon after these reports are made available to ISC, provided it is done before the submission deadline that currently stands at 12 months following an event occurrence.

With data constantly being reported to the ISC, even after the ISC has published its review, the total data shown as collected, in this chapter, is limited to two years after the time of the associated reading or event, i.e. any hypocentre data collected two years after the event are not reflected in the figures below.

7.2 Summary of Agency Reports to the ISC

A total of 142 agencies have reported data for January 2014 to June 2014. The parsing of these reports into the ISC database is summarised in Table 7.1.

Table 7.1: *Summary of the parsing of reports received by the ISC from a total of 142 agencies, containing data for this summary period.*

	Number of reports
Total collected	3457
Automatically parsed	2591
Manually parsed	866

Data collected by the ISC consists of multiple data types. These are typically one of:

- Bulletin, hypocentres with associated phase arrival observations.

- Catalogue, hypocentres only.
- Unassociated phase arrival observations.

In Table 7.2, the number of different data types reported to the ISC by each agency is listed. The number of each data type reported by each agency is also listed. Agencies reporting indirectly have their data type additionally listed for the agency that reported it. The agencies reporting indirectly may also have ‘hypocentres with associated phases’ but with no associated phases listed - this is because the association is being made by the agency reporting directly to the ISC. Summary maps of the agencies and the types of data reported are shown in Figure 7.1 and Figure 7.2.

Table 7.2: Agencies reporting to the ISC for this summary period. Entries in bold are for new or renewed reporting by agencies since the previous six-month period.

Agency	Country	Directly or indirectly reporting (D/I)	Hypocentres with associated phases	Hypocentres without associated phases	Associated phases	Unassociated phases	Amplitudes
TIR	Albania	D	376	11	3434	44	0
ALG	Algeria	I NEIC	0	0	21	0	0
CRAAG	Algeria	D	330	0	1723	305	0
LPA	Argentina	D	0	0	0	728	0
SJA	Argentina	D	1881	41	44484	0	10484
NSSP	Armenia	D	67	0	729	0	0
AUST	Australia	D	863	41	19889	0	0
IDC	Austria	D	17993	3	484637	0	355035
VIE	Austria	D	4721	91	41785	588	41415
AZER	Azerbaijan	D	37	40	2094	0	0
UCC	Belgium	D	0	0	0	5393	676
SCB	Bolivia	D	29	0	651	0	101
SAR	Bosnia and Herzegovina	I KRSZO	0	15	0	0	0
RHSSO	Bosnia-Herzegovina	D	755	0	13848	8043	0
VAO	Brazil	D	1126	1	26366	0	0
SOF	Bulgaria	D	185	3	1370	5411	0
OTT	Canada	D	1286	43	31938	0	1914
PGC	Canada	I HYB	920	3	24185	0	0
GUC	Chile	D	4643	486	134091	1428	35594
BJI	China	D	2025	35	102440	39456	72936
ASIES	Chinese Taipei	D	0	43	0	0	0
TAP	Chinese Taipei	D	18645	16	695335	0	0
RSNC	Colombia	D	6611	4	168431	18971	52068
HDC	Costa Rica	I NEIC	0	1	0	0	0
ICE	Costa Rica	I UCR	0	8	0	0	0
UCR	Costa Rica	D	881	20	22396	0	1395
ZAG	Croatia	D	0	0	0	52167	0
SSNC	Cuba	D	686	0	8097	0	3805
NIC	Cyprus	D	620	1	14401	0	6874
IPEC	Czech Republic	D	446	0	2889	24147	1360
PRU	Czech Republic	D	5905	25	53493	196	15957
WBNET	Czech Republic	D	2159	0	38630	0	38415
KEA	Democratic People's Republic of Korea	D	277	0	2101	0	0
DNK	Denmark	D	1	379	0	11413	2445
OSPL	Dominican Republic	D	400	4	4039	0	1289
IGQ	Ecuador	D	32	1	1328	0	0
HLW	Egypt	D	187	8	2213	0	0
SNET	El Salvador	D	1620	50	23717	43	3947
SSS	El Salvador	I UCR	2	6	0	0	0
EST	Estonia	I HEL	319	0	0	0	0

Table 7.2: (continued)

Agency	Country	Directly or indirectly reporting (D/I)	Hypocentres with associated phases	Hypocentres without associated phases	Associated phases	Unassociated phases	Amplitudes
AAE	Ethiopia	D	32	0	220	449	0
SKO	FYR Macedonia	D	1417	1	7817	4419	3305
FIA0	Finland	I HEL	14	1	0	0	0
HEL	Finland	D	6399	2905	119381	9	19078
CSEM	France	I BER	1512	791	0	0	0
LDG	France	D	3002	127	69429	14	27341
STR	France	D	1175	0	17832	0	0
PPT	French Polynesia	D	1255	7	9900	542	10352
TIF	Georgia	D	0	302	0	4897	0
AWI	Germany	D	2058	0	6631	46	0
BGR	Germany	D	900	386	23556	0	7272
BNS	Germany	I BGR	0	41	0	0	0
BRG	Germany	D	0	0	0	5585	4186
BUG	Germany	I BGR	19	5	0	0	0
CLL	Germany	D	53	0	0	10023	2910
GDNRW	Germany	I BGR	0	23	0	0	0
GFZ	Germany	I SJA	47	24	4	0	0
HLUG	Germany	I BGR	1	0	0	0	0
LEDBW	Germany	I BGR	18	6	0	0	0
ATH	Greece	D	16327	30	502471	0	155366
THE	Greece	D	6001	96	137722	5053	42179
GCG	Guatemala	D	859	0	5157	0	2
HKC	Hong Kong	D	0	0	0	42	0
BUD	Hungary	D	88	1	1624	505	0
REY	Iceland	D	17	0	515	0	0
HYB	India	D	1070	270	8538	1	2671
NDI	India	D	411	352	9028	3759	2938
DJA	Indonesia	D	3558	83	66348	0	84232
TEH	Iran	D	1422	30	33816	0	120
THR	Iran	D	330	30	2623	0	646
ISN	Iraq	D	187	0	1594	0	471
GII	Israel	D	463	1	8132	0	0
GEN	Italy	D	1209	0	13330	1141	0
MED_RCMT	Italy	D	0	176	0	0	0
OSUB	Italy	D	0	0	0	1458	0
RISSC	Italy	D	9	0	93	0	0
ROM	Italy	D	16189	184	940769	356428	627166
TRI	Italy	D	0	0	0	5728	0
LIC	Ivory Coast	D	1041	0	3374	0	2318
JSN	Jamaica	D	120	0	769	8	2
JMA	Japan	D	63813	0	543242	725	0
MAT	Japan	D	0	0	0	8145	0
NIED	Japan	D	0	721	0	0	0
SYO	Japan	D	0	0	0	4780	0
JSO	Jordan	D	15	0	243	0	257
NNC	Kazakhstan	D	8402	0	95853	0	89587
SOME	Kazakhstan	D	4696	219	71728	0	66724
KNET	Kyrgyzstan	D	1444	0	12170	0	2536
KRNET	Kyrgyzstan	D	4549	0	75222	0	0
LVSN	Latvia	D	278	0	3389	0	1668
GRAL	Lebanon	D	384	0	2550	470	0
LIT	Lithuania	D	233	230	2039	1194	515
MCO	Macao, China	D	0	0	0	15	0
GSDM	Malawi	D	0	0	0	106	0
KLM	Malaysia	D	605	0	2534	0	0
ECX	Mexico	D	650	5	12453	0	1793
MEX	Mexico	D	3292	244	34281	20	1
MOLD	Moldova	D	0	0	0	1697	566
PDG	Montenegro	D	539	0	13445	0	6714
CNRM	Morocco	D	1343	0	15767	0	0
NAM	Namibia	D	165	0	757	134	0
DMN	Nepal	D	1885	0	19392	0	14528

Table 7.2: (continued)

Agency	Country	Directly or indirectly reporting (D/I)	Hypocentres with associated phases	Hypocentres without associated phases	Associated phases	Unassociated phases	Amplitudes
DBN	Netherlands	I BGR	0	3	0	0	0
WEL	New Zealand	D	7520	16	242356	213	244767
INET	Nicaragua	D	0	1956	0	0	0
BER	Norway	D	2410	2025	45683	3246	10382
NAO	Norway	D	2550	979	6784	0	2142
OMAN	Oman	D	735	0	13718	0	0
MSSP	Pakistan	D	0	0	0	736	0
UPA	Panama	D	499	0	11552	0	37
ARE	Peru	I NEIC	20	26	0	0	0
LIM	Peru	I HYB	2	11	0	0	0
MAN	Philippines	D	0	2099	0	43264	14866
QCP	Philippines	D	0	0	0	160	0
WAR	Poland	D	0	0	0	11525	661
IGIL	Portugal	D	738	3	3265	0	1086
INMG	Portugal	D	1425	0	39549	1421	12952
PDA	Portugal	I SVSA	1	0	0	0	0
SVSA	Portugal	D	449	0	7645	1836	3377
BELR	Republic of Belarus	D	0	0	0	3269	621
BUC	Romania	D	963	25	16735	61271	5415
ASRS	Russia	D	121	174	4939	0	1721
BYKL	Russia	D	171	183	14278	0	4688
CMWS	Russia	I MOS	0	8	0	0	0
DRS	Russia	I MOS	105	148	0	0	0
IDG	Russia	I MOS	0	145	0	0	0
IEPN	Russia	D	288	0	2259	4590	1844
KOLA	Russia	D	136	197	497	0	0
KRAR	Russia	I MOS	0	574	0	0	0
KRSC	Russia	D	543	0	21107	0	0
MIRAS	Russia	D	54	83	479	0	239
MOS	Russia	D	2137	2177	336928	0	117733
NERS	Russia	D	152	57	2889	0	1339
NORS	Russia	I MOS	52	195	0	0	0
SKHL	Russia	D	539	549	16578	0	8041
VLA	Russia	I MOS	0	56	0	0	0
YARS	Russia	D	967	148	13678	0	9292
SGS	Saudi Arabia	D	12	12	114	0	0
BEO	Serbia	D	1671	17	30304	0	0
BRA	Slovakia	D	0	0	0	21069	0
LJU	Slovenia	D	2341	658	28514	4053	9364
HNR	Solomon Islands	D	0	0	0	1674	0
PRE	South Africa	D	705	0	9359	0	3118
MDD	Spain	D	1955	11	64003	0	47760
MRB	Spain	D	340	0	8861	0	3756
SFS	Spain	D	496	0	3585	570	0
UPP	Sweden	D	1252	1398	13656	0	0
ZUR	Switzerland	D	522	29	13961	0	6588
BKK	Thailand	D	835	0	9153	0	0
TRN	Trinidad and Tobago	D	4	1067	330	34874	0
TUN	Tunisia	D	17	0	81	0	0
ATA	Turkey	D	426	0	5117	0	0
DDA	Turkey	D	11798	3	239022	0	86148
ISK	Turkey	D	9040	24	142693	7721	83953
AEIC	U.S.A.	I NDI	2118	224	55955	0	0
ANF	U.S.A.	I IRIS	1622	874	0	0	0
BUT	U.S.A.	I NEIC	69	6	0	0	0
CERI	U.S.A.	I IRIS	9	8	0	0	0
GCMT	U.S.A.	D	0	2506	0	0	0
HON	U.S.A.	I HYB	0	10	0	0	0
HVO	U.S.A.	I NEIC	100	1	0	0	0
IRIS	U.S.A.	D	3558	2230	297868	0	0
LDO	U.S.A.	I IRIS	17	6	489	0	0

Table 7.2: (continued)

Agency	Country	Directly or indirectly reporting (D/I)	Hypocentres with associated phases	Hypocentres without associated phases	Associated phases	Unassociated phases	Amplitudes
NCEDC	U.S.A.	I IRIS	394	47	20396	0	0
NEIC	U.S.A.	D	18475	10001	1372018	0	561693
OGSO	U.S.A.	I NEIC	1	0	0	0	0
PAS	U.S.A.	I NEIC	130	16	15750	0	0
PMR	U.S.A.	I HYB	0	22	0	0	0
PNSN	U.S.A.	I IRIS	0	4	0	0	0
REN	U.S.A.	I NEIC	70	14	102	0	0
RSPR	U.S.A.	D	3428	13	43576	0	0
SCEDC	U.S.A.	I IRIS	266	67	0	0	0
SEA	U.S.A.	I NEIC	30	2	56	0	0
SLM	U.S.A.	I NEIC	32	0	1	0	0
TUL	U.S.A.	I NEIC	776	58	0	0	0
UUSS	U.S.A.	I NEIC	69	9	0	0	0
WES	U.S.A.	I IRIS	11	5	0	0	0
SIGU	Ukraine	D	113	116	2290	23	602
DSN	United Arab Emirates	D	467	0	5271	0	0
BGS	United Kingdom	D	398	12	12003	40	5184
EAF	Unknown	D	715	11	4020	6808	1
KRSZO	Unknown	D	98	143	8081	0	0
UNK	Unknown	I IRIS	1135	181	4939	0	0
ISU	Uzbekistan	D	83	0	772	582	0
CAR	Venezuela	I NEIC	2	8	0	0	0
FUNV	Venezuela	D	251	0	4042	0	0
LSZ	Zambia	D	145	0	459	183	7
BUL	Zimbabwe	D	1236	1	6044	1695	0

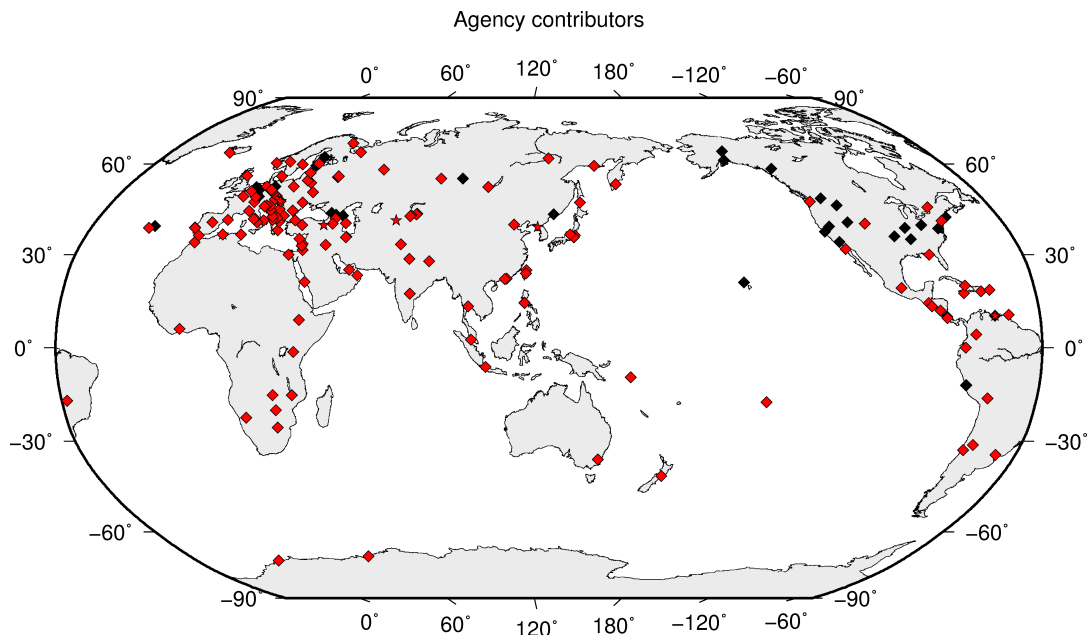


Figure 7.1: Map of agencies that have contributed data to the ISC for this summary period. Agencies that have reported directly to the ISC are shown in red. Those that have reported indirectly (via another agency) are shown in black. Any new or renewed agencies, since the last six-month period, are shown by a star. Each agency is listed in Table 7.2.

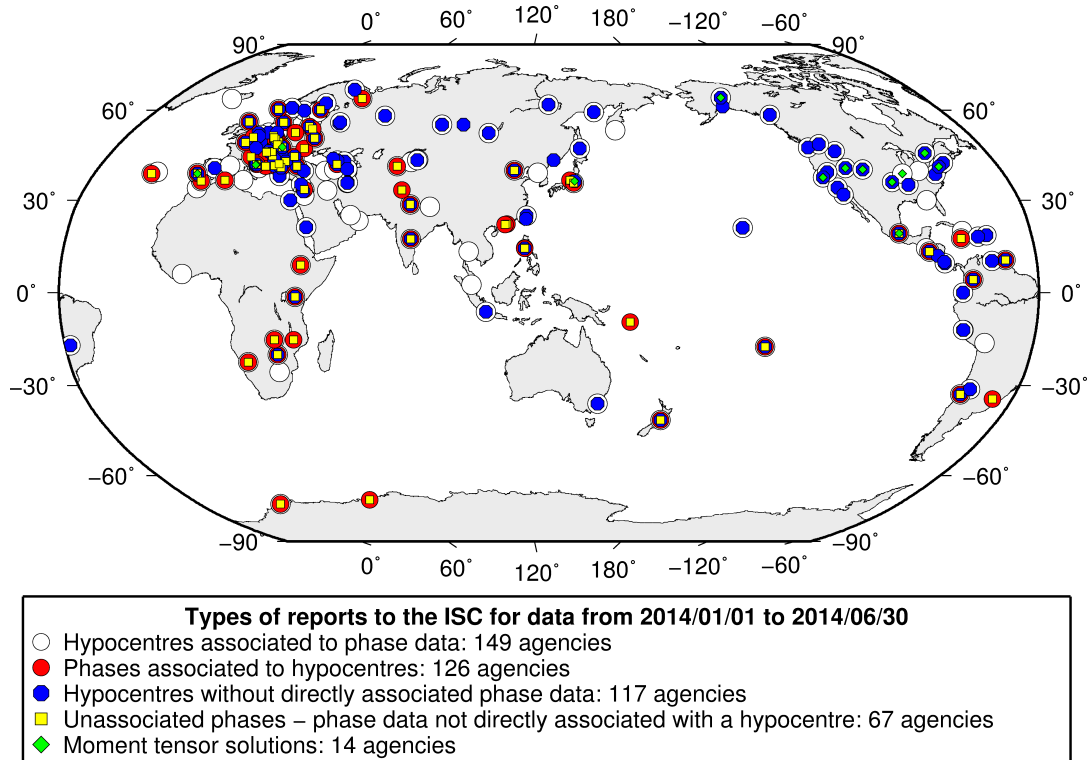


Figure 7.2: Map of the different data types reported by agencies to the ISC. A full list of the data types reported by each agency is shown in Table 7.2.

7.3 Arrival Observations

The collection of phase arrival observations at the ISC has increased dramatically with time. The increase in reported phase arrival observations is shown in Figure 7.3.

The reports with phase data are summarised in Table 7.3. This table is split into three sections, providing information on the reports themselves, the phase data, and the stations reporting the phase data. A map of the stations contributing these phase data is shown in Figure 7.4.

The ISC encourages the reporting of phase arrival times together with amplitude and period measurements whenever feasible. Figure 7.5 shows the percentage of events for which phase arrival times from each station are accompanied with amplitude and period measurements.

Figure 7.6 indicates the number of amplitude and period measurement for each station.

Together with the increase in the number of phases (Figure 7.3), there has been an increase in the number of stations reported to the ISC. The increase in the number of stations is shown in Figure 7.7. This increase can also be seen on the maps for stations reported each decade in Figure 7.8.

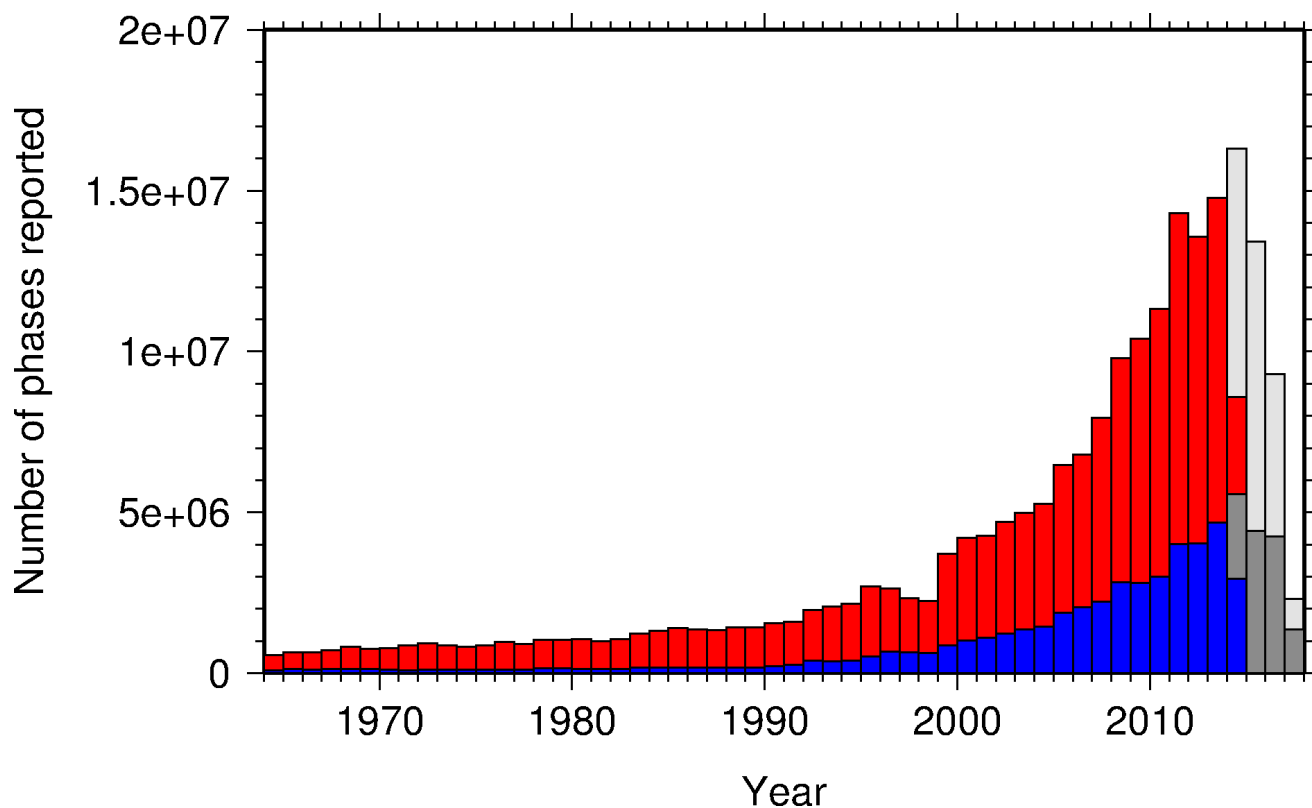


Figure 7.3: Histogram showing the number of phases (red) and number of amplitudes (blue) collected by the ISC for events each year since 1964. The data in grey covers the current period where data are still being collected before the ISC review takes place and is accurate at the time of publication.

Table 7.3: Summary of reports containing phase arrival observations.

Reports with phase arrivals	3321
Reports with phase arrivals including amplitudes	717
Reports with only phase arrivals (no hypocentres reported)	259
Total phase arrivals received	8586481
Total phase arrival-times received	7756535
Number of duplicate phase arrival-times	755969 (9.7%)
Number of amplitudes received	3065069
Stations reporting phase arrivals	7304
Stations reporting phase arrivals with amplitude data	4024
Max number of stations per report	1966

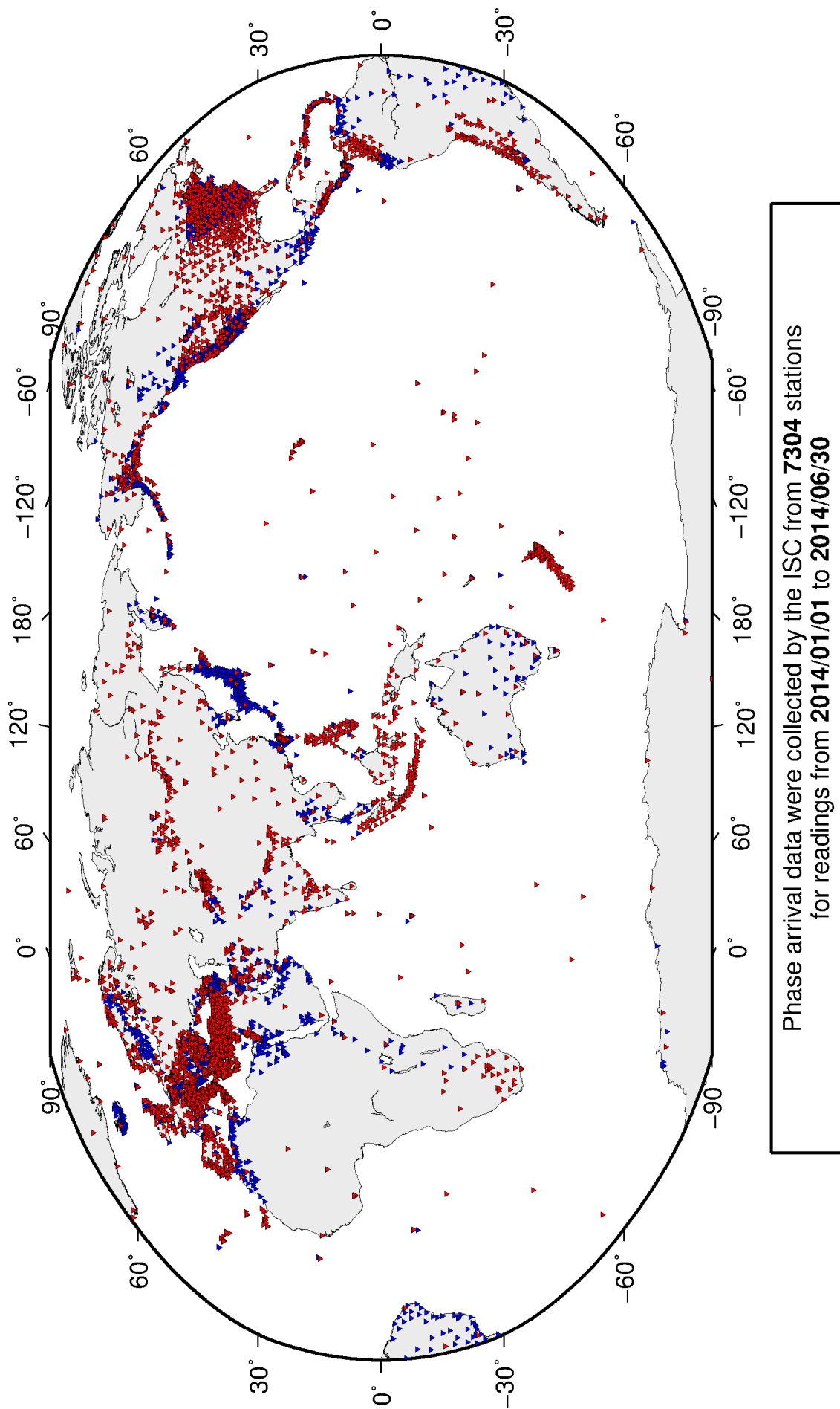


Figure 7.4: Stations contributing phase data to the ISC for readings from January 2014 to the end of June 2014. Stations in blue provided phase arrival times only; stations in red provided both phase arrival times and amplitude data.

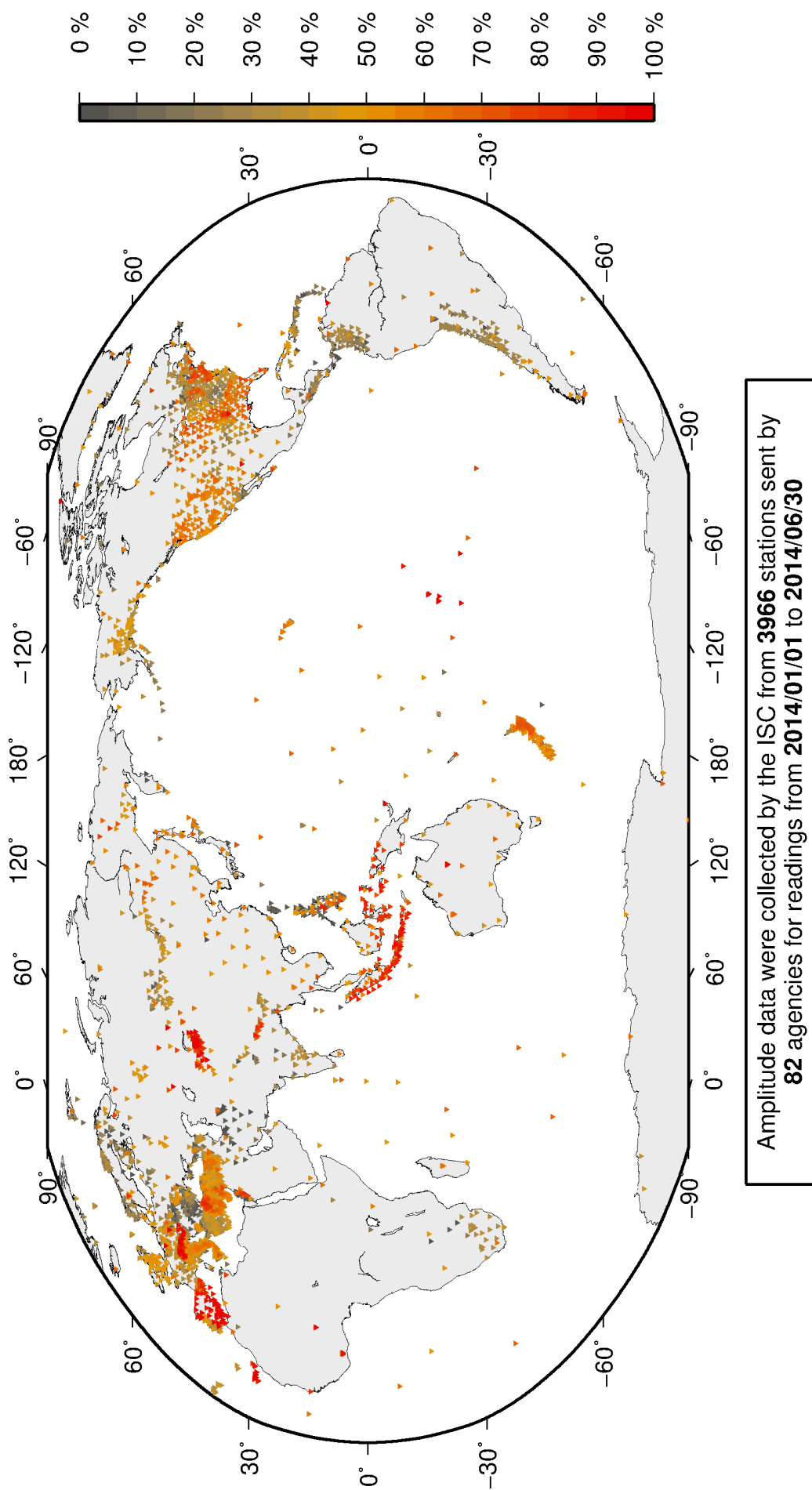
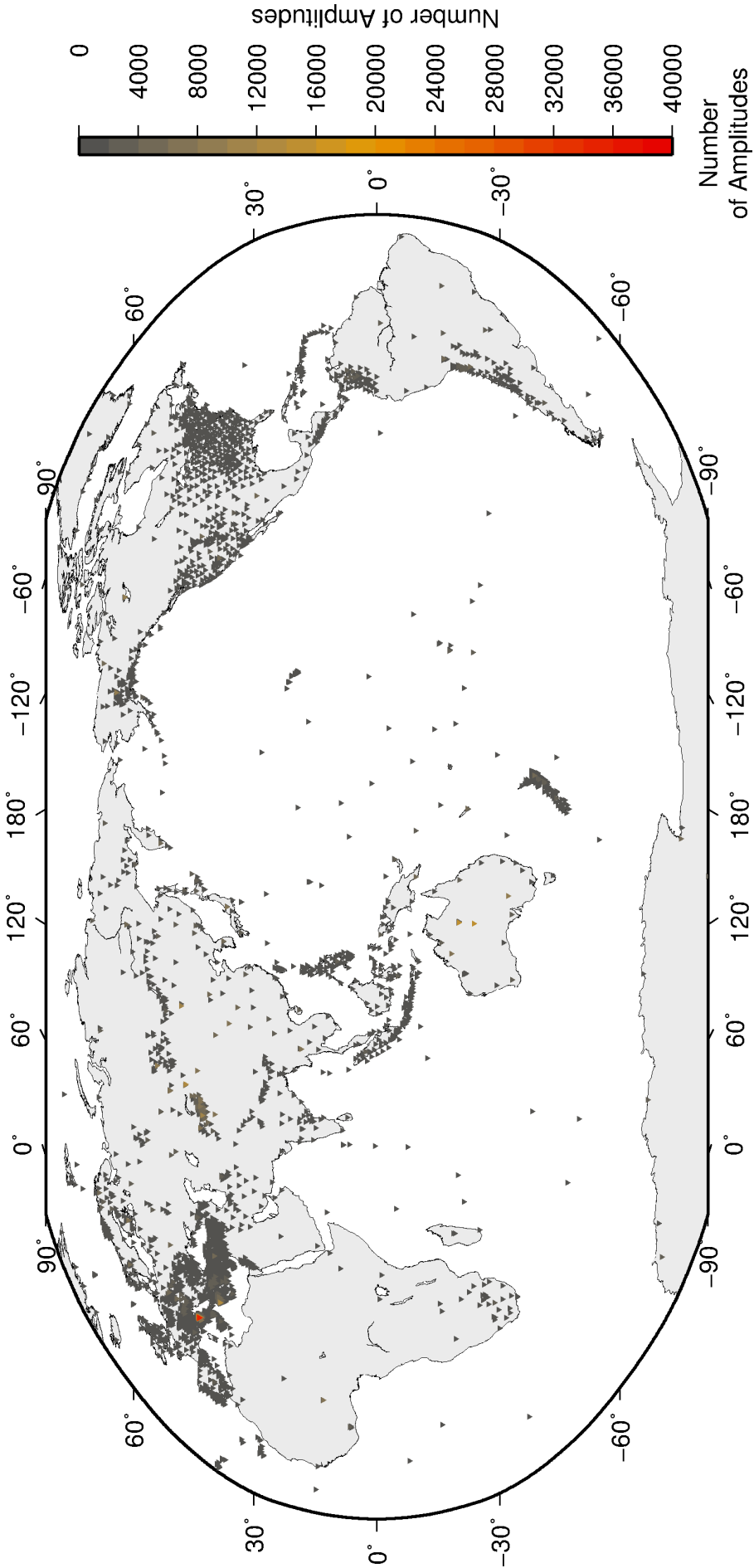


Figure 7.5: Percentage of events for which phase arrival times from each station are accompanied with amplitude and period measurements.



Amplitude data were collected by the ISC from **3966** stations sent by
82 agencies for readings from **2014/01/01** to **2014/06/30**

Figure 7.6: Number of amplitude and period measurements for each station.

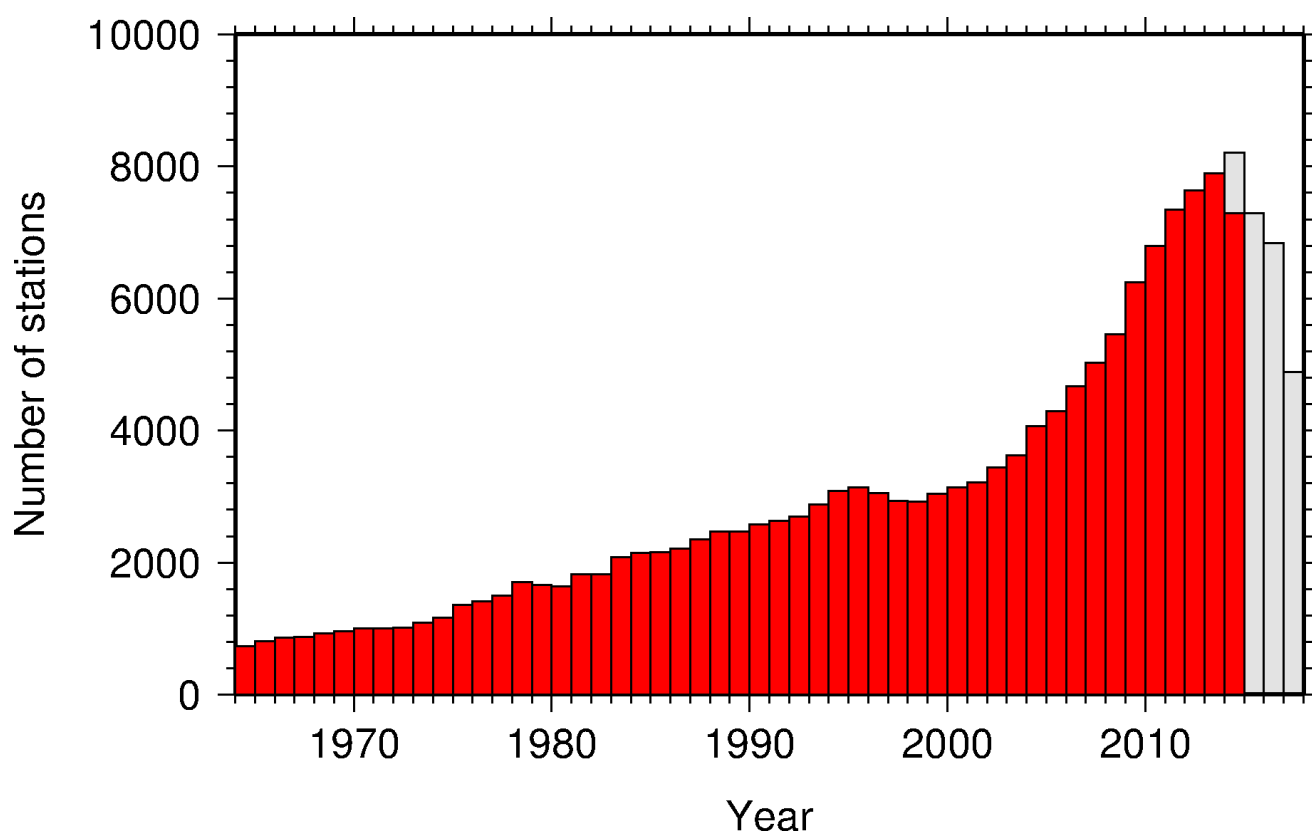


Figure 7.7: Histogram showing the number of stations reporting to the ISC each year since 1964. The data in grey covers the current period where station information is still being collected before the ISC review of events takes place and is accurate at the time of publication.

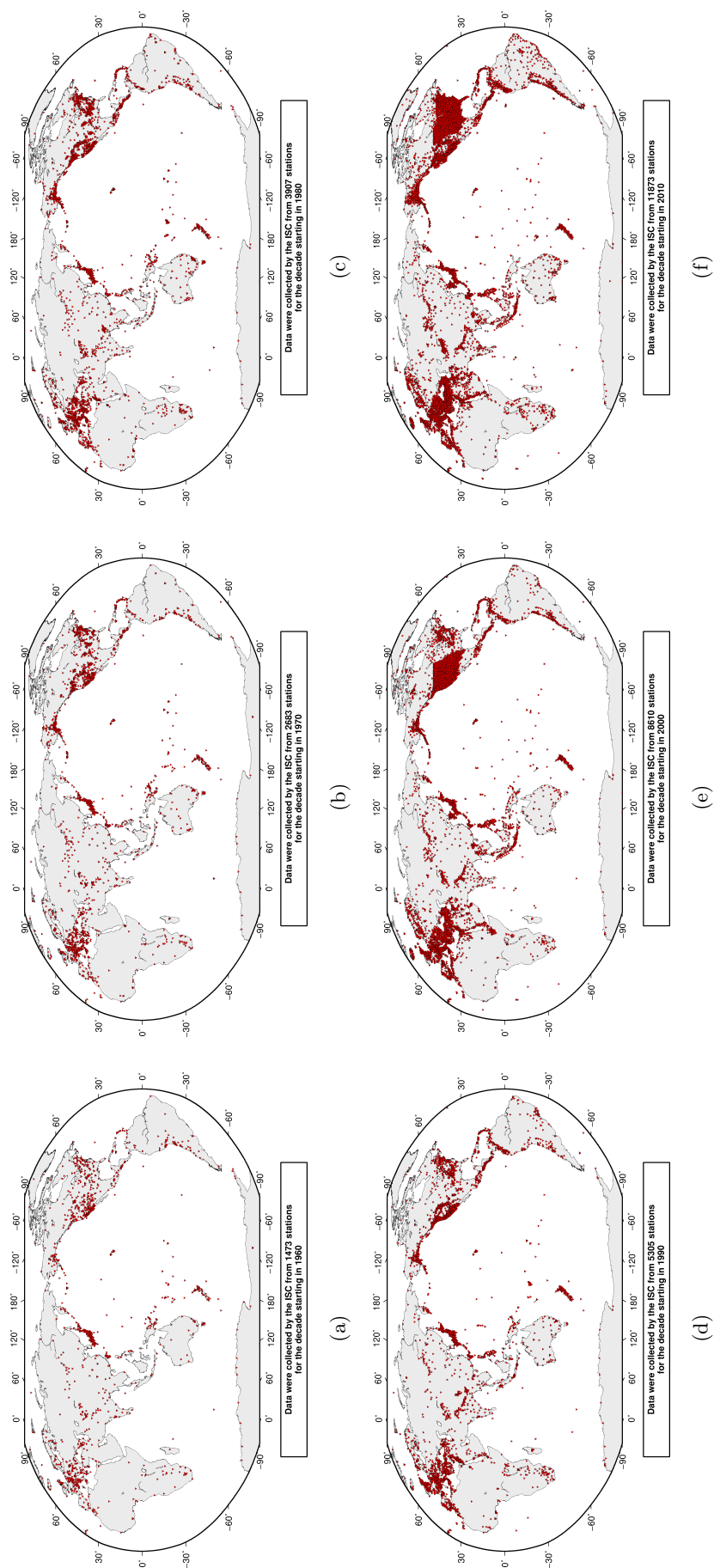


Figure 7.8: Maps showing the stations reported to the ISC for each decade since 1960. Note that the last map covers a shorter time period.

7.4 Hypocentres Collected

The ISC Bulletin groups multiple estimates of hypocentres into individual events, with an appropriate prime hypocentre solution selected. The collection of these hypocentre estimates are described in this section.

The reports containing hypocentres are summarised in Table 7.4. The number of hypocentres collected by the ISC has also increased significantly since 1964, as shown in Figure 7.9. A map of all hypocentres reported to the ISC for this summary period is shown in Figure 7.10. Where a network magnitude was reported with the hypocentre, this is also shown on the map, with preference given to reported values, first of M_W followed by M_S , m_b and M_L respectively (where more than one network magnitude was reported).

Table 7.4: Summary of the reports containing hypocentres.

Reports with hypocentres	3198
Reports of hypocentres only (no phase readings)	136
Total hypocentres received	337430
Number of duplicate hypocentres	9092 (2.7%)
Agencies determining hypocentres	169

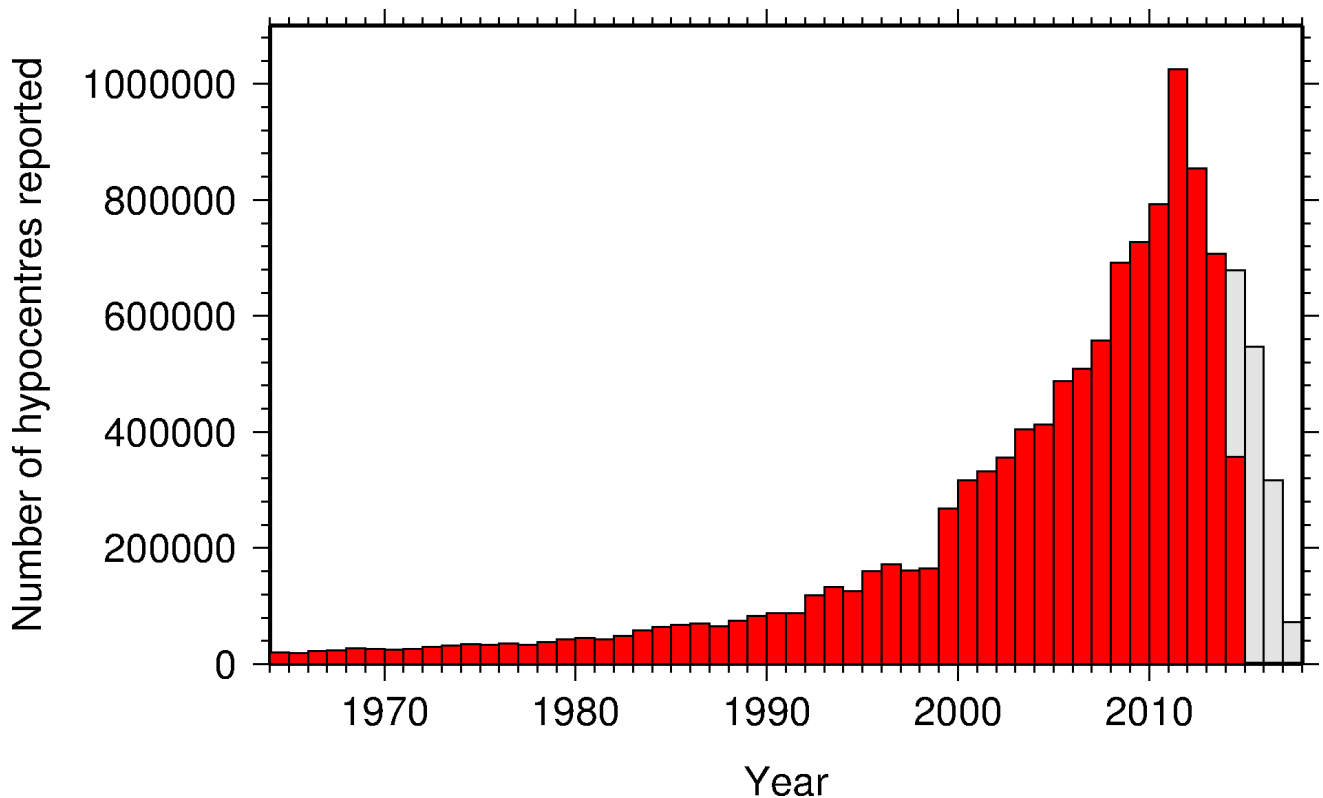


Figure 7.9: Histogram showing the number of hypocentres collected by the ISC for events each year since 1964. For each event, multiple hypocentres may be reported.

All the hypocentres that are reported to the ISC are automatically grouped into events, which form the basis of the ISC Bulletin. For this summary period 357287 hypocentres (including ISC) were grouped into 233815 events, the largest of these having 61 hypocentres in one event. The total number of events

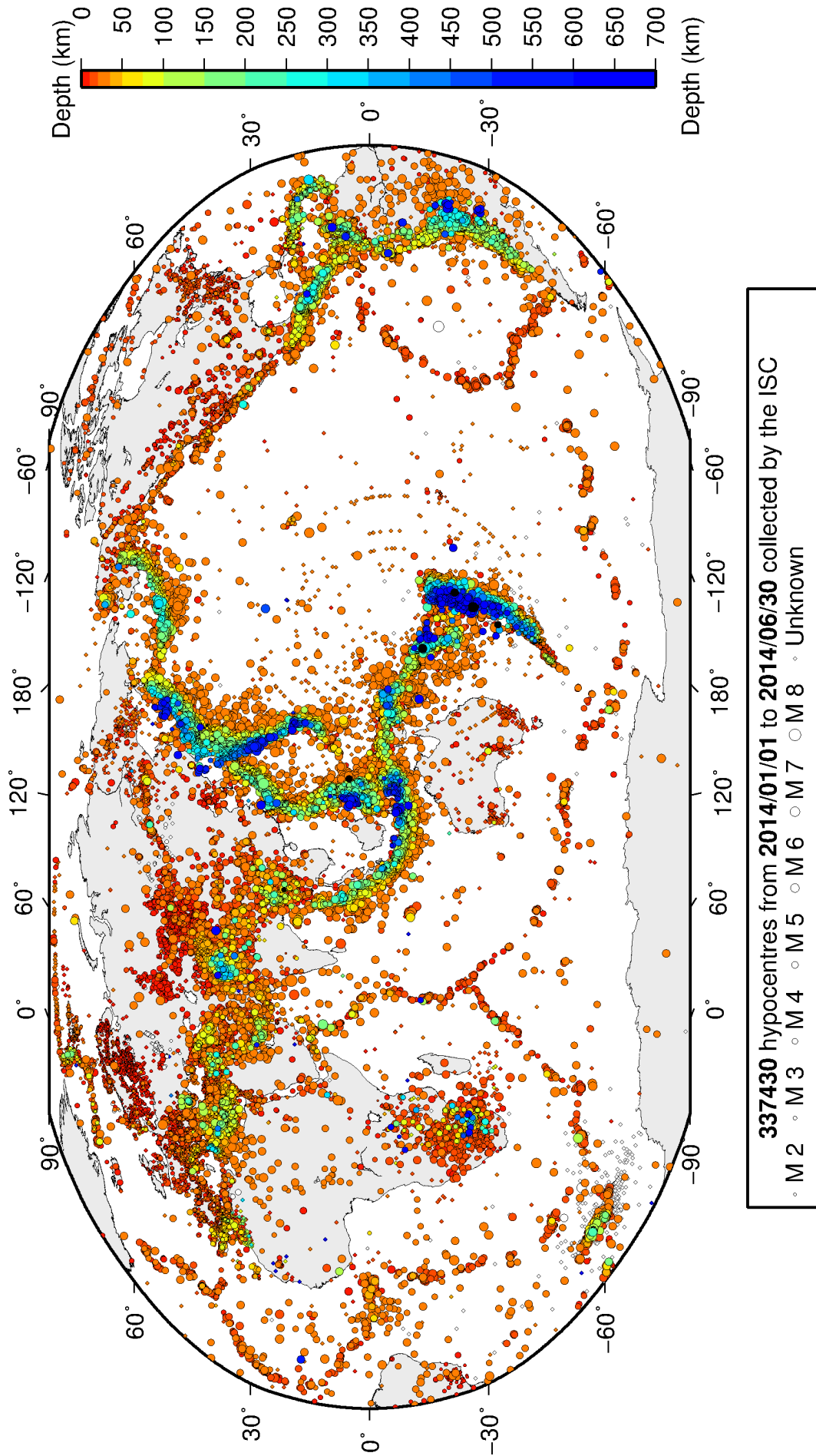


Figure 7.10: Map of all hypocentres collected by the ISC. The scatter shows the large variation of the multiple hypocentres that are reported for each event. The magnitude corresponds with the reported network magnitude. If more than one network magnitude type was reported, preference was given to values of M_W , M_S , m_b and M_L respectively. Compare with Figure 8.2

shown here is the result of an automatic grouping algorithm, and will differ from the total events in the published ISC Bulletin, where both the number of events and the number of hypocentre estimates will have changed due to further analysis. The process of grouping is detailed in Section 10.1.3. Figure 8.2 on page 92 shows a map of all prime hypocentres.

7.5 Collection of Network Magnitude Data

Data contributing agencies normally report earthquake hypocentre solutions along with magnitude estimates. For each seismic event, each agency may report one or more magnitudes of the same or different types. This stems from variability in observational practices at regional, national and global level in computing magnitudes based on a multitude of wave types. Differences in the amplitude measurement algorithm, seismogram component(s) used, frequency range, station distance range as well as the instrument type contribute to the diversity of magnitude types. Table 7.5 provides an overview of the complexity of reported network magnitudes reported for seismic events during the summary period.

Table 7.5: Statistics of magnitude reports to the ISC; M – average magnitude of estimates reported for each event.

	$M < 3.0$	$3.0 \leq M < 5.0$	$M \geq 5.0$
Number of seismic events	177308	34318	472
Average number of magnitude estimates per event	1.3	5.1	27.7
Average number of magnitudes (by the same agency) per event	1.1	2.7	3.8
Average number of magnitude types per event	1.2	4.1	13.2
Number of magnitude types	28	41	37

Table 7.6 gives the basic description, main features and scientific paper references for the most commonly reported magnitude types.

Table 7.6: Description of the most common magnitude types reported to the ISC.

Magnitude type	Description	References	Comments
M	Unspecified		Often used in real or near-real time magnitude estimations
mB	Medium-period and Broad-band body-wave magnitude	<i>Gutenberg</i> (1945a); <i>Gutenberg</i> (1945b); <i>IASPEI</i> (2005); <i>IASPEI</i> (2013); <i>Bormann et al.</i> (2009); <i>Bormann and Dewey</i> (2012)	
mb	Short-period body-wave magnitude	<i>IASPEI</i> (2005); <i>IASPEI</i> (2013); <i>Bormann et al.</i> (2009); <i>Bormann and Dewey</i> (2012)	Classical mb based on stations between 21°-100° distance

Table 7.6: *continued*

Magnitude type	Description	References	Comments
mb1	Short-period body-wave magnitude	<i>IDC</i> (1999) and references therein	Reported only by the IDC; also includes stations at distances less than 21°
mb1mx	Maximum likelihood short-period body-wave magnitude	<i>Ringdal</i> (1976); <i>IDC</i> (1999) and references therein	Reported only by the IDC
mbtmp	short-period body-wave magnitude with depth fixed at the surface	<i>IDC</i> (1999) and references therein	Reported only by the IDC
mbLg	Lg-wave magnitude	<i>Nuttli</i> (1973); <i>IASPEI</i> (2005); <i>IASPEI</i> (2013); <i>Bormann and Dewey</i> (2012)	Also reported as MN
Mc	Coda magnitude		
MD (Md)	Duration magnitude	<i>Bisztricsany</i> (1958); <i>Lee et al.</i> (1972)	
ME (Me)	Energy magnitude	<i>Choy and Boatwright</i> (1995)	Reported only by NEIC
MJMA	JMA magnitude	<i>Tsuboi</i> (1954)	Reported only by JMA
ML (Ml)	Local (Richter) magnitude	<i>Richter</i> (1935); <i>Hutton and Boore</i> (1987); <i>IASPEI</i> (2005); <i>IASPEI</i> (2013)	
MLS _n	Local magnitude calculated for S _n phases	<i>Balfour et al.</i> (2008)	Reported by PGC only for earthquakes west of the Cascadia subduction zone
ML _v	Local (Richter) magnitude computed from the vertical component		Reported only by DJA and BKK
MN (Mn)	Lg-wave magnitude	<i>Nuttli</i> (1973); <i>IASPEI</i> (2005)	Also reported as mbLg
MS (Ms)	Surface-wave magnitude	<i>Gutenberg</i> (1945c); <i>Vaněk et al.</i> (1962); <i>IASPEI</i> (2005)	Classical surface-wave magnitude computed from station between 20°-160° distance
Ms1	Surface-wave magnitude	<i>IDC</i> (1999) and references therein	Reported only by the IDC; also includes stations at distances less than 20°
ms1mx	Maximum likelihood surface-wave magnitude	<i>Ringdal</i> (1976); <i>IDC</i> (1999) and references therein	Reported only by the IDC

Table 7.6: *continued*

Magnitude type	Description	References	Comments
Ms7	Surface-wave magnitude	<i>Bormann et al.</i> (2007)	Reported only by BJI and computed from records of a Chinese-made long-period seismograph in the distance range 3°-177°
MW (Mw)	Moment magnitude	<i>Kanamori</i> (1977); <i>Dziewonski et al.</i> (1981)	Computed according to the <i>IASPEI</i> (2005) and <i>IASPEI</i> (2013) standard formula
Mw(mB)	Proxy Mw based on mB	<i>Bormann and Saul</i> (2008)	Reported only by DJA and BKK
Mwp	Moment magnitude from P-waves	<i>Tsuboi et al.</i> (1995)	Reported only by DJA and BKK and used in rapid response
mbh	Unknown		
mbv	Unknown		
MG	Unspecified type		Contact contributor
Mm	Unknown		
msh	Unknown		
MSV	Unknown		

Table 7.7 lists all magnitude types reported, the corresponding number of events in the ISC Bulletin and the agency codes along with the number of earthquakes.

Table 7.7: *Summary of magnitude types in the ISC Bulletin for this summary period. The number of events with values for each magnitude type is listed. The agencies reporting these magnitude types are listed, together with the total number of values reported.*

Magnitude type	Events	Agencies reporting magnitude type (number of values)
M	8794	WEL (6862), KRAR (574), MOS (197), BYKL (183), ASRS (174), YARS (148), IDG (145), KOLA (104), RSPR (83), NERS (57), VLA (56), MIRAS (48), PRU (32), BKK (27), IGQ (26), FDF (25), SCEDC (18), SKHL (10), CMWS (8), JSO (8), NCEDC (7), CERi (3), REN (2)
mB	2123	BJI (1591), DJA (737), WEL (151), KEA (11), BKK (5), STR (2)
mb	27804	IDC (17343), NEIC (8492), NNC (4591), KRNET (4545), MOS (1680), MAN (1668), BJI (1511), VIE (1433), DJA (1147), VAO (602), BGR (296), MDD (166), KLM (111), YARS (54), SIGU (42), GII (41), NDI (39), SOME (28), OMAN (20), DSN (14), STR (12), BKK (9), PGC (7), CRAAG (4), GUC (4), INET (3), IGIL (2), KRSZO (2), DMN (2), THR (2), SSNC (1), ROM (1), BGS (1)
mb1	17640	IDC (17640)
mb1mx	17640	IDC (17640)
mB_BB	39	BGR (39)

Table 7.7: Continued.

Magnitude type	Events	Agencies reporting magnitude type (number of values)
mb_Lg	93	NEIC (73), TEH (14), WES (4), OTT (1), MDD (1), OGSO (1)
mbLg	1756	MDD (1756)
mbR	121	VAO (121)
mbtmp	17645	IDC (17645)
Mc	1	BER (1)
MD	14797	MEX (3296), LDG (2522), ROM (2044), RSPR (1606), GCG (851), TRN (789), SSNC (666), ECX (624), UCR (409), GRAL (385), TIR (363), SVSA (311), DDA (205), SNET (205), GII (191), SOF (175), HLW (157), PDG (135), NCEDC (94), EAF (91), INET (71), JSN (63), LSZ (61), INMG (57), NAM (48), SJA (48), UPA (41), NIC (29), SLM (27), OSPL (25), BUT (18), TUN (17), BUL (15), ISK (9), HVO (6), SEA (4), CERI (4), BUG (4), PNSN (3), NDI (3), ATA (3), HDC (2), NEIC (1)
MJMA	60946	JMA (60946)
Mjma	8	JSO (8)
ML	124479	TAP (18666), ATH (16192), ROM (14691), DDA (11273), IDC (10106), ISK (9012), RSNC (6579), HEL (6395), THE (5991), WEL (5644), GUC (4826), LDG (2850), VIE (2772), ANF (2463), LJU (2247), UPP (2195), AEIC (2131), INET (1896), BER (1766), SJA (1762), MAN (1685), BEO (1661), SNET (1460), TEH (1341), GEN (1207), BUC (963), YARS (904), INMG (890), WBNET (877), TUL (760), RHSSO (754), PRE (705), SSNC (676), PGC (631), ECX (625), NIC (619), KRSC (541), PDG (490), IGIL (457), OMAN (450), IPEC (446), BJI (439), ATA (417), NAO (397), OSPL (385), UCR (379), SVSA (363), MRB (340), SFS (326), THR (319), LVSN (266), BGR (212), NEIC (206), KNET (199), CRAAG (188), ISN (186), DSN (172), BGS (168), HLW (156), PAS (123), DNK (103), HVO (95), NDI (93), BUD (86), KRSZO (78), USSS (63), SCEDC (60), NCEDC (58), PPT (56), OTT (55), CLL (53), ARE (53), MIRAS (52), BUT (49), REN (44), AZER (41), BNS (39), SCB (29), UPA (29), SEA (26), KEA (25), BUG (23), FIA0 (15), DMN (12), SGS (12), SSS (7), LDO (7), RISSC (6), JSO (5), TIR (5), ALG (5), ZUR (4), VAO (4), IASPEI (3), LSZ (3), CSEM (3), GCG (2), HYB (2), IGQ (1), CAR (1), PNSN (1), AUST (1), PRU (1)
MLh	623	ZUR (513), ASRS (110)
MLS _n	336	PGC (336)
ML _v	10624	WEL (7018), DJA (2501), STR (1175), BKK (27), JSO (8), ASRS (8)
M _m	133	GII (133)
MN	210	OTT (210)
mpv	4896	NNC (4896)
MPVA	304	NORS (241), MOS (157)

Table 7.7: Continued.

Magnitude type	Events	Agencies reporting magnitude type (number of values)
MS	10189	IDC (8236), MAN (2051), BJI (1329), MOS (442), BGR (134), NSSP (65), YARS (55), SOME (40), OMAN (28), VIE (9), KEA (8), LDG (3), SSNC (3), NDI (3), UPA (1), BER (1), IGIL (1), PPT (1)
Ms1	8145	IDC (8145)
ms1mx	8145	IDC (8145)
Ms7	1306	BJI (1306)
Ms_20	218	NEIC (218)
MW	6322	SJA (1749), GCMT (1183), NIED (708), RSNC (523), SSNC (515), UPA (476), PGC (360), DDA (305), ATA (296), FUNV (251), UCR (146), MED_RCMT (88), GUC (44), ASIES (43), ROM (28), INET (11), BER (9), DJA (6), SNET (4), IEC (4), SCEDC (3), NDI (2), IASPEI (1), OSPL (1), SIGU (1), SVSA (1), GFZ (1), SSS (1)
Mw(mB)	161	WEL (153), BKK (5), STR (3)
Mwb	228	NEIC (227), GUC (1), OTT (1)
Mwc	288	GCMT (288), NEIC (57)
Mwp	119	DJA (111), OMAN (9)
MWR	3	SCEDC (4), SLM (4)
Mwr	538	NEIC (442), NCEDC (29), SLM (28), OTT (13), GUC (12), CAR (7), PAS (7), UCR (5), REN (4), RSNC (4), CSEM (1), UPA (1)
Mww	234	NEIC (234)

The most commonly reported magnitude types are short-period body-wave, surface-wave, local (or Richter), moment, duration and JMA magnitude type. For a given earthquake, the number and type of reported magnitudes greatly vary depending on its size and location. The large earthquake of October 25, 2010 gives an example of the multitude of reported magnitude types for large earthquakes (Listing 7.1). Different magnitude estimates come from global monitoring agencies such as the IDC, NEIC and GCMT, a local agency (GUC) and other agencies, such as MOS and BJI, providing estimates based on the analysis of their networks. The same agency may report different magnitude types as well as several estimates of the same magnitude type, such as NEIC estimates of M_w obtained from W-phase, centroid and body-wave inversions.

Listing 7.1: Example of reported magnitudes for a large event

[illegible]

MLv	7.0	0.2	26	DJA	01268475
	7.1	0.4	117	DJA	01268475
Mwp	6.9	0.2	102	DJA	01268475
mb	6.4		49	MOS	16742129
MS	7.2		70	MOS	16742129
mb	6.5		110	NEIC	01288303
NE	7.3			NEIC	01288303
MS	7.3		143	NEIC	01288303
MW	7.7			NEIC	01288303
MW	7.8		130	GCMT	00125427
mb	5.9			KLM	00255772
ML	6.7			KLM	00255772
MS	7.6			KLM	00255772
mb	6.4		20	BGR	16815854
Ms	7.2		2	BGR	16815854
mb	6.3	0.3	250	ISC	01346132
MS	7.3	0.1	237	ISC	01346132

An example of a relatively small earthquake that occurred in northern Italy for which we received magnitude reports of mostly local and duration type from six agencies in Italy, France and Austria is given in Listing 7.2.

Listing 7.2: Example of reported magnitudes for a small event

Event 15089710 Northern Italy																
Date	Time	Err	RMS	Latitude	Longitude	Smaj	Smin	Az	Depth	Err	Ndef	Nsta	Gap	mdist	Mdist	Qual
2010/08/08	15:20:46.22	0.94	0.778	45.4846	8.3212	2.900	2.539	110	28.6	9.22	172	110	82	0.41	5.35	m i ke
(#PRIME)																
Author																
OrigID																
01249414																
Magnitude																
Err																
Nsta																
Author																
OrigID																
ML 2.4 10 ZUR 15925566																
Md 2.6 0.2 19 ROM 16861451																
Ml 2.2 0.2 9 ROM 16861451																
ML 2.5 GEN 00554757																
ML 2.6 0.3 28 CSEM 00554756																
Md 2.3 0.0 3 LDG 14797570																
Ml 2.6 0.3 32 LDG 14797570																

Figure 7.11 shows a distribution of the number of agencies reporting magnitude estimates to the ISC according to the magnitude value. The peak of the distribution corresponds to small earthquakes where many local agencies report local and/or duration magnitudes. The number of contributing agencies rapidly decreases for earthquakes of approximately magnitude 5.5 and above, where magnitudes are mostly given by global monitoring agencies.

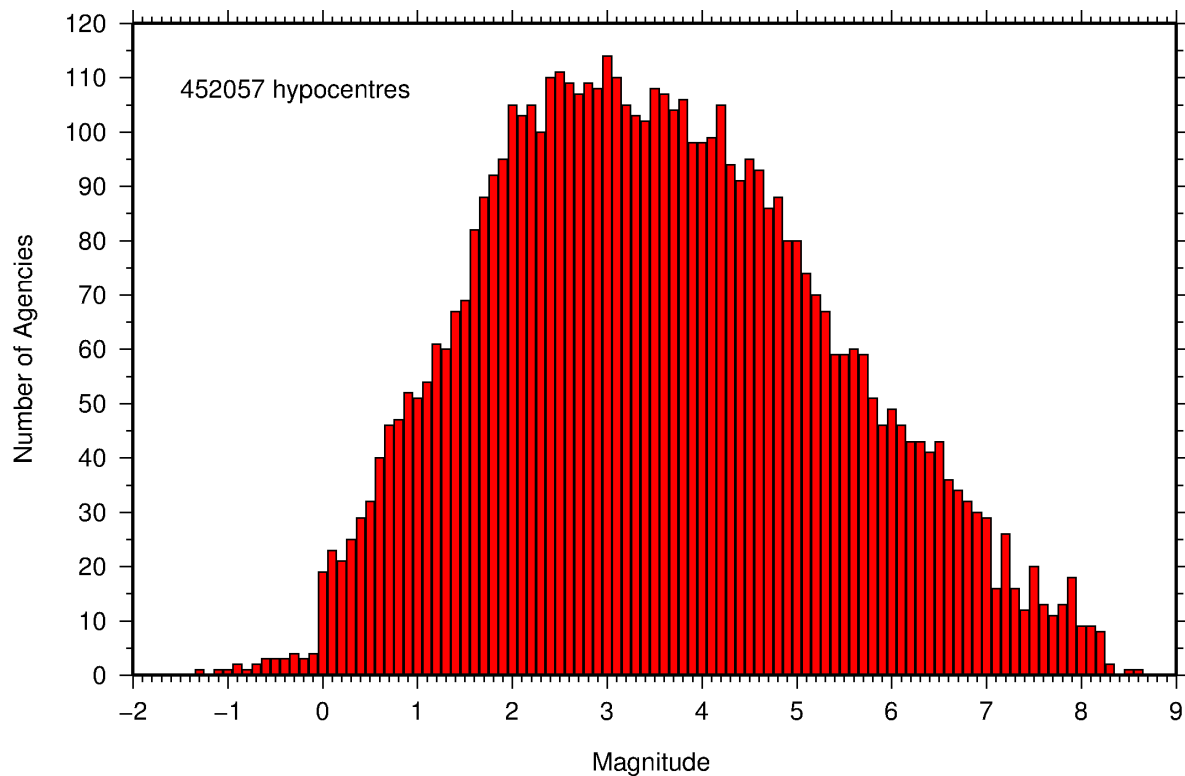


Figure 7.11: Histogram showing the number of agencies that reported network magnitude values. All magnitude types are included.

7.6 Moment Tensor Solutions

The ISC Bulletin publishes moment tensor solutions, which are reported to the ISC by other agencies. The collection of moment tensor solutions is summarised in Table 7.8. A histogram showing all moment tensor solutions collected throughout the ISC history is shown in Figure 7.12. Several moment tensor solutions from different authors and different moment tensor solutions calculated by different methods from the same agency may be present for the same event.

Table 7.8: Summary of reports containing moment tensor solutions.

Reports with Moment Tensors	43
Total moment tensors received	5708
Agencies reporting moment tensors	14

The number of moment tensors for this summary period, reported by each agency, is shown in Table 7.9. The moment tensor solutions are plotted in Figure 7.13.

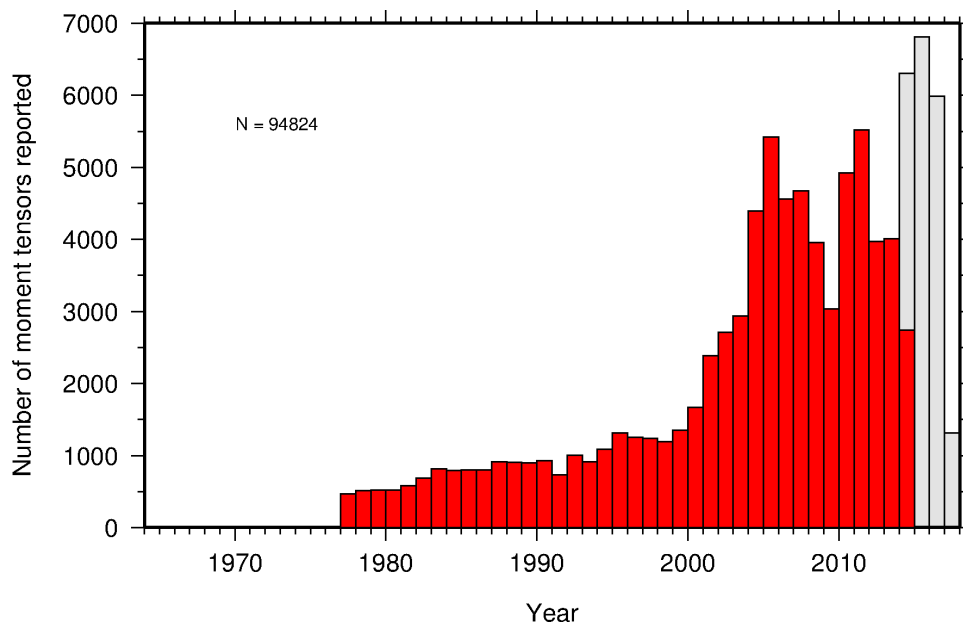
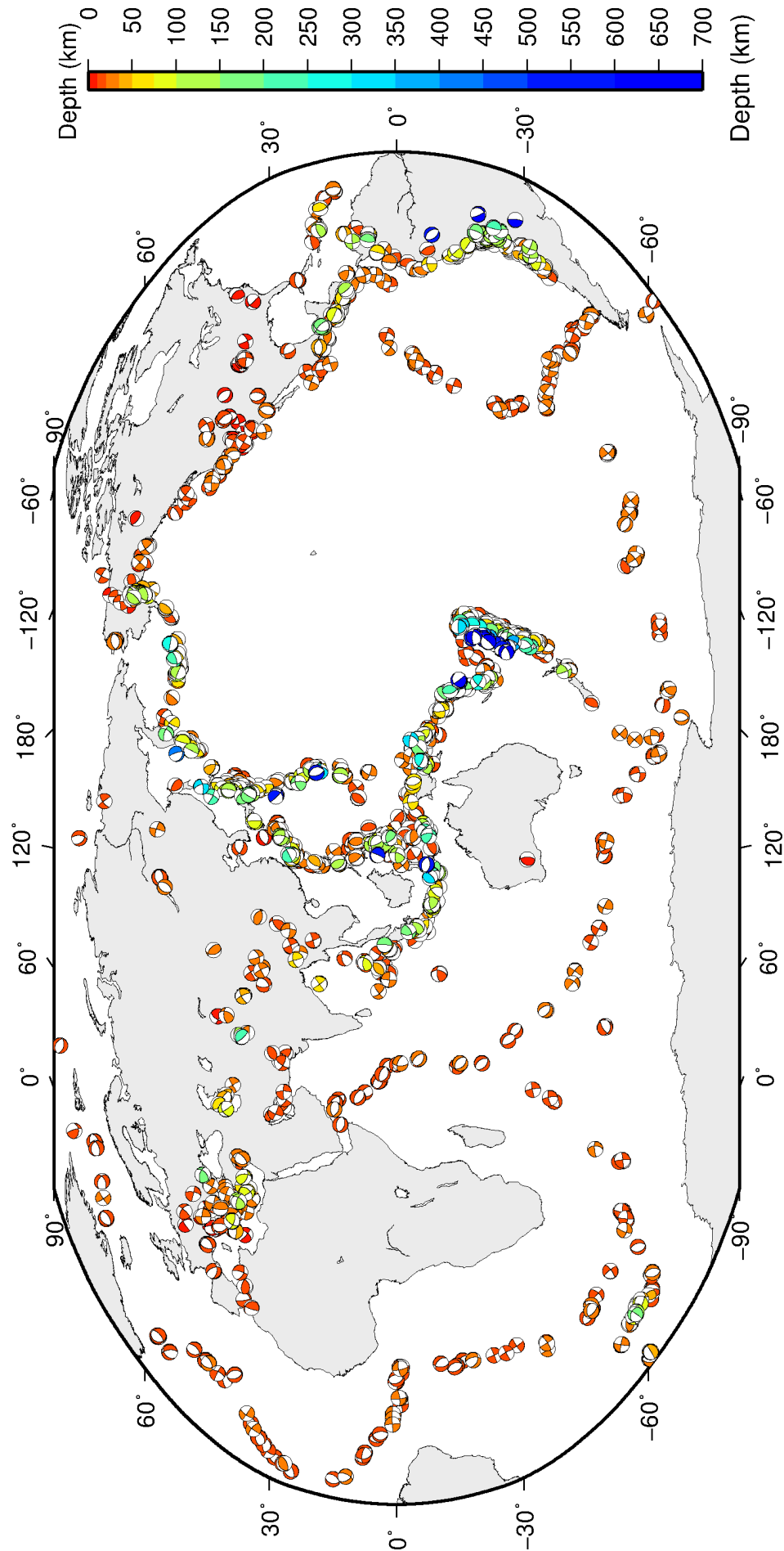


Figure 7.12: Histogram showing the number of moment tensors reported to the ISC since 1964. The regions in grey represent data that are still being actively collected.



ISC Bulletin: 2714 focal mechanism solutions for 1721 events from 2014/01/01 to 2014/06/30

Figure 7.13: Map of all moment tensor solutions in the ISC Bulletin for this summary period.

Table 7.9: Summary of moment tensor solutions in the ISC Bulletin reported by each agency.

Agency	Number of moment tensor solutions
NEIC	1364
GCMT	1183
JMA	514
MED_RCMT	88
RSNC	73
ROM	28
MOS	26
UCR	14
NCEDC	14
NIED	13
TUL	13
ECX	13
IEC	8
UPA	6
AEIC	6
BER	4
UOSS	3
OSPL	3
SNET	2
SLM	2
GUC	1

7.7 Timing of Data Collection

Here we present the timing of reports to the ISC. Please note, this does not include provisional alerts, which are replaced at a later stage. Instead, it reflects the final data sent to the ISC. The absolute timing of all hypocentre reports, regardless of magnitude, is shown in Figure 7.14. In Figure 7.15 the reports are grouped into one of six categories - from within three days of an event origin time, to over one year. The histogram shows the distribution with magnitude (for hypocentres where a network magnitude was reported) for each category, whilst the map shows the geographic distribution of the reported hypocentres.

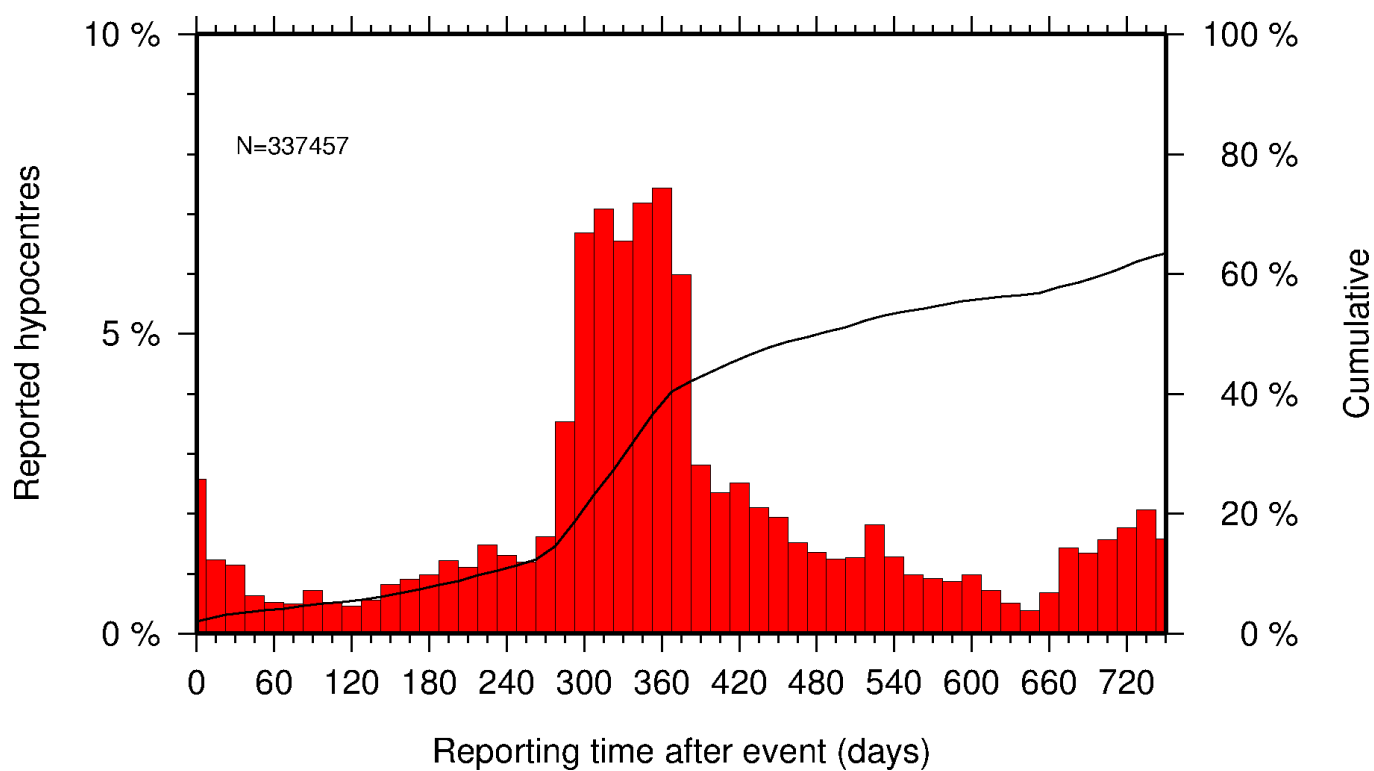


Figure 7.14: Histogram showing the timing of final reports of the hypocentres (total of N) to the ISC. The cumulative frequency is shown by the solid line.

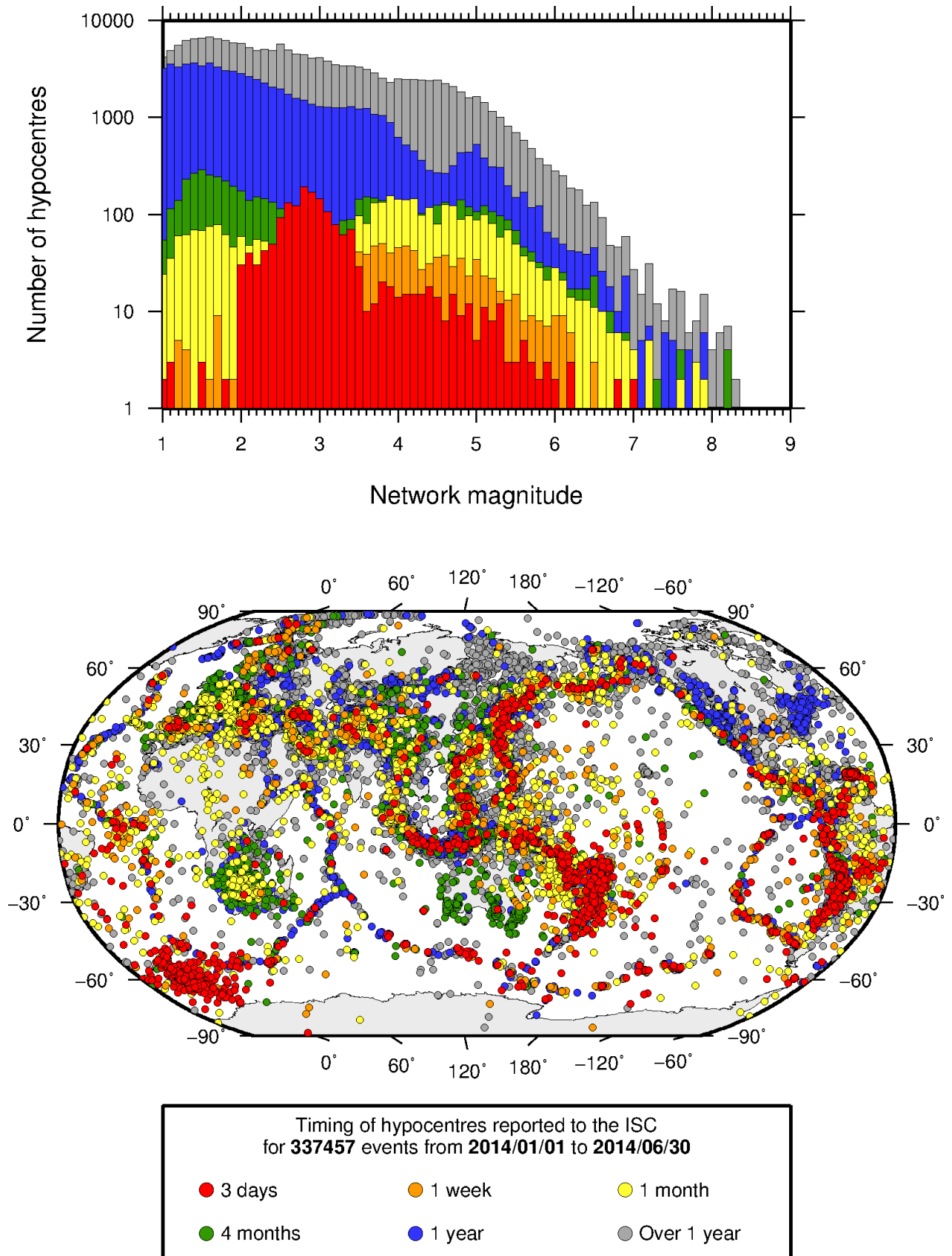


Figure 7.15: Timing of hypocentres reported to the ISC. The colours show the time after the origin time that the corresponding hypocentre was reported. The histogram shows the distribution with magnitude. If more than one network magnitude was reported, preference was given to a value of M_W followed by M_S , m_b and M_L respectively; all reported hypocentres are included on the map. Note: early reported hypocentres are plotted over later reported hypocentres, on both the map and histogram.

8

Overview of the ISC Bulletin

This chapter provides an overview of the seismic event data in the ISC Bulletin. We indicate the differences between all ISC events and those ISC events that are reviewed or located. We describe the wealth of phase arrivals and phase amplitudes and periods observed at seismic stations worldwide, reported in the ISC Bulletin and often used in the ISC location and magnitude determination. Finally, we make some comparisons of the ISC magnitudes with those reported by other agencies, and discuss magnitude completeness of the ISC Bulletin.

8.1 Events

The ISC Bulletin had 225544 reported events in the summary period between January and June 2014. Some 91% (206237) of the events were identified as earthquakes, the rest (19307) were of anthropogenic origin (including mining and other chemical explosions, rockbursts and induced events) or of unknown origin. As discussed in Section 10.1.3, typically about 20% of the events are selected for ISC review, and about half of the events selected for review are located by the ISC. In this summary period 12% of the events were reviewed and 8% of the events were located by the ISC. For events that are not located by the ISC, the prime hypocentre is identified according to the rules described in Section 10.1.3.

Of the 8642683 reported phase observations, 36% are associated to ISC-reviewed events, and 34% are associated to events selected for ISC location. Note that all large events are reviewed and located by the ISC. Since large events are globally recorded and thus reported by stations worldwide, they will provide the bulk of observations. This explains why only about one-fifth of the events in any given month is reviewed although the number of phases associated to reviewed events has increased nearly exponentially in the past decades.

Figure 8.1 shows the daily number of events throughout the summary period. Figure 8.2 shows the locations of the events in the ISC Bulletin; the locations of ISC-reviewed and ISC-located events are shown in Figures 8.3 and 8.4, respectively.

Figure 8.5 shows the hypocentral depth distributions of events in the ISC Bulletin for the summary period. The vast majority of events occur in the Earth's crust. Note that the peaks at 0, 10, 35 km, and at every 50 km intervals deeper than 100 km are artifacts of analyst practices of fixing the depth to a nominal value when the depth cannot be reliably resolved.

Figure 8.6 shows the depth distribution of free-depth solutions in the ISC Bulletin. The depth of a hypocentre reported to the ISC is assumed to be determined as a free parameter, unless it is explicitly labelled as a fixed-depth solution. On the other hand, as described in Section 10.1.4, the ISC locator attempts to get a free-depth solution if, and only if, there is resolution for the depth in the data, i.e. if

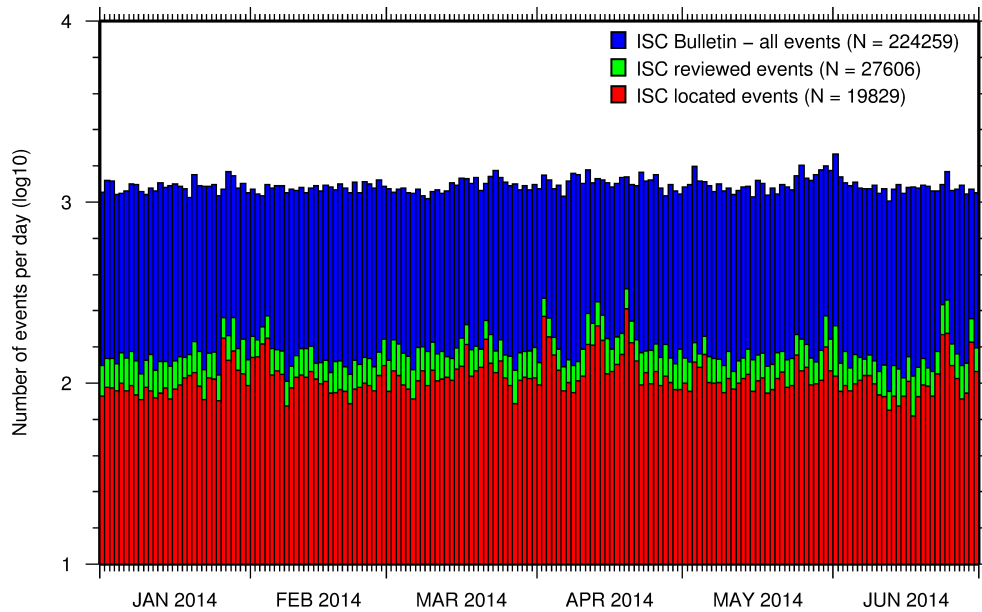


Figure 8.1: Histogram showing the number of events in the ISC Bulletin for the current summary period. The vertical scale is logarithmic.

there is a local network and/or sufficient depth-sensitive phases are reported.

Figure 8.7 shows the depth distribution of fixed-depth solutions in the ISC Bulletin. Except for a fraction of events whose depth is fixed to a shallow depth, this set comprises mostly ISC-located events. If there is no resolution for depth in the data, the ISC locator fixes the depth to a value obtained from the ISC default depth grid file, or if no default depth exists for that location, to a nominal default depth assigned to each Flinn-Engdahl region (see details in Section 10.1.4). During the ISC review editors are inclined to accept the depth obtained from the default depth grid, but they typically change the depth of those solutions that have a nominal (10 or 35 km) depth. When doing so, they usually fix the depth to a round number, preferably divisible by 50.

For events selected for ISC location, the number of stations typically increases as arrival data reported by several agencies are grouped together and associated to the prime hypocentre. Consequently, the network geometry, characterised by the secondary azimuthal gap (the largest azimuthal gap a single station closes), is typically improved. Figure 8.8 illustrates that the secondary azimuthal gap is indeed generally smaller for ISC-located events than that for all events in the ISC Bulletin. Figure 8.9 shows the distribution of the number of associated stations. For large events the number of associated stations is usually larger for ISC-located events than for any of the reported event bulletins. On the other hand, events with just a few reporting stations are rarely selected for ISC location. The same is true for the number of defining stations (stations with at least one defining phase that were used in the location). Figure 8.10 indicates that because the reported observations from multiple agencies are associated to the prime, large ISC-located events typically have a larger number of defining stations than any of the reported event bulletins.

The formal uncertainty estimates are also typically smaller for ISC-located events. Figure 8.11 shows the distribution of the area of the 90% confidence error ellipse for ISC-located events during the summary period. The distribution suffers from a long tail indicating a few poorly constrained event locations. Nevertheless, half of the events are characterised by an error ellipse with an area less than 190 km², 90%

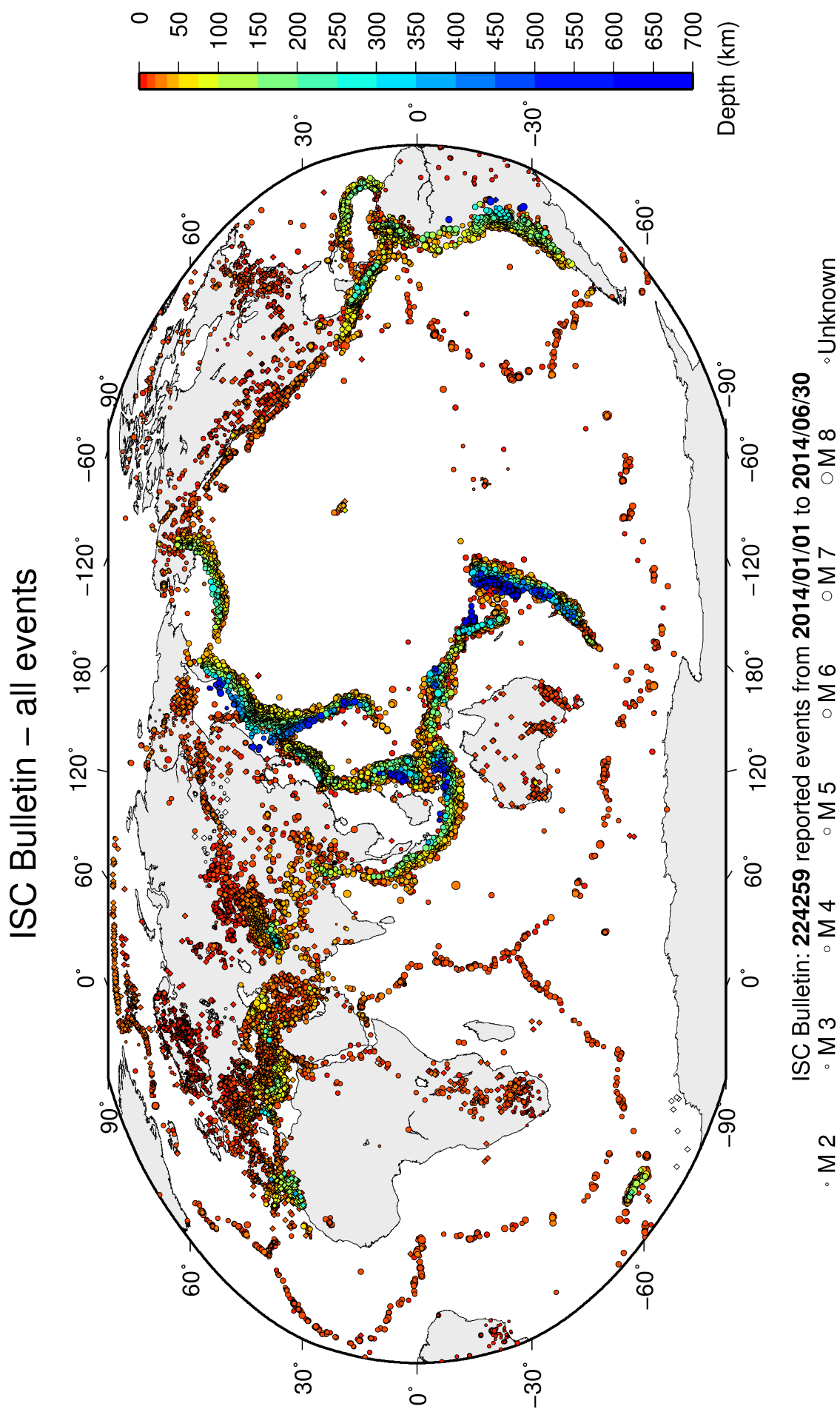


Figure 8.2: Map of all events in the ISC Bulletin. Prime hypocentre locations are shown. Compare with Figure 7.10.

ISC Bulletin – reviewed events

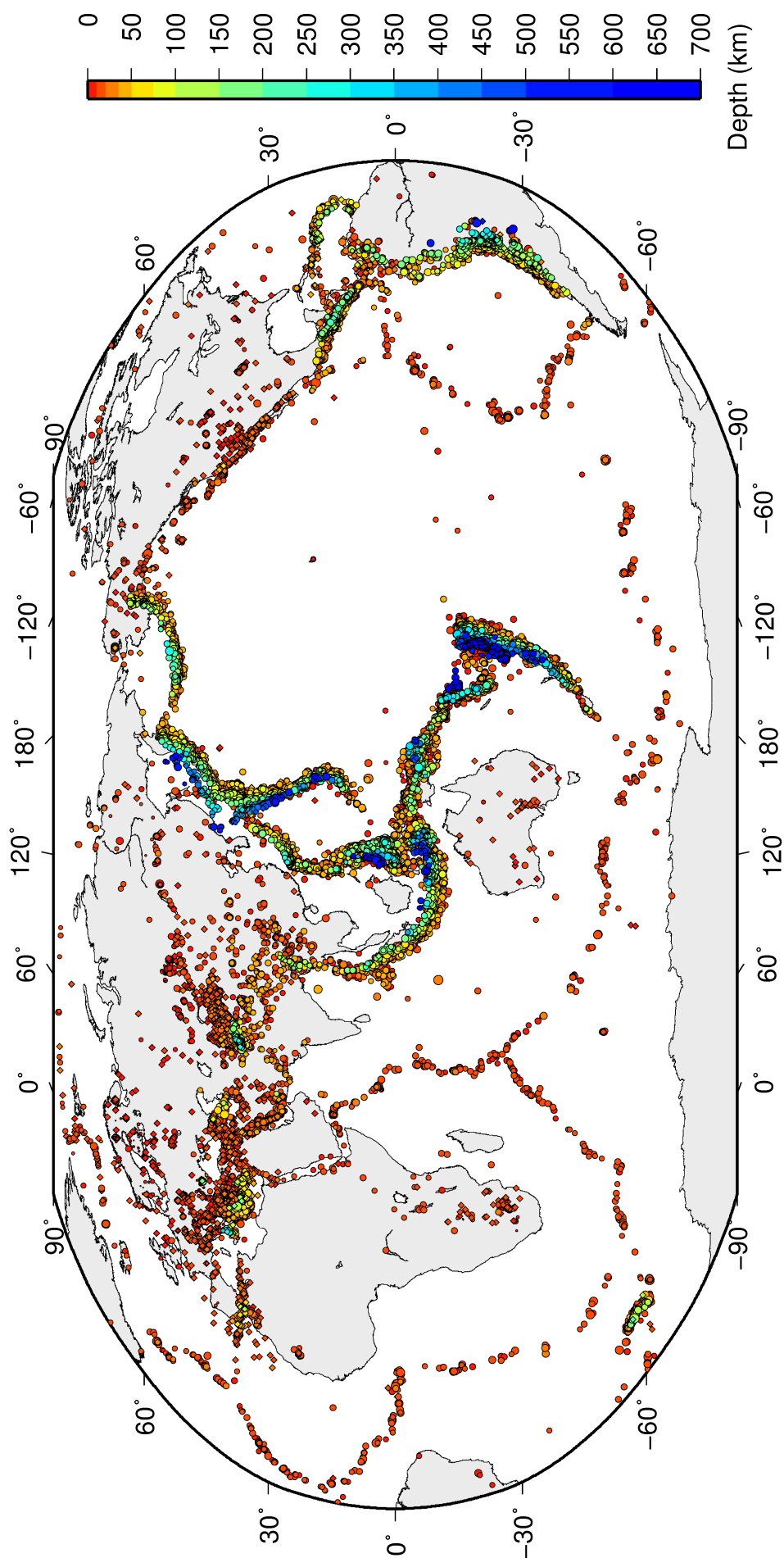
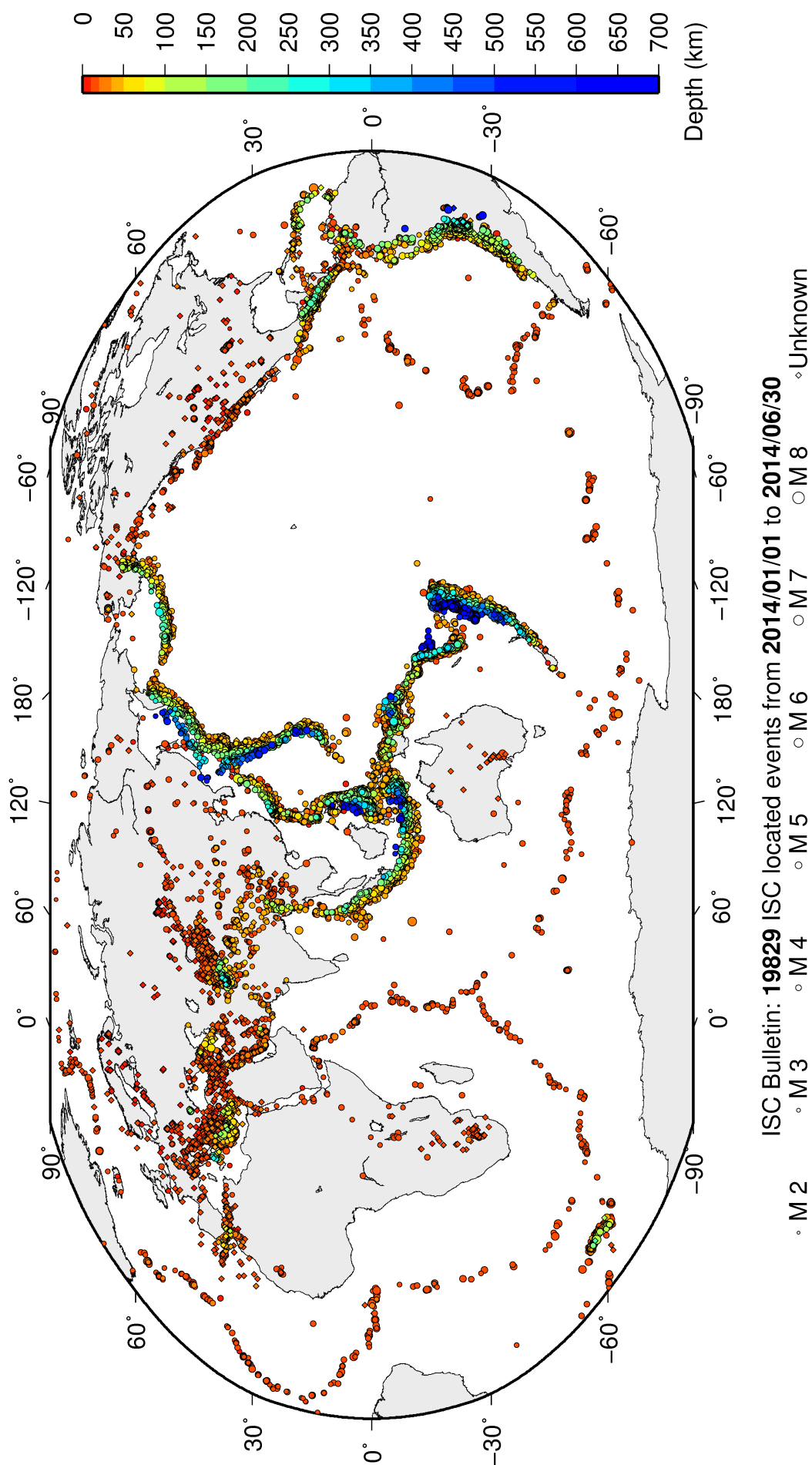


Figure 8.3: Map of all events reviewed by the ISC for this time period. Prime hypocentre locations are shown.

ISC Bulletin – ISC located events



ISC Bulletin: 19829 ISC located events from 2014/01/01 to 2014/06/30

◦ M 2 ◦ M 3 ◦ M 4 ◦ M 5 ◦ M 6 ◦ M 7 ◦ M 8 ◊ Unknown

Figure 8.4: Map of all events located by the ISC for this time period. ISC determined hypocentre locations are shown.

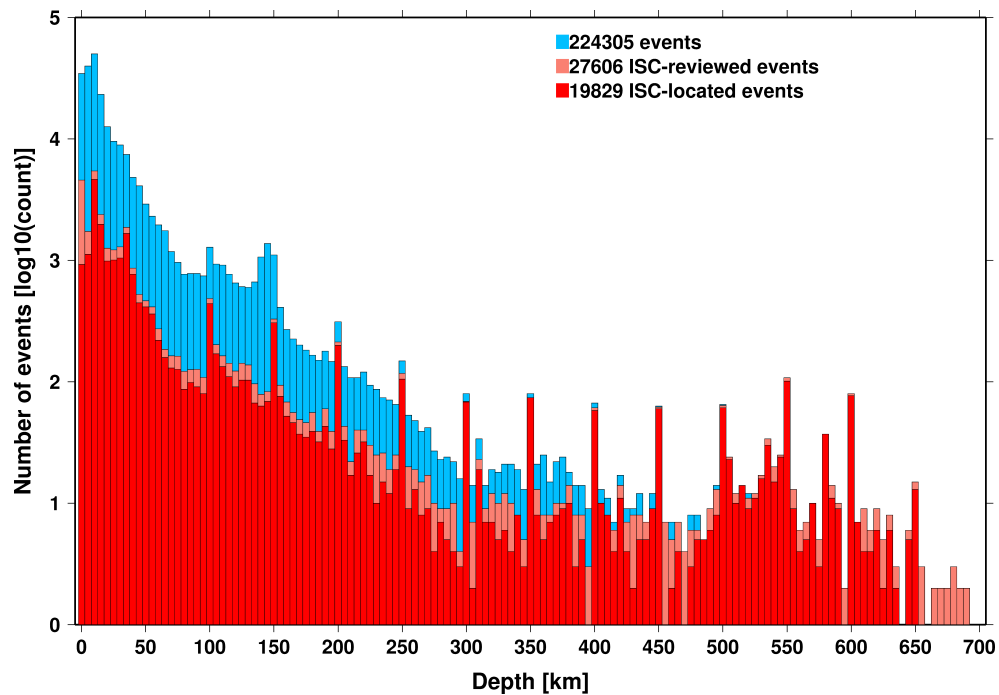


Figure 8.5: Distribution of event depths in the ISC Bulletin (blue) and for the ISC-reviewed (pink) and the ISC-located (red) events during the summary period. All ISC-located events are reviewed, but not all reviewed events are located by the ISC. The vertical scale is logarithmic.

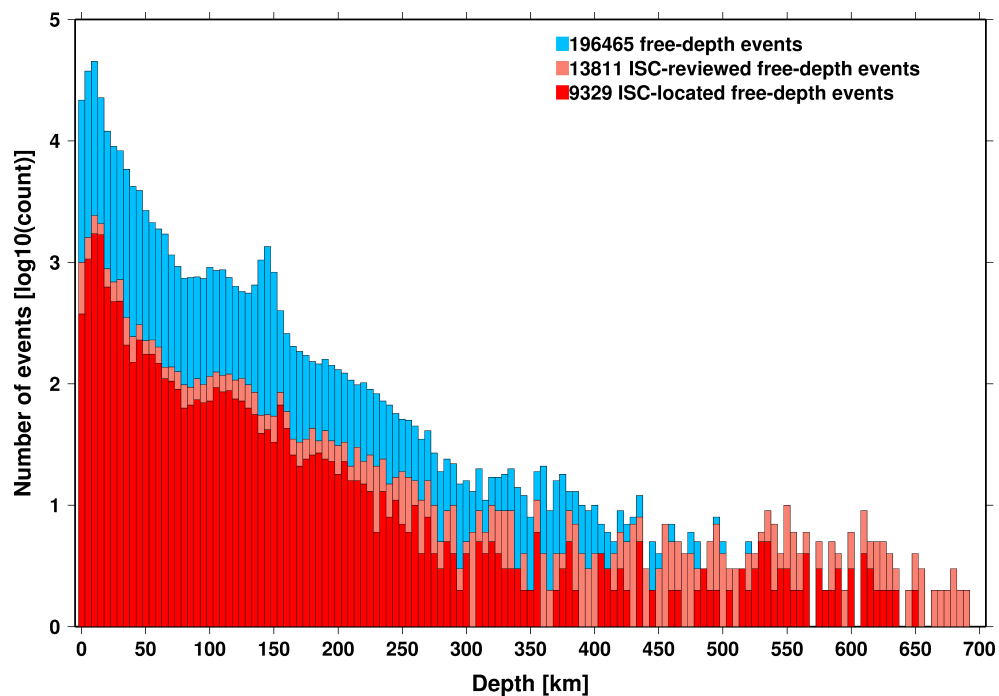


Figure 8.6: Hypocentral depth distribution of events where the prime hypocentres are reported/located with a free-depth solution in the ISC Bulletin. The vertical scale is logarithmic.

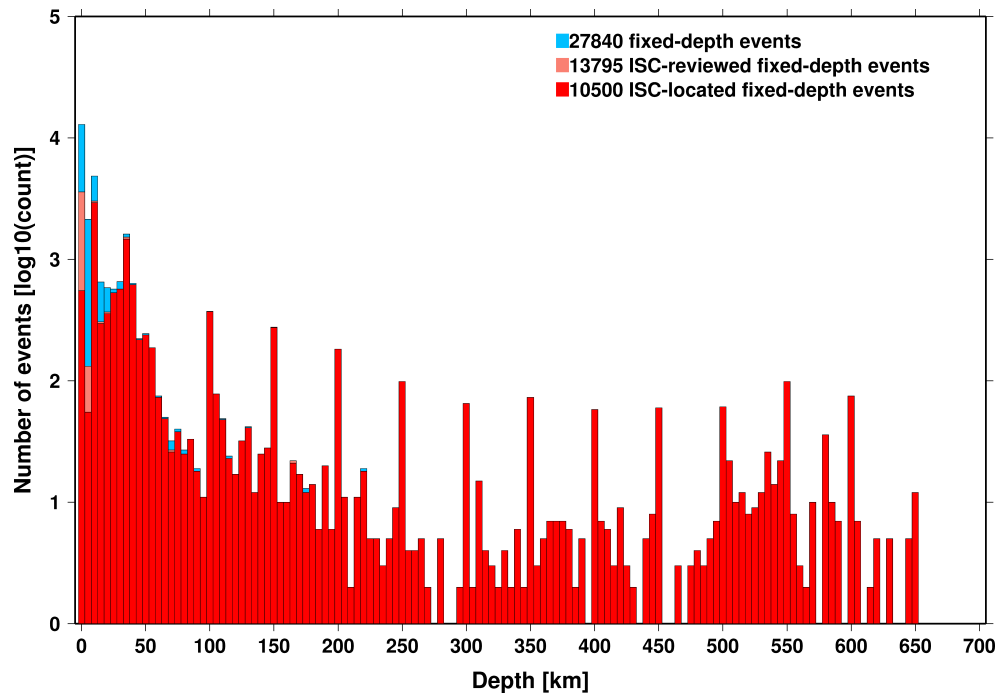


Figure 8.7: Hypocentral depth distribution of events where the prime hypocentres are reported/located with a fixed-depth solution in the ISC Bulletin. The vertical scale is logarithmic.

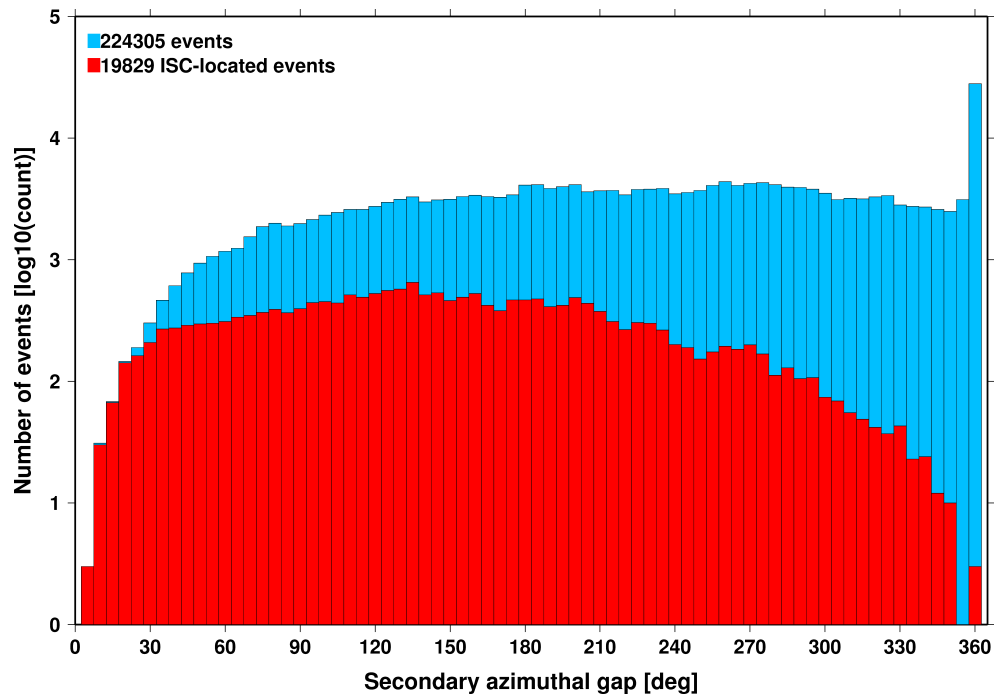


Figure 8.8: Distribution of secondary azimuthal gap for events in the ISC Bulletin (blue) and those selected for ISC location (red). The vertical scale is logarithmic.

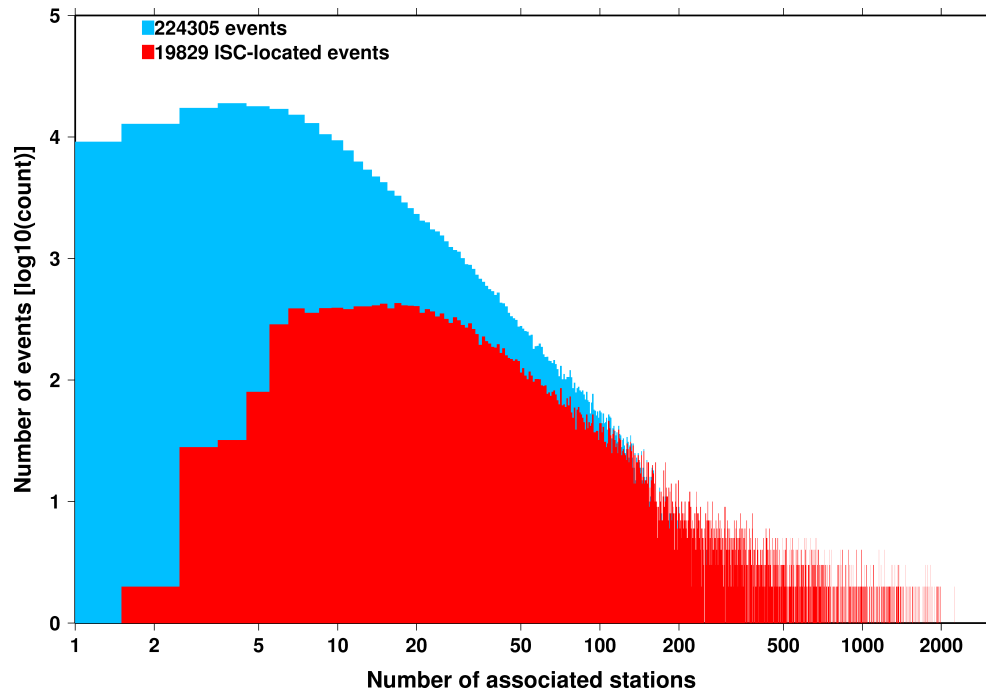


Figure 8.9: Distribution of the number of associated stations for events in the ISC Bulletin (blue) and those selected for ISC location (red). The vertical scale is logarithmic.

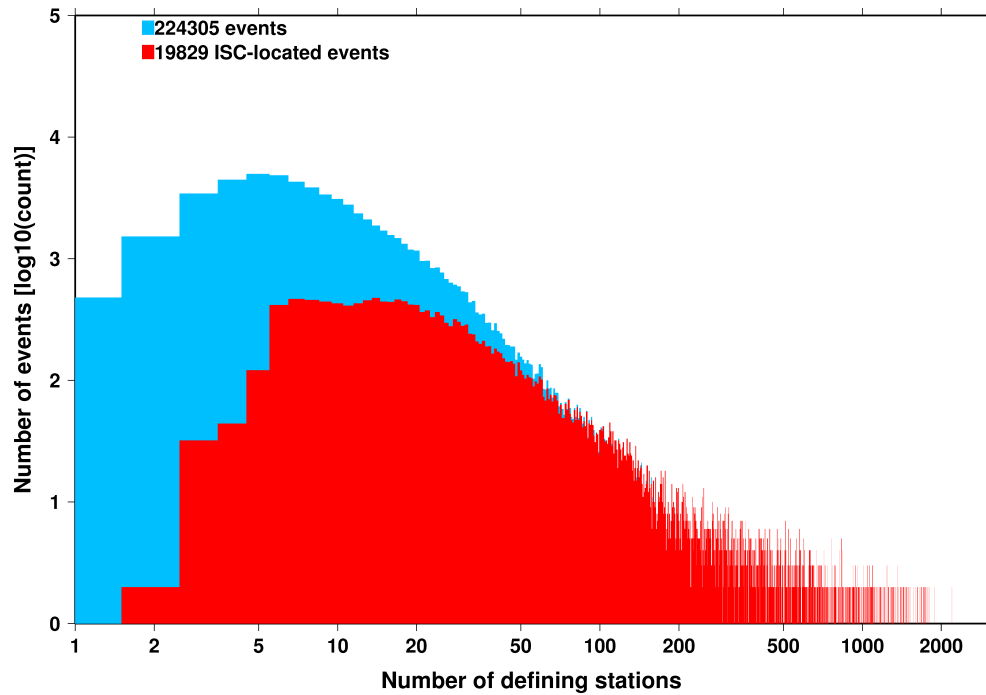


Figure 8.10: Distribution of the number of defining stations for events in the ISC Bulletin (blue) and those selected for ISC location (red). The vertical scale is logarithmic.

of the events have an error ellipse area less than 1135 km^2 , and 95% of the events have an error ellipse area less than 1765 km^2 .

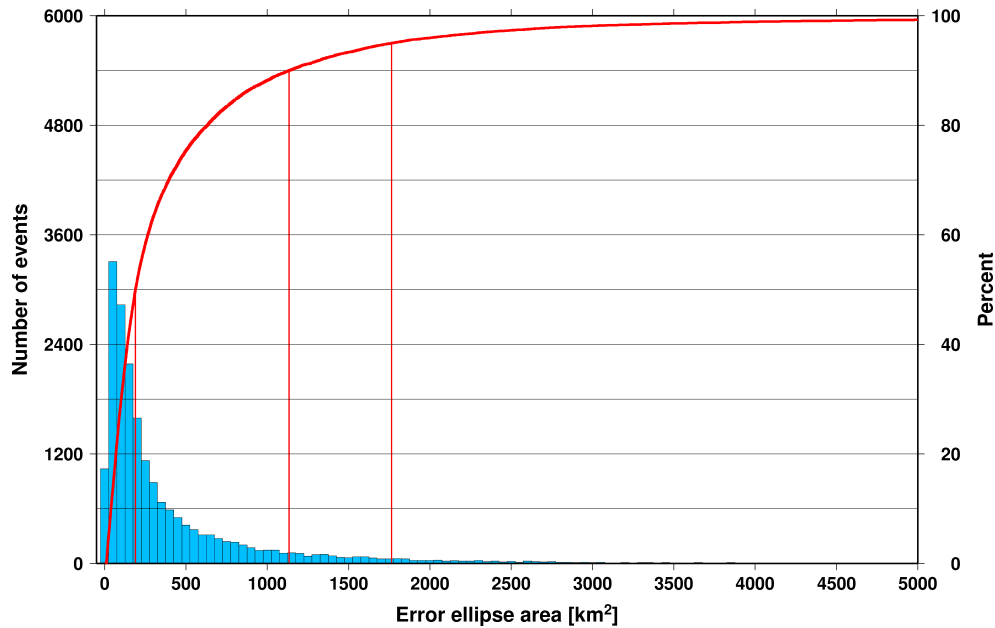


Figure 8.11: Distribution of the area of the 90% confidence error ellipse of the ISC-located events. Vertical red lines indicate the 50th, 90th and 95th percentile values.

Figure 8.12 shows one of the major characteristic features of the ISC location algorithm (Bondár and Storchak, 2011). Because the ISC locator accounts for correlated travel-time prediction errors due to unmodelled velocity heterogeneities along similar ray paths, the area of the 90% confidence error ellipse does not decrease indefinitely with increasing number of stations, but levels off once the information carried by the network geometry is exhausted, thus providing more realistic uncertainty estimates.

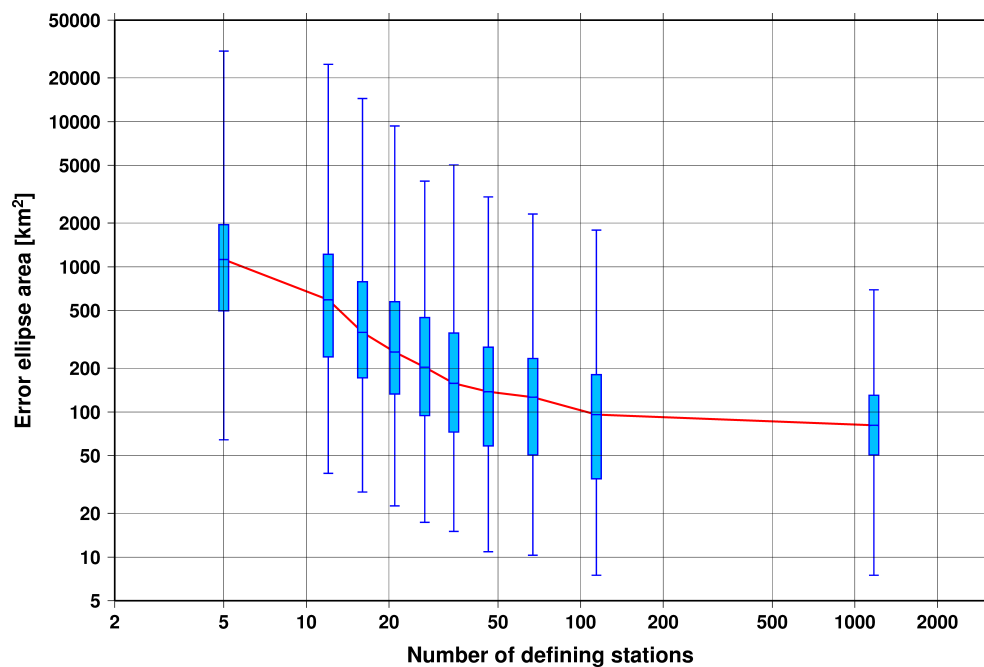


Figure 8.12: Box-and-whisker plot of the area of the 90% confidence error ellipse of the ISC-located events as a function of the number of defining stations. Each box represents one-tenth-worth of the total number of data. The red line indicates the median 90% confidence error ellipse area.

8.2 Seismic Phases and Travel-Time Residuals

The number of phases that are associated to events over the summary period in the ISC Bulletin is shown in Figure 8.13. Phase types and their total number in the ISC Bulletin is shown in the Appendix, Table 10.3. A summary of phase types is indicated in Figure 8.14.

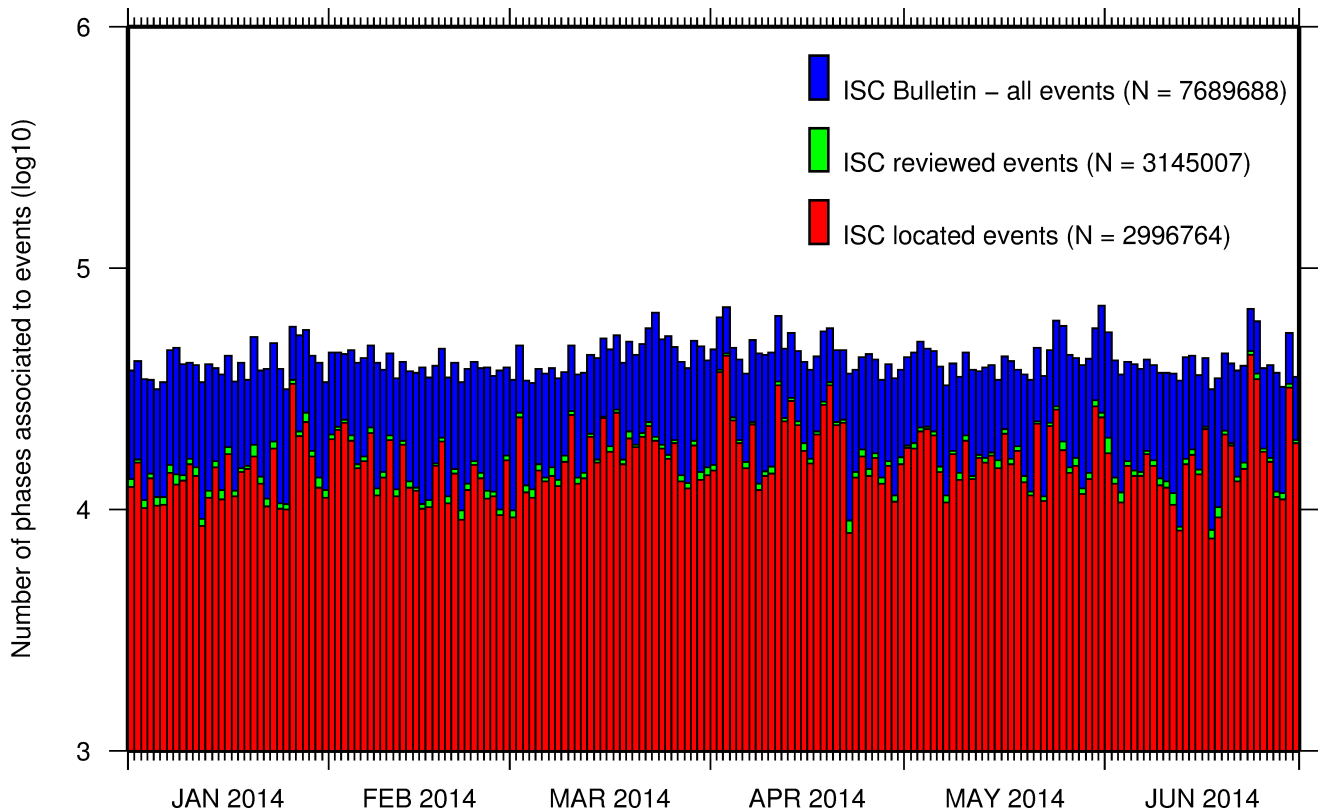


Figure 8.13: Histogram showing the number of phases (N) that the ISC has associated to events within the ISC Bulletin for the current summary period.

In computing ISC locations, the current (for events since 2009) ISC location algorithm (*Bondár and Storchak, 2011*) uses all *ak135* phases where possible. Within the Bulletin, the phases that contribute to an ISC location are labelled as *time defining*. In this section, we summarise these time defining phases.

In Figure 8.15, the number of defining phases is shown in a histogram over the summary period. Each defining phase is listed in Table 8.1, which also provides a summary of the number of defining phases per event. A pie chart showing the proportion of defining phases is shown in Figure 8.16. Figure 8.17 shows travel times of seismic waves. The distribution of residuals for these defining phases is shown for the top five phases in Figures 8.18 through 8.22.

Table 8.1: Numbers of ‘time defining’ phases (N) within the ISC Bulletin for 19829 ISC located events.

Phase	Number of ‘defining’ phases	Number of events	Max per event	Median per event
P	950978	14521	2548	15
Pn	514627	18444	862	14
Sn	167581	15876	212	6
Pb	90905	8361	121	6
Pg	78684	6489	148	7
PKPdf	74743	4821	971	2
Sg	62150	6303	117	6
Sb	58403	8145	86	5

Table 8.1: (continued)

Phase	Number of 'defining' phases	Number of events	Max per event	Median per event
PKiKP	51805	4221	492	2
S	39221	3516	547	3
PKPbc	28373	4204	276	2
PKPab	21737	3354	164	2
PcP	12855	3572	118	2
PP	11745	1959	390	1
Pdif	11423	1059	549	2
pP	8887	1302	266	2
ScP	4251	1122	78	2
SS	4129	1006	76	2
SKSac	3017	401	153	2
PKKPbc	2592	495	101	2
sP	2511	770	54	2
pwP	1379	440	56	1
pPKPdf	1171	438	41	1
SKPbc	1070	316	43	2
PnPn	1007	612	10	1
ScS	979	451	34	1
SnSn	763	460	14	1
P'P'df	687	171	32	2
SKiKP	686	312	32	1
PKKPdf	586	274	20	1
PS	562	149	42	2
pPKPab	554	210	38	1
PKKPab	542	243	17	1
sS	513	259	34	1
pPKPbc	433	238	17	1
SKKSac	370	215	16	1
sPKPdf	364	217	11	1
SKSdf	357	200	22	1
SKPab	323	166	14	1
PKSdf	321	278	4	1
PcS	317	266	13	1
SKPdf	291	88	21	1
sPKPab	219	92	12	1
sPKPbc	188	108	26	1
Sdif	171	88	9	1
SP	164	63	12	1
PnS	148	88	4	1
SKKPbc	137	43	25	1
pPKiKP	56	37	5	1
pPdif	51	25	12	1
pS	47	43	2	1
P'P'bc	39	25	6	1
PbPb	22	17	4	1
PKSbc	20	9	6	1
SKKPab	19	13	4	1
SPn	15	14	2	1
sPn	14	5	9	1
SKKSdf	11	10	2	1
pSKSac	9	2	5	4
SKKPdf	9	6	2	2
sPdif	8	5	3	1
P'P'ab	8	6	2	1
sSKSac	7	1	7	7
sPKiKP	6	6	1	1
pPn	6	4	3	1
SbSb	5	5	1	1
PgPg	4	3	2	1
S'S'ac	3	3	1	1
SgSg	1	1	1	1
PKSab	1	1	1	1
PgS	1	1	1	1
sSb	1	1	1	1
sPb	1	1	1	1

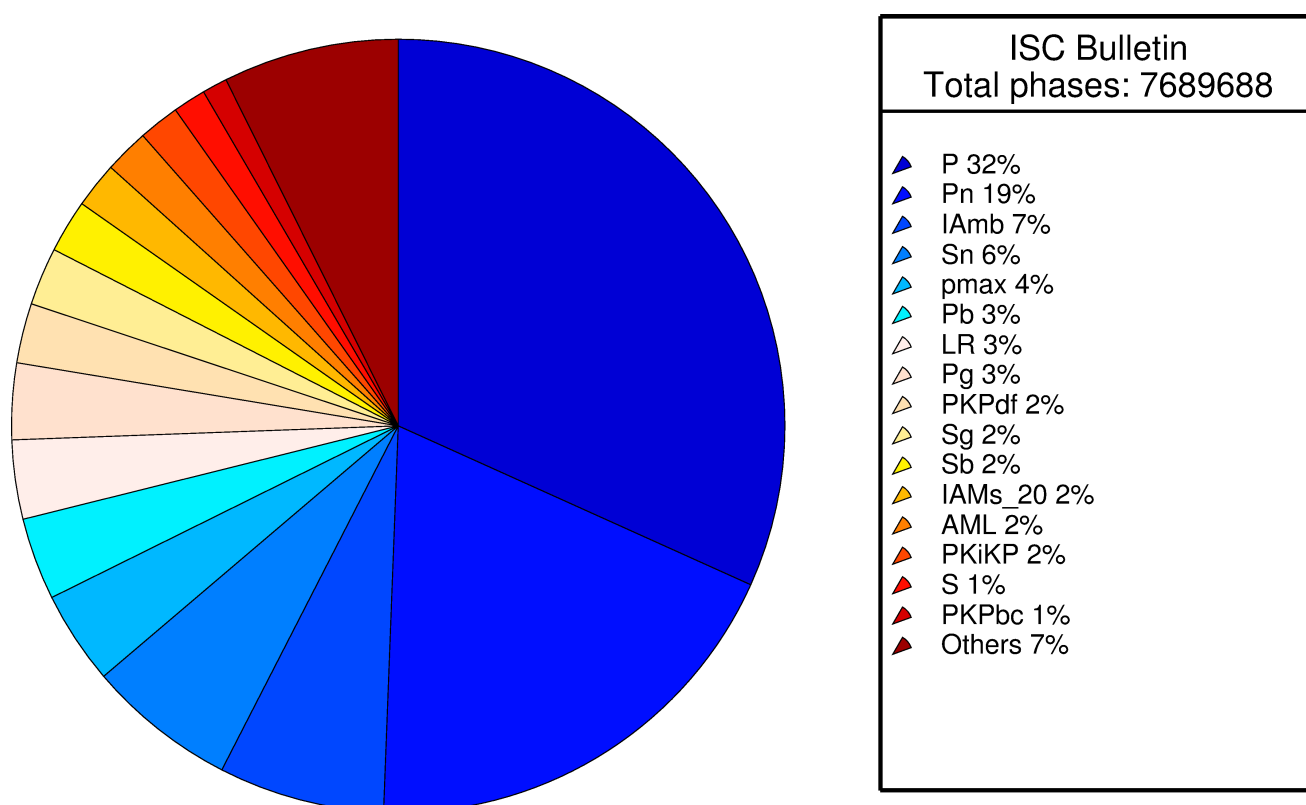


Figure 8.14: Pie chart showing the fraction of various phase types in the ISC Bulletin for this summary period.

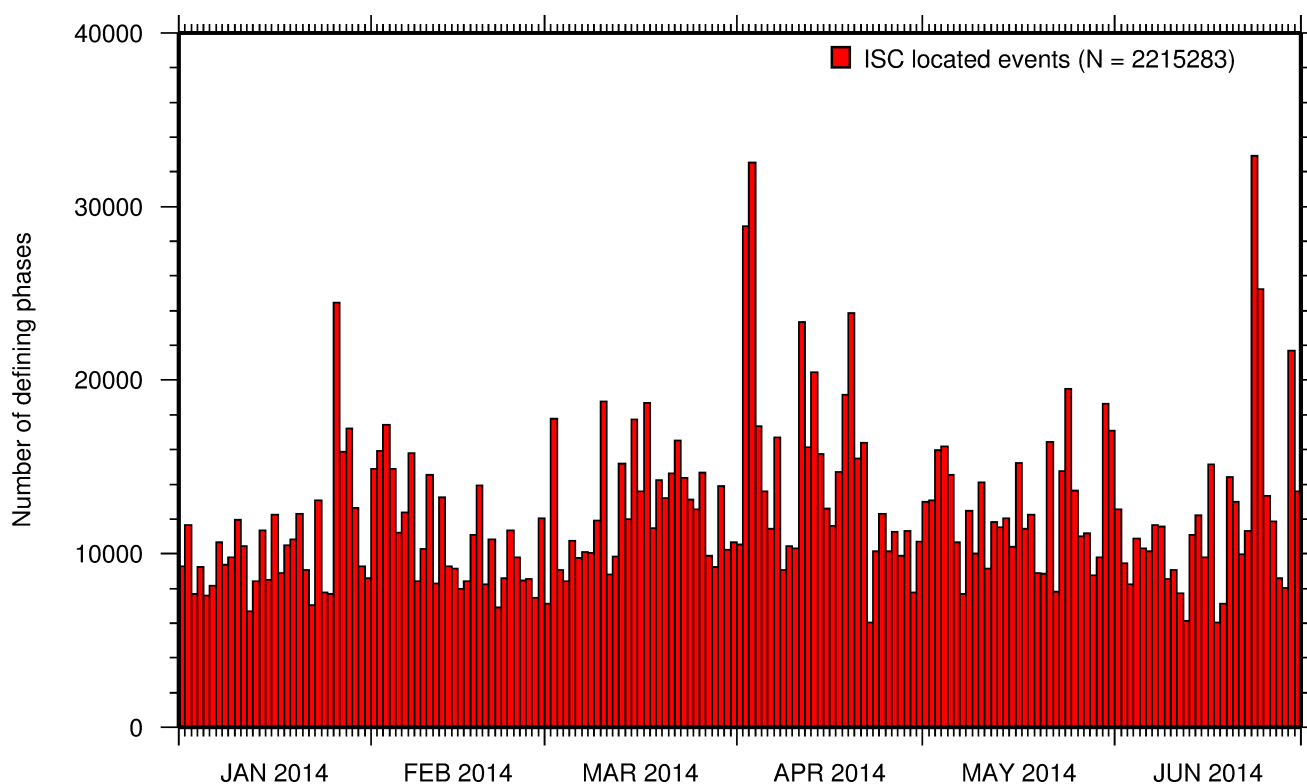


Figure 8.15: Histogram showing the number of defining phases in the ISC Bulletin, for events located by the ISC.

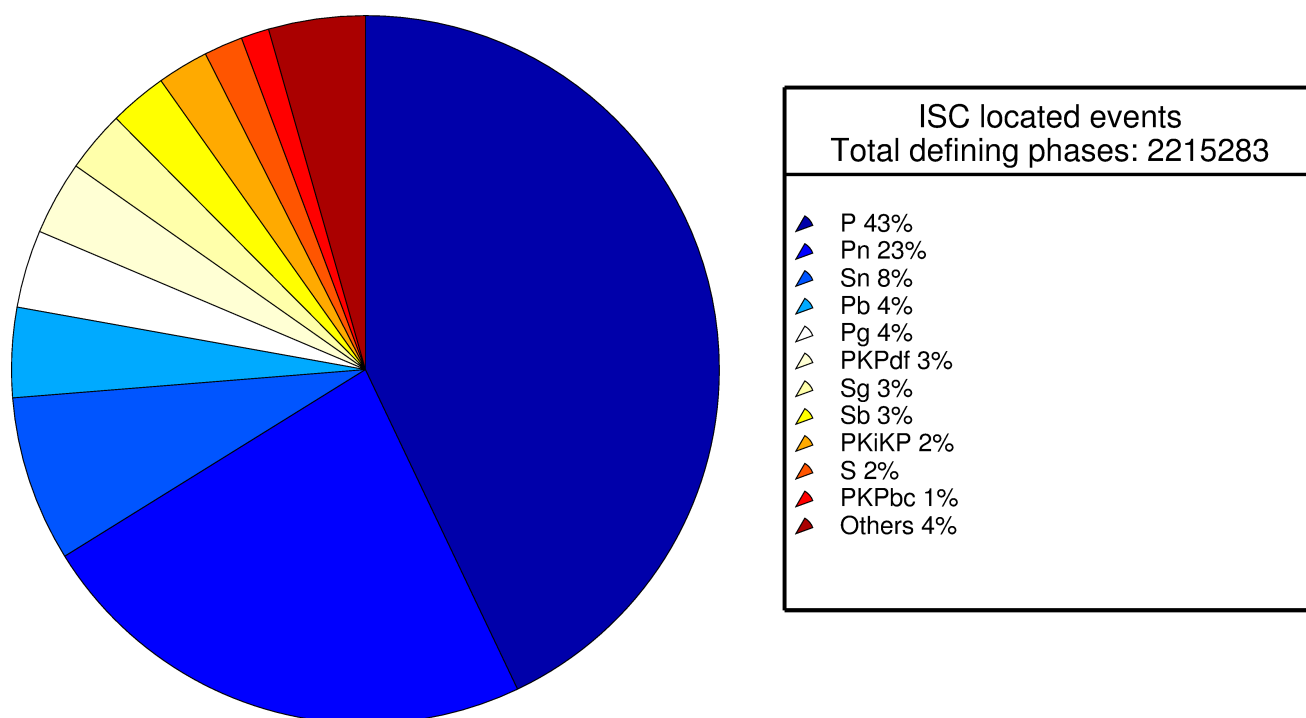


Figure 8.16: Pie chart showing the defining phases in the ISC Bulletin, for events located by the ISC. A complete list of defining phases is shown in Table 8.1.

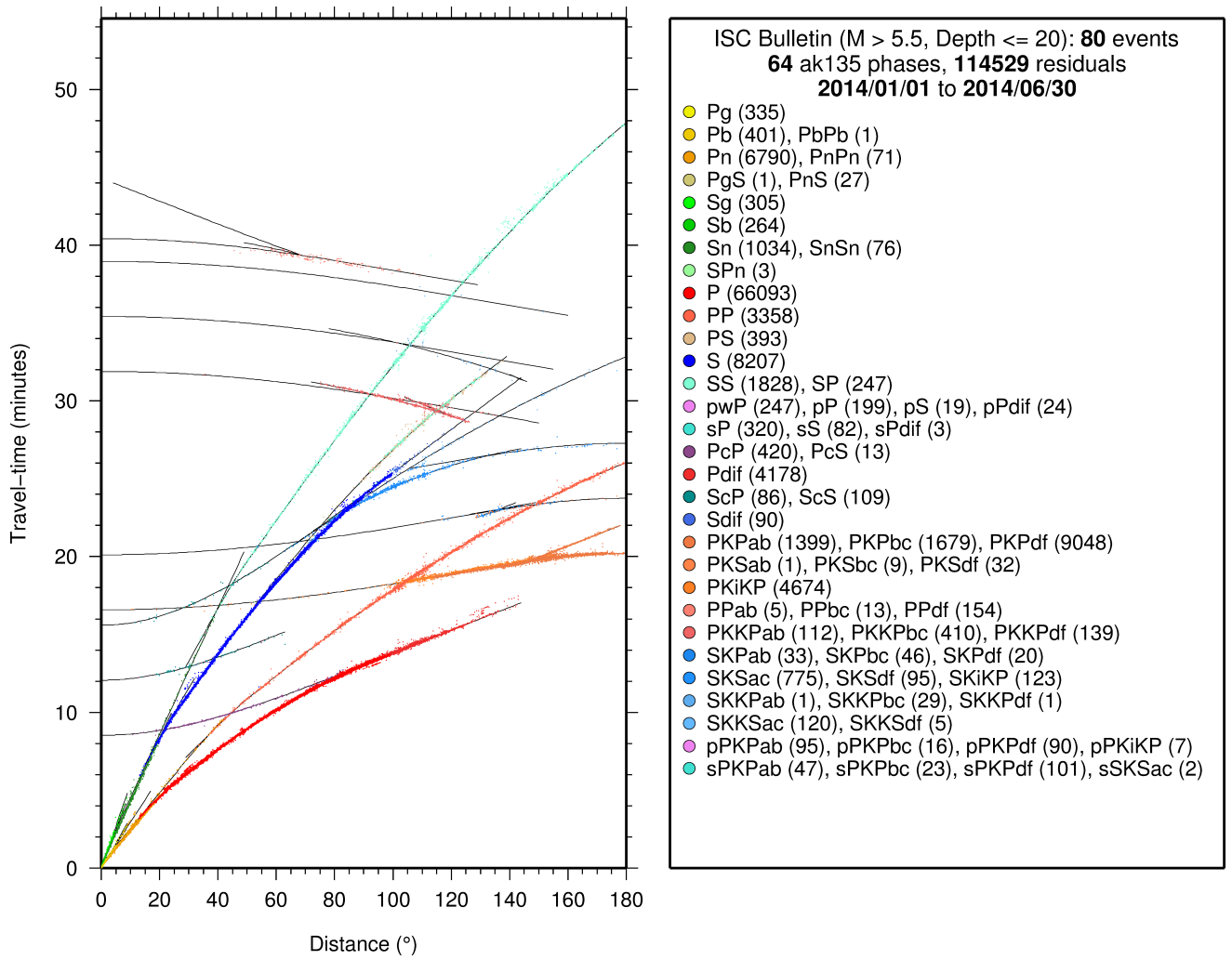


Figure 8.17: Distribution of travel-time observations in the ISC Bulletin for events with $M > 5.5$ and depth less than 20 km. The travel-time observations are shown relative to a 0 km source and compared with the theoretical ak135 travel-time curves (solid lines). The legend lists the number of each phase plotted.

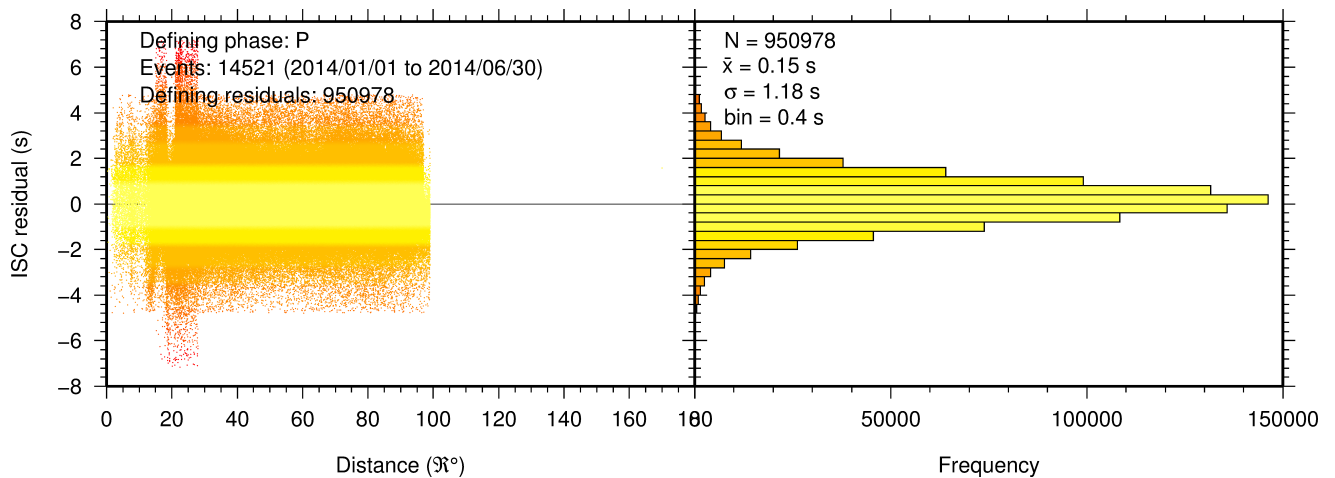


Figure 8.18: Distribution of travel-time residuals for the defining P phases used in the computation of ISC located events in the Bulletin.

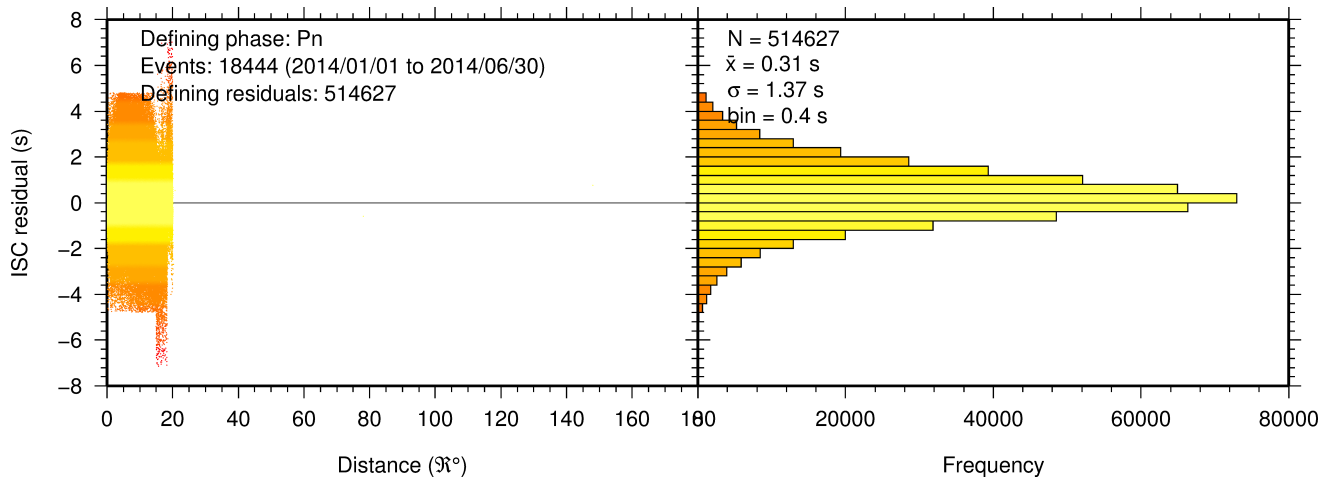


Figure 8.19: Distribution of travel-time residuals for the defining Pn phases used in the computation of ISC located events in the Bulletin.

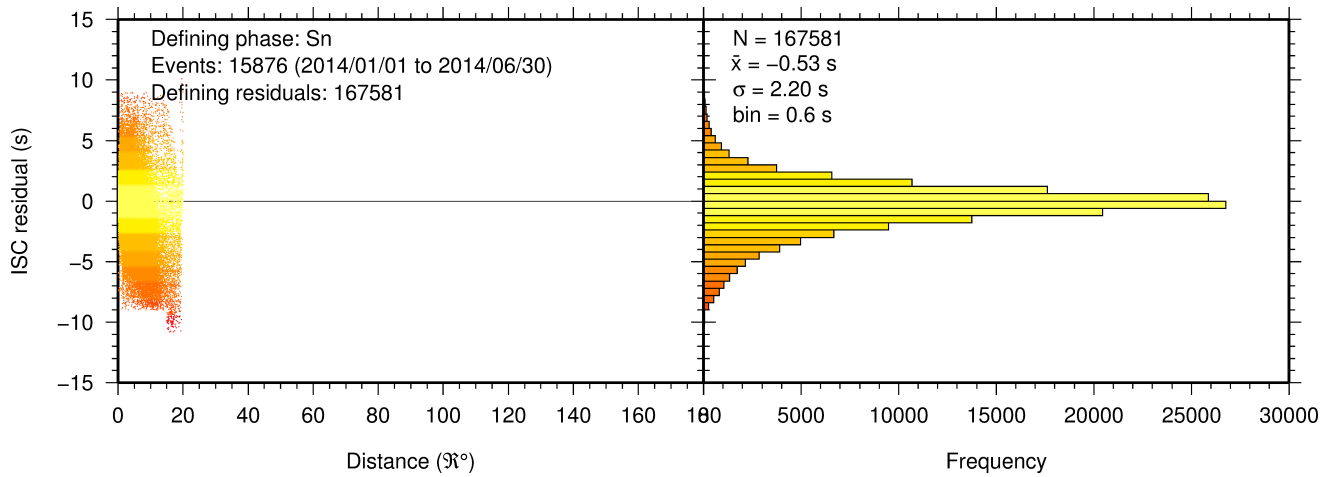


Figure 8.20: Distribution of travel-time residuals for the defining Sn phases used in the computation of ISC located events in the Bulletin.

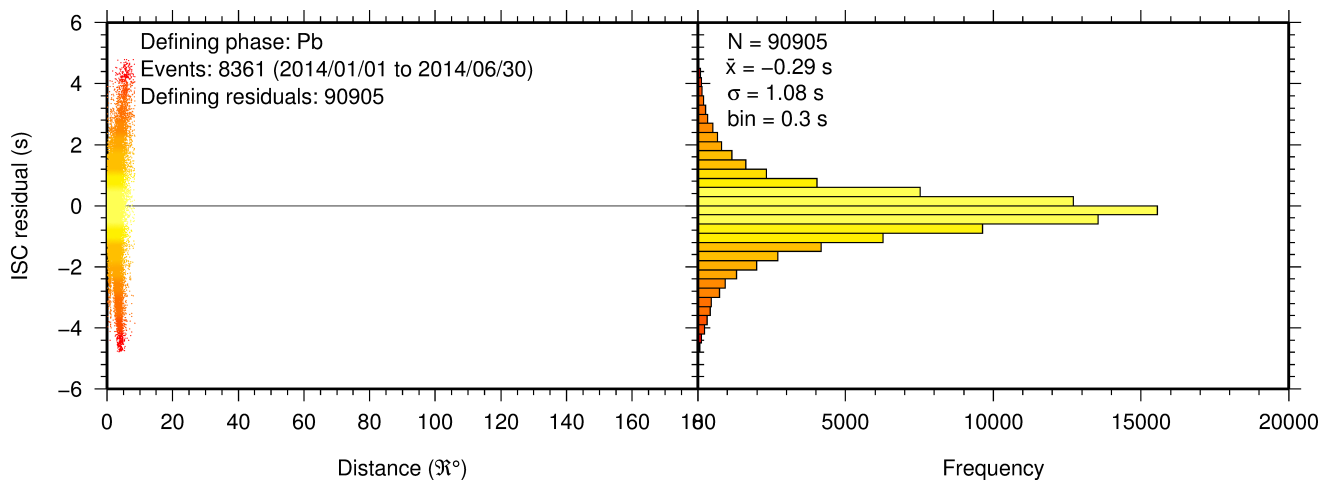


Figure 8.21: Distribution of travel-time residuals for the defining Pb phases used in the computation of ISC located events in the Bulletin.

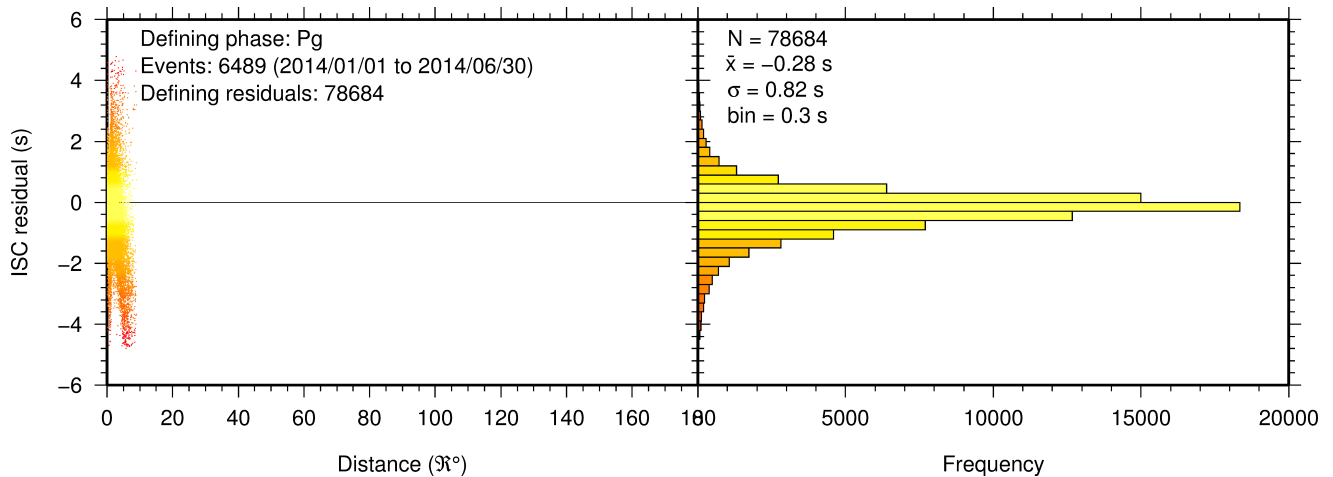


Figure 8.22: Distribution of travel-time residuals for the defining Pg phases used in the computation of ISC located events in the Bulletin.

8.3 Seismic Wave Amplitudes and Periods

The ISC Bulletin contains a variety of seismic wave amplitudes and periods measured by reporting agencies. For this Bulletin Summary, the total of collected amplitudes and periods is 3065069 (see Section 7.3). For the determination of the ISC magnitudes MS and mb , only a fraction of such data can be used. Indeed, the ISC network magnitudes are computed only for ISC located events. Here we recall the main features of the ISC procedure for MS and mb computation (see detailed description in Section 10.1.4). For each amplitude-period pair in a reading the ISC algorithm computes the magnitude (a reading can include several amplitude-period measurements) and the reading magnitude is assigned to the maximum A/T in the reading. If more than one reading magnitude is available for a station, the station magnitude is the median of the reading magnitudes. The network magnitude is computed then as the 20% alpha-trimmed median of the station magnitudes (at least three required). MS is computed for shallow earthquakes (depth ≤ 60 km) only and using amplitudes and periods on all three components (when available) if the period is within 10-60 s and the epicentral distance is between 20° and 160° . mb is computed also for deep earthquakes (depth down to 700 km) but only with amplitudes on the vertical component measured at periods ≤ 3 s in the distance range 21° - 100° .

Table 8.2 is a summary of the amplitude and period data that contributed to the computation of station and ISC MS and mb network magnitudes for this Bulletin Summary.

Table 8.2: Summary of the amplitude-period data used by the ISC Locator to compute MS and mb .

	MS	mb
Number of amplitude-period data	133894	450776
Number of readings	120176	446482
Percentage of readings in the ISC located events with qualifying data for magnitude computation	13.4	43.4
Number of station magnitudes	115573	402860
Number of network magnitudes	3080	12600

A small percentage of the readings with qualifying data for MS and mb calculation have more than one

amplitude-period pair. Notably, only 13% of the readings for the ISC located (shallow) events included qualifying data for MS computation, whereas for mb the percentage is much higher at 43%. This is due to the seismological practice of reporting agencies. Agencies contributing systematic reports of amplitude and period data are listed in Appendix Table 10.4. Obviously the ISC Bulletin would benefit if more agencies included surface wave amplitude-period data in their reports.

Figure 8.23 shows the distribution of the number of station magnitudes versus distance. For mb there is a significant increase in the distance range 70° - 90° , whereas for MS most of the contributing stations are below 100° . The increase in number of station magnitude between 70° - 90° for mb is partly due to the very dense distribution of seismic stations in North America and Europe with respect to earthquake occurring in various subduction zones around the Pacific Ocean.

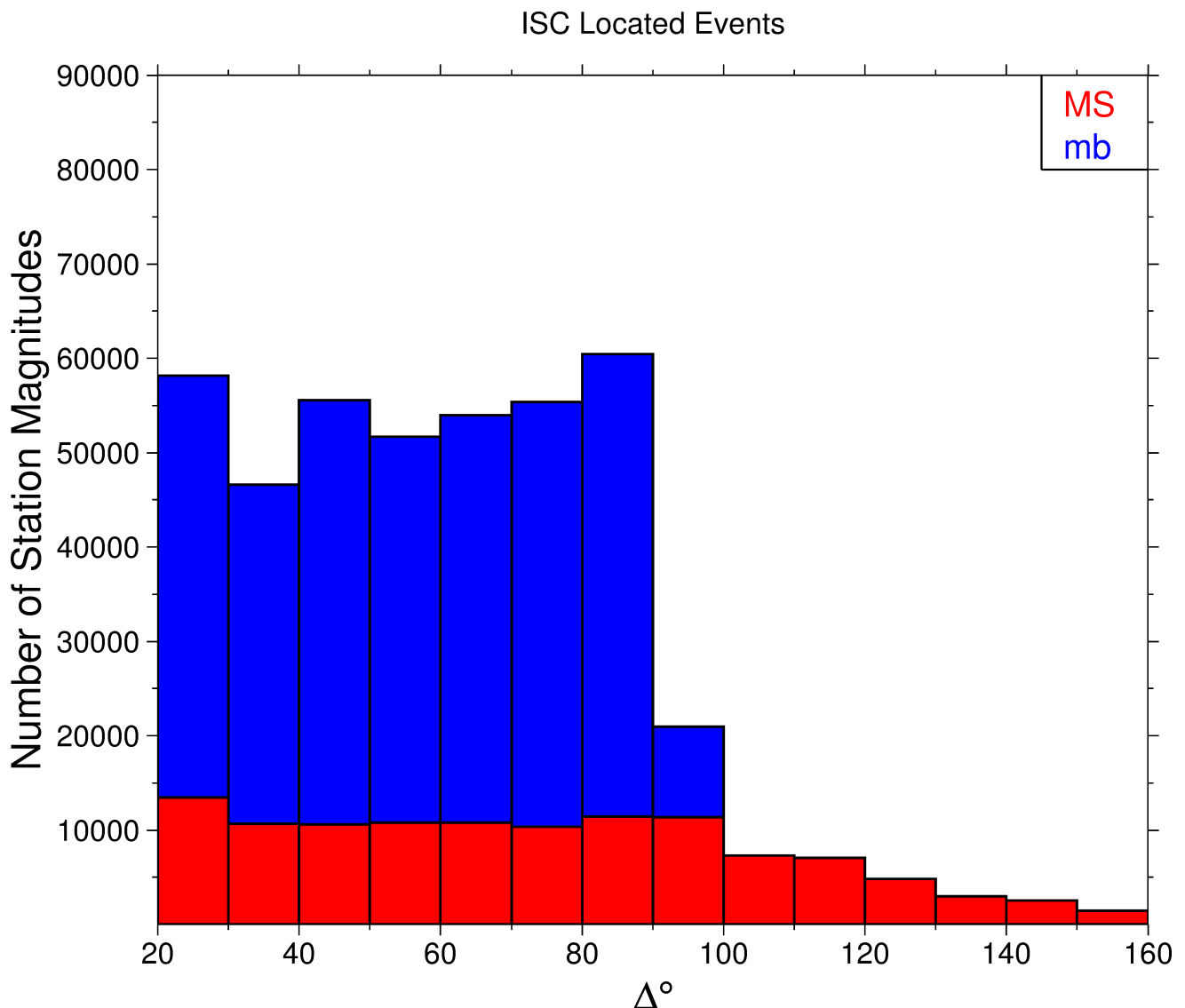


Figure 8.23: Distribution of the number of station magnitudes computed by the ISC Locator for mb (blue) and MS (red) versus distance.

Finally, Figure 8.24 shows the distribution of network MS and mb as well as the median number of stations for magnitude bins of 0.2. Clearly with increasing magnitude the number of events is smaller but with a general tendency of having more stations contributing to the network magnitude.

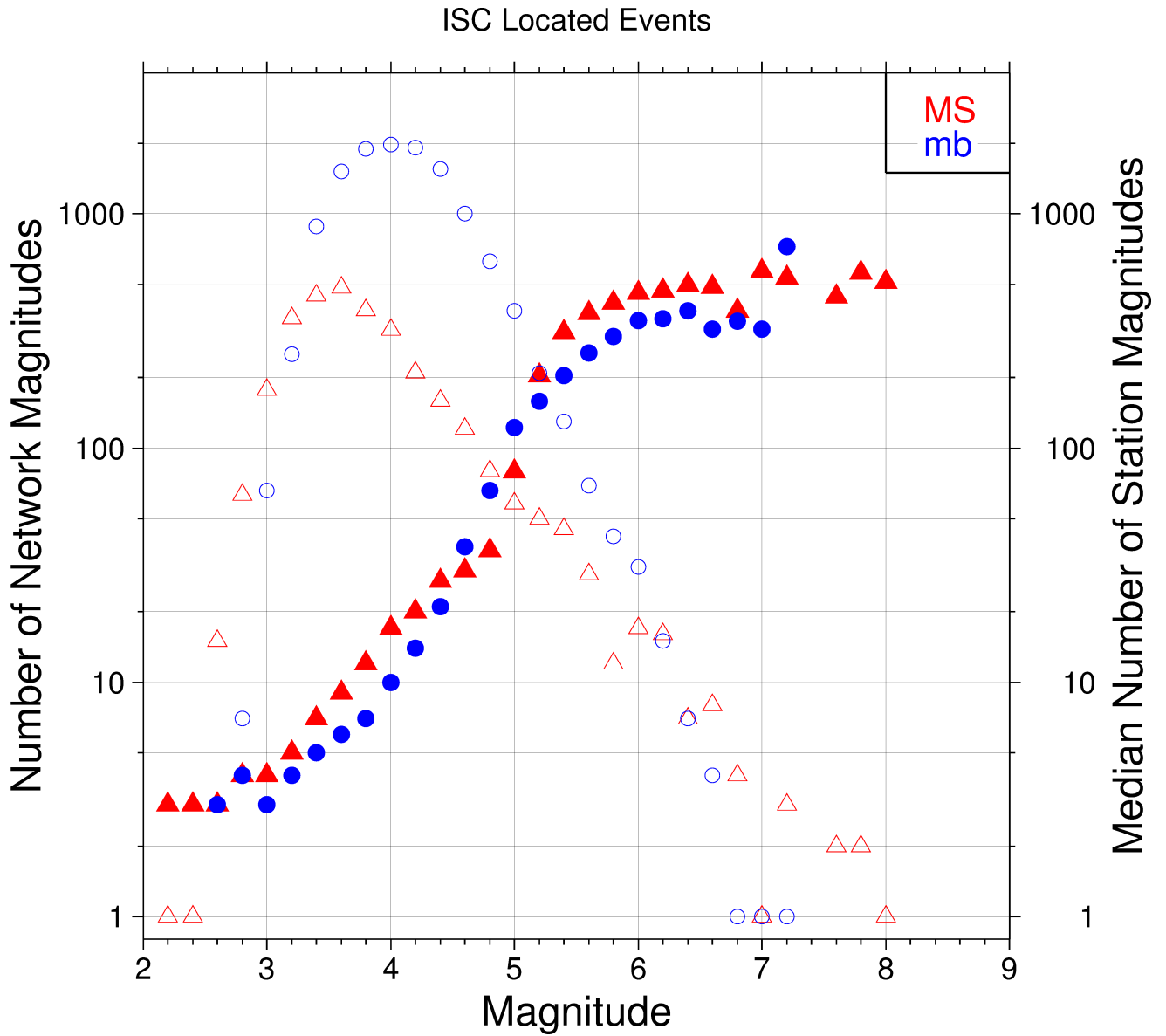


Figure 8.24: Number of network magnitudes (open symbols) and median number of stations magnitudes (filled symbols). Blue circles refer to mb and red triangles to MS. The width of the magnitude interval δM is 0.2, and each symbol includes data with magnitude in $M \pm \delta M/2$.

8.4 Completeness of the ISC Bulletin

The completeness of the ISC Bulletin can be expressed as a magnitude value, above which we expect the Bulletin to contain 100% of events. This magnitude of completeness, M_C can be measured as the point where the seismicity no longer follows the Gutenberg-Richter relationship. We compute an estimate of M_C using the maximum curvature technique of *Woessner and Wiemer (2005)*.

The completeness of the ISC Bulletin for this summary period is shown in Figure 8.25. A history of completeness for the ISC Bulletin is shown in Figure 8.26. The step change in 1996 corresponds with the inclusion of the Prototype IDC (EIDC) Bulletin, followed by the Reviewed Event Bulletin (REB) of the IDC.

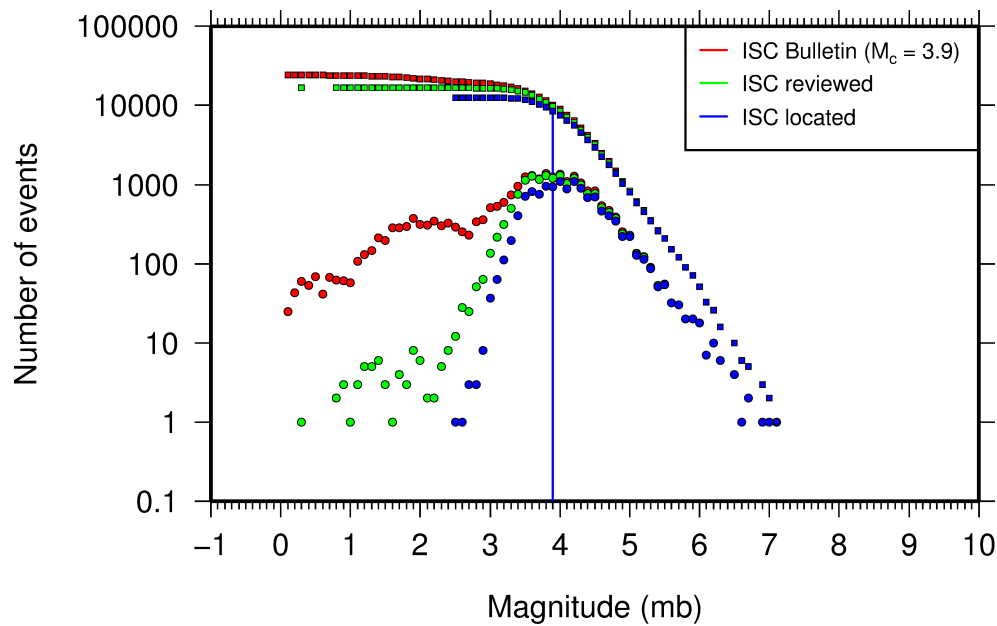


Figure 8.25: Frequency and cumulative frequency magnitude distribution for all events in the ISC Bulletin, ISC reviewed events and events located by the ISC. The magnitude of completeness (M_C) is shown for the ISC Bulletin. Note: only events with values of mb are represented in the figure.

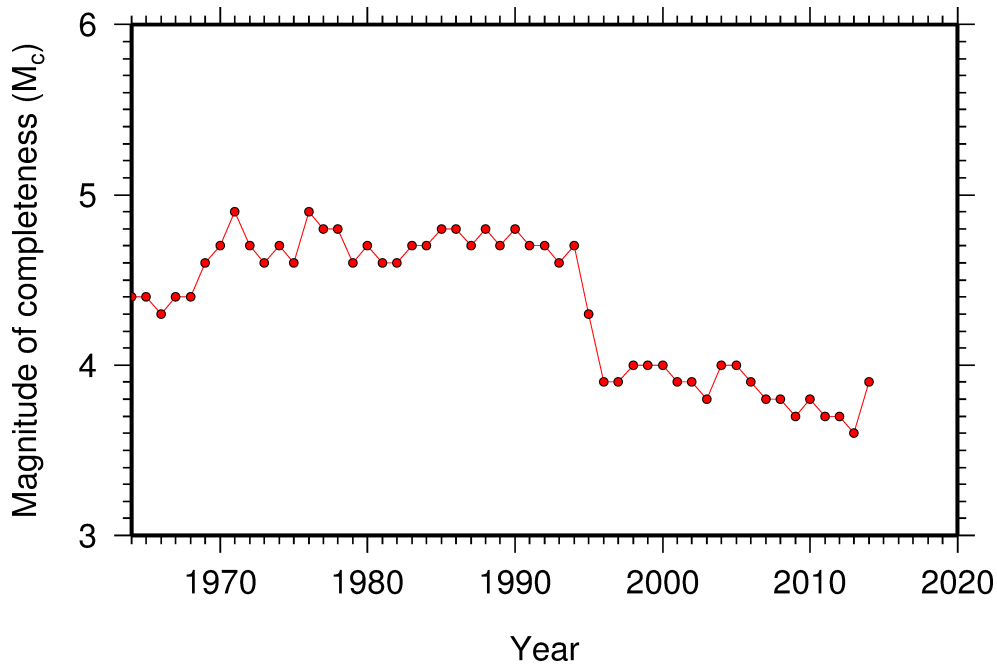


Figure 8.26: Variation of magnitude of completeness (M_C) for each year in the ISC Bulletin. Note: M_C is calculated only using those events with values of mb .

8.5 Magnitude Comparisons

The ISC Bulletin publishes network magnitudes reported by multiple agencies to the ISC. For events that have been located by the ISC, where enough amplitude data has been collected, the MS and mb magnitudes are calculated by the ISC (MS is computed only for depths ≤ 60 km). In this section, ISC magnitudes and some other reported magnitudes in the ISC Bulletin are compared.

The comparison between MS and mb computed by the ISC locator for events in this summary period is shown in Figure 8.27, where the large number of data pairs allows a colour coding of the data density. The scatter in the data reflects the fundamental differences between these magnitude scales.

Similar plots are shown in Figure 8.28 and 8.29, respectively, for comparisons of ISC mb and ISC MS with M_W from the GCMT catalogue. Since M_W is not often available below magnitude 5, these distributions are mostly for larger, global events. Not surprisingly, the scatter between mb and M_W is larger than the scatter between MS and M_W . Also, the saturation effect of mb is clearly visible for earthquakes with $M_W > 6.5$. In contrast, MS scales well with $M_W > 6$, whereas for smaller magnitudes MS appears to be systematically smaller than M_W .

In Figure 8.30 ISC values of mb are compared with all reported values of mb , values of mb reported by NEIC and values of mb reported by IDC. Similarly in Figure 8.31, ISC values of MS are compared with all reported values of MS , values of MS reported by NEIC and values of MS reported by IDC. There is a large scatter between the ISC magnitudes and the mb and MS reported by all other agencies.

The scatter decreases both for mb and MS when ISC magnitudes are compared just with NEIC and IDC magnitudes. This is not surprising as the latter two agencies provide most of the amplitudes and periods used by the ISC locator to compute MS and mb . However, ISC mb appears to be smaller than NEIC mb for $mb < 4$ and larger than IDC mb for $mb > 4$. Since NEIC does not include IDC amplitudes,

it seems these features originate from observations at the high-gain, low-noise sites reported by the IDC. For the MS comparisons between ISC and NEIC a similar but smaller effect is observed for $MS < 4.5$, whereas a good scaling is generally observed for the MS comparisons between ISC and IDC.

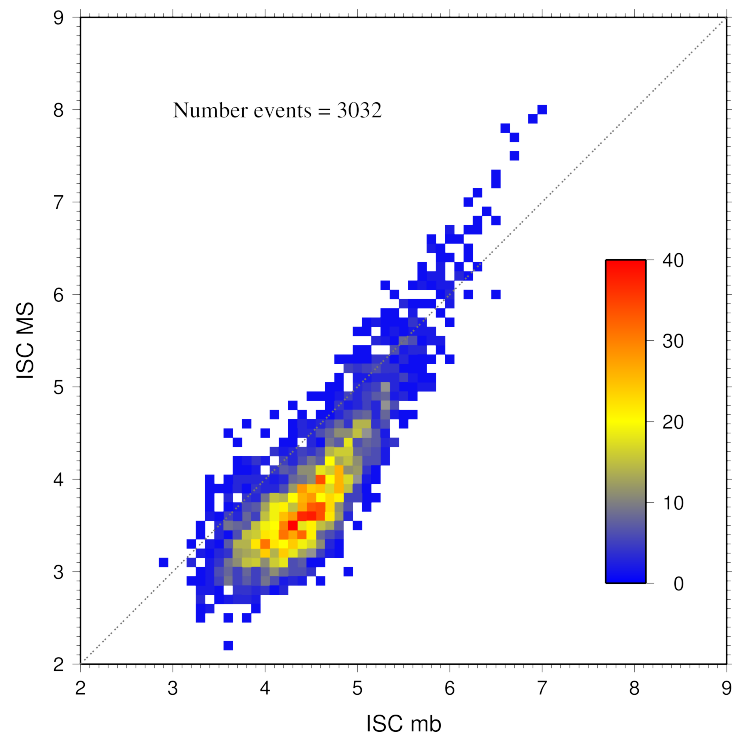


Figure 8.27: Comparison of ISC values of MS with mb for common event pairs.

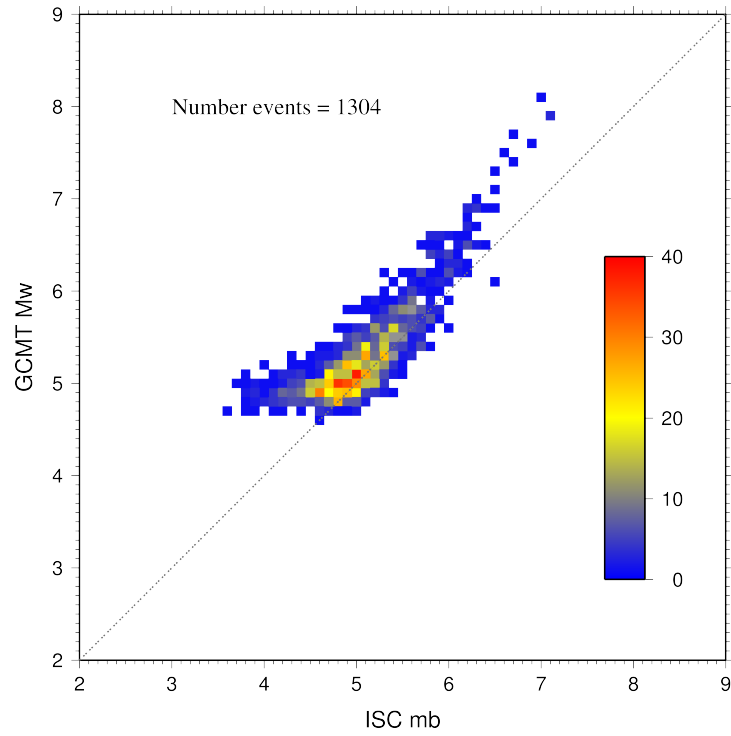


Figure 8.28: Comparison of ISC values of m_b with GCMT M_W for common event pairs.

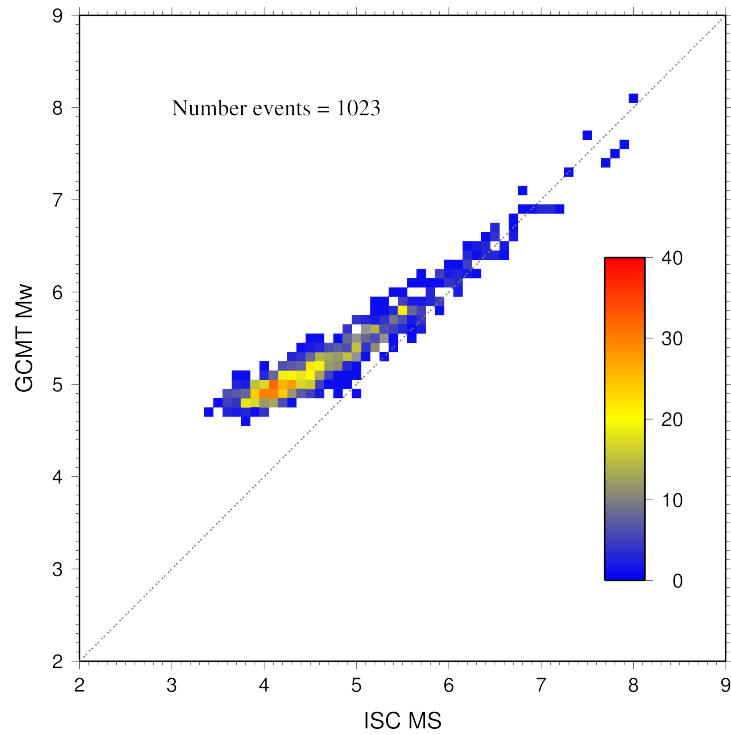


Figure 8.29: Comparison of ISC values of M_S with GCMT M_W for common event pairs.

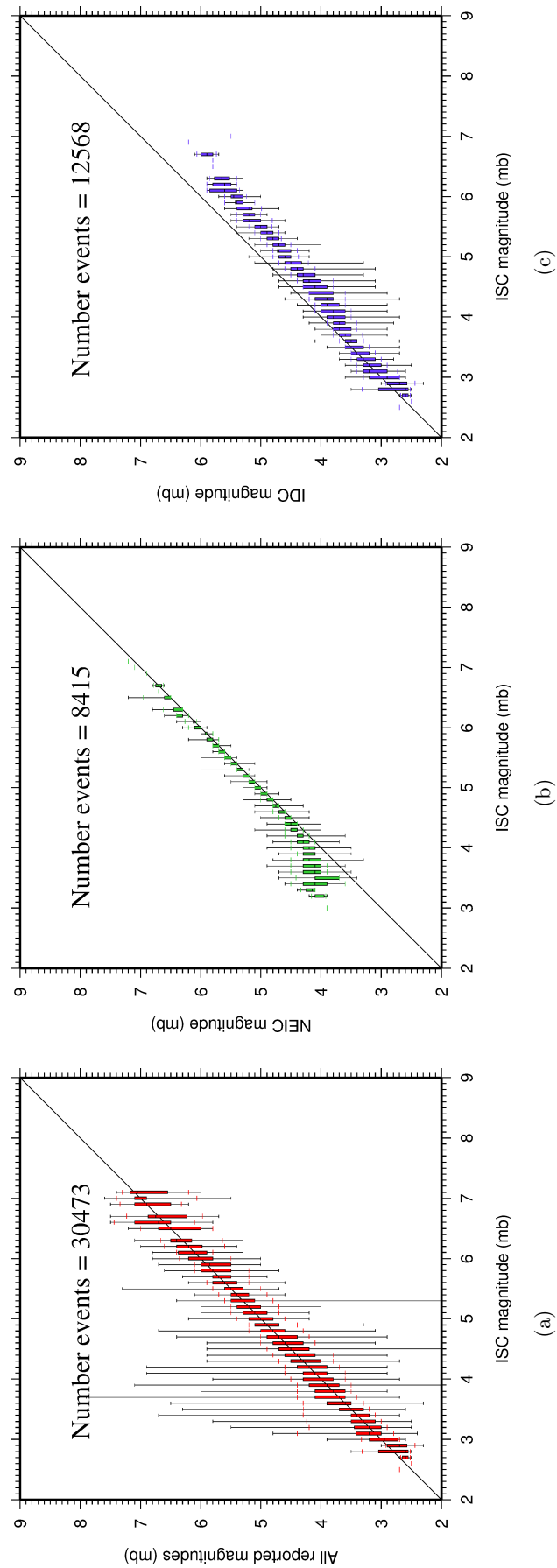


Figure 8.30: Comparison of ISC magnitude data (mb) with additional agency magnitudes (mb). The statistical summary is shown in box-and-whisker plots where the 10th and 90th percentiles are shown in addition to the max and min values. (a): All magnitudes reported; (b): NEIC magnitudes; (c): IDC magnitudes.

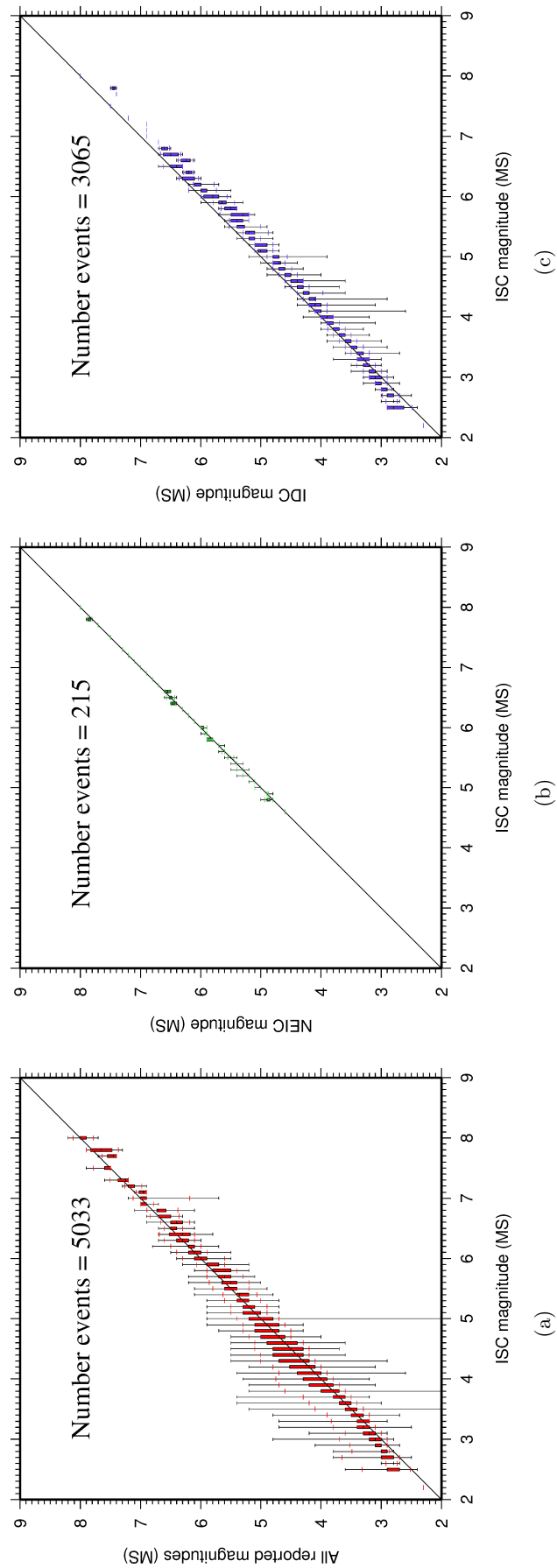


Figure 8.31: Comparison of ISC magnitude data (MS) with additional agency magnitudes (MS). The statistical summary is shown in the box-and-whisker plots where the 10th and 90th percentiles are shown in addition to the max and min values. (a): All magnitudes reported; (b): NEIC magnitudes; (c): IDC magnitudes.

9

The Leading Data Contributors

For the current six-month period, 142 agencies reported related bulletin data. Although we are grateful for every report, we nevertheless would like to acknowledge those agencies that made the most useful or distinct contributions to the contents of the ISC Bulletin. Here we note those agencies that:

- provided a comparatively large volume of parametric data (see Section 9.1),
- reported data that helped quite considerably to improve the quality of the ISC locations or magnitude determinations (see Section 9.2),
- helped the ISC by consistently reporting data in one of the standard recognised formats and in-line with the ISC data collection schedule (see Section 9.3).

We do not aim to discourage those numerous small networks who provide comparatively smaller yet still most essential volumes of regional data regularly, consistently and accurately. Without these reports the ISC Bulletin would not be as comprehensive and complete as it is today.

9.1 The Largest Data Contributors

We acknowledge the contribution of IDC, NEIC, MOS, BJI, CLL, DJA and a few others (Figure 9.1) that reported the majority of moderate to large events recorded at teleseismic distances. The contributions of NEIC, IDC, JMA, and several others are also acknowledged with respect to smaller seismic events. The contributions of JMA, NEIC, IDC, TAP, ROM, and a number of others are also acknowledged with respect to small seismic events. Note that the NEIC bulletin accumulates a contribution of all regional networks in the USA. Several agencies monitoring highly seismic regions routinely report large volumes of small to moderate magnitude events, such as those in Japan, Chinese Taipei, Turkey, Chile, Italy, Greece, New Zealand, Mexico and Columbia. Contributions of small magnitude events by agencies in regions of low seismicity, such as Finland are also gratefully received.

We also would like to acknowledge contributions of those agencies that report a large portion of arrival time and amplitude data (Figure 9.2). For small magnitude events, these are local agencies in charge of monitoring local and regional seismicity. For moderate to large events, contributions of IDC, USArray, NEIC, MOS are especially acknowledged. Notably, three agencies (IDC, NEIC and MOS) together reported over 82% of all amplitude measurements made for teleseismically recorded events. We hope that other agencies would also be able to update their monitoring routines in the future to include the amplitude reports for teleseismic events compliant with the IASPEI standards.

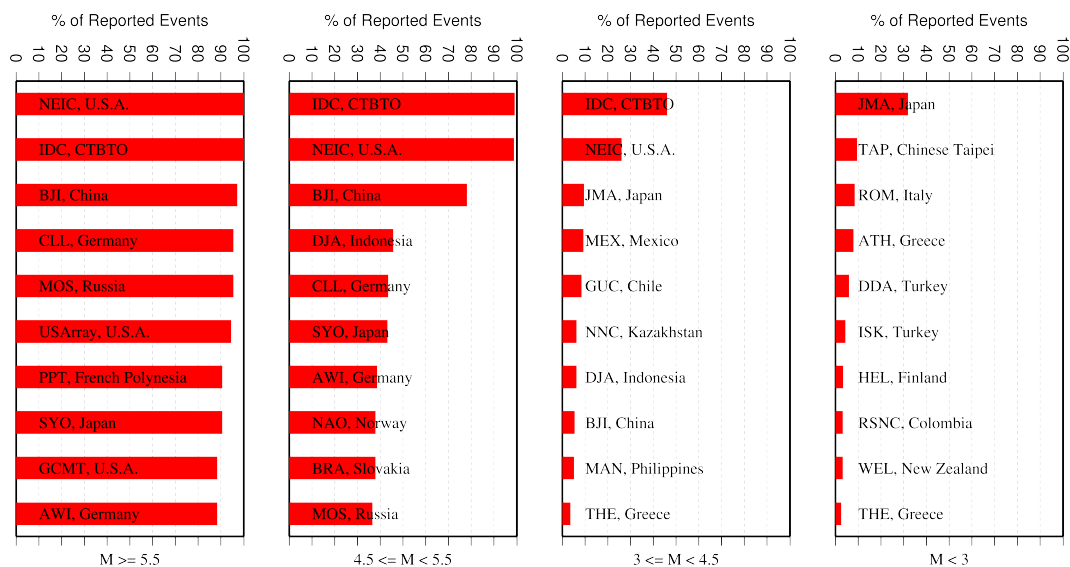


Figure 9.1: Frequency of events in the ISC Bulletin for which an agency reported at least one item of data: a moment tensor, a hypocentre, a station arrival time or an amplitude. The top ten agencies are shown for four magnitude intervals.

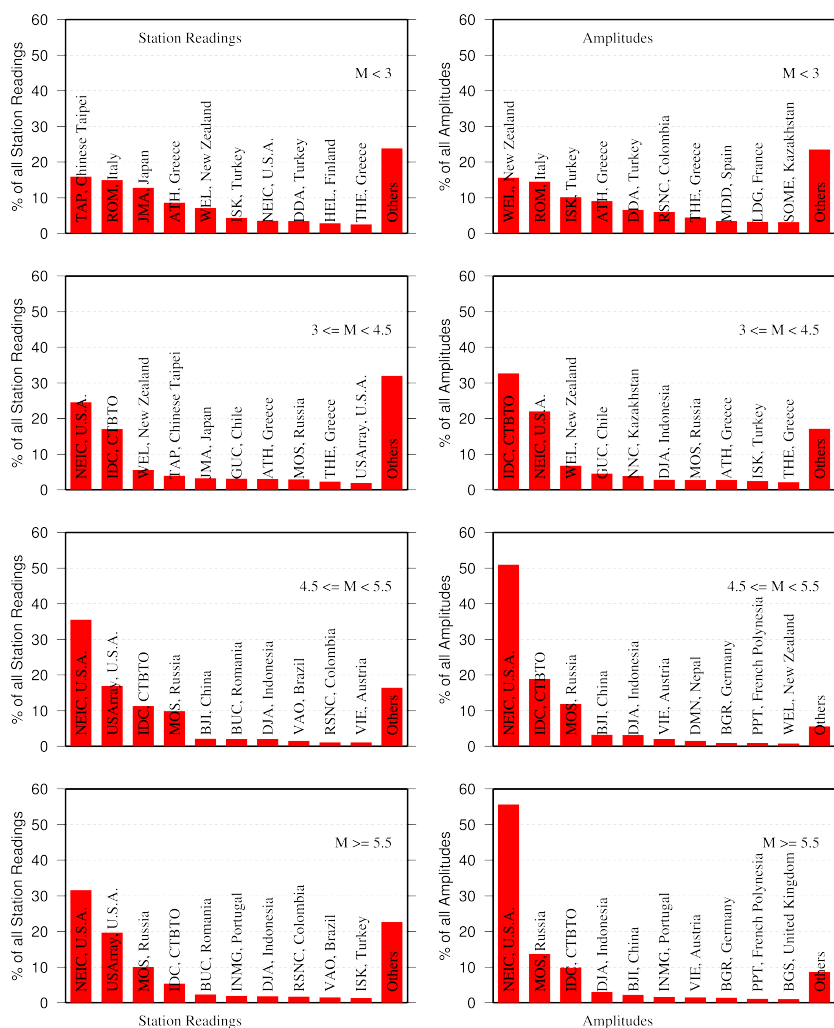


Figure 9.2: Contributions of station arrival time readings (left) and amplitudes (right) of agencies to the ISC Bulletin. Top ten agencies are shown for four magnitude intervals.

9.2 Contributors Reporting the Most Valuable Parameters

One of the main ISC duties is to re-calculate hypocentre estimates for those seismic events where a collective wealth of all station reports received from all agencies is likely to improve either the event location or depth compared to the hypocentre solution from each single agency. For areas with a sparse local seismic network or an unfavourable station configuration, readings made by other networks at teleseismic distances are very important. All events near mid-oceanic ridges as well as those in the majority of subduction zones around the world fall into this category. Hence we greatly appreciate the effort made by many agencies that report data for remote earthquakes (Figure 9.3). For some agencies, such as the IDC and the NEIC, it is part of their mission. For instance, the IDC reports almost every seismic event that is large enough to be recorded at teleseismic distance (20 degrees and beyond). This is largely because the International Monitoring System of primary arrays and broadband instruments is distributed at quiet sites around the world in order to be able to detect possible violations of the Comprehensive Nuclear-Test-Ban Treaty. The NEIC reported over 33% of those events as their mission requires them to report events above magnitude 4.5 outside the United States of America. For other agencies reporting distant events it is an extra effort that they undertake to notify their governments and relief agencies as well as to help the ISC and academic research in general. Hence these agencies usually report on the larger magnitude events. BJI, NAO, CLL, MOS, SYO, DMN, BRA and AWI each reported individual station arrivals for several percent of all relevant events. We encourage other agencies to report distant events to us.

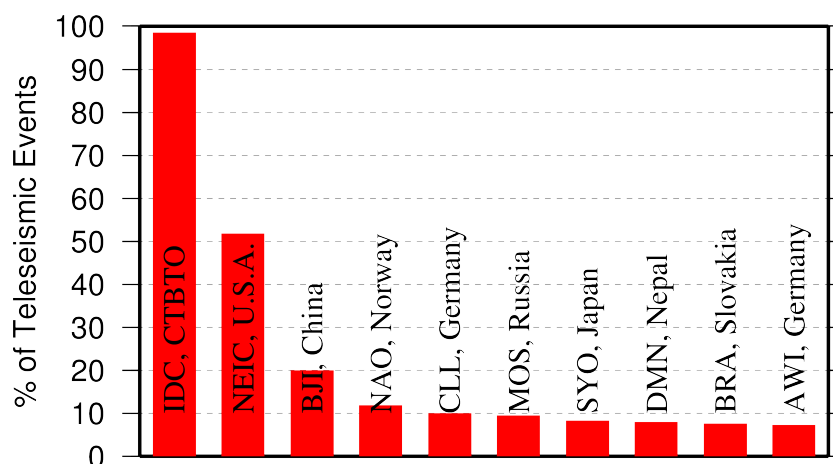


Figure 9.3: Top ten agencies that reported teleseismic phase arrivals for a large portion of ISC events.

In addition to the first arriving phase we encourage reporters to contribute observations of secondary seismic phases that help constrain the event location and depth: S, Sn, Sg and pP, sP, PcP (Figure 9.4). We expect though that these observations are actually made from waveforms, rather than just predicted by standard velocity models and modern software programs. It is especially important that these arrivals are manually reviewed by an operator (as we know takes place at the IDC and NEIC), as opposed to some lesser attempts to provide automatic phase readings that are later rejected by the ISC due to a generally poor quality of unreviewed picking.

Another important long-term task that the ISC performs is to compute the most definitive values of MS and mb network magnitudes that are considered reliable due to removal of outliers and consequent

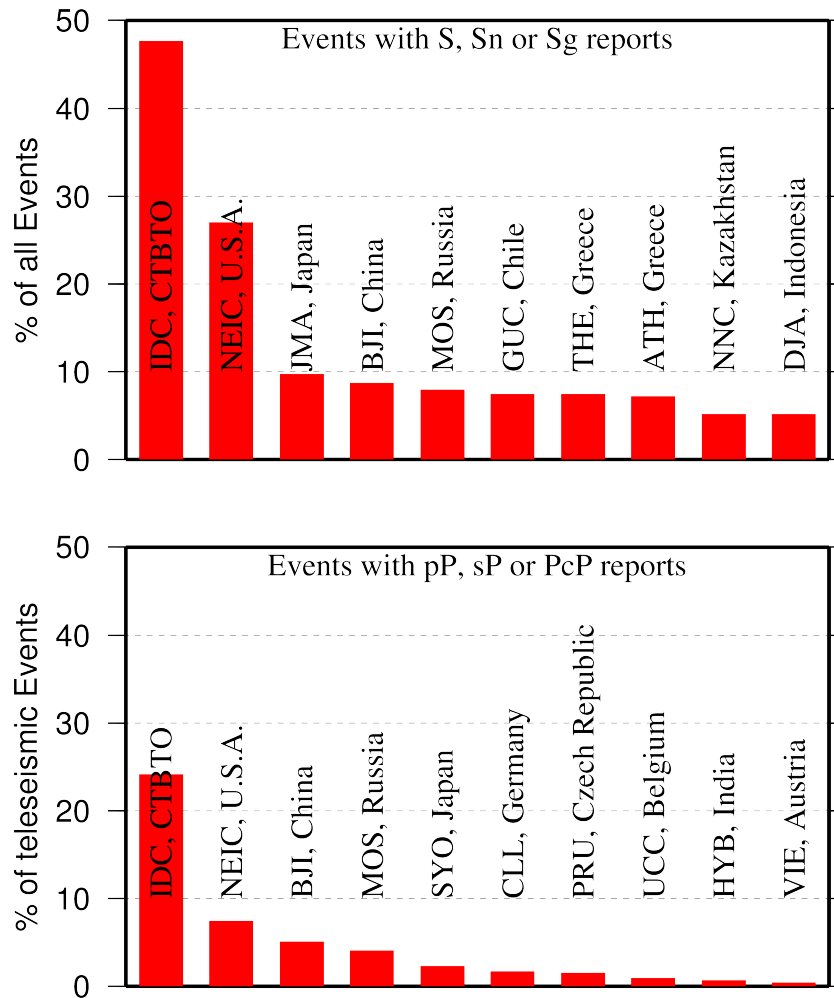


Figure 9.4: Top ten agencies that reported secondary phases important for an accurate epicentre location (top) and focal depth determination (bottom).

averaging (using alpha-trimmed median) across the largest network of stations, generally not feasible for a single agency. Despite concern over the bias at the lower end of m_b introduced by the body wave amplitude data from the IDC, other agencies are also known to bias the results. This topic is further discussed in Section 8.5.

Notably, the IDC reports almost 100% of all events for which MS and m_b are estimated. This is due to the standard routine that requires determination of body and surface wave magnitudes useful for discrimination purposes. NEIC, BJI, MOS, PPT, NAO and a few other agencies (Figure 9.5) are also responsible for the majority of the amplitude and period reports that contribute towards the ISC magnitudes.

Since the ISC does not routinely process waveforms, we rely on other agencies to report moment magnitudes as well as moment tensor determinations (Figure 9.6).

Among other event parameters the ISC Bulletin also contains information on event type. We cannot independently verify the type of each event in the Bulletin and thus rely on other agencies to report the event type to us. Practices of reporting non-tectonic events vary greatly from country to country. Many agencies do not include anthropogenic events in their reports. Suppression of such events from reports to the ISC may lead to a situation where a neighbouring agency reports the anthropogenic event

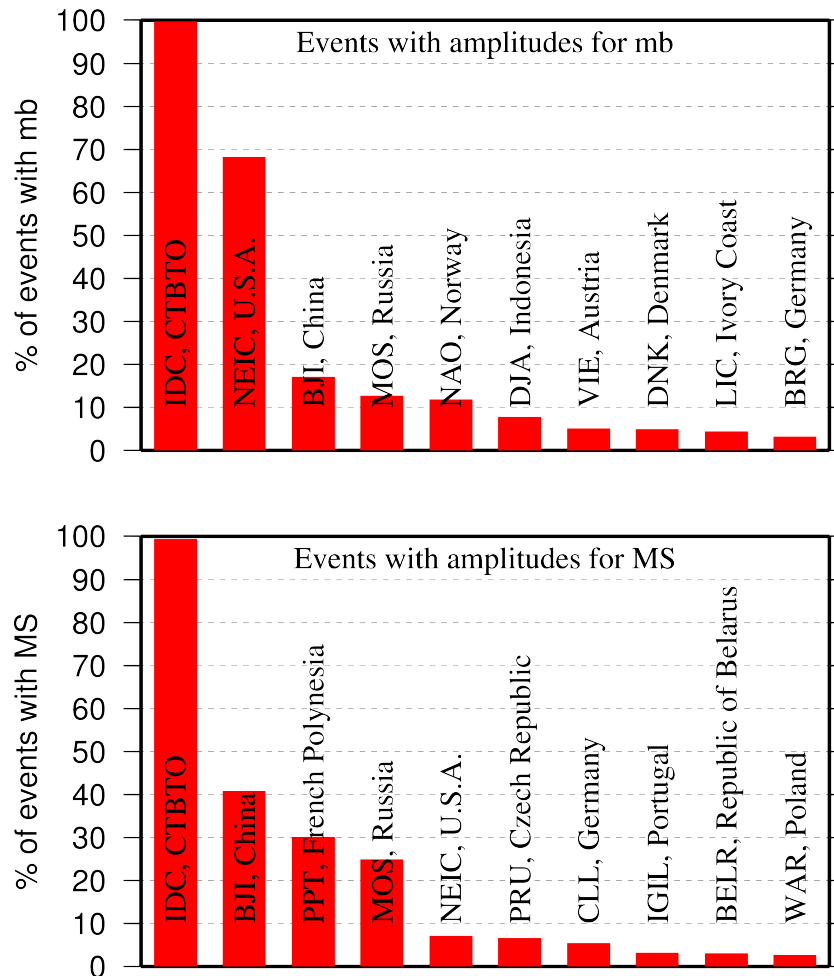


Figure 9.5: Agencies that report defining body (top) and surface (bottom) wave amplitudes and periods for the largest fraction of those ISC Bulletin events with MS/mb determinations.

as an earthquake for which expected data are missing. This in turn is detrimental to ISC Bulletin users studying natural seismic hazard. Hence we encourage all agencies to join the agencies listed on Figure 9.7 and several others in reporting both natural and anthropogenic events to the ISC.

The ISC Bulletin also contains felt and damaging information when local agencies have reported it to us. Agencies listed on Figure 9.8 provide such information for the majority of all felt or damaging events in the ISC Bulletin.

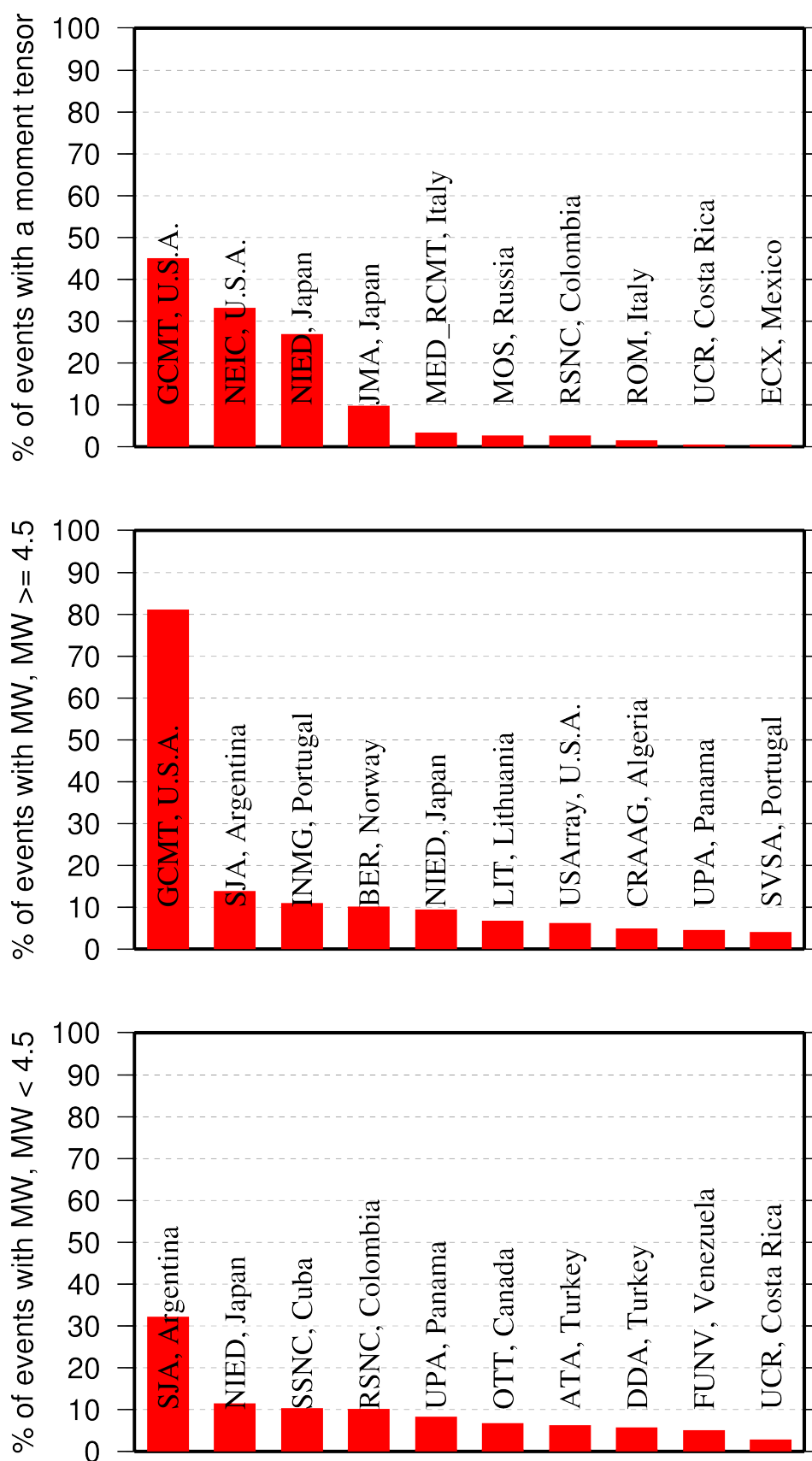


Figure 9.6: Top ten agencies that most frequently report determinations of seismic moment tensor (top) and moment magnitude (middle/bottom for M greater/smaller than 4.5).

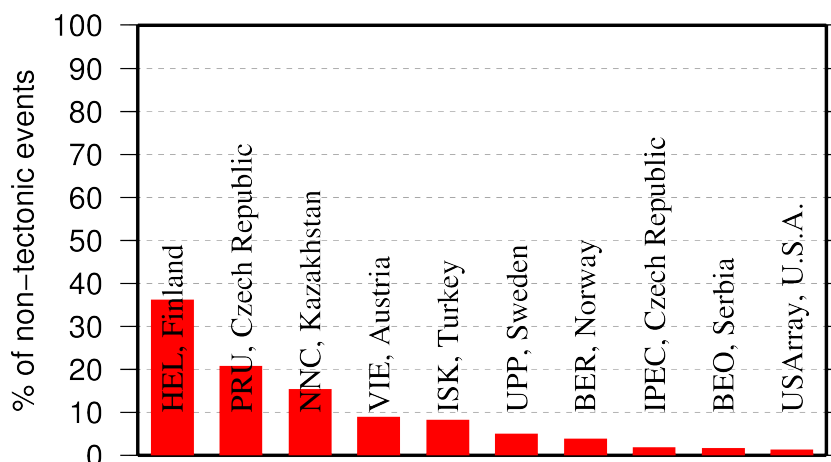


Figure 9.7: Top ten agencies that most frequently report non-tectonic seismic events to the ISC.

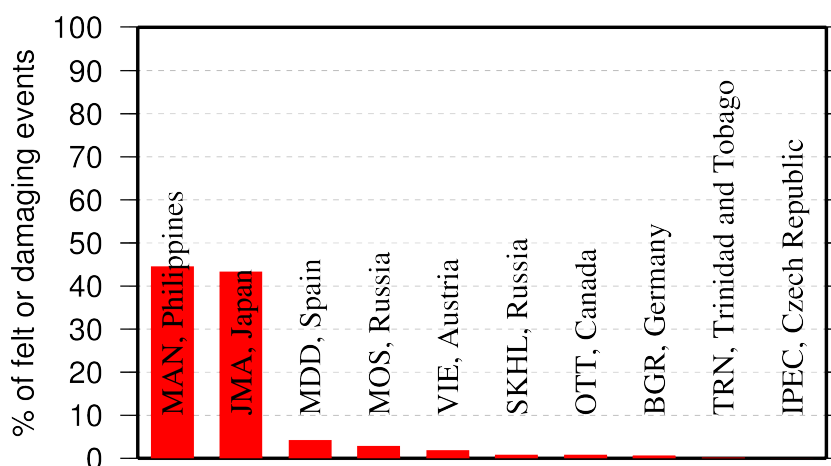


Figure 9.8: Top ten agencies that most frequently report macroseismic information to the ISC.

9.3 The Most Consistent and Punctual Contributors

During this six-month period, 29 agencies reported their bulletin data in one of the standard seismic formats (ISF, IMS, GSE, Nordic or QuakeML) and within the current 12-month deadline. Here we must reiterate that the ISC accepts reviewed bulletin data after a final analysis as soon as they are ready. These data, even if they arrive before the deadline, are immediately parsed into the ISC database, grouped with other data and become available to the ISC users on-line as part of the preliminary ISC Bulletin. There is no reason to wait until the deadline to send the data to the ISC. Table 9.1 lists all agencies that have been helpful to the ISC in this respect during the six-month period.

Table 9.1: Agencies that contributed reviewed bulletin data to the ISC in one of the standard international formats before the submission deadline.

Agency Code	Country	Average Delay from real time (days)
PPT	French Polynesia	20
LIC	Ivory Coast	24
NAO	Norway	28
IGIL	Portugal	31
IDC	Austria	49
SVSA	Portugal	54
UCC	Belgium	67
INMG	Portugal	70
KRSC	Russia	77
LDG	France	81
ISN	Iraq	91
BUL	Zimbabwe	93
AUST	Australia	97
THE	Greece	104
BJI	China	106
ISK	Turkey	124
STR	France	165
BEO	Serbia	171
BGS	United Kingdom	186
IRIS	U.S.A.	210
ZUR	Switzerland	216
LIT	Lithuania	246
BYKL	Russia	286
ATA	Turkey	289
ATH	Greece	309
BUD	Hungary	319
BGR	Germany	338
VIE	Austria	340
QCP	Philippines	362

10

Appendix

10.1 ISC Operational Procedures

10.1.1 Introduction

The relational database at the ISC is the primary source for the ISC Bulletin. This database is also the source for the ISC web-based search, the ISC CD-ROMs and this printed Summary. The ISC database is also mirrored at several institutions such as the Data Management Center of the Incorporated Research Institutions for Seismology (IRIS DMC), Earthquake Research Institute (ERI) of the University of Tokyo and a few others.

The database holds information about ISC events, both natural and anthropogenic. Information on each event may include hypocentre estimates, moment tensors, event type, felt and damaging reports and associated station observations reported by different agencies and grouped together per physical event.

The majority of the ISC events ($\sim 80\%$) are small and are not reviewed by the ISC analysts. Those that are reviewed ($\sim 20\%$, usually magnitude greater than 3.5) may or may not include an ISC hypocentre solution and magnitude estimates. The decision depends on whether the wealth of combined information from several agencies as compared to the data of each single agency alone warrants the ISC location. The events are called ISC events regardless of whether they have been reviewed or located by the ISC or not.

All events located by the ISC are reviewed by the ISC analysts but not the other way round. Analyst review involves an examination of the integrity of all reported parametric information. It does not involve review of waveforms. Even if waveforms from all of the $\sim 6,000$ stations included in a typical recent month of the ISC Bulletin were freely available, it would be an unmanageable task to inspect them all.

We shall now describe briefly current processes and procedures involved in producing the Bulletin of the International Seismological Centre. These have been developed from former practices described in the Introduction to earlier issues of the ISC Bulletin to account for modern methods and technologies of data collection and analysis.

10.1.2 Data Collection

Parametric data, mainly comprising seismic event hypocentre solutions, phase arrival observations and associated magnitude data, are now mostly emailed to the ISC (seismo@isc.ac.uk) by agencies around the world. Other macroseismic and source information associated with seismic events may also be incorporated in accordance with modern standards. The process of data collection at the ISC involves

the automatic parsing of these data into the ISC relational database. The ISC now has over 200 individual parsers to account for legacy and current bulletin data formats used by data reporters.

Figure 10.1 shows the 313 agencies that have reported bulletin data to the ISC, directly or via regional data centres, during the entire period of the ISC existence: these agencies are also listed in Table 10.2 of the Appendix. In Figure 10.1, corresponding countries are shown shaded in red. Please note that the continent of Antarctica appears white on the map despite a steady stream of bulletin data from Antarctic stations: the agencies that run these stations are based elsewhere.

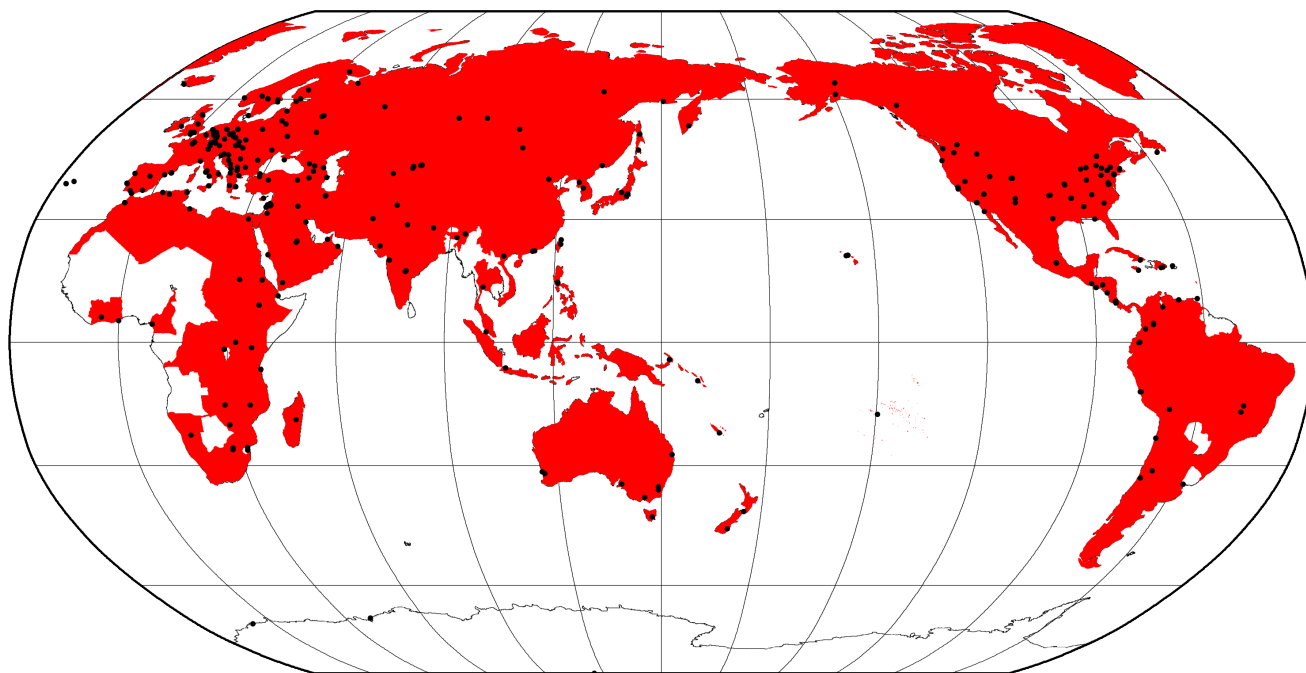


Figure 10.1: Map of 313 agencies and corresponding countries that have reported seismic bulletin data to the ISC at least once during the entire period of the ISC operations, either directly or via regional data centres. Corresponding countries are shaded in red.

10.1.3 ISC Automatic Procedures

Grouping

Grouping is the automatic process by which the many hypocentre solutions sent by the agencies reporting to the ISC for the same physical event are merged together into a single ISC event. This process possibly begins with an alert message and ends before a final review by ISC analysts. The process periodically runs through a set time interval of the input data stream, typically one day, looking for hypocentres in newly received data that are not yet grouped into an ISC event. Thus it considers only data more recent than the last data month reviewed by the ISC analysts. Immediately after grouping the seismic arrival associator is run on the same time interval, dealing with new phase arrival data not associated with any hypocentre.

The first stage of grouping gets a score where possible for each hypocentre to determine whether the reported hypocentre will be considered to be the primary estimate, or prime, for an ISC event. This score is based on the station arrival times reported in association with the hypocentre in four epicentral

distance zones that characterise the networks of stations reporting:

1. Whole network
2. Local, 0 - 150 km
3. Near-regional, 3° - 10°
4. Teleseismic, 28° - 180°

For each distance zone, the azimuthal gap, the secondary azimuthal gap (the largest azimuthal gap filled by a single station), the minimum and maximum epicentral distance and number of stations are all used to calculate the value of dU , the normalised absolute deviation from best fitting uniformly distributed stations (*Bondár and McLaughlin, 2009a*). Clearly, this procedure can only use:

1. Bulletin data with hypocentres and sufficient associated seismic arrivals
2. Data for stations that are in the International Registry (IR)
3. Station data that are actually reported to ISC: CENC (China), for example, reports at most 24 stations, whilst many more may have been used to determine the hypocentre.

The hypocentres are then each considered in turn for grouping using one of two methods, the first by searching for a similar hypocentre, and the second by searching for the best fit of the reported phase arrival data that are associated with the candidate hypocentre. The method chosen for a reporter is based on feedback gained from ISC analysts.

For finding similar hypocentres, three sets of limits for origin-time difference and epicentral separation are used according to the type of bulletin data, be it alert, provisional or final: these limits are, respectively:

- ± 2 minutes and 10°
- ± 2 minutes and 4°
- ± 1 minutes and 2°

If there is no overlap with the hypocentre of an existing ISC event, a new event is formed. For each candidate hypocentre, a proximity score is otherwise calculated based on differences in time, t , and distance, s , between the candidate hypocentre and a hypocentre in an event with which it could potentially be grouped.

$$\text{Proximity score} = 2 - (dt/dt_{max}) - (ds/ds_{max})$$

where ds_{max} is the maximum distance between hypocentres and dt_{max} the maximum difference in origin time.

As long as there is no duplication of hypocentre (with the same author, origin time and location within tight limits) the candidate hypocentre together with the associated phase data is grouped with the prime

hypocentre of the event and the initial dU score is used to reassess the prime hypocentre designation. Apparent duplicated hypocentre estimations, including preliminary solutions relayed by other agencies, need to be assessed to determine whether they should really be split between different events. Should there be two or more equally valid events, these can be assessed in turn and may eventually be merged together.

Grouping by fit of the associated phase arrival data is simpler. The residuals of the arrival data are calculated using ak135 travel times for all suitable prime hypocentres within the widest proximity limits given above for similar hypocentres. The hypocentre and associated phase arrival data is then grouped with the event with the best fitting prime hypocentre, which may similarly be re-designated according to the dU scores. Associations of phase arrival data are updated to be with the prime hypocentre estimate of each ISC event.

It follows that a hypocentre and associated phase arrival data submitted by a reporter will have the reported hypocentre set as the prime hypocentre in the ISC event if no other submitted hypocentre estimate is a closer match. It follows also that a hypocentre submitted without phase data can only be grouped with a similar hypocentre. Generally, early arriving data may be superseded by later arriving data: the data will still be in the ISC database but be deprecated, that is, marked as being no longer useful for further processes.

Association

Association is the automatic procedure, run routinely after grouping, that links reported phase arrivals at IR stations with the prime hypocentres of ISC events. As grouping took care of those phases associated with reported hypocentres, by associating the phases to the respective prime hypocentres of the ISC events without further checks, this procedure is only required for phase arrival observations that were sent without any association of event made for them by the reporter. Currently only 5% of arrival data is sent unassociated compared with 25% ten years ago.

If a phase arrival is found to be very similar to another already reported, it is placed in the same event, otherwise the procedure below is followed.

For associating a phase arrival, suitable events are sought with prime hypocentre origin-times in the window 40 minutes before and 100 s after the arrival time. For each phase arrival and prime hypocentre an ak135 travel-time residual is calculated for either the reported arrival phase name or an alternative from a default list if appropriate. Possible timing errors that are multiples of 60 s (a minute) are considered if the phase arrival is at a station not known to be digitally recording. A reporting likelihood is then determined based on the reported event magnitude: a magnitude default of 3.0 is used if no magnitude is given.

A final score is calculated from the residuals, from the likelihood of the phase observations for the magnitude of the event and from the S-P misfit. A phase arrival along with all other phase arrivals in that reading for the station is then associated with the prime hypocentre with the best score. If no suitable match is found, the reading remains unassociated but may be used at some later stage.

Thresholding

Thresholding is the process determining which events are to be reviewed by the ISC analysts. In former times, before email transmission of data was convenient, all events were reviewed, with magnitudes nearly always 3.5 or above. Nowadays, data contributors are encouraged to send all their data, which are stored in the ISC database. The overwhelming amount of data, including that for many more smaller events and from many more seismograph stations, led to the advent of ISC Comprehensive Bulletin, for all events, and the ISC Reviewed Bulletin, for selected events reviewed by ISC analysts. Thresholding has been under constant review since the start of the 1999 data year.

Several criteria are considered to decide which events merit review. Once a decision is made, whether or not an event is to be reviewed, further criteria are not considered.

In this section, M is the maximum magnitude reported by any agency for the event. The sequence of tests in the automatic decision process for reviewing events is currently:

- All events reported by the International Data Centre (IDC) of the Comprehensive Nuclear-Test-Ban Treaty Organization (CTBTO) are reviewed.
- If M is greater than or equal to 3.5, the event is reviewed.
- If M is less than 2.5, the event is not reviewed.
- If M is unknown, the number of data sources of hypocentres and phase arrivals is used. Care is taken here to avoid counting indirect reports arriving via agencies such as NEIC, CSEM and CASC, which compile regional and global data:
 - If the number of hypocentre authors is greater than two and the maximum epicentral distance of arrival data is greater than 10° , the event is reviewed.
 - If the number of arrival authors is greater than two and the maximum epicentral distance of arrival data is greater than 10° , the event is reviewed.
 - Otherwise the event is not reviewed.
- If M is between 2.5 and 3.5:
 - If the number of hypocentre and seismic arrival authors is less than two, the event is not reviewed.
 - If any bulletin contributing to the event has at least ten stations within 3° and the secondary azimuthal gap (the largest azimuthal gap filled by a single station) is less than 135° , the event is not reviewed.

Location by the ISC

The automatic processes group and associate incoming data into ISC events as indicated above. These data are available to users before review by the ISC analysts but there will be no ISC hypocentre solutions for any of the events. The candidate events due for review by the ISC analysts are determined by the

thresholding process, which is why many smaller events remain without an ISC hypocentre solution even after the analyst review.

Several further checks of the data are made in preparation for the analyst review, and initial trial estimates for ISC hypocentres are then generated using the accumulated data. If sufficiently robust, the ISC hypocentre estimation will be retained and be made the prime solution for the event, but this, of course, will itself be subject to the analyst review.

It is important to note that not all reviewed events will have an ISC hypocentre. For the reviewed events certain criteria must be met for an initial ISC location of an event to be made. These criteria are shown below:

- All events with an IDC hypocentre, unless IDC is the only hypocentre author and there are less than six associated phases.
- Two or more reporters of data
- Phase data at epicentral distance $\geq 20^\circ$

The ISC locator also needs an initial seed location; in all events except those with eight or more reporters of data where the existing prime is used, this is calculated using a Neighbourhood Algorithm (NA) (*Sambridge, 1999; Sambridge and Kennett, 2001*). More information about the ISC location algorithm and initial seed is given in the next section.

10.1.4 ISC Location Algorithm

The new ISC location algorithm is described in detail in *Bondár and Storchak (2011)* (doi: 10.1111/j.1365-246X.2011.05107.x, Manual www.isc.ac.uk/iscbulletin/iscloc/); here we give a short summary of the major features. Ever since the ISC came into existence in 1964, it has been committed to providing a homogeneous bulletin that benefits scientific research. Hence the location algorithm used by the ISC, except for some minor modifications, has remained largely unchanged for the past 40 years (*Adams et al., 1982; Bolt, 1960*). While the ISC location procedures have served the scientific community well in the past, they can certainly be improved.

Linearised location algorithms are very sensitive to the initial starting point for the location. The old procedures made the assumption that a good initial hypocentre is available among the reported hypocentres. However, there is no guarantee that any of the reported hypocentres are close to the global minimum in the search space. Furthermore, attempting to find a free-depth solution was futile when the data had no resolving power for depth (e.g. when the first arrival is not within the inflection point of the P travel-time curve). When there was no depth resolution, the algorithm would simply pick a point on the origin time – depth trade-off curve. The old ISC locator assumed that the observational errors are independent. The recent years have seen a phenomenal growth both in the number of reported events and phases, owing to the ever-increasing number of stations worldwide. Similar ray paths will produce correlated travel-time prediction errors due to unmodelled heterogeneities in the Earth, resulting in underestimated location uncertainties and for unfavourable network geometries, location bias. Hence,

accounting for correlated travel-time prediction errors becomes imperative if we want to improve (or simply maintain) location accuracy as station networks become progressively denser. Finally, publishing network magnitudes that may have been derived from a single station measurement was rather prone to producing erroneous event magnitude estimates.

To meet the challenge imposed by the ever-increasing data volume from heavily unbalanced networks we introduced a new ISC location algorithm to ensure the efficient handling of data and to further improve the location accuracy of events reviewed by the ISC. The new ISC location algorithm

- Uses all ak135 (*Kennett et al.*, 1995) predicted phases (including depth phases) in the location;
- Obtains the initial hypocentre guess via the Neighbourhood Algorithm (NA) (*Sambridge*, 1999; *Sambridge and Kennett*, 2001);
- Performs iterative linearised inversion using an *a priori* estimate of the full data covariance matrix to account for correlated model errors (*Bondár and McLaughlin*, 2009b);
- Attempts a free-depth solution if and only if there is depth resolution, otherwise it fixes the depth to a region-dependent default depth;
- Scales uncertainties to 90% confidence level and calculates location quality metrics for various distance ranges;
- Obtains a depth-phase depth estimate based on reported surface reflections via depth-phase stacking (*Murphy and Barker*, 2006);
- Provides robust network magnitude estimates with uncertainties.

Seismic Phases

One of the major advantages of using the ak135 travel-time predictions (*Kennett et al.*, 1995) is that they do not suffer from the baseline difference between P, S and PKP phases compared with the Jeffreys-Bullen tables (*Jeffreys and Bullen*, 1940). Furthermore, ak135 offers an abundance of phases from the IASPEI Standard Seismic List (*Storchak et al.*, 2003; 2011) that can be used in the location, most notably the PKP branches and depth-sensitive phases. Elevation and ellipticity corrections (*Dziewonski and Gilbert*, 1976; *Engdahl et al.*, 1998; *Kennett et al.*, 1996), using the WG84 ellipsoid parameters, are added to the ak135 predictions. For depth phases, bounce point (elevation correction at the surface reflection point) and water depth (for pwP) corrections are calculated using the algorithm of *Engdahl et al.* (1998). We use the ETOPO1 global relief model (*Amante and Eakins*, 2009) to obtain the elevation or the water depth at the bounce point.

Phase picking errors are described by *a priori* measurement error estimates derived from the inspection of the distribution of ground truth residuals (residuals calculated with respect to the ground truth location) from the IASPEI Reference Event List (*Bondár and McLaughlin*, 2009a). For phases that do not have a sufficient number of observations in the ground truth database we establish *a priori* measurement errors so that the consistency of the relative weighting schema is maintained. First-arriving P-type phases (P, Pn, Pb, Pg) are picked more accurately than later phases, so their measurement error estimates are

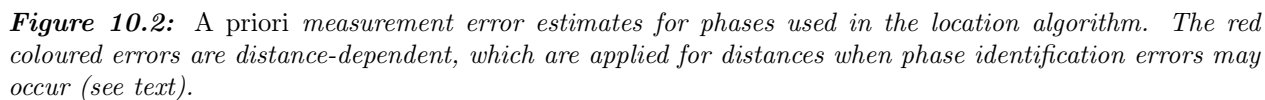
the smallest, 0.8 s. The measurement error for first-arriving S-phases (S, Sn, Sb, Sg) is set to 1.5 s. Phases traversing through or reflecting from the inner/outer core of the Earth have somewhat larger (1.3 s for PKP, PKS, PKKP, PKKS and P'P' branches as well as PKiKP, PcP and PcS, and 1.8 s for SKP, SKS, SKKP, SKKS and S'S' branches as well as SKiKP, ScP and ScS) measurement error estimates to account for possible identification errors among the various branches. Free-surface reflections and conversions (PnPn, PbPb, PgPg, PS, PnS, PgS and SnSn, SbSb, SgSg, SP, SPn, SPg) are observed less frequently and with larger uncertainty, and therefore suffer from large, 2.5 s, measurement errors. Similarly, a measurement error of 2.8 s is assigned to the longer period and typically emergent diffracted phases (Pdif, Sdif, PKPdif). The *a priori* measurement error for the commonly observed depth phases (pP, sP, pS, sS and pwP) is set to 1.3 s, while the remaining depth phases (pPKP, sPKP, pSKS, sSKS branches and pPb, sPb, sSb, pPn, sPn, sSn) have the measurement error estimate set to 1.8 s. We set the measurement error estimate to 2.5 s for the less reliable depth phases (pPg, sPg, sSg, pPdif, pSdif, sPdif and sSdif). Note that we also allow for distance-dependent measurement errors. For instance, to account for possible phase identification errors at far-regional distances the *a priori* measurement error for Pn and P is increased from 0.8 s to 1.2 s and for Sn and S from 1.5 s to 1.8 s between 15° and 28°. The measurement errors between 40° and 180° are set to 1.3 s and 1.8 s for the prominent PP and SS arrivals respectively, but they are increased to 1.8 s and 2.5 s between 25° and 40°.

The relative weighting scheme (Figure 10.2) described above ensures that arrivals picked less reliably or prone to phase identification errors are down-weighted in the location algorithm. Since the ISC works with reported parametric data with wildly varying quality, we opted for a rather conservative set of *a priori* measurement error estimates.

Correlated Travel-Time Prediction Error Structure

Most location algorithms, either linearised or non-linear, assume that all observational errors are independent. This assumption is violated when the separation between stations is less than the scale length of local velocity heterogeneities. When correlated travel-time prediction errors are present, the data covariance matrix is no longer diagonal, and the redundancy in the observations reduces the effective number of degrees of freedom. Thus, ignoring the correlated error structure inevitably results in underestimated location uncertainty estimates. For events located by an unbalanced seismic network this may also lead to a biased location estimate. *Chang et al.* (1983) demonstrated that accounting for correlated error structure in a linearised location algorithm is relatively straightforward once an estimate of the non-diagonal data covariance matrix is available. To determine the data covariance matrix we follow the approach described by *Bondár and McLaughlin* (2009b). They assume that the similarity between ray paths is well approximated by the station separation. This simplifying assumption allows for the estimation of covariances between station pairs from a generic P variogram model derived from ground truth residuals. Because the overwhelming number of phases in the ISC Bulletin is teleseismic P, we expect that the generic variogram model will perform reasonably well anywhere on the globe.

Since in this representation the covariances depend only on station separations, the covariance matrix (and its inverse) needs to be calculated only once. We assume that different phases owing to the different ray paths they travel along as well as station pairs with a separation larger than 1000 km are uncorrelated. Hence, the data covariance matrix is a sparse, block-diagonal matrix. Furthermore, if the stations in



each phase block are ordered by their nearest neighbour distance, the phase blocks themselves become block-diagonal. To reduce the computational time of inverting large matrices we exploit the inherent block-diagonal structure by inverting the covariance matrix block-by-block. The *a priori* measurement error variances are added to the diagonal of the data covariance matrix.

Depth Resolution

In principle, depth can be resolved if there is a mixture of upgoing and downgoing waves emanating from the source, that is, if there are stations covering the distance range where the vertical partial derivative of the travel-time of the first-arriving phase changes sign (local networks), or if there are phases with vertical slowness of opposite sign (depth phases). Core reflections, such as PcP, and to a lesser extent, secondary phases (S in particular) could also help in resolving the depth.

We developed a number of criteria to test whether the reported data for an event have sufficient depth resolution:

- local network: one or more stations within 0.2° with time-defining phases
- depth phases: five or more time-defining depth phases reported by at least two agencies (to reduce a chance of misinterpretation by a single inexperienced analyst)
- core reflections: five or more time-defining core reflections (PcP, ScS) reported by at least two agencies
- local/near regional S: five or more time-defining S and P pairs within 3°

We attempt a free-depth solution if any of the above criteria are satisfied; otherwise we fix the depth to a default depth dependent on the epicentre location. The default depth grid was derived from the EHB (*Engdahl et al.*, 1998) free-depth solutions, including the fixed-depth EHB earthquakes that were flagged as having reliable depth estimate (personal communication with Bob Engdahl), as well as from free-depth solutions obtained by the new locator when locating the entire ISC Bulletin data-set. As Figure 10.3 indicates, the default depth grid provides a reasonable depth estimate where seismicity is well established. Note that the depths of known anthropogenic events and landslides are fixed to the surface.

Depth-Phase Stack

While we use depth phases directly in the location, the depth-phase stacking method (*Murphy and Barker*, 2006) provides an independent means to obtain robust depth estimates. Because the depth obtained from the depth-phase stacking method implicitly depends on the epicentre itself, we perform the depth-phase stack only twice: first, with respect to the initial location in order to obtain a reasonable starting point for the depth in the grid search described in the following section; second, with respect to the final location to obtain the final estimate for the depth-phase constrained depth.

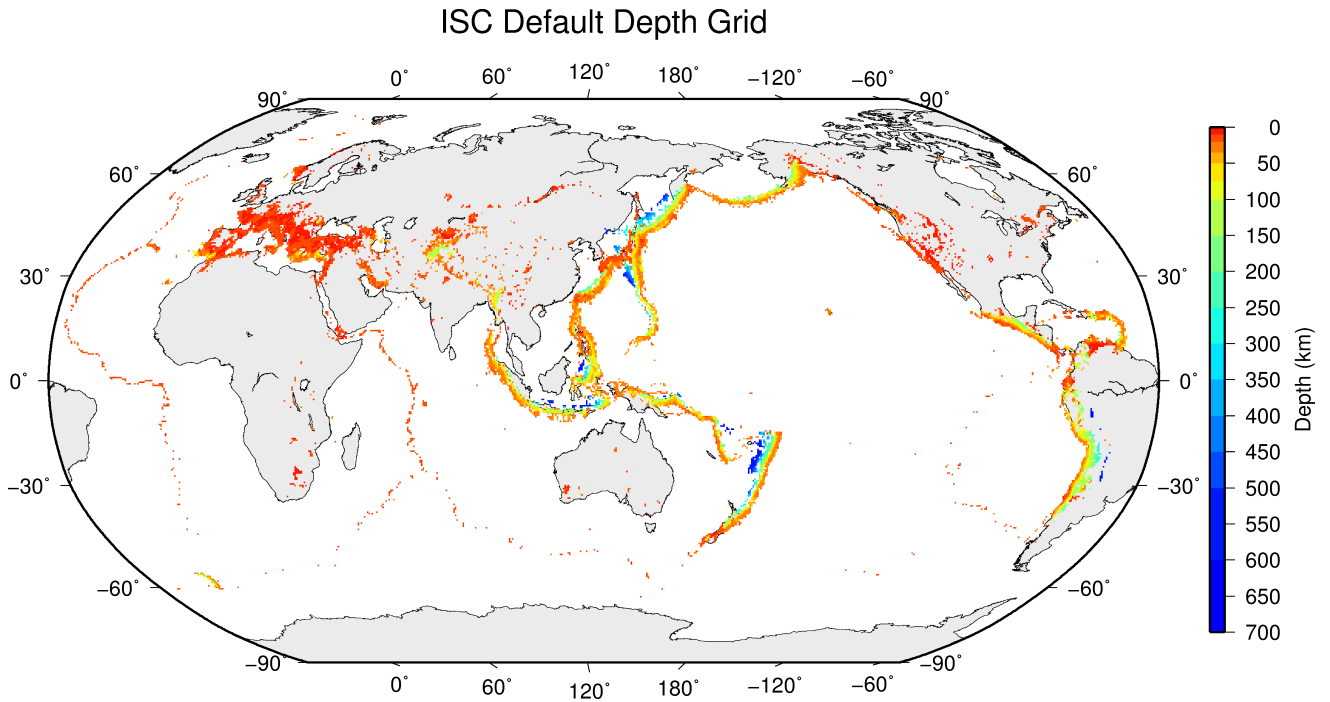


Figure 10.3: Default depths on a 0.5×0.5 degree grid derived from EHB free-depth solutions and EHB events flagged as reliable depth, as well as free-depth solutions from the entire ISC Bulletin located with the new locator.

Initial Hypocentre

For poorly recorded events the reported hypocentres may exhibit a large scatter and they could suffer from large location errors, especially if they are only recorded teleseismically. In order to obtain a good initial hypocentre guess for the linearised location algorithm we employ the Neighbourhood Algorithm (NA) (Sambridge, 1999; Sambridge and Kennett, 2001). NA is a nonlinear grid search method capable of exploring a large search space and rapidly closing in on the global optimum. Kennett (2006) discusses in detail the NA algorithm and its use for locating earthquakes.

We perform a search around the median of reported hypocentre parameters with a generously defined search region – within a 2° radius circle around the median epicentre, 10 s around the median origin time and 150 km around the median reported depth. These default search parameters were obtained by trial-and-error runs to achieve a compromise between execution time and allowance for gross errors in the median reported hypocentre parameters. Note that if our test for depth resolution fails, we fix the depth to the region-dependent default depth. The initial hypocentre estimate will be the one with the smallest L1-norm misfit among the NA trial hypocentres. Once close to the global optimum, we proceed with the linearised location algorithm to obtain the final solution and corresponding formal uncertainties.

Iterative Linearised Location Algorithm

We adopt the location algorithm described in detail in Bondár and McLaughlin (2009b). Recall that in the presence of correlated travel-time prediction errors the data covariance matrix is no longer diagonal. Using the singular value decomposition of the data covariance matrix we construct a projection matrix

that orthogonalises the data set and projects redundant observations into the null space. In other words, we solve the inversion problem in the eigen coordinate system in which the transformed observations are independent.

The model covariance matrix yields the four-dimensional error ellipsoid whose projections provide the two-dimensional error ellipse and one-dimensional errors for depth and origin time. These uncertainties are scaled to the 90% confidence level. Note that since we projected the system of equations into the eigen coordinate system, the number of independent observations is less than the total number of observations. Hence, the estimated location error ellipses necessarily become larger, providing a more realistic representation of the location uncertainties. The major advantage of this approach is that the projection matrix is calculated only once for each event location.

Validation Tests

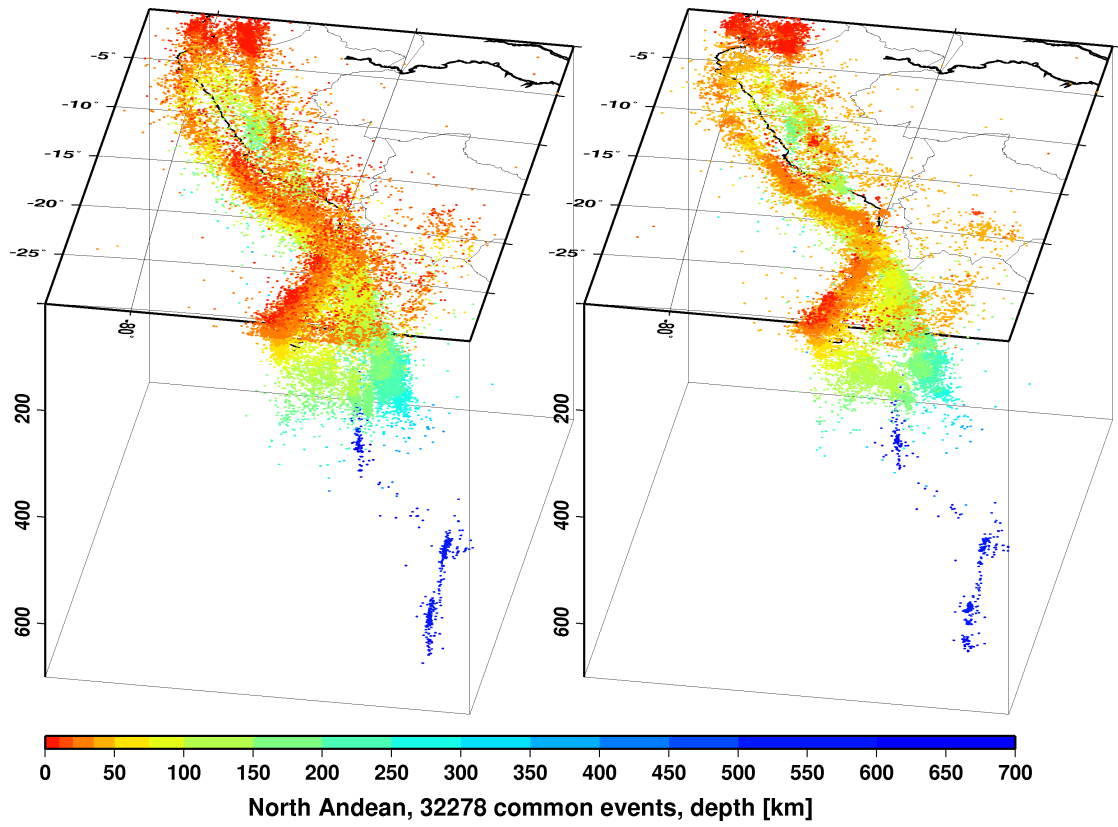
To demonstrate improvements due to the new location procedures, we located some 7,200 GT0-5 events in the IASPEI Reference Event List (*Bondár and McLaughlin, 2009a*) both with the old ISC locator (which constitutes the baseline) and with the new location algorithm. We also located the entire (1960-2010) ISC Bulletin, including four years of the International Seismological Summary (ISS, the predecessor of the ISC) catalogue (*Villaseñor and Engdahl, 2005; 2007*).

The location of GT events demonstrated that the new ISC location algorithm provides small but consistent location improvements, considerable improvements in depth determination and significantly more accurate formal uncertainty estimates. Even using a 1-D model and a variogram model that fits teleseismic observations we could achieve realistic uncertainty estimates, as the 90% confidence error ellipses cover the true locations 80-85% of the time. The default depth grid provides reasonable depth estimates where there is seismicity. We have shown that the location and depth accuracy obtained by the new algorithm matches or surpasses the EHB accuracy.

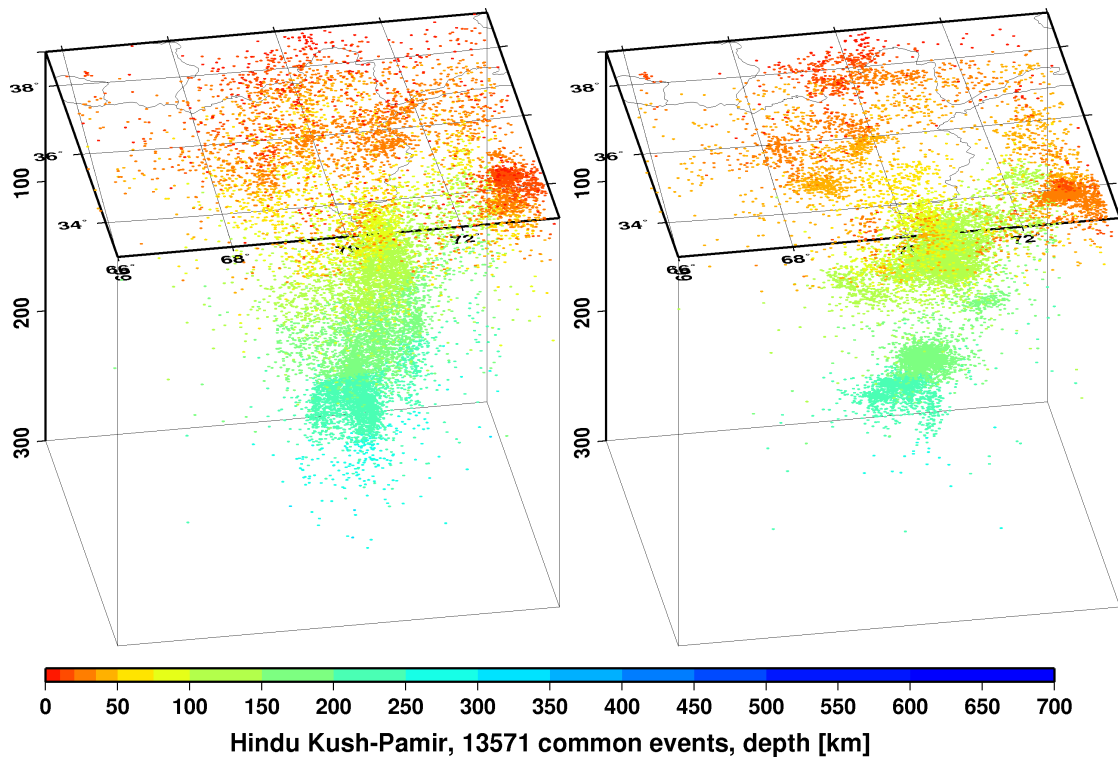
We noted above that the location improvements for the ground truth events are consistent, but minor. This is not surprising as most of the events in the IASPEI Reference Event List are very well-recorded with a small azimuthal gap and dominated by P-type phases. In these circumstances we could expect significant location improvements only for heavily unbalanced networks where large numbers of correlated ray paths conspire to introduce location bias. On the other hand, the ISC Bulletin represents a plethora of station configurations ranging from reasonable to the most unfavourable network geometries. Hence, we could expect more dramatic location improvements when locating the entire ISC Bulletin. Although in this case we cannot measure the improvement in location accuracy due to the lack of ground truth information, we show that with the new locator we obtain significantly better clustering of event locations (Figure 10.4), thus providing an improved view of the seismicity of the Earth.

Magnitude Calculation

Currently the ISC locator calculates body and surface wave magnitudes. MS is calculated for shallow events (depth < 60 km) only. At least three station magnitudes are required for a network (mb or MS) magnitude. The network magnitude is defined as the median of the station magnitudes, and its



(a)



(b)

Figure 10.4: Comparison of seismicity maps for common events in the reviewed ISC Bulletin (old locator, left) and the located ISC Bulletin (new locator, right) for the North Andean (a) and Hindu Kush - Pamir regions (b). The events are better clustered when located with the new locator.

uncertainty is defined as the standard median absolute deviation (SMAD) of the alpha-trimmed ($\alpha = 20\%$) station magnitudes.

The station magnitude is defined as the median of reading magnitudes for a station. The reading magnitude is defined as the magnitude computed from the maximal $\log(A/T)$ in a reading. Amplitude magnitudes are calculated for each reported amplitude-period pair.

Body-Wave Magnitudes

Body-wave magnitudes are calculated for each reported amplitude-period pair, provided that the phase is in the list of phases that can contribute to mb (P, pP, sP, AMB, IAmb, pmax), the station is between the epicentral distances $21 - 100^\circ$ and the period is less than 3 s.

A reading contains all parametric data reported by a single agency for an event at a station, and it may have several reported amplitude and periods. The amplitudes are measured as zero-to-peak values in nanometres. For each pair an amplitude mb is calculated.

$$mb_{amp} = \log(A/T) + Q(\Delta, h) - 3 \quad (10.1)$$

If no amplitude-period pairs are reported for a reading, the body-wave magnitude is calculated using the reported \logat values for $\log(A/T)$.

$$mb_{amp} = \logat + Q(\Delta, h) - 3 \quad (10.2)$$

where the magnitude attenuation $Q(\Delta, h)$ value is calculated using the Gutenberg-Richter tables (*Gutenberg and Richter, 1956*).

For each reading the ISC locator finds the reported amplitude-period pair for which A/T is maximal:

$$mb_{rd} = \log(\max(A/T)) + Q(\Delta, h) - 3 \quad (10.3)$$

Or, if no amplitude-period pairs were reported for the reading:

$$mb_{rd} = \max(\logat) + Q(\Delta, h) - 3 \quad (10.4)$$

Several agencies may report data from the same station. The station magnitude is defined as the median of the reading magnitudes for a station.

$$mb_{sta} = \text{median}(mb_{rd}) \quad (10.5)$$

Once all station mb values are determined, the station magnitudes are sorted and the lower and upper alpha percentiles are made non-defining. The network mb and its uncertainty are then calculated as the median and the standard median absolute deviation (SMAD) of the alpha-trimmed station magnitudes, respectively.

Surface-Wave Magnitudes

Surface-wave magnitudes are calculated for each reported amplitude-period pair, provided that the phase is in the list of phases that can contribute to MS (AMS , $IAMS_{20}$, LR , MLR , M , L), the station is between the epicentral distances $20 - 160^\circ$ and the period is between $10 - 60$ s.

For each reported amplitude-period pair MS is calculated using the Prague formula (*Vaněk et al.*, 1962). Amplitude MS is calculated for each component (Z, E, N) separately.

$$MS_{amp} = \log(A/T) + 1.66 * \log(\Delta) + 0.3 \quad (10.6)$$

To calculate the reading MS , the ISC locator first finds the reported amplitude-period pair for which A/T is maximal on the vertical component.

$$MS_Z = \log(\max(A_Z/T_Z)) + 1.66 * \log(\Delta) + 0.3 \quad (10.7)$$

Then it finds the $\max(A/T)$ for the E and N components for which the period measured on the horizontal components is within ± 5 s from the period measured on the vertical component.

$$MS_E = \log(\max(A_E/T_E)) + 1.66 * \log(\Delta) + 0.3 \quad (10.8)$$

$$MS_N = \log(\max(A_N/T_N)) + 1.66 * \log(\Delta) + 0.3 \quad (10.9)$$

The horizontal MS is calculated as

$$\max(A/T)_h = \begin{cases} \sqrt{2(\max(A_E/T_E))^2} & \text{if } MS_N \text{ does not exist} \\ \sqrt{(\max(A_E/T_E))^2 + (\max(A_N/T_N))^2} & \text{if } MS_E \text{ and } MS_N \text{ exist} \\ \sqrt{2(\max(A_N/T_N))^2} & \text{if } MS_E \text{ does not exist} \end{cases} \quad (10.10)$$

$$MS_H = \log(\max(A/T)_h) + 1.66 * \log(\Delta) + 0.3 \quad (10.11)$$

The reading MS is defined as

$$MS = \begin{cases} (MS_Z + MS_H)/2 & \text{if } MS_Z \text{ and } MS_H \text{ exist} \\ MS_H & \text{if } MS_Z \text{ does not exist} \\ MS_Z & \text{if } MS_H \text{ does not exist} \end{cases} \quad (10.12)$$

Several agencies may report data from the same station. The station magnitude is defined as the median of the reading magnitudes for a station.

$$MS_{sta} = \text{median}(MS_{rd}) \quad (10.13)$$

Once all station MS values are determined, the station magnitudes are sorted and the lower and upper alpha percentiles are made non-defining. The network MS and its uncertainty are calculated as the median and the standard median absolute deviation (SMAD) of the alpha-trimmed station magnitudes, respectively.

10.1.5 Review Process

Typically, for each month, the ISC analysts now review approximately 20% of the events in the ISC database, currently 3,500-5,000 per data month. This review is done about 24 months behind real time to allow for the comprehensive collection of data from networks and data centres worldwide.

Users of the ISC Bulletin can be assured that all ISC Bulletin events with an ISC hypocentre solution have been reviewed by the ISC analysts. Not all reviewed events will end up having an ISC hypocentre solution, but events that have not been reviewed are flagged accordingly.

An automatic process creates a monthly listing of the events for the analysts to review. The analysis is performed in batches: thus, events are generally not finalised one at a time, and a completed month of events is published after all the analysis is finished.

The first batch of editing involves careful examination of all events selected for review for the month. The entire month is then reprocessed incorporating the editing changes deemed necessary by the analysts. The analysts next review the same events again in a second pass through the data, checking for each event where there is a change that the result was as could be expected by comparing the revised solution against the initial solution. When the analysts are satisfied with an event, it is no longer revised in a subsequent pass but analysis continues in several passes until all events are considered satisfactory.

The analysts initially print the entire monthly listing, which is split into sections each with about 150 events. Each event, uniquely identified in the monthly printout, shows the reported hypocentres, magnitudes and phase arrivals grouped and associated for the event, as well as an ISC solution of hypocentre, if there is one, along with quality metrics, error estimates, redetermined magnitudes and phase arrival-time residuals. Ancillary information including the geographic region and reported macroseismic observations is also present in the listing for each pass.

The analysts have the capability to execute a variety of commands that can be used to merge or split events, to move phase arrivals or hypocentres from one event to another or to modify the reported phase names. Each of these changes initiates a new revision of the relevant events and ISC hypocentre solutions. There are also several commands to change the starting depth or location in the location algorithm.

The main tasks in reviewing the ISC Bulletin are to:

1. Check that the grouping of hypocentres and association of phase arrivals is appropriate.
2. Check that the depth and location is appropriate for the region and reported phase arrivals.
3. Check that no data are missing for an event, given the region and magnitude, and that included data are appropriate.

4. Examine the phase arrival-time residuals to check that the ISC hypocentre solution is appropriate.
5. Look for outliers in the observations and for misassociated phases.

As well as examining each event closely, it is also important to scan the hypocentres and phase arrivals of adjacent events, close in time and space, to ensure that there is uniformity in the composition of the events. In some cases, two events should be merged into one event, as apparent in some other case. In other cases, one apparent event needs to be split into two events, when the automatic grouping has erroneously created one event with more than one reported hypocentre out of the observations for two real events that are distinct but closely occurring.

Misassociated phase arrivals are returned to the unassociated data stream, if not immediately placed by the analyst in another event where they belong. These unassociated phases are then available to be associated with some other event if the time and location is appropriate. The analysts also check that no phase is associated to more than one event.

Towards the end of the monthly analysis, the ISC ‘Search’ procedure runs, attempting to build events from the remaining set of unassociated phase arrivals. The algorithm is based on the methodology of *Engdahl and Gunst* (1966). Candidate events are validated or rejected by attempting to find ISC hypocentres for them using the ISC locator. The surviving events are then reviewed. Those events with phase arrival observations reported by stations from at least two networks are added to the ISC Bulletin if the solutions meet the standards set by the ISC analysts. These events have only an ISC determination of hypocentre.

At the end of analysis for a data month, a set of final checks is run for quality control, with the results reviewed by an analyst and the defects rectified. These are checks for inconsistencies and errors to ensure the general integrity of the ISC Bulletin.

10.1.6 History of Operational Changes

- From data-month January 2001 onwards, both P and S groups of arrival times are used in location.
- From data-month September 2002 onwards, the printed ISC Bulletins have been generated directly from the ISC Relational Database.
- From data-month October 2002, a new location program ISCloc has been used in operations. Also, the IASPEI standard phase list has now been adopted by the ISC. Please see Section 10.2.1 for details.
- From data-month January 2003 onwards, an updated regionalisation scheme has been adopted (*Young et al.*, 1996).
- From data-month January 2006 the ISC hypocentres are computed using the *ak135* earth velocity model (*Kennett et al.*, 1995) and then reviewed by ISC seismologists. The ISC still produces the hypocentre solutions based on Jeffreys-Bullen travel time tables (agency code ISCJB), yet these solutions are no longer reviewed.

Currently, the ISC is re-computing the entire ISC Bulletin as part of the Rebuild Project using *ak135* and the new location program (Section 10.1.4) in order to assure homogeneity and consistency of the data in the ISC Bulletin.

- From data-month January 2009, a new location program (*Bondár and Storchak, 2011*) has been used in operations. The new program uses all predicted *ak135* phases and accounts for correlated model errors. An overview of the location algorithm is provided in this volume (Section 10.1.4).

10.2 IASPEI Standards

10.2.1 Standard Nomenclature of Seismic Phases

The following list of seismic phases was approved by the IASPEI Commission on Seismological Observation and Interpretation (CoSOI) and adopted by IASPEI on 9th July 2003. More details can be found in *Storchak et al. (2003)* and *Storchak et al. (2011)*. Ray paths for some of these phases are shown in Figures 10.5–10.10.

Crustal Phases

Pg	At short distances, either an upgoing P wave from a source in the upper crust or a P wave bottoming in the upper crust. At larger distances also, arrivals caused by multiple P-wave reverberations inside the whole crust with a group velocity around 5.8 km/s.
Pb	Either an upgoing P wave from a source in the lower crust or a P wave bottoming in the lower crust (alt: P*)
Pn	Any P wave bottoming in the uppermost mantle or an upgoing P wave from a source in the uppermost mantle
PnPn	Pn free-surface reflection
PgPg	Pg free-surface reflection
PmP	P reflection from the outer side of the Moho
PmPN	PmP multiple free surface reflection; <i>N</i> is a positive integer. For example, PmP2 is PmPPmP.
PmS	P to S reflection/conversion from the outer side of the Moho
Sg	At short distances, either an upgoing S wave from a source in the upper crust or an S wave bottoming in the upper crust. At larger distances also, arrivals caused by superposition of multiple S-wave reverberations and SV to P and/or P to SV conversions inside the whole crust.
Sb	Either an upgoing S wave from a source in the lower crust or an S wave bottoming in the lower crust (alt: S*)
Sn	Any S wave bottoming in the uppermost mantle or an upgoing S wave from a source in the uppermost mantle
SnSn	Sn free-surface reflection
SgSg	Sg free-surface reflection
SmS	S reflection from the outer side of the Moho
SmSN	SmS multiple free-surface reflection; <i>N</i> is a positive integer. For example, SmS2 is SmSSmS.
SmP	S to P reflection/conversion from the outer side of the Moho
Lg	A wave group observed at larger regional distances and caused by superposition of multiple S-wave reverberations and SV to P and/or P to SV conversions inside the whole crust. The maximum energy travels with a group velocity of approximately 3.5 km/s
Rg	Short-period crustal Rayleigh wave

Mantle Phases

P	A longitudinal wave, bottoming below the uppermost mantle; also an upgoing longitudinal wave from a source below the uppermost mantle
PP	Free-surface reflection of P wave leaving a source downward
PS	P, leaving a source downward, reflected as an S at the free surface. At shorter distances the first leg is represented by a crustal P wave.
PPP	Analogous to PP
PPS	PP which is converted to S at the second reflection point on the free surface; travel time matches that of PSP
PSS	PS reflected at the free surface
PcP	P reflection from the core-mantle boundary (CMB)
PcS	P converted to S when reflected from the CMB
PcPN	PcP reflected from the free surface $N - 1$ times; N is a positive integer. For example PcP2 is PcPPcP.
Pz+P	(alt: PzP) P reflection from outer side of a discontinuity at depth z ; z may be a positive numerical value in km. For example, P660+P is a P reflection from the top of the 660 km discontinuity.
Pz-P	P reflection from inner side of a discontinuity at depth z . For example, P660-P is a P reflection from below the 660 km discontinuity, which means it is precursory to PP.
Pz+S	(alt: PzS) P converted to S when reflected from outer side of discontinuity at depth z
Pz-S	P converted to S when reflected from inner side of discontinuity at depth z
PScS	P (leaving a source downward) to ScS reflection at the free surface
Pdif	P diffracted along the CMB in the mantle (old: Pdiff)
S	Shear wave, bottoming below the uppermost mantle; also an upgoing shear wave from a source below the uppermost mantle
SS	Free-surface reflection of an S wave leaving a source downward
SP	S, leaving a source downward, reflected as P at the free surface. At shorter distances the second leg is represented by a crustal P wave.
SSS	Analogous to SS
SSP	SS converted to P when reflected from the free surface; travel time matches that of SPS
SPP	SP reflected at the free surface
ScS	S reflection from the CMB
ScP	S converted to P when reflected from the CMB
ScSN	ScS multiple free-surface reflection; N is a positive integer. For example ScS2 is ScSScS.
Sz+S	S reflection from outer side of a discontinuity at depth z ; z may be a positive numerical value in km. For example S660+S is an S reflection from the top of the 660 km discontinuity. (alt: SzS)
Sz-S	S reflection from inner side of discontinuity at depth z . For example, S660-S is an S reflection from below the 660 km discontinuity, which means it is precursory to SS.
Sz+P	(alt: SzP) S converted to P when reflected from outer side of discontinuity at depth z
Sz-P	S converted to P when reflected from inner side of discontinuity at depth z
ScSP	ScS to P reflection at the free surface
Sdif	S diffracted along the CMB in the mantle (old: Sdiff)

Core Phases

PKP	Unspecified P wave bottoming in the core (alt: P')
PKPab	P wave bottoming in the upper outer core; ab indicates the retrograde branch of the PKP caustic (old: PKP2)
PKPbc	P wave bottoming in the lower outer core; bc indicates the prograde branch of the PKP caustic (old: PKP1)
PKPdf	P wave bottoming in the inner core (alt: PKIKP)

PKPpre	A precursor to PKPdf due to scattering near or at the CMB (old: PKhKP)
PKPdif	P wave diffracted at the inner core boundary (ICB) in the outer core
PKS	Unspecified P wave bottoming in the core and converting to S at the CMB
PKSab	PKS bottoming in the upper outer core
PKSbc	PKS bottoming in the lower outer core
PKSdf	PKS bottoming in the inner core
P'P'	Free-surface reflection of PKP (alt: PKPPKP)
P'N	PKP reflected at the free surface $N - 1$ times; N is a positive integer. For example, P'3 is P'P'P'. (alt: PKPN)
P'z-P'	PKP reflected from inner side of a discontinuity at depth z outside the core, which means it is precursory to P'P'; z may be a positive numerical value in km
P'S'	(alt: PKPSKS) PKP converted to SKS when reflected from the free surface; other examples are P'PKS, P'SKP
PS'	P (leaving a source downward) to SKS reflection at the free surface (alt: PSKS)
PKKP	Unspecified P wave reflected once from the inner side of the CMB
PKKPab	PKKP bottoming in the upper outer core
PKKPbc	PKKP bottoming in the lower outer core
PKKPdf	PKKP bottoming in the inner core
PNKP	P wave reflected $N - 1$ times from inner side of the CMB; N is a positive integer.
PKKPpre	A precursor to PKKP due to scattering near the CMB
PKiKP	P wave reflected from the inner core boundary (ICB)
PKNIKP	P wave reflected $N - 1$ times from the inner side of the ICB
PKJKP	P wave traversing the outer core as P and the inner core as S
PKKS	P wave reflected once from inner side of the CMB and converted to S at the CMB
PKKSab	PKKS bottoming in the upper outer core
PKKSbc	PKKS bottoming in the lower outer core
PKKSdf	PKKS bottoming in the inner core
PcPP'	PcP to PKP reflection at the free surface; other examples are PcPS', PcSP', PcSS', PcPSKP, PcSSKP. (alt: PcPPKP)
SKS	unspecified S wave traversing the core as P (alt: S')
SKSac	SKS bottoming in the outer core
SKSdf	SKS bottoming in the inner core (alt: SKIKS)
SPdifKS	SKS wave with a segment of mantleside Pdif at the source and/or the receiver side of the ray path (alt: SKPdifS)
SKP	Unspecified S wave traversing the core and then the mantle as P
SKPab	SKP bottoming in the upper outer core
SKPbc	SKP bottoming in the lower outer core
SKPdf	SKP bottoming in the inner core
S'S'	Free-surface reflection of SKS (alt: SKSSKS)
S'N	SKS reflected at the free surface $N - 1$ times; N is a positive integer
S'z-S'	SKS reflected from inner side of discontinuity at depth z outside the core, which means it is precursory to S'S'; z may be a positive numerical value in km.
S'P'	(alt: SKSPKP) SKS converted to PKP when reflected from the free surface; other examples are S'SKP, S'PKS.
S'P	(alt: SKSP) SKS to P reflection at the free surface
SKKS	Unspecified S wave reflected once from inner side of the CMB
SKKSac	SKKS bottoming in the outer core
SKKSdf	SKKS bottoming in the inner core
SNKS	S wave reflected $N - 1$ times from inner side of the CMB; N is a positive integer.
SKiKS	S wave traversing the outer core as P and reflected from the ICB
SKJKS	S wave traversing the outer core as P and the inner core as S
SKKP	S wave traversing the core as P with one reflection from the inner side of the CMB and then continuing as P in the mantle

SKKPab	SKKP bottoming in the upper outer core
SKKPbc	SKKP bottoming in the lower outer core
SKKPdf	SKKP bottoming in the inner core
ScSS'	ScS to SKS reflection at the free surface; other examples are ScPS', ScSP', ScPP', ScSSKP, ScPSKP. (alt: ScSSKS)

Near-source Surface reflections (Depth Phases)

pPy	All P-type onsets (<i>Py</i>), as defined above, which resulted from reflection of an upgoing P wave at the free surface or an ocean bottom. WARNING: The character <i>y</i> is only a wild card for any seismic phase, which could be generated at the free surface. Examples are pP, pPKP, pPP, pPcP, etc.
sPy	All <i>Py</i> resulting from reflection of an upgoing S wave at the free surface or an ocean bottom; for example, sP, sPKP, sPP, sPcP, etc.
pSy	All S-type onsets (<i>Sy</i>), as defined above, which resulted from reflection of an upgoing P wave at the free surface or an ocean bottom; for example, pS, pSKS, pSS, pScP, etc.
sSy	All <i>Sy</i> resulting from reflection of an upgoing S wave at the free surface or an ocean bottom; for example, sSn, sSS, sScS, sSdif, etc.
pwPy	All <i>Py</i> resulting from reflection of an upgoing P wave at the ocean's free surface
pmPy	All <i>Py</i> resulting from reflection of an upgoing P wave from the inner side of the Moho

Surface Waves

L	Unspecified long-period surface wave
LQ	Love wave
LR	Rayleigh wave
G	Mantle wave of Love type
GN	Mantle wave of Love type; <i>N</i> is integer and indicates wave packets traveling along the minor arcs (odd numbers) or major arc (even numbers) of the great circle
R	Mantle wave of Rayleigh type
RN	Mantle wave of Rayleigh type; <i>N</i> is integer and indicates wave packets traveling along the minor arcs (odd numbers) or major arc (even numbers) of the great circle
PL	Fundamental leaking mode following P onsets generated by coupling of P energy into the waveguide formed by the crust and upper mantle SPL S wave coupling into the PL waveguide; other examples are SSPL, SSSPL.

Acoustic Phases

H	A hydroacoustic wave from a source in the water, which couples in the ground
HPg	H phase converted to Pg at the receiver side
HSg	H phase converted to Sg at the receiver side
HRg	H phase converted to Rg at the receiver side
I	An atmospheric sound arrival which couples in the ground
IPg	I phase converted to Pg at the receiver side
ISg	I phase converted to Sg at the receiver side
IRg	I phase converted to Rg at the receiver side
T	A tertiary wave. This is an acoustic wave from a source in the solid earth, usually trapped in a low-velocity oceanic water layer called the SOFAR channel (SOund Fixing And Ranging).
TPg	T phase converted to Pg at the receiver side
TSg	T phase converted to Sg at the receiver side
TRg	T phase converted to Rg at the receiver side

Amplitude Measurement Phases

The following set of amplitude measurement names refers to the IASPEI Magnitude Standard (see www.iaspei.org/commissions/CSOI/Summary_of_WG_recommendations.pdf)

compliance to which is indicated by the presence of leading letter I. The absence of leading letter I indicates that a measurement is non-standard. Letter A indicates a measurement in *nm* made on a displacement seismogram, whereas letter V indicates a measurement in *nm/s* made on a velocity seismogram.

IAML	Displacement amplitude measured according to the IASPEI standard for local magnitude <i>ML</i>
IAMs_20	Displacement amplitude measured according to IASPEI standard for surface-wave magnitude <i>MS</i> (20)
IVMs_BB	Velocity amplitude measured according to IASPEI standard for broadband surface-wave magnitude <i>MS</i> (<i>BB</i>)
IAMB	Displacement amplitude measured according to IASPEI standard for short-period teleseismic body-wave magnitude <i>mb</i>
IVmB_BB	Velocity amplitude measured according to IASPEI standard for broadband teleseismic body-wave magnitude <i>mB</i> (<i>BB</i>)
AX_IN	Displacement amplitude of phase of type <i>X</i> (e.g., PP, S, etc), measured on an instrument of type IN (e.g., SP - short-period, LP - long-period, BB - broadband)
VX_IN	Velocity amplitude of phase of type <i>X</i> and instrument of type IN (as above)
A	Unspecified displacement amplitude measurement
V	Unspecified velocity amplitude measurement
AML	Displacement amplitude measurement for nonstandard local magnitude
AMs	Displacement amplitude measurement for nonstandard surface-wave magnitude
Amb	Displacement amplitude measurement for nonstandard short-period body-wave magnitude
AmB	Displacement amplitude measurement for nonstandard medium to long-period body-wave magnitude
END	Time of visible end of record for duration magnitude

Unidentified Arrivals

x	unidentified arrival (old: i, e, NULL)
rx	unidentified regional arrival (old: i, e, NULL)
tx	unidentified teleseismic arrival (old: i, e, NULL)
Px	unidentified arrival of P type (old: i, e, NULL, (P), P?)
Sx	unidentified arrival of S type (old: i, e, NULL, (S), S?)

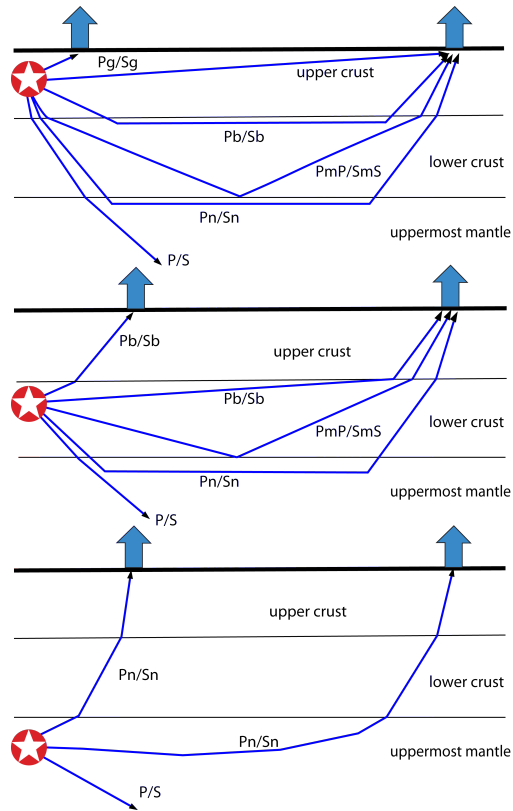


Figure 10.5: Seismic ‘crustal phases’ observed in the case of a two-layer crust in local and regional distance ranges ($0^\circ < D < \text{about } 20^\circ$) from the seismic source in the: upper crust (top); lower crust (middle); and uppermost mantle (bottom).

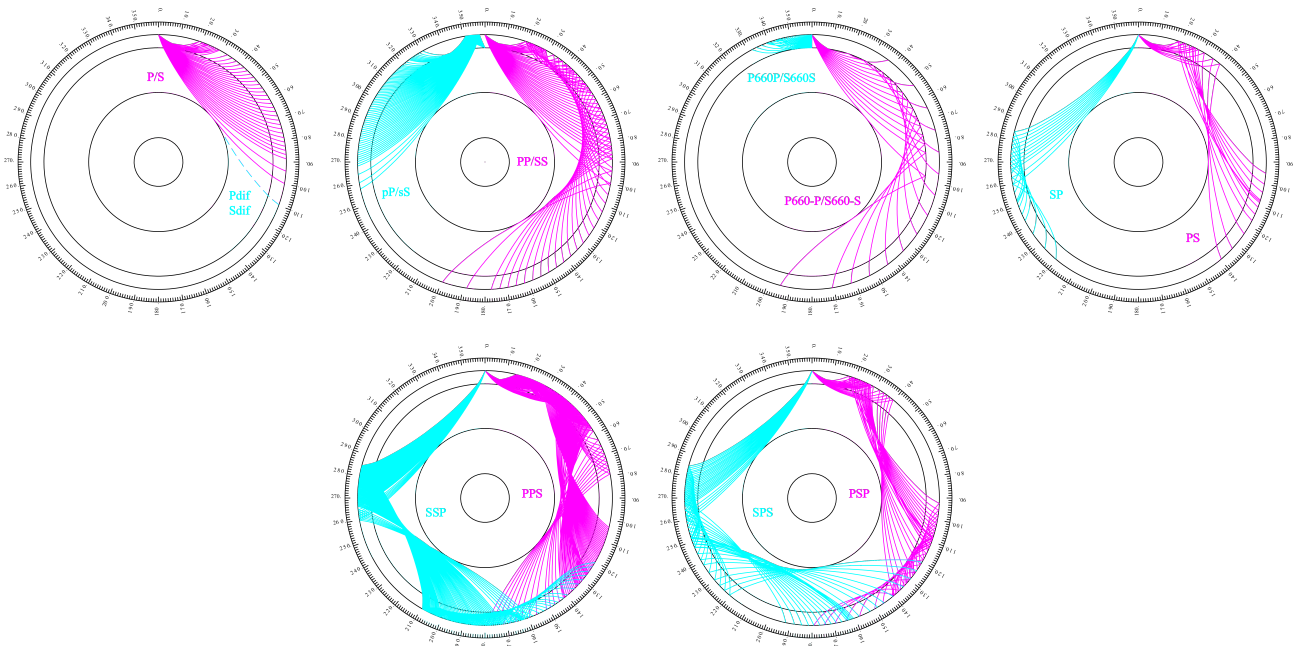


Figure 10.6: Mantle phases observed at the teleseismic distance range $D > \text{about } 20^\circ$.

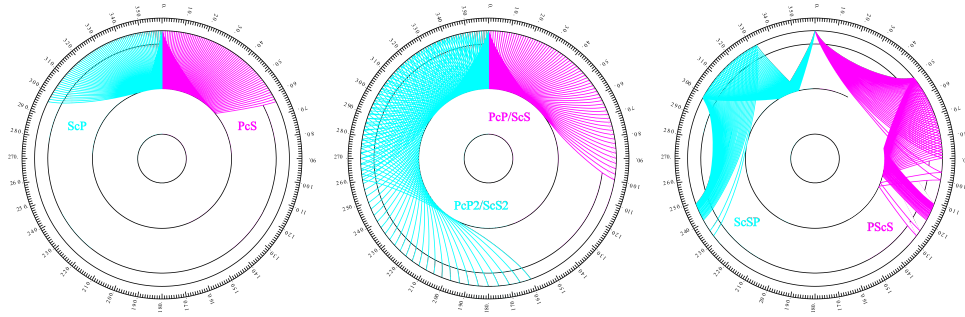


Figure 10.7: Reflections from the Earth's core.

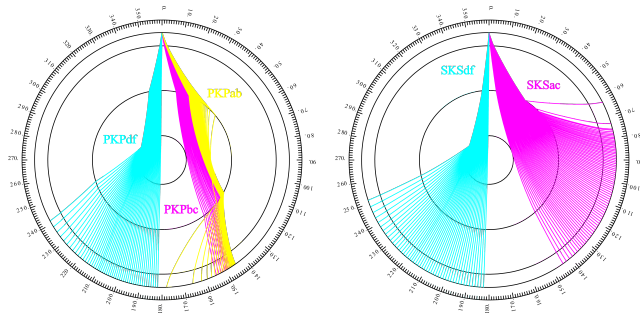


Figure 10.8: Seismic rays of direct core phases.

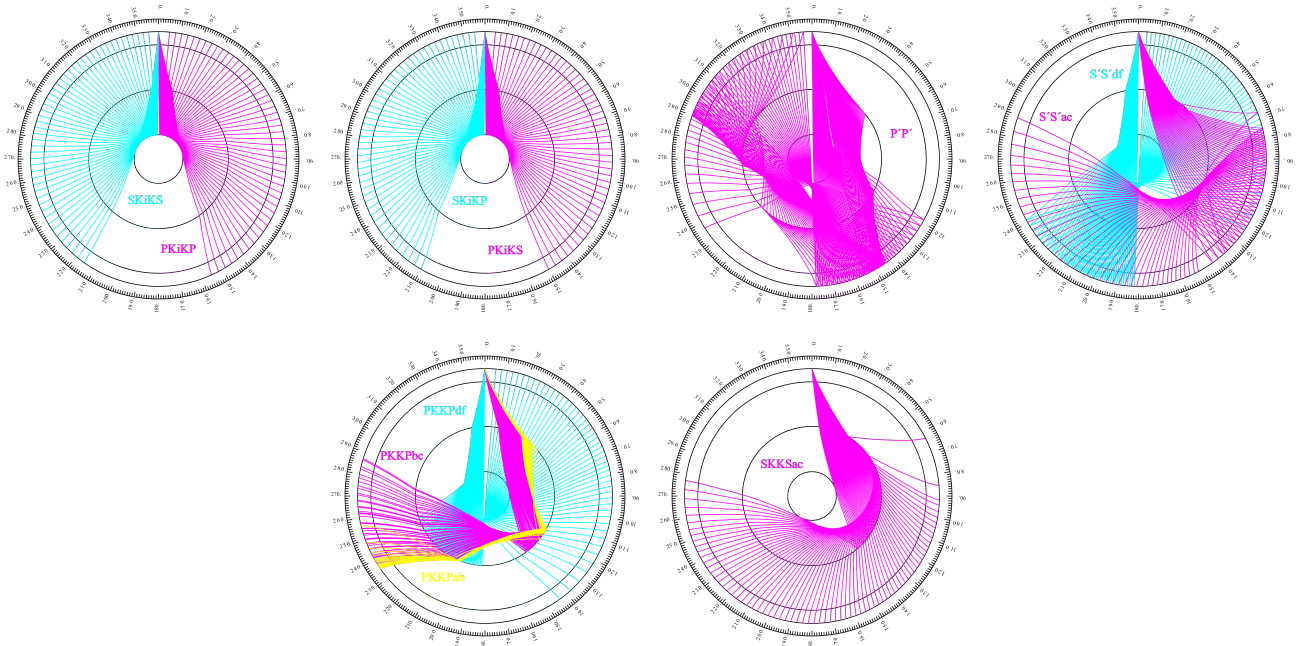


Figure 10.9: Seismic rays of single-reflected core phases.

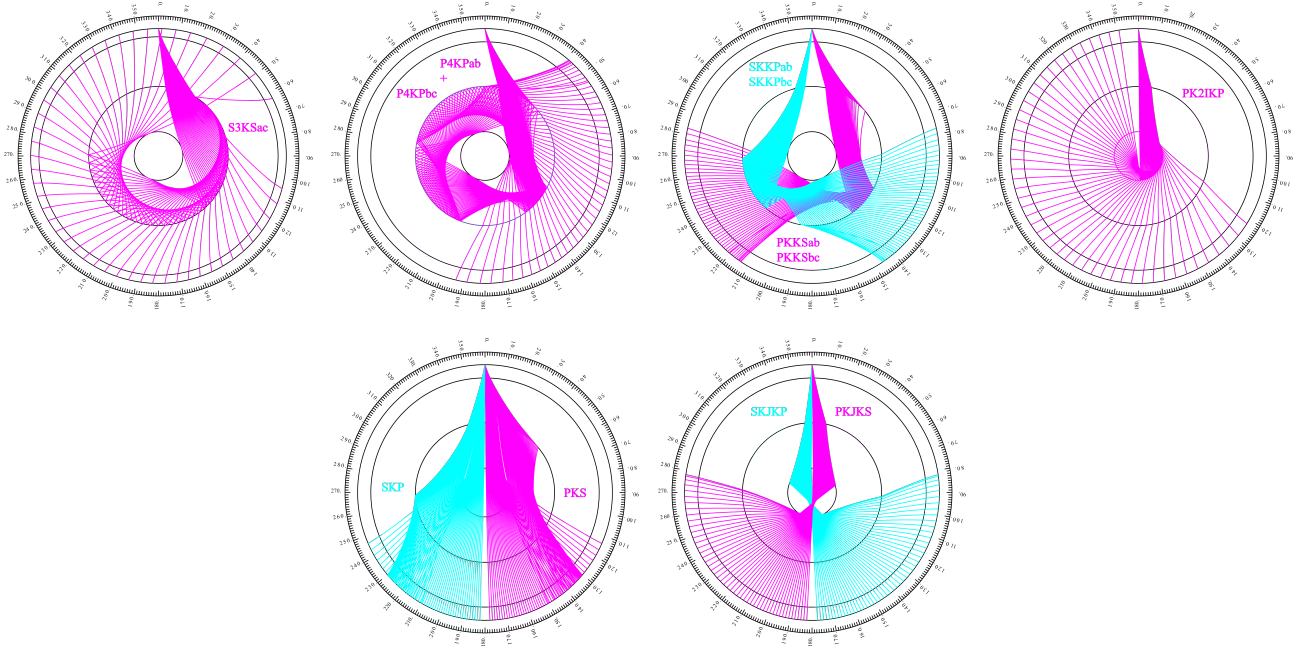


Figure 10.10: Seismic rays of multiple-reflected and converted core phases.

10.2.2 Flinn-Engdahl Regions

The Flinn-Engdahl regions were first proposed by *Flinn and Engdahl* (1965), with the standard defined by *Flinn et al.* (1974). The latest version of the schema, published by *Young et al.* (1996), divides the Earth into 50 seismic regions (Figure 10.11), which are further subdivided producing a total of 754 geographical regions (listed below). The geographic regions are numbered 1 to 757 with regions 172, 299 and 550 no longer in use. The boundaries of these regions are defined at one-degree intervals.

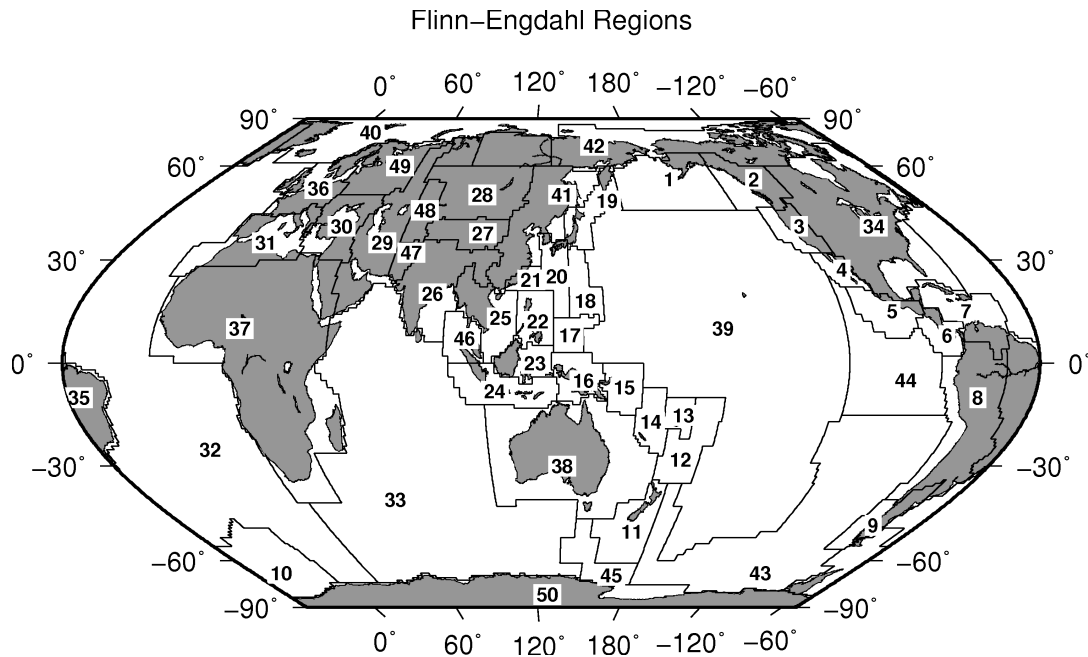


Figure 10.11: Map of all Flinn-Engdahl seismic regions.

Seismic Region 1

Alaska-Aleutian Arc

1. Central Alaska
2. Southern Alaska
3. Bering Sea
4. Komandorsky Islands region
5. Near Islands
6. Rat Islands
7. Andreanof Islands
8. Pribilof Islands
9. Fox Islands
10. Unimak Island region
11. Bristol Bay
12. Alaska Peninsula
13. Kodiak Island region
14. Kenai Peninsula
15. Gulf of Alaska
16. South of Aleutian Islands
17. South of Alaska

Seismic Region 2

Eastern Alaska to Vancouver Island

18. Southern Yukon Territory
19. Southeastern Alaska
20. Off coast of southeastern Alaska
21. West of Vancouver Island
22. Queen Charlotte Islands region
23. British Columbia
24. Alberta
25. Vancouver Island region
26. Off coast of Washington
27. Near coast of Washington
28. Washington-Oregon border region
29. Washington

Seismic Region 3

California-Nevada Region

30. Off coast of Oregon
31. Near coast of Oregon
32. Oregon
33. Western Idaho
34. Off coast of northern California
35. Near coast of northern California
36. Northern California
37. Nevada
38. Off coast of California
39. Central California
40. California-Nevada border region
41. Southern Nevada
42. Western Arizona
43. Southern California
44. California-Arizona border region
45. California-Baja California border region
46. Western Arizona-Sonora border

region

Seismic Region 4

Lower California and Gulf of California

47. Off west coast of Baja California
48. Baja California
49. Gulf of California
50. Sonora
51. Off coast of central Mexico
52. Near coast of central Mexico

Seismic Region 5

Mexico-Guatemala Area

53. Revilla Gigedo Islands region
54. Off coast of Jalisco
55. Near coast of Jalisco
56. Near coast of Michoacan
57. Michoacan
58. Near coast of Guerrero
59. Guerrero
60. Oaxaca
61. Chiapas
62. Mexico-Guatemala border region
63. Off coast of Mexico
64. Off coast of Michoacan
65. Off coast of Guerrero
66. Near coast of Oaxaca
67. Off coast of Oaxaca
68. Off coast of Chiapas
69. Near coast of Chiapas
70. Guatemala
71. Near coast of Guatemala
730. Northern East Pacific Rise

Seismic Region 6

Central America

72. Honduras
73. El Salvador
74. Near coast of Nicaragua
75. Nicaragua
76. Off coast of central America
77. Off coast of Costa Rica
78. Costa Rica
79. North of Panama
80. Panama-Costa Rica border region
81. Panama
82. Panama-Colombia border region
83. South of Panama

Seismic Region 7

Caribbean Loop

84. Yucatan Peninsula
85. Cuba region
86. Jamaica region

87. Haiti region

88. Dominican Republic region
89. Mona Passage
90. Puerto Rico region
91. Virgin Islands
92. Leeward Islands
93. Belize
94. Caribbean Sea
95. Windward Islands
96. Near north coast of Colombia
97. Near coast of Venezuela
98. Trinidad
99. Northern Colombia
100. Lake Maracaibo
101. Venezuela
731. North of Honduras

Seismic Region 8

Andean South America

102. Near west coast of Colombia
103. Colombia
104. Off coast of Ecuador
105. Near coast of Ecuador
106. Colombia-Ecuador border region
107. Ecuador
108. Off coast of northern Peru
109. Near coast of northern Peru
110. Peru-Ecuador border region
111. Northern Peru
112. Peru-Brazil border region
113. Western Brazil
114. Off coast of Peru
115. Near coast of Peru
116. Central Peru
117. Southern Peru
118. Peru-Bolivia border region
119. Northern Bolivia
120. Central Bolivia
121. Off coast of northern Chile
122. Near coast of northern Chile
123. Northern Chile
124. Chile-Bolivia border region
125. Southern Bolivia
126. Paraguay
127. Chile-Argentina border region
128. Jujuy Province
129. Salta Province
130. Catamarca Province
131. Tucuman Province
132. Santiago del Estero Province
133. Northeastern Argentina
134. Off coast of central Chile
135. Near coast of central Chile
136. Central Chile
137. San Juan Province
138. La Rioja Province
139. Mendoza Province

140. San Luis Province
141. Cordoba Province
142. Uruguay

Seismic Region 9

Extreme South America

143. Off coast of southern Chile
144. Southern Chile
145. Southern Chile-Argentina border region
146. Southern Argentina

Seismic Region 10

Southern Antilles

147. Tierra del Fuego
148. Falkland Islands region
149. Drake Passage
150. Scotia Sea
151. South Georgia Island region
152. South Georgia Rise
153. South Sandwich Islands region
154. South Shetland Islands
155. Antarctic Peninsula
156. Southwestern Atlantic Ocean
157. Weddell Sea
732. East of South Sandwich Islands

Seismic Region 11

New Zealand Region

158. Off west coast of North Island
159. North Island
160. Off east coast of North Island
161. Off west coast of South Island
162. South Island
163. Cook Strait
164. Off east coast of South Island
165. North of Macquarie Island
166. Auckland Islands region
167. Macquarie Island region
168. South of New Zealand

Seismic Region 12

Kermadec-Tonga-Samoa Area

169. Samoa Islands region
170. Samoa Islands
171. South of Fiji Islands
172. West of Tonga Islands (REGION NOT IN USE)
173. Tonga Islands
174. Tonga Islands region
175. South of Tonga Islands
176. North of New Zealand
177. Kermadec Islands region
178. Kermadec Islands
179. South of Kermadec Islands

Seismic Region 13

Fiji Area

180. North of Fiji Islands
181. Fiji Islands region
182. Fiji Islands

Seismic Region 14

Vanuatu (New Hebrides)

183. Santa Cruz Islands region
184. Santa Cruz Islands
185. Vanuatu Islands region
186. Vanuatu Islands
187. New Caledonia
188. Loyalty Islands
189. Southeast of Loyalty Islands

Seismic Region 15

Bismarck and Solomon Islands

190. New Ireland region
191. North of Solomon Islands
192. New Britain region
193. Bougainville-Solomon Islands region
194. D'Entrecasteaux Islands region
195. South of Solomon Islands

Seismic Region 16

New Guinea

196. Irian Jaya region
197. Near north coast of Irian Jaya
198. Ninigo Islands region
199. Admiralty Islands region
200. Near north coast of New Guinea
201. Irian Jaya
202. New Guinea
203. Bismarck Sea
204. Aru Islands region
205. Near south coast of Irian Jaya
206. Near south coast of New Guinea
207. Eastern New Guinea region
208. Arafura Sea

Seismic Region 17

Caroline Islands to Guam

209. Western Caroline Islands
210. South of Mariana Islands

Seismic Region 18

Guam to Japan

211. Southeast of Honshu
212. Bonin Islands region
213. Volcano Islands region
214. West of Mariana Islands
215. Mariana Islands region
216. Mariana Islands

Seismic Region 19

Japan-Kurils-Kamchatka

217. Kamchatka Peninsula
218. Near east coast of Kamchatka Peninsula
219. Off east coast of Kamchatka Peninsula
220. Northwest of Kuril Islands
221. Kuril Islands
222. East of Kuril Islands
223. Eastern Sea of Japan
224. Hokkaido region
225. Off southeast coast of Hokkaido
226. Near west coast of eastern Honshu
227. Eastern Honshu
228. Near east coast of eastern Honshu
229. Off east coast of Honshu
230. Near south coast of eastern Honshu

Seismic Region 20

Southwestern Japan and Ryukyu Islands

231. South Korea
232. Western Honshu
233. Near south coast of western Honshu
234. Northwest of Ryukyu Islands
235. Kyushu
236. Shikoku
237. Southeast of Shikoku
238. Ryukyu Islands
239. Southeast of Ryukyu Islands
240. West of Bonin Islands
241. Philippine Sea

Seismic Region 21

Taiwan

242. Near coast of southeastern China
243. Taiwan region
244. Taiwan
245. Northeast of Taiwan
246. Southwestern Ryukyu Islands
247. Southeast of Taiwan

Seismic Region 22

Philippines

248. Philippine Islands region
249. Luzon
250. Mindoro
251. Samar
252. Palawan
253. Sulu Sea
254. Panay

- 255. Cebu
- 256. Leyte
- 257. Negros
- 258. Sulu Archipelago
- 259. Mindanao
- 260. East of Philippine Islands

Seismic Region 23

Borneo-Sulawesi

- 261. Borneo
- 262. Celebes Sea
- 263. Talaud Islands
- 264. North of Halmahera
- 265. Minahassa Peninsula, Sulawesi
- 266. Northern Molucca Sea
- 267. Halmahera
- 268. Sulawesi
- 269. Southern Molucca Sea
- 270. Ceram Sea
- 271. Buru
- 272. Seram

Seismic Region 24

Sunda Arc

- 273. Southwest of Sumatera
- 274. Southern Sumatera
- 275. Java Sea
- 276. Sunda Strait
- 277. Jawa
- 278. Bali Sea
- 279. Flores Sea
- 280. Banda Sea
- 281. Tanimbar Islands region
- 282. South of Jawa
- 283. Bali region
- 284. South of Bali
- 285. Sumbawa region
- 286. Flores region
- 287. Sumba region
- 288. Savu Sea
- 289. Timor region
- 290. Timor Sea
- 291. South of Sumbawa
- 292. South of Sumba
- 293. South of Timor

Seismic Region 25

Myanmar and Southeast Asia

- 294. Myanmar-India border region
- 295. Myanmar-Bangladesh border region
- 296. Myanmar
- 297. Myanmar-China border region
- 298. Near south coast of Myanmar
- 299. Southeast Asia (REGION NOT IN USE)
- 300. Hainan Island

- 301. South China Sea
- 733. Thailand
- 734. Laos
- 735. Kampuchea
- 736. Vietnam
- 737. Gulf of Tongking

Seismic Region 26

India-Xizang-Szechwan-Yunnan

- 302. Eastern Kashmir
- 303. Kashmir-India border region
- 304. Kashmir-Xizang border region
- 305. Western Xizang-India border region
- 306. Xizang
- 307. Sichuan
- 308. Northern India
- 309. Nepal-India border region
- 310. Nepal
- 311. Sikkim
- 312. Bhutan
- 313. Eastern Xizang-India border region
- 314. Southern India
- 315. India-Bangladesh border region
- 316. Bangladesh
- 317. Northeastern India
- 318. Yunnan
- 319. Bay of Bengal

Seismic Region 27

Southern Xinjiang to Gansu

- 320. Kyrgyzstan-Xinjiang border region
- 321. Southern Xinjiang
- 322. Gansu
- 323. Western Nei Mongol
- 324. Kashmir-Xinjiang border region
- 325. Qinghai

Seismic Region 28

Alma-Ata to Lake Baikal

- 326. Southwestern Siberia
- 327. Lake Baykal region
- 328. East of Lake Baykal
- 329. Eastern Kazakhstan
- 330. Lake Issyk-Kul region
- 331. Kazakhstan-Xinjiang border region
- 332. Northern Xinjiang
- 333. Tuva-Buryatia-Mongolia border region
- 334. Mongolia

Seismic Region 29

Western Asia

- 335. Ural Mountains region
- 336. Western Kazakhstan
- 337. Eastern Caucasus
- 338. Caspian Sea
- 339. Northwestern Uzbekistan
- 340. Turkmenistan
- 341. Iran-Turkmenistan border region
- 342. Turkmenistan-Afghanistan border region
- 343. Turkey-Iran border region
- 344. Iran-Armenia-Azerbaijan border region
- 345. Northwestern Iran
- 346. Iran-Iraq border region
- 347. Western Iran
- 348. Northern and central Iran
- 349. Northwestern Afghanistan
- 350. Southwestern Afghanistan
- 351. Eastern Arabian Peninsula
- 352. Persian Gulf
- 353. Southern Iran
- 354. Southwestern Pakistan
- 355. Gulf of Oman
- 356. Off coast of Pakistan

Seismic Region 30

Middle East-Crimea-Eastern Balkans

- 357. Ukraine-Moldova-Southwestern Russia region
- 358. Romania
- 359. Bulgaria
- 360. Black Sea
- 361. Crimea region
- 362. Western Caucasus
- 363. Greece-Bulgaria border region
- 364. Greece
- 365. Aegean Sea
- 366. Turkey
- 367. Turkey-Georgia-Armenia border region
- 368. Southern Greece
- 369. Dodecanese Islands
- 370. Crete
- 371. Eastern Mediterranean Sea
- 372. Cyprus region
- 373. Dead Sea region
- 374. Jordan-Syria region
- 375. Iraq

Seismic Region 31

Western Mediterranean Area

- 376. Portugal
- 377. Spain

378. Pyrenees
379. Near south coast of France
380. Corsica
381. Central Italy
382. Adriatic Sea
383. Northwestern Balkan Peninsula
384. West of Gibraltar
385. Strait of Gibraltar
386. Balearic Islands
387. Western Mediterranean Sea
388. Sardinia
389. Tyrrhenian Sea
390. Southern Italy
391. Albania
392. Greece-Albania border region
393. Madeira Islands region
394. Canary Islands region
395. Morocco
396. Northern Algeria
397. Tunisia
398. Sicily
399. Ionian Sea
400. Central Mediterranean Sea
401. Near coast of Libya

Seismic Region 32

Atlantic Ocean

402. North Atlantic Ocean
403. Northern Mid-Atlantic Ridge
404. Azores Islands region
405. Azores Islands
406. Central Mid-Atlantic Ridge
407. North of Ascension Island
408. Ascension Island region
409. South Atlantic Ocean
410. Southern Mid-Atlantic Ridge
411. Tristan da Cunha region
412. Bouvet Island region
413. Southwest of Africa
414. Southeastern Atlantic Ocean
738. Reykjanes Ridge
739. Azores-Cape St. Vincent Ridge

Seismic Region 33

Indian Ocean

415. Eastern Gulf of Aden
416. Socotra region
417. Arabian Sea
418. Lakshadweep region
419. Northeastern Somalia
420. North Indian Ocean
421. Carlsberg Ridge
422. Maldive Islands region
423. Laccadive Sea
424. Sri Lanka
425. South Indian Ocean
426. Chagos Archipelago region

427. Mauritius-Reunion region
428. Southwest Indian Ridge
429. Mid-Indian Ridge
430. South of Africa
431. Prince Edward Islands region
432. Crozet Islands region
433. Kerguelen Islands region
434. Broken Ridge
435. Southeast Indian Ridge
436. Southern Kerguelen Plateau
437. South of Australia
740. Owen Fracture Zone region
741. Indian Ocean Triple Junction
742. Western Indian-Antarctic Ridge

Seismic Region 34

Eastern North America

438. Saskatchewan
439. Manitoba
440. Hudson Bay
441. Ontario
442. Hudson Strait region
443. Northern Quebec
444. Davis Strait
445. Labrador
446. Labrador Sea
447. Southern Quebec
448. Gaspé Peninsula
449. Eastern Quebec
450. Anticosti Island
451. New Brunswick
452. Nova Scotia
453. Prince Edward Island
454. Gulf of St. Lawrence
455. Newfoundland
456. Montana
457. Eastern Idaho
458. Hebgen Lake region, Montana
459. Yellowstone region
460. Wyoming
461. North Dakota
462. South Dakota
463. Nebraska
464. Minnesota
465. Iowa
466. Wisconsin
467. Illinois
468. Michigan
469. Indiana
470. Southern Ontario
471. Ohio
472. New York
473. Pennsylvania
474. Vermont-New Hampshire region
475. Maine
476. Southern New England

477. Gulf of Maine
478. Utah
479. Colorado
480. Kansas
481. Iowa-Missouri border region
482. Missouri-Kansas border region
483. Missouri
484. Missouri-Arkansas border region
485. Missouri-Illinois border region
486. New Madrid region, Missouri
487. Cape Girardeau region, Missouri
488. Southern Illinois
489. Southern Indiana
490. Kentucky
491. West Virginia
492. Virginia
493. Chesapeake Bay region
494. New Jersey
495. Eastern Arizona
496. New Mexico
497. Northwestern Texas-Oklahoma border region
498. Western Texas
499. Oklahoma
500. Central Texas
501. Arkansas-Oklahoma border region
502. Arkansas
503. Louisiana-Texas border region
504. Louisiana
505. Mississippi
506. Tennessee
507. Alabama
508. Western Florida
509. Georgia
510. Florida-Georgia border region
511. South Carolina
512. North Carolina
513. Off east coast of United States
514. Florida Peninsula
515. Bahama Islands
516. Eastern Arizona-Sonora border region
517. New Mexico-Chihuahua border region
518. Texas-Mexico border region
519. Southern Texas
520. Near coast of Texas
521. Chihuahua
522. Northern Mexico
523. Central Mexico
524. Jalisco
525. Veracruz
526. Gulf of Mexico
527. Bay of Campeche

Seismic Region 35

Eastern South America

- 528. Brazil
- 529. Guyana
- 530. Suriname
- 531. French Guiana

Seismic Region 36

Northwestern Europe

- 532. Eire
- 533. United Kingdom
- 534. North Sea
- 535. Southern Norway
- 536. Sweden
- 537. Baltic Sea
- 538. France
- 539. Bay of Biscay
- 540. The Netherlands
- 541. Belgium
- 542. Denmark
- 543. Germany
- 544. Switzerland
- 545. Northern Italy
- 546. Austria
- 547. Czech and Slovak Republics
- 548. Poland
- 549. Hungary

Seismic Region 37

Africa

- 550. Northwest Africa (REGION NOT IN USE)
- 551. Southern Algeria
- 552. Libya
- 553. Egypt
- 554. Red Sea
- 555. Western Arabian Peninsula
- 556. Chad region
- 557. Sudan
- 558. Ethiopia
- 559. Western Gulf of Aden
- 560. Northwestern Somalia
- 561. Off south coast of northwest Africa
- 562. Cameroon
- 563. Equatorial Guinea
- 564. Central African Republic
- 565. Gabon
- 566. Congo
- 567. Zaire
- 568. Uganda
- 569. Lake Victoria region
- 570. Kenya
- 571. Southern Somalia
- 572. Lake Tanganyika region
- 573. Tanzania
- 574. Northwest of Madagascar

- 575. Angola
- 576. Zambia
- 577. Malawi
- 578. Namibia
- 579. Botswana
- 580. Zimbabwe
- 581. Mozambique
- 582. Mozambique Channel
- 583. Madagascar
- 584. South Africa
- 585. Lesotho
- 586. Swaziland
- 587. Off coast of South Africa
- 743. Western Sahara
- 744. Mauritania
- 745. Mali
- 746. Senegal-Gambia region
- 747. Guinea region
- 748. Sierra Leone
- 749. Liberia region
- 750. Cote d'Ivoire
- 751. Burkina Faso
- 752. Ghana
- 753. Benin-Togo region
- 754. Niger
- 755. Nigeria

Seismic Region 38

Australia

- 588. Northwest of Australia
- 589. West of Australia
- 590. Western Australia
- 591. Northern Territory
- 592. South Australia
- 593. Gulf of Carpentaria
- 594. Queensland
- 595. Coral Sea
- 596. Northwest of New Caledonia
- 597. New Caledonia region
- 598. Southwest of Australia
- 599. Off south coast of Australia
- 600. Near coast of South Australia
- 601. New South Wales
- 602. Victoria
- 603. Near southeast coast of Australia
- 604. Near east coast of Australia
- 605. East of Australia
- 606. Norfolk Island region
- 607. Northwest of New Zealand
- 608. Bass Strait
- 609. Tasmania region
- 610. Southeast of Australia

Seismic Region 39

Pacific Basin

- 611. North Pacific Ocean

- 612. Hawaiian Islands region
- 613. Hawaiian Islands
- 614. Eastern Caroline Islands region
- 615. Marshall Islands region
- 616. Enewetak Atoll region
- 617. Bikini Atoll region
- 618. Gilbert Islands region
- 619. Johnston Island region
- 620. Line Islands region
- 621. Palmyra Island region
- 622. Kiritimati region
- 623. Tuvalu region
- 624. Phoenix Islands region
- 625. Tokelau Islands region
- 626. Northern Cook Islands
- 627. Cook Islands region
- 628. Society Islands region
- 629. Tubuai Islands region
- 630. Marquesas Islands region
- 631. Tuamotu Archipelago region
- 632. South Pacific Ocean

Seismic Region 40

Arctic Zone

- 633. Lomonosov Ridge
- 634. Arctic Ocean
- 635. Near north coast of Kalaallit Nunaat
- 636. Eastern Kalaallit Nunaat
- 637. Iceland region
- 638. Iceland
- 639. Jan Mayen Island region
- 640. Greenland Sea
- 641. North of Svalbard
- 642. Norwegian Sea
- 643. Svalbard region
- 644. North of Franz Josef Land
- 645. Franz Josef Land
- 646. Northern Norway
- 647. Barents Sea
- 648. Novaya Zemlya
- 649. Kara Sea
- 650. Near coast of northwestern Siberia
- 651. North of Severnaya Zemlya
- 652. Severnaya Zemlya
- 653. Near coast of northern Siberia
- 654. East of Severnaya Zemlya
- 655. Laptev Sea

Seismic Region 41

Eastern Asia

- 656. Southeastern Siberia
- 657. Priamurye-Northeastern China border region
- 658. Northeastern China
- 659. North Korea

660. Sea of Japan
661. Primorye
662. Sakhalin Island
663. Sea of Okhotsk
664. Southeastern China
665. Yellow Sea
666. Off east coast of southeastern China

Seismic Region 42

Northeastern Asia, Northern Alaska to Greenland

667. North of New Siberian Islands
668. New Siberian Islands
669. Eastern Siberian Sea
670. Near north coast of eastern Siberia
671. Eastern Siberia
672. Chukchi Sea
673. Bering Strait
674. St. Lawrence Island region
675. Beaufort Sea
676. Northern Alaska
677. Northern Yukon Territory
678. Queen Elizabeth Islands
679. Northwest Territories
680. Western Kalaallit Nunaat
681. Baffin Bay
682. Baffin Island region

Seismic Region 43

Southeastern and Antarctic Pacific Ocean

683. Southeastcentral Pacific Ocean
684. Southern East Pacific Rise
685. Easter Island region
686. West Chile Rise

687. Juan Fernandez Islands region
688. East of North Island
689. Chatham Islands region
690. South of Chatham Islands
691. Pacific-Antarctic Ridge
692. Southern Pacific Ocean
756. Southeast of Easter Island

Seismic Region 44

Galapagos Area

693. Eastcentral Pacific Ocean
694. Central East Pacific Rise
695. West of Galapagos Islands
696. Galapagos Islands region
697. Galapagos Islands
698. Southwest of Galapagos Islands
699. Southeast of Galapagos Islands
757. Galapagos Triple Junction region

Seismic Region 45

Macquarie Loop

700. South of Tasmania
701. West of Macquarie Island
702. Balleny Islands region

Seismic Region 46

Andaman Islands to Sumatera

703. Andaman Islands region
704. Nicobar Islands region
705. Off west coast of northern Sumatera
706. Northern Sumatera
707. Malay Peninsula
708. Gulf of Thailand

Seismic Region 47

Baluchistan

709. Southeastern Afghanistan
710. Pakistan
711. Southwestern Kashmir
712. India-Pakistan border region

Seismic Region 48

Hindu Kush and Pamir

713. Central Kazakhstan
714. Southeastern Uzbekistan
715. Tajikistan
716. Kyrgyzstan
717. Afghanistan-Tajikistan border region
718. Hindu Kush region
719. Tajikistan-Xinjiang border region
720. Northwestern Kashmir

Seismic Region 49

Northern Eurasia

721. Finland
722. Norway-Murmansk border region
723. Finland-Karelia border region
724. Baltic States-Belarus-Northwestern Russia
725. Northwestern Siberia
726. Northern and central Siberia

Seismic Region 50

Antarctica

727. Victoria Land
728. Ross Sea
729. Antarctica

10.2.3 IASPEI Magnitudes

The ISC publishes a diversity of magnitude data. Although trying to be as complete and specific as possible, preference is now given to magnitudes determined according to standard procedures recommended by the Working Group on Magnitude Measurements of the IASPEI Commission on Seismological Observation and Interpretation (CoSOI). So far, such standards have been agreed upon for the local magnitude ML , the local-regional mb_Lg , and for two types each of body-wave (mb and mB_BB) and surface-wave magnitudes (Ms_20 and Ms_BB). With the exception of ML , all other standard magnitudes are measured on vertical-component records only. BB stands for direct measurement on unfiltered velocity broadband records in a wide range of periods, provided that their passband covers at least the period range within which mB_BB and Ms_BB are supposed to be measured. Otherwise, a deconvolution has to be applied prior to the amplitude and period measurement so as to assure that this specification is met. In contrast, mb_Lg , mb and Ms_20 are based on narrowband amplitude measurements around periods of 1 s and 20 s, respectively.

ML is consistent with the original definition of the local magnitude by *Richter* (1935) and mB_BB in close agreement with the original definition of medium-period body-wave magnitude mB measured in a wide range of periods between some 2 to 20 s and calibrated with the *Gutenberg and Richter* (1956) Q -function for vertical-component P waves. Similarly, Ms_BB is best tuned to the unbiased use of the IASPEI (1967) recommended standard magnitude formula for surface-wave amplitudes in a wide range of periods and distances, as proposed by its authors *Vaněk et al.* (1962). In contrast, mb and Ms_20 are chiefly based on measurement standards defined by US agencies in the 1960s in conjunction with the global deployment of the World-Wide Standard Seismograph Network (WWSSN), which did not include medium or broadband recordings. Some modifications were made in the 1970s to account for IASPEI recommendations on extended measurement time windows for mb . Although not optimal for calibrating narrow-band spectral amplitudes measured around 1 s and 20 s only, mb and Ms_20 use the same original calibrations functions as mB_BB and Ms_BB . But mb and Ms_20 data constitute by far the largest available magnitude data sets. Therefore they continue to be used, with appreciation for their advantages (e.g., mb is by far the most frequently measured teleseismic magnitude and often the only available and reasonably good magnitude estimator for small earthquakes) and their shortcomings (see section 3.2.5.2 of Chapter 3 in NMSOP-2).

Abbreviated descriptions of the standard procedures for ML , mb_Lg , mb , mB_BB and Ms_BB are summarised below. For more details, including also the transfer functions of the simulation filters to be used, see www.iaspei.org/commissions/CSOI/Summary_WG-Recommendations_20130327.pdf.

All amplitudes used in the magnitude formulas below are in most circumstances to be measured as one-half the maximum deflection of the seismogram trace, peak-to-adjacent-trough or trough-to-adjacent-peak, where the peak and trough are separated by one crossing of the zero-line: this measurement is sometimes described as “one-half peak-to-peak amplitude.” The periods are to be measured as twice the time-intervals separating the peak and adjacent-trough from which the amplitudes are measured. The amplitude-phase arrival-times are to be measured and reported too as the time of the zero-crossing between the peak and adjacent-trough from which the amplitudes are measured. The issue of amplitude and period measuring procedures, and circumstances under which alternative procedures are acceptable or preferable, is discussed further in Section 5 of IS 3.3 and in section 3.2.3.3 of Chapter 3 of NMSOP-2.

Amplitudes measured according to recommended IASPEI standard procedures should be reported with the following ISF amplitude “phase names”: IAML, IAmb_Lg, IAmb, IAMs_20, IVmB_BB and IVMs_BB. “T” stands for “International” or “IASPEI”, “A” for displacement amplitude, measured in nm, and “V” for velocity amplitude, measured in nm/s. Although the ISC will calculate standard surface-wave magnitudes only for earthquakes shallower than 60 km, contributing agencies or stations are encouraged to report standard amplitude measurements of IAMs_20 and IVMs_BB for deeper earthquakes as well.

Note that the commonly known classical calibration relationships have been modified in the following to be consistent with displacements measured in nm, and velocities in nm/s, which is now common with high-resolution digital data and analysis tools. With these general definitions of the measurement parameters, where R is hypocentral distance in km (typically less than 1000 km), Δ is epicentral distance in degrees and h is hypocentre depth in km, the standard formulas and procedures read as follows:

ML :

$$ML = \log_{10}(A) + 1.11 \log_{10} R + 0.00189R - 2.09 \quad (10.14)$$

for crustal earthquakes in regions with attenuative properties similar to those of southern California, and with A being the maximum trace amplitude in nm that is measured on output from a horizontal-component instrument that is filtered so that the response of the seismograph/filter system replicates that of a Wood-Anderson standard seismograph (but with a static magnification of 1). For the normalised simulated response curve and related poles and zeros see Figure 1 and Table 1 in IS 3.3 of NMSOP-2.

Equation (10.14) is an expansion of that of *Hutton and Boore* (1987). The constant term in equation (10.14), -2.09 , is based on an experimentally determined static magnification of the Wood-Anderson of 2080 (see *Uhrhammer and Collins* (1990)), rather than the theoretical magnification of 2800 that was specified by the seismograph’s manufacturer. The formulation of equation (10.14) assures that reported ML amplitude data are not affected by uncertainty in the static magnification of the Wood-Anderson seismograph.

For seismographic stations containing two horizontal components, amplitudes are measured independently from each horizontal component and each amplitude is treated as a single datum. There is no effort to measure the two observations at the same time, and there is no attempt to compute a vector average. For crustal earthquakes in regions with attenuative properties that are different from those of coastal California and for measuring magnitudes with vertical-component seismographs the constants in the above equation have to be re-determined to adjust for the different regional attenuation and travel paths as well as for systematic differences between amplitudes measured on horizontal and vertical seismographs.

mb_Lg :

$$mb_Lg = \log_{10}(A) + 0.833 \log_{10} R + 0.434\gamma(R - 10) - 0.87 \quad (10.15)$$

where A = “sustained ground-motion amplitude” in nm, defined as the third largest amplitude in the time window corresponding to group velocities of 3.6 to 3.2 km/s, in the period (T) range 0.7 s to 1.3

s; R = epicentral distance in km, γ = coefficient of attenuation in km^{-1} . γ is related to the quality factor Q through the equation $\gamma = \pi/(QU T)$, where U is group velocity and T is the wave period of the L_g wave. γ is a strong function of crustal structure and should be determined specifically for the region in which the mb_Lg is to be used. A and T are measured on output from a vertical-component instrument that is filtered so that the frequency response of the seismograph/filter system replicates that of a WWSSN short-period seismograph (see Figure 1 and Table 1 in IS 3.3 of NMSOP-2). Arrival times with respect to the origin of the seismic disturbance are used, along with epicentral distance, to compute group velocity U .

mb :

$$mb = \log_{10}(A/T) + Q(\Delta, h) - 3.0 \quad (10.16)$$

where A = vertical component P-wave ground amplitude in nm measured at distances $20^\circ \leq \Delta \leq 100^\circ$ and calculated from the maximum trace-amplitude with $T < 3$ s in the entire P-phase train (time spanned by P, pP, sP, and possibly PcP and their codas, and ending preferably before PP). A and T are measured on output from an instrument that is filtered so that the frequency response of the seismograph/filter system replicates that of a WWSSN short-period seismograph (see Figure 1 and Table 1 in IS 3.3 of NMSOP-2). A is determined by dividing the maximum trace amplitude by the magnification of the simulated WWSSN-SP response at period T .

$Q(\Delta, h)$ = attenuation function for PZ (P-waves recorded on vertical component seismographs) established by *Gutenberg and Richter* (1956) in the tabulated or algorithmic form as used by the U.S. Geological Survey/National Earthquake Information Center (USGS/NEIC) (see Table 2 in IS 3.3 and program description PD 3.1 in NMSOP-2);

mB_BB :

$$mB_BB = \log_{10}(Vmax/2\pi) + Q(\Delta, h) - 3.0 \quad (10.17)$$

where $Vmax$ = vertical component ground velocity in nm/s at periods between $0.2 \text{ s} < T < 30 \text{ s}$, measured in the range $20^\circ \leq \Delta \leq 100^\circ$. $Vmax$ is calculated from the maximum trace-amplitude in the entire P-phase train (see mb), as recorded on a seismogram that is proportional to velocity at least in the period range of measurements. $Q(\Delta, h)$ = attenuation function for PZ established by *Gutenberg and Richter* (1956) (see 10.16). Equation (10.16) differs from the equation for mB of *Gutenberg and Richter* (1956) by virtue of the $\log_{10}(Vmax/2\pi)$ term, which replaces the classical $\log_{10}(A/T)_{max}$ term. Contributors should continue to send observations of A and T to ISC.

Ms_20 :

$$Ms_20 = \log_{10}(A/T) + 1.66 \log_{10} \Delta + 0.3 \quad (10.18)$$

where A = vertical-component ground displacement in nm at $20^\circ \leq \Delta \leq 160^\circ$ epicentral distance measured from the maximum trace amplitude of a surface-wave phase having a period T between 18 s and 22 s on a waveform that has been filtered so that the frequency response of the seismograph/filter

replicates that of a WWSSN long-period seismograph (see Figure 1 and Table 1 in IS 3.3 of NMSOP-2). A is determined by dividing the maximum trace amplitude by the magnification of the simulated WWSSN-LP response at period T . Equation (10.18) is formally equivalent to the Ms equation proposed by *Vaněk et al.* (1962) but is here applied to vertical motion measurements in a narrow range of periods.

Ms_BB :

$$Ms_BB = \log_{10} (Vmax/2\pi) + 1.66 \log_{10} \Delta + 0.3 \quad (10.19)$$

where $Vmax$ = vertical-component ground velocity in nm/s associated with the maximum trace-amplitude in the surface-wave train at periods between $3 \text{ s} < T < 60 \text{ s}$ as recorded at distances $2^\circ \leq \Delta \leq 160^\circ$ on a seismogram that is proportional to velocity in that range of considered periods. Equation (10.19) is based on the Ms equation proposed by *Vaněk et al.* (1962), but is here applied to vertical motion measurements and is used with the $\log_{10} (Vmax/2\pi)$ term replacing the $\log_{10} (A/T)_{max}$ term of the original. As for mB_BB , observations of A and T should be reported to ISC.

Mw :

$$Mw = (\log_{10} M_0 - 9.1) / 1.5 \quad (10.20)$$

Moment magnitude Mw is calculated from data of the scalar seismic moment M_0 (when given in Nm), or

$$Mw = (\log_{10} M_0 - 16.1) / 1.5 \quad (10.21)$$

its CGS equivalent when M_0 is in dyne-cm.

Please note that the magnitude nomenclature used in this Section uses the IASPEI standards as the reference. However, the magnitude type is typically written in plain text in most typical data reports and so it is in this document. Moreover, writing magnitude types in plain text allows us to reproduce the magnitude type as stored in the database and provides a more direct identification of the magnitude type reported by different agencies. A short description of the common magnitude types available in this Summary is given in table 7.6.

10.2.4 The IASPEI Seismic Format (ISF)

The ISF is the IASPEI approved standard format for the exchange of parametric seismological data (hypocentres, magnitudes, phase arrivals, moment tensors etc.) and is one of the formats used by the ISC. It was adopted as standard in August 2001 and is an extension of the International Monitoring System 1.0 (IMS1.0) standard, which was developed for exchanging data used to monitor the Comprehensive Nuclear-Test-Ban Treaty. An example of the ISF is shown in Listing 10.1.

Bulletins which use the ISF are comprised of origin and arrival information, provided in a series of data blocks. These include: a bulletin title block; an event title block; an origin block; a magnitude sub-block; an effect block; a reference block; and a phase block.

Within these blocks an important extension of the IMS1.0 standard is the ability to add additional comments and thus provide further parametric information. The ISF comments are distinguishable within the open parentheses required for IMS1.0 comments by beginning with a hash mark (#) followed by a keyword identifying the type of formatted comment. Each additional line required in the ISF comment begins with the hash (within the comment parentheses) followed by blank spaces at least as long as the keyword. Optional lines within the comment are signified with a plus sign (+) instead of a hash mark. The keywords include **PRIME** (to designate a prime origin of a hypocentre); **CENTROID** (to indicate the centroid origin); **MOMTENS** (moment tensor solution); **FAULT_PLANE** (fault plane solution); **PRINAX** (principal axes); **PARAM** (an origin parameter e.g. hypocentre depth given by a depth phase).

The full documentation for the ISF is maintained at the ISC and can be downloaded from:
www.isc.ac.uk/doc/code/isf/isf.pdf

The documentation for the IMS1.0 standard can be downloaded from:
www.isc.ac.uk/doc/code/isf/ims1_0.pdf

Listing 10.1: Example of an ISF formatted event

```

Event 15146084 Near east coast of eastern Honshu
Date Time Err RMS Latitude Longitude SmaJ Smin Az Depth Err Ndef Nsta Gap mdist Mdlist Qual Author OrigID
2010/09/01 07:32:00 37.9000 141.9000f 37.0 44.0 71 281 11.00 51.10 uk BJI 15275482
(#MOMTENS sc MO fCLVD MRR MTT MPP MRT MTP MPR NST1 NST2 Author )
(# eMO eCLVD eRR eTT ePP eRT eTP ePR NCO1 NCO2 Duration )
(# 16 5.760 NIED )
(# )
(#FAULT_PLANE Typ Strike Dip Rake NP NS Plane Author )
(# BDC 199.00 19.00 86.00 NIED )
(+ 23.00 71.00 91.00 )
(Epicenter information from JMA Focal Mechanism Solution Determined Manually Variance reduction = 96.98%)
2010/09/01 07:32:47.50 1.470 37.8300 142.2400 6.7 4.5 110 44.0 114 490 478 122 0.65 92.01 m i fe ISCJB 16741494
2010/09/01 07:32:52.20 0.92 38.0320 141.8090 6.7 4.5 110 44.0 114 490 478 122 0.65 92.01 m i fe ISCJB 16741494
2010/09/01 07:32:52.53 0.35 0.889 37.9202 141.8229 4.090 2.740 145 49.7 2.76 490 478 122 0.65 92.01 m i fe ISCJB 16741494
(#PARAM pP_DEPTH=41.11021)
2010/09/01 07:32:52.60 0.10 37.9100 141.8700 1.1 0.9 -1 43.0 1.0 fe JMA 16271222
(Felt I=III-III J1)
2010/09/01 07:32:53.66 0.42 0.770 37.9250 141.7880 5.1 3.4 140 44.4 3.9 102 127 3.17 127.67 fe NEIC 01134459
(#MOMTENS sc MO fCLVD MRR MTT MPP MRT MTP MPR NST1 NST2 Author )
(# eMO eCLVD eRR eTT ePP eRT eTP ePR NCO1 NCO2 Duration )
(# 16 5.800 3.600 -0.550 -3.040 1.850 -1.140 4.150 NIED )
(# )
(#FAULT_PLANE Typ Strike Dip Rake NP NS Plane Author )
(# BDC 199.00 19.00 86.00 NIED )
(+ 23.00 71.00 91.00 )
(Recorded [3 JMA] in Miyagi; [2 JMA] in Fukushima and Iwate; [1 JMA] in Akita, Aomori, Ibaraki, Tochigi and Yamagata.)
2010/09/01 07:32:53.70 0.20 37.9300 142.0600 2.224 1.112 -1 50.3 1.0 262 89 GCMT 00124877
(#CENTROID)
(#MOMTENS sc MO fCLVD MRR MTT MPP MRT MTP MPR NST1 NST2 Author )
(# eMO eCLVD eRR eTT ePP eRT eTP ePR NCO1 NCO2 Duration )
(# 16 6.891 5.430 -0.440 -4.990 1.500 -2.070 3.710 64 89 GCMT )
(# 0.173 0.118 0.120 0.100 0.094 0.110 102 160 0.90 )
(#FAULT_PLANE Typ Strike Dip Rake NP NS Plane Author )
(# BDC 22.00 63.00 91.00 GCMT )
(+ 201.00 27.00 89.00 )
(#PRINAX sc T_val T_azim T_pl B_val B_azim B_pl P_val P_azim P_pl Author )
(# 16 6.711 293.00 72.00 0.360 201.00 0.00 -7.072 111.00 18.00 GCMT )
(nsta1 refers to body waves, cutoff=40s. nsta2 refers to surface waves, cutoff=50s.)
2010/09/01 07:32:55.05 1.77 1.070 37.8692 141.9450 12.9 10.4 100 63.6 16.8 36 127 3.24 117.04 uk IDC 16680924
2010/09/01 07:32:52.23 0.30 1.333 37.8836 141.9148 5.558 4.001 142 38.9 2.33 542 478 61 0.72 141.68 m i se ISC 01237353
(#PRIME)
(#PARAM pP_DEPTH=39.00000)

Magnitude Err Nsta Author OrigID
Mw 5.1 NIED 17047453
Ms 4.8 61 BJI 15275482
Ms7 4.6 58 BJI 15275482
mb 5.1 48 BJI 15275482
mb 5.0 63 BJI 15275482
MS 4.7 19 MOS 16741494
mb 5.2 49 MOS 16741494
MS 4.6 43 ISCJB 01631732
mb 4.9 138 ISCJB 01631732
mb 5.0 JMA 16271222
mb 5.0 55 NEIC 01134459
MW 5.1 NIED 01134459
MW 5.2 89 GCMT 00124877
MS 4.4 0.1 28 IDC 16680924
Msl 4.4 0.1 28 IDC 16680924
mb 4.4 0.1 27 IDC 16680924
mbi 4.5 0.0 33 IDC 16680924
mbimx 4.4 0.0 37 IDC 16680924
mbtmp 4.7 0.1 33 IDC 16680924
mslmx 4.3 0.1 31 IDC 16680924
MS 4.7 0.2 43 ISC 01237353
mb 4.9 0.2 145 ISC 01237353

Sta Dist EvAz Phase Time TRes Azim AzRes Slow SRes Def SNR Amp Per Qual Magnitude ArrID
JIO 0.72 322.1 Pn 07:33:05.9 -0.06 90.9 T-- 49540510
JIO 0.72 322.1 Sn 07:33:15.0 -0.82 T-- 49540511
JMM 0.89 269.2 Sn 07:33:08.4 0.2 T-- 49540512
JMM 0.89 269.2 Sn 07:33:19.2 -0.68 T-- 49540513
JFK 0.97 238.3 Pn 07:33:09.5 0.1 T-- 49540514
JFK 0.97 238.3 Sn 07:33:21.5 -0.54 T-- 49540515
JOU 1.10 296.4 Pn 07:33:11.5 0.4 T-- 49540516
JOU 1.10 296.4 Sn 07:33:25.4 0.3 T-- 49540517
UNAJ 1.18 229.0 Pn 07:33:12.4 0.1 T-- 49540530
JMK 1.20 333.1 Pn 07:33:12.5 0.0 T-- 49540518
JMK 1.20 333.1 Sn 07:33:27.1 -0.39 T-- 49540519
OFUJ 1.21 350.9 Pn 07:33:12.3 -0.34 T-- 49540531
.
.
532A 91.05 49.8 P 07:45:52.799 -0.00 90.9 T-- 05504129
334A 91.18 47.9 P 07:45:54.012 0.7 91.0 T-- 05504128
H06N1 91.36 64.9 T 09:27:33.559 --- 6.0 --- 58438458
MIAR 91.43 42.9 P 07:45:54.85 0.5 91.2 T-- 05504179
Y39A 91.60 43.6 P 07:45:55.543 0.4 91.4 T-- 05504214
534A 91.98 49.0 P 07:45:57.308 0.2 91.8 T-- 05504130
KEST 94.59 323.1 LR 08:33:52.432 320.5 38.70 --- 466.5 18.65 --- 58438480
ESDC 96.70 334.2 LR 08:34:40.011 345.0 38.30 --- 375.8 20.18 --- 58438449
TORO 117.01 315.6 PKPdf 07:51:32.55 -0.82 17.7 2.30 T-- 5.1 0.4 0.70 --- 58438504
TORO 117.01 315.6 PP 07:52:39.3 -2.90 31.2 6.30 T-- 6.5 1.3 0.68 --- 58438505
QSPA 127.62 180.0 PKPdf 07:51:52.02 -0.16 T-- 23535420
SNA 141.68 197.1 PKPdf 07:52:13.751 -4.52 T-- 20375340
VNA2 143.24 196.3 PKPbc 07:52:18.562 0.4 122.0 2.31 --- 20375338
VNA1 143.64 196.2 PKPbc 07:52:19.77 0.6 --- 20375339

```

10.2.5 Ground Truth (GT) Events

Accurate locations are crucial in testing Earth models derived from body and surface wave tomography as well as in location calibration studies. ‘Ground Truth’ (GT) events are well-established source locations and origin times. A database of IASPEI reference events (GT earthquakes and explosions) is hosted at the ISC (www.isc.ac.uk). A full description of GT selection criteria can be found in *Bondár and McLaughlin* (2009a).

The events are coded by category GT0, GT1, GT2 or GT5, where the epicentre of a GT X event is known to within X km to a 95% confidence level. A map of all IASPEI reference events is shown in Figure 10.12 and the types of event are categorised in Figure 10.13. GT0 are explosions with announced locations and origin times. GT1 and GT2 are typically explosions, mine blasts or rock bursts either associated to explosion phenomenology located upon overhead imagery with seismically determined origin times, or precisely located by in-mine seismic networks. GT1-2 events are assumed to be shallow, but depth is unknown.

The database consists of nuclear explosions of GT0–5 quality, adopted from the Nuclear Explosion Database (*Bennett et al.*, 2010); GT0–5 chemical explosions, rock bursts, mine-induced events, as well as a few earthquakes, inherited from the reference event set by *Bondár et al.* (2004); GT5 events (typically earthquakes with crustal depths) which have been identified using either the method of *Bondár et al.* (2008) (2,275 events) or *Bondár and McLaughlin* (2009a) (updated regularly from the EHB catalogue (*Engdahl et al.*, 1998)), which uses the following criteria:

- 10 or more stations within 150 km from the epicentre
- one or more stations within 10 km
- $\Delta U \leq 0.35$
- a secondary azimuthal gap $\leq 160^\circ$

where ΔU is the network quality metric defined as the mean absolute deviation between the best-fitting uniformly distributed network of stations and the actual network:

$$\Delta U = \frac{4 \sum |esaz_i - (unif_i + b)|}{360N}, 0 \leq \Delta U \leq 1 \quad (10.22)$$

where N is the number of stations, $esaz_i$ is the i th event-to-station azimuth, $unif_i = 360i/N$ for $i = 0, \dots, N - 1$, and $b = \text{avg}(esaz_i) - \text{avg}(unif_i)$. ΔU is normalised so that it is 0 when the stations are uniformly distributed in azimuth and 1 when all the stations are at the same azimuth.

The seismological community is invited to participate in this project by nominating seismic events for the reference event database. Submitters may be contacted for further confirmation and for arrival time data. The IASPEI Reference Event List will be periodically published both in written and electronic form with proper acknowledgement of all submitters.

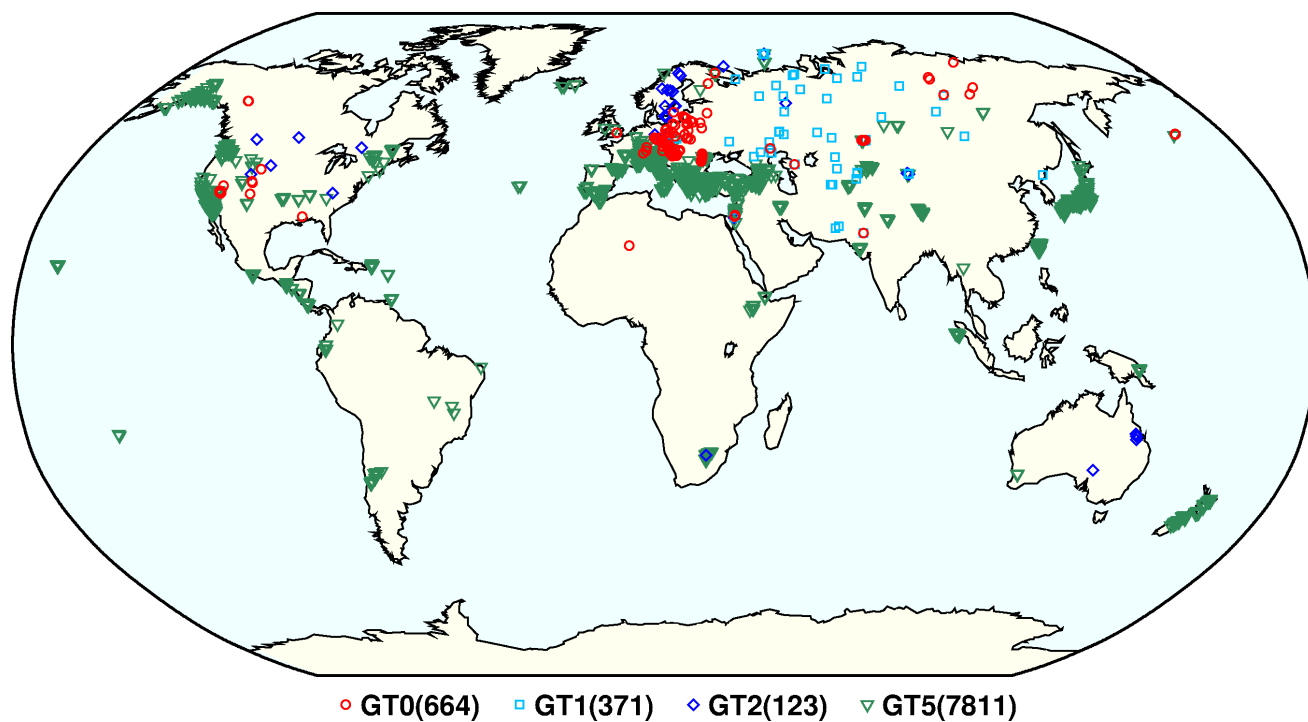


Figure 10.12: Map of all IASPEI Reference Events as of December 2016.

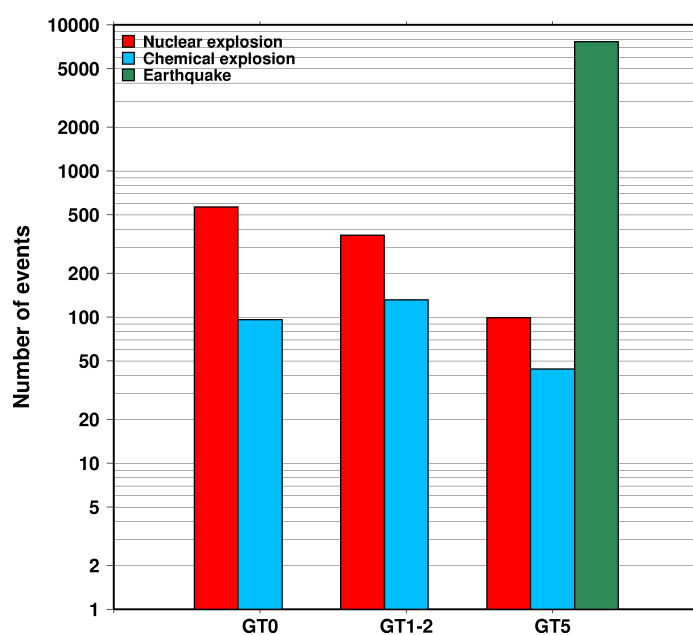


Figure 10.13: Histogram showing the event types within the IASPEI Reference Event list as of December 2016.

10.2.6 Nomenclature of Event Types

The nomenclature of event types currently used in the ISC Bulletin takes its origin from the IASPEI International Seismic Format (ISF).

Event type codes are composed of a leading character that generally indicates the confidence with which the type of the event is asserted and a trailing character that generally gives the type of the event. The leading and trailing characters may be used in any combination.

The **leading** characters are:

- s = suspected
- k = known
- f = felt (implies known)
- d = damaging (implies felt and known)

The **trailing** characters are:

- c = meteoritic event
- e = earthquake
- h = chemical explosion
- i = induced event
- l = landslide
- m = mining explosion
- n = nuclear explosion
- r = rock burst
- x = experimental explosion

A chemical explosion might be for mining or experimental purposes, and it is conceivable that other types of event might be assigned two or more different event type codes. This is deliberate, and matches the ambiguous identification of events in existing databases.

In addition, the code **uk** is used for events of unknown type and **ls** is used for known landslides.

The frequency of the different event types designated in the ISC Bulletin since 1964 is indicated in Figure 10.14.

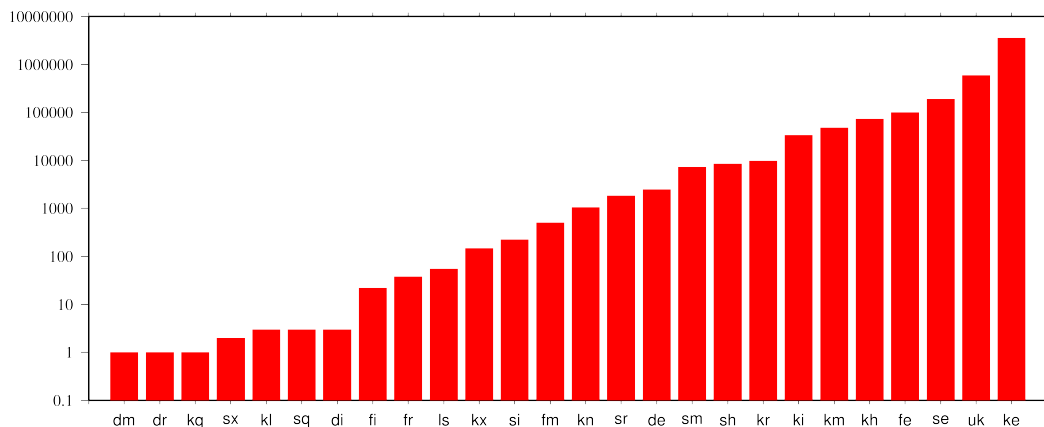


Figure 10.14: Event types in the ISC Bulletin

There are currently plans to revise this nomenclature as part of the coordination process between the National Earthquake Information Center (NEIC/USGS), European-Mediterranean Seismological Centre (CSEM) and the ISC.

10.3 Tables

Table 10.2: Listing of all 337 agencies that have directly reported to the ISC. The 142 agencies highlighted in bold have reported data to the ISC Bulletin for the period of this Bulletin Summary.

Agency Code	Agency Name
AAA	Alma-ata, Kazakhstan
AAE	University of Addis Ababa, Ethiopia
AAM	University of Michigan, USA
ADE	Primary Industries and Resources SA, Australia
ADH	Observatorio Afonso Chaves, Portugal
AEIC	Alaska Earthquake Information Center, USA
AFAR	The Afar Depression: Interpretation of the 1960-2000 Earthquakes, Israel
AFUA	University of Alabama, USA
ALG	Algiers University, Algeria
ANF	USArray Array Network Facility, USA
ANT	Antofagasta, Chile
ARE	Instituto Geofísico del Peru, Peru
ARO	Observatoire Géophysique d'Arta, Djibouti
ASIES	Institute of Earth Sciences, Academia Sinica, Chinese Taipei
ASL	Albuquerque Seismological Laboratory, USA
ASM	University of Asmara, Eritrea
ASRS	Altai-Sayan Seismological Centre, GS SB RAS, Russia
ATA	The Earthquake Research Center Ataturk University, Turkey
ATH	National Observatory of Athens, Greece
AUST	Geoscience Australia, Australia
AWI	Alfred Wegener Institute for Polar and Marine Research, Germany
AZER	Republic Center of Seismic Survey, Azerbaijan
BCIS	Bureau Central International de Sismologie, France
BDF	Observatório Sismológico da Universidade de Brasília, Brazil

Table 10.2: Continued.

Agency Code	Agency Name
BELR	Centre of Geophysical Monitoring of the National Academy of Sciences of Belarus, Republic of Belarus
BEO	Seismological Survey of Serbia, Serbia
BER	University of Bergen, Norway
BERK	Berkheimer H, Germany
BGR	Bundesanstalt für Geowissenschaften und Rohstoffe, Germany
BGS	British Geological Survey, United Kingdom
BHJ2	Study of Aftershocks of the Bhuj Earthquake by Japanese Research Team, Japan
BIAK	Biak earthquake aftershocks (17-Feb-1996), USA
BJI	China Earthquake Networks Center, China
BKK	Thai Meteorological Department, Thailand
BNS	Erdbebenstation, Geologisches Institut der Universität, Köl, Germany
BOG	Universidad Javeriana, Colombia
BRA	Geophysical Institute, Slovak Academy of Sciences, Slovakia
BRG	Seismological Observatory Berggießhübel, TU Bergakademie Freiberg, Germany
BRK	Berkeley Seismological Laboratory, USA
BRS	Brisbane Seismograph Station, Australia
BUC	National Institute for Earth Physics, Romania
BUD	Geodetic and Geophysical Research Institute, Hungary
BUG	Institute of Geology, Mineralogy & Geophysics, Germany
BUL	Goetz Observatory, Zimbabwe
BUT	Montana Bureau of Mines and Geology, USA
BYKL	Baykal Regional Seismological Centre, GS SB RAS, Russia
CADCG	Central America Data Centre, Costa Rica
CAN	Australian National University, Australia
CANSK	Canadian and Scandinavian Networks, Sweden
CAR	Instituto Sismológico de Caracas, Venezuela
CASC	Central American Seismic Center, Costa Rica
CENT	Centennial Earthquake Catalog, USA
CERI	Center for Earthquake Research and Information, USA
CFUSG	Inst. of Seismology and Geodynamics, V.I. Vernadsky Crimean Federal University, Republic of Crimea
CLL	Geophysikalisches Observatorium Collm, Germany
CMWS	Laboratory of Seismic Monitoring of Caucasus Mineral Water Region, GSRAS, Russia
CNG	Seismographic Station Chagalane, Mozambique
CNRM	Centre National de Recherche, Morocco
COSMOS	Consortium of Organizations for Strong Motion Observations, USA
CRAAG	Centre de Recherche en Astronomie, Astrophysique et Géophysique, Algeria
CSC	University of South Carolina, USA
CSEM	Centre Sismologique Euro-Méditerranéen (CSEM/EMSC), France
CUPWA	Curtin University, Australia
DASA	Defense Atomic Support Agency, USA
DBN	Koninklijk Nederlands Meteorologisch Instituut, Netherlands

Table 10.2: Continued.

Agency Code	Agency Name
DDA	Disaster and Emergency Management Presidency, Turkey
DHMR	Yemen National Seismological Center, Yemen
DIAS	Dublin Institute for Advanced Studies, Ireland
DJA	Badan Meteorologi, Klimatologi dan Geofisika, Indonesia
DMN	National Seismological Centre, Nepal, Nepal
DNK	Geological Survey of Denmark and Greenland, Denmark
DRS	Dagestan Branch, Geophysical Survey, Russian Academy of Sciences, Russia
DSN	Dubai Seismic Network, United Arab Emirates
DUSS	Damascus University, Syria, Syria
EAF	East African Network, Unknown
EAGLE	Ethiopia-Afar Geoscientific Lithospheric Experiment, Unknown
EBR	Observatori de l'Ebre, Spain
EBSE	Ethiopian Broadband Seismic Experiment, Unknown
ECX	Centro de Investigación Científica y de Educación Superior de Ensenada, Mexico
EFATE	OBS Experiment near Efate, Vanuatu, USA
EHB	Engdahl, van der Hilst and Buland, USA
EIDC	Experimental (GSETT3) International Data Center, USA
EKA	Eskdalemuir Array Station, United Kingdom
ENT	Geological Survey and Mines Department, Uganda
EPSI	Reference events computed by the ISC for EPSI project, United Kingdom
ERDA	Energy Research and Development Administration, USA
EST	Geological Survey of Estonia, Estonia
FBR	Fabra Observatory, Spain
FDF	Fort de France, Martinique
FIA0	Finessa Array, Finland
FOR	Unknown Historical Agency, Unknown - historical agency
FUNV	Fundación Venezolana de Investigaciones Sismológicas, Venezuela
FUR	Geophysikalisches Observatorium der Universität München, Germany
GBZT	Marmara Research Center, Turkey
GCG	INSIVUMEH, Guatemala
GCMT	The Global CMT Project, USA
GDNRW	Geologischer Dienst Nordrhein-Westfalen, Germany
GEN	Dipartimento per lo Studio del Territorio e delle sue Risorse (RSNI), Italy
GFZ	Helmholtz Centre Potsdam GFZ German Research Centre For Geosciences, Germany
GII	The Geophysical Institute of Israel, Israel
GOM	Observatoire Volcanologique de Goma, Democratic Republic of the Congo
GRAL	National Council for Scientific Research, Lebanon
GSDM	Geological Survey Department Malawi, Malawi
GTFE	German Task Force for Earthquakes, Germany
GUC	Centro Sismológico Nacional, Universidad de Chile, Chile
HAN	Hannover, Germany

Table 10.2: Continued.

Agency Code	Agency Name
HDC	Observatorio Vulcanológico y Sismológico de Costa Rica, Costa Rica
HEL	Institute of Seismology, University of Helsinki, Finland
HFS	Hagfors Observatory, Sweden
HFS1	Hagfors Observatory, Sweden
HFS2	Hagfors Observatory, Sweden
HKC	Hong Kong Observatory, Hong Kong
HLUG	Hessisches Landesamt für Umwelt und Geologie, Germany
HLW	National Research Institute of Astronomy and Geophysics, Egypt
HNR	Ministry of Mines, Energy and Rural Electrification, Solomon Islands
HON	Pacific Tsunami Warning Center - NOAA, USA
HRVD	Harvard University, USA
HRVD_LR	Department of Geological Sciences, Harvard University, USA
HVO	Hawaiian Volcano Observatory, USA
HYB	National Geophysical Research Institute, India
HYD	National Geophysical Research Institute, India
IAG	Instituto Andaluz de Geofísica, Spain
IASPEI	IASPEI Working Group on Reference Events, USA
ICE	Instituto Costarricense de Electricidad, Costa Rica
IDC	International Data Centre, CTBTO, Austria
IDG	Institute of Dynamics of Geosphere, Russian Academy of Sciences, Russia
IEPN	Institute of Environmental Problems of the North, Russian Academy of Sciences, Russia
IGIL	Instituto Geofísico do Infante Dom Luiz, Portugal
IGQ	Servicio Nacional de Sismología y Vulcanología, Ecuador
IGS	Institute of Geological Sciences, United Kingdom
INDEPTH3	International Deep Profiling of Tibet and the Himalayas, USA
INET	Instituto Nicaragüense de Estudios Territoriales, Nicaragua
INMG	Instituto Português do Mar e da Atmosfera, I.P., Portugal
IPEC	The Institute of Physics of the Earth (IPEC), Czech Republic
IPER	Institute of Physics of the Earth, Academy of Sciences, Moscow, Russia
IPGP	Institut de Physique du Globe de Paris, France
IPRG	Institute for Petroleum Research and Geophysics, Israel
IRIS	IRIS Data Management Center, USA
IRSM	Institute of Rock Structure and Mechanics, Czech Republic
ISK	Kandilli Observatory and Research Institute, Turkey
ISN	Iraqi Meteorological and Seismology Organisation, Iraq
ISS	International Seismological Summary, United Kingdom
IST	Institute of Physics of the Earth, Technical University of Istanbul, Turkey
ISU	Institute of Seismology, Academy of Sciences, Republic of Uzbekistan, Uzbekistan
JEN	Geodynamisches Observatorium Moxa, Germany
JMA	Japan Meteorological Agency, Japan
JOH	Bernard Price Institute of Geophysics, South Africa
JSN	Jamaica Seismic Network, Jamaica

Table 10.2: Continued.

Agency Code	Agency Name
JSO	Jordan Seismological Observatory, Jordan
KBC	Institut de Recherches Géologiques et Minières, Cameroon
KEA	Korea Earthquake Administration, Democratic People's Republic of Korea
KEW	Kew Observatory, United Kingdom
KHC	Geofysikalni Ustav, Ceske Akademie Ved, Czech Republic
KISR	Kuwait Institute for Scientific Research, Kuwait
KLM	Malaysian Meteorological Service, Malaysia
KMA	Korea Meteorological Administration, Republic of Korea
KNET	Kyrgyz Seismic Network, Kyrgyzstan
KOLA	Kola Regional Seismic Centre, GS RAS, Russia
KRAR	Krasnoyarsk Scientific Research Inst. of Geology and Mineral Resources, Russia, Russia
KRL	Geodätisches Institut der Universität Karlsruhe, Germany
KRNET	Institute of Seismology, Academy of Sciences of Kyrgyz Republic, Kyrgyzstan
KRSC	Kamchatkan Experimental and Methodical Seismological Department, GS RAS, Russia
KRSZO	Old BUD, Unknown
KSA	Observatoire de Ksara, Lebanon
KUK	Geological Survey Department of Ghana, Ghana
LAO	Large Aperture Seismic Array, USA
LDG	Laboratoire de Détection et de Géophysique/CEA, France
LDN	University of Western Ontario, Canada
LDO	Lamont-Doherty Earth Observatory, USA
LED	Landeserdbebendienst Baden-Württemberg, Germany
LEDBW	Landeserdbebendienst Baden-Württemberg, Germany
LER	Besucherbergwerk Binweide Station, Germany
LIB	Tripoli, Libya
LIC	Station Géophysique de Lamto, Ivory Coast
LIM	Lima, Peru
LIS	Instituto de Meteorologia, Portugal
LIT	Geological Survey of Lithuania, Lithuania
LJU	Slovenian Environment Agency, Slovenia
LPA	Universidad Nacional de La Plata, Argentina
LSZ	Geological Survey Department of Zambia, Zambia
LVSN	Latvian Seismic Network, Latvia
MAN	Philippine Institute of Volcanology and Seismology, Philippines
MAT	The Matsushiro Seismological Observatory, Japan
MCO	Macao Meteorological and Geophysical Bureau, Macao, China
MDD	Instituto Geográfico Nacional, Spain
MED_RCMT	MedNet Regional Centroid - Moment Tensors, Italy
MERI	Maharashtra Engineering Research Institute, India
MES	Messina Seismological Observatory, Italy
MEX	Instituto de Geofísica de la UNAM, Mexico
MIRAS	Mining Institute of the Ural Branch of the Russian Academy of Sciences, Russia

Table 10.2: Continued.

Agency Code	Agency Name
MOLD	Institute of Geophysics and Geology, Moldova
MOS	Geophysical Survey of Russian Academy of Sciences, Russia
MOZ	Direccao Nacional de Geologia, Mozambique
MRB	Institut Cartogràfic i Geològic de Catalunya, Spain
MSI	Messina Seismological Observatory, Italy
MSSP	Micro Seismic Studies Programme, PINSTECH, Pakistan
MUN	Mundaring Observatory, Australia
NAI	University of Nairobi, Kenya
NAM	The Geological Survey of Namibia, Namibia
NAO	Stiftelsen NORSAR, Norway
NCEDC	Northern California Earthquake Data Center, USA
NDI	National Centre for Seismology of the Ministry of Earth Sciences of India, India
NEIC	National Earthquake Information Center, USA
NEIS	National Earthquake Information Service, USA
NERS	North Eastern Regional Seismological Centre, GS RAS, Russia
NIC	Cyprus Geological Survey Department, Cyprus
NIED	National Research Institute for Earth Science and Disaster Prevention, Japan
NNC	National Nuclear Center, Kazakhstan
NORS	North Ossetia (Alania) Branch, Geophysical Survey, Russian Academy of Sciences, Russia
NOU	IRD Centre de Nouméa, New Caledonia
NSSC	National Syrian Seismological Center, Syria
NSSP	National Survey of Seismic Protection, Armenia
OBM	Research Centre of Astronomy and Geophysics, Mongolia
OGSO	Ohio Geological Survey, USA
OMAN	Sultan Qaboos University, Oman
ORF	Orfeus Data Center, Netherlands
OSPL	Observatorio Sismologico Politecnico Loyola, Dominican Republic
OSUB	Osservatorio Sismologico Universita di Bari, Italy
OTT	Canadian Hazards Information Service, Natural Resources Canada, Canada
PAL	Palisades, USA
PAS	California Institute of Technology, USA
PDA	Universidade dos Açores, Portugal
PDG	Seismological Institute of Montenegro, Montenegro
PEK	Peking, China
PGC	Pacific Geoscience Centre, Canada
PLV	National Center for Scientific Research, Vietnam
PMEL	Pacific seismicity from hydrophones, USA
PMR	Alaska Tsunami Warning Center,, USA
PNNL	Pacific Northwest National Laboratory, USA
PNSN	Pacific Northwest Seismic Network, USA
PPT	Laboratoire de Géophysique/CEA, French Polynesia
PRE	Council for Geoscience, South Africa

Table 10.2: Continued.

Agency Code	Agency Name
PRU	Geophysical Institute, Academy of Sciences of the Czech Republic, Czech Republic
PTO	Instituto Geofísico da Universidade do Porto, Portugal
PTWC	Pacific Tsunami Warning Center, USA
QCP	Manila Observatory, Philippines
QUE	Pakistan Meteorological Department, Pakistan
QUI	Escuela Politécnica Nacional, Ecuador
RAB	Rabaul Volcanological Observatory, Papua New Guinea
RBA	Université Mohammed V, Morocco
REN	MacKay School of Mines, USA
REY	Icelandic Meteorological Office, Iceland
RHSSO	Republic Hydrometeorological Service, Seismological Observatory, Banja Luka, Bosnia-Herzegovina
RISSC	Laboratory of Research on Experimental and Computational Seimology, Italy
RMIT	Royal Melbourne Institute of Technology, Australia
ROC	Odenbach Seismic Observatory, USA
ROM	Istituto Nazionale di Geofisica e Vulcanologia, Italy
RRLJ	Regional Research Laboratory Jorhat, India
RSMAC	Red Sísmica Mexicana de Apertura Continental, Mexico
RSNC	Red Sismológica Nacional de Colombia, Colombia
RSPR	Red Sísmica de Puerto Rico, USA
RYD	King Saud University, Saudi Arabia
SAPSE	Southern Alps Passive Seismic Experiment, New Zealand
SAR	Sarajevo Seismological Station, Bosnia and Herzegovina
SCB	Observatorio San Calixto, Bolivia
SCEDC	Southern California Earthquake Data Center, USA
SDD	Universidad Autonoma de Santo Domingo, Dominican Republic
SEA	Geophysics Program AK-50, USA
SET	Setif Observatory, Algeria
SFS	Real Instituto y Observatorio de la Armada, Spain
SGS	Saudi Geological Survey, Saudi Arabia
SHL	Central Seismological Observatory, India
SIGU	Subbotin Institute of Geophysics, National Academy of Sciences, Ukraine
SIK	Seismic Institute of Kosovo, Unknown
SIO	Scripps Institution of Oceanography, USA
SJA	Instituto Nacional de Prevención Sísmica, Argentina
SJS	Instituto Costarricense de Electricidad, Costa Rica
SKHL	Sakhalin Experimental and Methodological Seismological Expedition, GS RAS, Russia
SKL	Sakhalin Complex Scientific Research Institute, Russia
SKO	Seismological Observatory Skopje, FYR Macedonia
SLC	Salt Lake City, USA
SLM	Saint Louis University, USA
SNET	Servicio Nacional de Estudios Territoriales, El Salvador
SNM	New Mexico Institute of Mining and Technology, USA

Table 10.2: Continued.

Agency Code	Agency Name
SNSN	Saudi National Seismic Network, Saudi Arabia
SOF	Geophysical Institute, Bulgarian Academy of Sciences, Bulgaria
SOME	Seismological Experimental Methodological Expedition, Kazakhstan
SPA	USGS - South Pole, Antarctica
SPGM	Service de Physique du Globe, Morocco
SRI	Stanford Research Institute, USA
SSN	Sudan Seismic Network, Sudan
SSNC	Servicio Sismológico Nacional Cubano, Cuba
SSS	Centro de Estudios y Investigaciones Geotecnicas del San Salvador, El Salvador
STK	Stockholm Seismological Station, Sweden
STR	Institut de Physique du Globe, France
STU	Stuttgart Seismological Station, Germany
SVSA	Sistema de Vigilância Sismológica dos Açores, Portugal
SYO	National Institute of Polar Research, Japan
SZGRF	Seismologisches Zentralobservatorium Gräfenberg, Germany
TAC	Estación Central de Tacubaya, Mexico
TAN	Antananarivo, Madagascar
TANZANIA	Tanzania Broadband Seismic Experiment, USA
TAP	CWB, Chinese Taipei
TAU	University of Tasmania, Australia
TEH	Tehran University, Iran
TEIC	Center for Earthquake Research and Information, USA
THE	Department of Geophysics, Aristotle University of Thessaloniki, Greece
THR	International Institute of Earthquake Engineering and Seismology (IIEES), Iran
TIF	Institute of Earth Sciences/ National Seismic Monitoring Center, Georgia
TIR	The Institute of Seismology, Academy of Sciences of Albania, Albania
TRI	Istituto Nazionale di Oceanografia e di Geofisica Sperimentale (OGS), Italy
TRN	The Seismic Research Centre, Trinidad and Tobago
TTG	Titograd Seismological Station, Montenegro
TUL	Oklahoma Geological Survey, USA
TUN	Institut National de la Météorologie, Tunisia
TVA	Tennessee Valley Authority, USA
TZN	University of Dar Es Salaam, Tanzania
UAF	Department of Geosciences, USA
UAV	Red Sismológica de Los Andes Venezolanos, Venezuela
UCC	Royal Observatory of Belgium, Belgium
UCR	Sección de Sismología, Vulcanología y Exploración Geofísica, Costa Rica
UGN	Institute of Geonics AS CR, Czech Republic
ULE	University of Leeds, United Kingdom

Table 10.2: Continued.

Agency Code	Agency Name
UNAH	Universidad Nacional Autonoma de Honduras, Honduras
UPA	Universidad de Panama, Panama
UPIES	Institute of Earth- and Environmental Science, Germany
UPP	University of Uppsala, Sweden
UPSL	University of Patras, Department of Geology, Greece
USAEC	United States Atomic Energy Commission, USA
USCGS	United States Coast and Geodetic Survey, USA
USGS	United States Geological Survey, USA
UUSS	The University of Utah Seismograph Stations, USA
UVC	Universidad del Valle, Colombia
VAO	Instituto Astronomico e Geofisico, Brazil
VIE	Zentralanstalt für Meteorologie und Geodynamik (ZAMG), Austria
VKMS	Lab. of Seismic Monitoring, Voronezh region, GSRAS & Voronezh State University, Russia
VLA	Vladivostok Seismological Station, Russia
VSI	University of Athens, Greece
WAR	Institute of Geophysics, Polish Academy of Sciences, Poland
WBNET	West Bohemia Seismic Network, Czech Republic
WEL	Institute of Geological and Nuclear Sciences, New Zealand
WES	Weston Observatory, USA
WUSTL	Washington University Earth and Planetary Sciences, USA
YARS	Yakutiya Regional Seismological Center, GS SB RAS, Russia
ZAG	Seismological Survey of the Republic of Croatia, Croatia
ZUR	Swiss Seismological Service (SED), Switzerland
ZUR_RMT	Zurich Moment Tensors, Switzerland

Table 10.3: Phases reported to the ISC. These include phases that could not be matched to an appropriate ak135 phases. Those agencies that reported at least 10% of a particular phase are also shown.

Reported Phase	Total	Agencies reporting
P	3529658	ROM (13%)
S	1621614	TAP (21%), JMA (16%), ROM (14%)
AML	779007	ROM (78%), ATH (20%)
IAmb	437484	NEIC (99%)
NULL	404275	NEIC (36%), AEIC (14%), RSNC (13%), IDC (11%)
Pn	212794	NEIC (31%), IDC (12%)
Pg	176784	NNC (13%), LDG (11%)
IAML	168972	DDA (51%), GUC (21%)
Sg	138368	LDG (15%), ZAG (11%)
pmax	124980	MOS (75%), BJI (25%)
IAMs_20	117190	NEIC (99%)
LR	105666	IDC (57%), BJI (36%)
PG	105492	ISK (55%), HEL (17%), PRU (13%)
Sn	89288	LDG (14%), IDC (13%), NEIC (13%)
SG	87578	ISK (32%), PRU (24%), HEL (24%), IPEC (11%)
PN	77536	ISK (69%), MOS (12%)
Lg	58173	NNC (47%), MDD (32%)
PKP	33018	IDC (56%), BJI (11%)
T	26447	IDC (93%)
PKPbc	20434	IDC (63%), BGR (13%)
PKIKP	19931	MOS (97%)
MSG	19119	HEL (99%)
pP	18643	BJI (42%), IDC (19%)
MLR	17217	MOS (100%)
SN	16884	HEL (50%), ISK (22%), BRA (12%)
END	16477	ROM (100%)
A	15494	INMG (53%), SKHL (28%), SVSA (19%)
PP	14657	BJI (32%), IDC (21%)
PcP	12277	IDC (64%), VIE (11%)
PKPdf	10822	NEIC (35%), BGR (12%), BER (11%)
Sb	9561	IRIS (95%)
PKiKP	8726	IRIS (41%), VIE (26%), IDC (21%)
PKPab	8493	IDC (38%), VIE (15%), NEIC (13%), BGR (12%)
SS	8325	BJI (34%), MOS (31%)
PB	7947	HEL (100%)
sP	7717	BJI (82%)
SB	7356	HEL (100%)
smax	7107	MOS (73%), BJI (27%)
Pb	6352	IRIS (89%)
x	5468	NDI (50%), PRU (34%)
AMB	4776	SKHL (66%), BJI (34%)
AMS	4284	PRU (81%), SKHL (12%)
Pdiff	4220	IRIS (64%), IDC (14%)
PKP2	3936	MOS (91%)
ScP	3841	IDC (83%)
IAmb_Lg	2999	NEIC (100%)

Table 10.3: (continued)

Reported Phase	Total	Agencies reporting
PKKPbc	2971	IDC (94%)
LG	2885	BRA (87%), OTT (13%)
*PP	2391	MOS (100%)
LQ	2259	PPT (41%), INMG (27%), IEPN (15%), BELR (11%)
Smax	2095	BYKL (100%)
sS	1966	BJI (94%)
Trac	1916	OTT (100%)
pPKP	1872	BJI (47%), IDC (29%), PRU (15%)
AMP	1834	IEPN (76%), HLW (19%)
PKhKP	1722	IDC (100%)
IVMs_BB	1718	HYB (52%), BER (46%)
PPP	1666	MOS (76%)
Pmax	1600	BYKL (98%)
PS	1533	MOS (42%)
X	1494	JMA (69%), SYO (28%)
SKPbc	1452	IDC (92%)
SKS	1433	BJI (44%), PRU (20%), INMG (13%)
L	1394	BGR (47%), WAR (33%)
E	1376	ZAG (99%)
SSS	1285	MOS (51%), CLL (18%), BELR (12%)
PKHKP	1135	MOS (100%)
Sgmax	1046	NERS (100%)
SKSac	1037	BER (40%), HYB (12%), INMG (11%)
PKPPKP	993	IDC (94%)
sPKP	973	BJI (96%)
max	965	BYKL (100%)
Pdif	889	BER (33%), HYB (14%), BJI (12%)
PKPAB	883	PRU (100%)
IVmB_BB	865	BER (64%), HYB (34%)
ScS	861	BJI (72%), IDC (16%)
pPKPbc	847	IDC (51%), BGR (25%), VIE (17%)
SKKS	775	BJI (85%)
PKPDF	748	PRU (100%)
pPKPdf	712	VIE (43%), BER (20%), NEIC (16%)
LRM	692	BELR (53%), MOLD (46%)
SP	641	BER (30%), MOS (27%), PRU (14%)
PDIFF	637	PRU (43%), BRA (31%), IPEC (15%)
H	538	IDC (100%)
PKP1	525	LIC (85%)
*SP	522	MOS (100%)
PKS	477	BJI (84%)
PKKP	472	IDC (83%)
SKP	412	IDC (73%), PRU (15%)
PcS	406	BJI (85%)
Lm	392	CLL (100%)
pPKPab	390	VIE (50%), CLL (15%), IDC (14%), BGR (11%)
*SS	347	MOS (100%)

Table 10.3: (continued)

Reported Phase	Total	Agencies reporting
Sgm	323	SIGU (100%)
SKKPbc	301	IDC (92%)
PKKPab	301	IDC (83%)
PPS	290	CLL (56%), MOS (21%), MOLD (18%)
PKP2bc	288	IDC (100%)
Pgmax	283	NERS (100%)
pPKiKP	239	VIE (64%), UCC (13%), CLL (12%)
LmV	228	CLL (100%)
IVmBBB	228	HYB (52%), BER (48%)
PKPpre	211	NEIC (53%), PRU (36%)
SKPdf	210	BER (43%), VIE (33%), CLL (17%)
LMZ	195	WAR (100%)
(P)	189	BRG (69%), CLL (31%)
P3KPbc	189	IDC (100%)
Sm	181	SIGU (100%)
Pm	174	SIGU (100%)
AMd	173	NIC (100%)
PM	165	BELR (100%)
AMb	161	IGIL (79%), NDI (20%)
PCP	148	PRU (46%), LPA (38%)
SSSS	143	CLL (83%), ISC (17%)
Rg	136	NAO (42%), BER (29%), IDC (18%)
IVMsBB	132	HYB (53%), BER (46%)
LmH	131	CLL (100%)
Pgm	130	SIGU (100%)
pPdiff	130	VIE (67%), SYO (31%)
PmP	128	BGR (83%), ZUR (17%)
SKPab	128	VIE (58%), IDC (27%), BGR (12%)
SmS	118	BGR (98%)
SKKSac	117	CLL (44%), IEPN (24%), HYB (20%)
sPKPdf	114	VIE (79%), CLL (16%)
PnPn	112	UCC (78%), SYO (22%)
PKKPdf	104	VIE (77%), NEIC (12%)
Pd0	101	ATH (100%)
m	93	SIGU (100%)
Sdif	89	CLL (53%), INMG (27%), PPT (11%)
P'P'df	87	VIE (92%)
P4KPbc	84	IDC (100%)
Snm	83	SIGU (100%)
pPcP	81	IDC (91%)
SKSdf	74	BER (70%), VIE (20%)
sPKPab	72	VIE (82%), CLL (11%)
Lmax	71	CLL (100%)
Pc0	70	ATH (100%)
PKP2ab	64	IDC (100%)
pPP	57	CLL (47%), LPA (32%), BGR (16%)
p	56	MAN (91%)

Table 10.3: (continued)

Reported Phase	Total	Agencies reporting
sPKiKP	54	VIE (67%), UCC (19%), CLL (13%)
SDIFF	54	BRG (72%), LPA (19%)
rx	52	SKHL (100%)
sPP	48	CLL (98%)
SCS	47	LPA (85%)
sPKPbc	47	VIE (81%), CLL (11%)
SKIKS	42	LPA (100%)
P*	41	BGR (59%), BUD (24%)
PKPM	41	BELR (98%)
PKSdf	39	BER (62%), CLL (31%)
Sdiff	38	LJU (50%), VIE (21%), IDC (16%), OMAN (13%)
PSKS	37	CLL (100%)
LQM	35	BELR (86%), MOLD (14%)
SH	35	SYO (100%)
PKPdiff	34	CLL (100%)
PgPg	34	BYKL (88%), UCC (12%)
pPn	34	UCC (91%)
(sP)	33	CLL (100%)
RG	31	IPEC (87%), HEL (13%)
SKKP	31	IDC (74%), BRG (16%)
sPn	30	UCC (90%)
SKSP	30	BELR (47%), MOLD (33%), CLL (20%)
MSN	29	HEL (83%), BER (17%)
PPPP	27	CLL (100%)
SgSg	27	BYKL (100%)
P3KP	26	IDC (100%)
AMSG	25	BER (100%)
Pnm	24	SIGU (100%)
SKIKP	23	LPA (100%)
s	23	SFS (78%), MAN (22%)
(PP)	23	CLL (100%)
pPdif	23	HYB (65%), CLL (30%)
PKPPKPdf	22	CLL (100%)
SM	21	BELR (86%), ISU (14%)
SKiKP	20	IDC (75%), IEPN (25%)
AMPG	20	BER (100%)
MPN	19	HEL (58%), BER (42%)
sSS	18	CLL (100%)
SCP	18	PRU (61%), IPEC (22%), BRG (17%)
(Sn)	17	OSUB (82%), CLL (18%)
sPdif	16	CLL (69%), HYB (31%)
PSP	16	LPA (100%)
R	15	LDG (100%)
PbPb	14	UCC (100%)
PPM	14	BELR (100%)
Plp	14	CLL (100%)
PA	13	JSN (69%), ATA (31%)

Table 10.3: (continued)

Reported Phase	Total	Agencies reporting
SPP	13	MOS (46%), CLL (31%), BELR (23%)
(pP)	13	CLL (100%)
SKSp	12	BRA (100%)
LV	12	CLL (100%)
sPPP	11	CLL (100%)
PPPrev	11	CLL (100%)
Sglp	11	CLL (100%)
SKKKS	11	BELR (100%)
PsP	11	MOLD (82%), BELR (18%)
P'P'bc	11	VIE (82%), NEIC (18%)
sSKSac	11	HYB (73%), CLL (27%)
AMs_VX	11	NEIC (100%)
(Pg)	11	CLL (100%)
pSKPab	10	BGR (100%)
(S)	10	CLL (100%)
(pPKPdf)	10	CLL (100%)
S*	10	BUD (70%), BGR (30%)
(SSS)	10	CLL (100%)
Li	10	MOLD (100%)
tx	9	SOME (78%), IEPN (22%)
SKPDF	9	BRA (100%)
(PKPdf)	9	CLL (100%)
PPlp	9	CLL (100%)
(SS)	9	CLL (100%)
PSPS	9	CLL (100%)
(Pdif)	8	CLL (100%)
PKSbc	8	CLL (75%), LJU (25%)
SnSn	8	UCC (75%), SVSA (25%)
(Pn)	8	CLL (88%), OSUB (12%)
(PKPab)	7	CLL (100%)
Lm(360	7	CLL (100%)
Cod	7	SFS (100%)
PSS	6	CLL (83%), BRG (17%)
PKKS	6	IEPN (50%), BRG (33%), IDC (17%)
(PKP)	6	CLL (50%), BRG (50%)
PK	6	EAF (50%), MDD (33%), SVSA (17%)
(sPP)	6	CLL (100%)
pwP	6	NEIC (100%)
(SSSS)	6	CLL (100%)
PKPdif	6	NEIC (83%), CLL (17%)
(Sg)	6	CLL (83%), OSUB (17%)
(PPS)	6	CLL (100%)
PPP(2)	5	LPA (100%)
sPdiff	5	SYO (100%)
PKIKS	5	LPA (100%)
sSn	5	UCC (100%)
pPDIFF	5	BRG (100%)

Table 10.3: (continued)

Reported Phase	Total	Agencies reporting
SKKSacre	5	CLL (100%)
(PKiKP)	5	CLL (100%)
PgC	5	BUD (100%)
n	5	BUD (100%)
IPZ	5	SJA (100%)
(PPP)	5	CLL (100%)
del	5	AUST (60%), KNET (40%)
pSKSac	5	HYB (100%)
SKSSKSac	4	CLL (100%)
P(2)	4	CLL (100%)
Pd2	4	ATH (100%)
(PS)	4	CLL (100%)
(sPKPdf)	4	CLL (100%)
P'P'ab	4	PPT (100%)
PPmax	4	CLL (100%)
(PcP)	4	CLL (100%)
PKPlp	4	CLL (100%)
sPcP	4	CLL (100%)
pScP	4	IDC (100%)
SKKSdf	3	CLL (67%), LJU (33%)
(Sdif)	3	CLL (100%)
SKPd	3	BER (100%)
i-	3	INMG (100%)
PKiKPd	3	BUD (100%)
SKKPdf	3	CLL (100%)
PZ	3	SJA (100%)
SKPPKPdf	3	CLL (100%)
(SKPdf)	3	CLL (100%)
I	3	NDI (67%), SOME (33%)
sSSSS	3	CLL (100%)
SSmax	3	CLL (100%)
pS	3	CLL (100%)
PSSrev	3	CLL (100%)
SKKPab	3	IDC (67%), IEPN (33%)
(pPKPab)	3	CLL (100%)
sPS	3	CLL (100%)
SKKSacr	2	CLL (100%)
(sS)	2	CLL (100%)
sSKKSac	2	CLL (100%)
sSb	2	UCC (100%)
PKPab(2)	2	CLL (100%)
Pdiffmax	2	CLL (100%)
PKPbc(2)	2	CLL (100%)
(SKSac)	2	CLL (100%)
EP	2	AAE (100%)
Sx	2	YARS (100%)
LH	2	CLL (100%)

Table 10.3: (continued)

Reported Phase	Total	Agencies reporting
sPKPPKPd	2	CLL (100%)
pPKPPKPd	2	CLL (100%)
SSSmax	2	CLL (100%)
G	2	SCB (100%)
P4KP	2	IDC (100%)
Sk	2	CLL (100%)
SKPPKPab	2	CLL (100%)
sSSS	2	CLL (100%)
(pPKPbc)	2	CLL (100%)
sPDIFF	2	BRG (100%)
PcPPKPre	2	CLL (100%)
Pnd	2	WAR (100%)
PSPSrev	2	CLL (100%)
ES	2	AAE (100%)
sPPS	2	CLL (100%)
PGN	2	HEL (100%)
PKiKPD	2	BUD (100%)
PKPPKPbc	2	CLL (100%)
(sPKiKP)	2	CLL (100%)
SKPPKPbc	2	CLL (100%)
(sPdif)	1	CLL (100%)
pPg	1	UCC (100%)
PPPPmax	1	CLL (100%)
PN2	1	SJA (100%)
dif	1	INMG (100%)
(pPKiKP)	1	CLL (100%)
-ML	1	SVSA (100%)
PKP(2)	1	CLL (100%)
PD	1	UPA (100%)
Q	1	BELR (100%)
KP	1	BRG (100%)
pSKP	1	BRG (100%)
s_20	1	RSNC (100%)
PPPmax	1	CLL (100%)
(sSdiff)	1	CLL (100%)
pPPPP	1	CLL (100%)
sPKSdf	1	CLL (100%)
(PSKS)	1	CLL (100%)
PKPdf22	1	CLL (100%)
(PKPpre)	1	CLL (100%)
Pc2	1	ATH (100%)
3PKP	1	CLL (100%)
SKPa	1	NAO (100%)
sPPPP	1	CLL (100%)
(PSPS)	1	CLL (100%)
LRM1	1	BELR (100%)
(sPKPab)	1	CLL (100%)

Table 10.3: (continued)

Reported Phase	Total	Agencies reporting
P M	1	BELR (100%)
(sSS)	1	CLL (100%)
LRN	1	MOLD (100%)
pSKKPbc	1	CLL (100%)
PPrev	1	CLL (100%)
(SKKSac)	1	CLL (100%)
Pe	1	UPA (100%)
PKIK	1	LPA (100%)
sSKSP	1	CLL (100%)
SSrev	1	CLL (100%)
Z	1	EAF (100%)
PnC	1	BUD (100%)
Pd1	1	ATH (100%)
(SSSm)	1	CLL (100%)
PKSdfp	1	CLL (100%)
SbSb	1	UCC (100%)
PKP1M	1	BELR (100%)
(Sb)	1	CLL (100%)
IAM	1	GUC (100%)
sSSP	1	CLL (100%)
pPKSdf	1	CLL (100%)
RQ	1	MOLD (100%)
sPKS	1	BELR (100%)
DMd	1	NEIC (100%)
SSSrev	1	CLL (100%)
(pPPS)	1	CLL (100%)
P9	1	NDI (100%)
pPPS	1	CLL (100%)
SHS	1	SFS (100%)
pPmax	1	CLL (100%)
(SG)	1	BRG (100%)
pp	1	SYO (100%)
(SKPbc)	1	CLL (100%)
(sPPP)	1	CLL (100%)
Amb	1	AAE (100%)
P*P	1	ZUR (100%)
(L)	1	CLL (100%)
KIKP	1	LPA (100%)
SRS	1	KEA (100%)
Pg(2)	1	CLL (100%)
IP	1	BELR (100%)
PxPxbc	1	BGR (100%)
SN2	1	SJA (100%)
(sPKPbc)	1	CLL (100%)
SKS	1	INMG (100%)
SKSacmax	1	CLL (100%)
pPKSbc	1	CLL (100%)

Table 10.3: *(continued)*

Reported Phase	Total	Agencies reporting
PDIF	1	PRU (100%)
PKPbclp	1	CLL (100%)
AP	1	MOS (100%)
Sd1	1	ATH (100%)
sP)	1	CLL (100%)
PKKSdf	1	CLL (100%)
pZP	1	SYO (100%)
pSKPbc	1	CLL (100%)
(pPP)	1	CLL (100%)
PKPPKPab	1	CLL (100%)
PPPPrev	1	CLL (100%)
(sKKSac)	1	CLL (100%)
SSS(2)	1	LPA (100%)
PKPdiff2	1	CLL (100%)
(SSm)	1	CLL (100%)
(SKKPbc)	1	CLL (100%)
sPg	1	UCC (100%)
(PKSdf)	1	CLL (100%)
pP(2)	1	CLL (100%)
Sdiffmax	1	CLL (100%)
pPKKPbc	1	CLL (100%)
sSdiff	1	CLL (100%)
(SKSP)	1	CLL (100%)
pSKKPdf	1	CLL (100%)
(pPdif)	1	CLL (100%)
PgD	1	BUD (100%)

Table 10.4: *Reporters of amplitude data*

Agency	Number of reported amplitudes	Number of amplitudes in ISC located events	Number used for ISC <i>mb</i>	Number used for ISC <i>MS</i>
ROM	627166	9923	0	0
NEIC	561726	268405	187405	56093
IDC	355017	337212	140880	35907
WEL	244767	16172	0	0
ATH	155366	29774	0	0
MOS	117731	115254	59571	12264
NNC	89587	28098	114	0
DDA	86147	11140	0	0
DJA	84232	50079	11712	0
ISK	83953	13936	0	0
BJI	72934	64074	13904	18714
SOME	66724	19115	1519	0
RSNC	52068	5067	0	0
MDD	47760	9982	0	0
THE	42179	11987	0	0
VIE	41415	23331	7135	0
WBNET	38415	273	0	0
GUC	35594	12172	13	0
LDG	27341	4425	2	0
HEL	19078	426	0	0
PRU	15957	5232	0	2038
MAN	14866	4571	0	0
DMN	14528	13965	956	0
INMG	12952	6812	3459	0
SJA	10484	5963	12	0
BER	10382	2385	0	0
PPT	10352	9018	985	2768
LJU	9364	363	0	0
YARS	9292	642	1	0
SKHL	8041	5847	1	0
BGR	7272	6698	5162	0
NIC	6874	2729	0	0
PDG	6714	4570	0	0
ZUR	6588	748	0	0
BUC	5415	1344	0	0
BGS	5184	3038	1303	955
BYKL	4688	1230	0	0
BRG	4186	2453	434	0
SNET	3947	1782	0	0
SSNC	3805	242	0	0
MRB	3756	197	0	0
SVSA	3377	545	410	0
SKO	3305	560	0	0
PRE	3118	308	0	0

Table 10.4: Continued.

Agency	Number of reported amplitudes	Number of amplitudes in ISC located events	Number used for ISC <i>mb</i>	Number used for ISC <i>MS</i>
NDI	2938	2596	1017	129
CLL	2909	2501	380	295
HYB	2671	2621	1051	0
KNET	2536	875	0	0
DNK	2445	2208	1614	0
LIC	2318	2079	1267	0
NAO	2142	2114	1495	0
OTT	1914	217	0	0
IEPN	1844	1456	32	0
ECX	1793	292	0	0
ASRS	1721	796	0	0
LVSN	1668	255	0	0
ATA	1528	421	0	0
UCR	1395	1369	0	0
IPEC	1360	272	0	0
NERS	1339	94	0	0
OSPL	1289	465	0	0
IGIL	1086	573	103	256
KRSZO	794	271	0	0
UCC	676	462	351	0
WAR	661	628	0	494
THR	646	465	0	0
BELR	621	567	1	239
SIGU	602	302	0	0
MOLD	566	308	43	0
LIT	515	421	171	0
ISN	471	297	0	0
JSO	257	207	0	0
MIRAS	239	28	0	0
TEH	119	8	0	0
SCB	101	91	0	0
UPA	37	4	0	0
LSZ	7	3	0	0
JSN	2	2	0	0
GCG	2	1	0	0
MEX	1	0	0	0
EAF	1	0	0	0

11

Glossary of ISC Terminology

- Agency/ISC data contributor

An academic or government institute, seismological organisation or company, geological/meteorological survey, station operator or author that reports or contributed data in the past to the ISC or one of its predecessors. Agencies may contribute data to the ISC directly, or indirectly through other ISC data contributors.

- Agency code

A unique, maximum eight-character code for a data reporting agency (e.g. NEIC, GFZ, BUD) or author (e.g. ISC, EHB, IASPEI). Often the agency code is the commonly used acronym of the reporting institute.

- Arrival

A phase pick at a station is characterised by a phase name and an arrival time.

- Associated phase

Associated phase arrival or amplitude measurements represent a collection of observations belonging to (i.e. generated by) an event. The complete set of observations are associated to the prime hypocentre.

- Azimuthal gap/Secondary azimuthal gap

The azimuthal gap for an event is defined as the largest angle between two stations with defining phases when the stations are ordered by their event-to-station azimuths. The secondary azimuthal gap is the largest azimuthal gap a single station closes.

- BAAS

Seismological bulletins published by the British Association for the Advancement of Science (1913-1917) under the leadership of H.H. Turner. These bulletins are the predecessors of the ISS Bulletins and include reports from stations distributed worldwide.

- Bulletin

An ordered list of event hypocentres, uncertainties, focal mechanisms, network magnitudes, as well as phase arrival and amplitude observations associated to each event. An event bulletin may list all the reported hypocentres for an event. The convention in the ISC Bulletin is that the preferred (prime) hypocentre appears last in the list of reported hypocentres for an event.

- Catalogue

An ordered list of event hypocentres, uncertainties and magnitudes. An event catalogue typically lists only the preferred (prime) hypocentres and network magnitudes.

- CoSOI/IASPEI

Commission on Seismological Observation and Interpretation, a commission of IASPEI that prepares and discusses international standards and procedures in seismological observation and interpretation.

- Defining/Non-defining phase

A defining phase is used in the location of the event (time-defining) or in the calculation of the network magnitude (magnitude-defining). Non-defining phases are not used in the calculations because they suffer from large residuals or could not be identified.

- Direct/Indirect report

A data report sent (e-mailed) directly to the ISC, or indirectly through another ISC data contributor.

- Duplicates

Nearly identical phase arrival time data reported by one or more agencies for the same station. Duplicates may be created by agencies reporting observations from other agencies, or several agencies independently analysing the waveforms from the same station.

- Event

A natural (e.g. earthquake, landslide, asteroid impact) or anthropogenic (e.g. explosion) phenomenon that generates seismic waves and its source can be identified by an event location algorithm.

- Grouping

The ISC algorithm that organises reported hypocentres into groups of events. Phases associated to any of the reported hypocentres will also be associated to the preferred (prime) hypocentre. The grouping algorithm also attempts to associate phases that were reported without an accompanying hypocentre to events.

- Ground Truth

An event with a hypocentre known to certain accuracy at a high confidence level. For instance, GT0 stands for events with exactly known location, depth and origin time (typically explosions); GT5 stands for events with their epicentre known to 5 km accuracy at the 95% confidence level, while their depth and origin time may be known with less accuracy.

- Ground Truth database

On behalf of IASPEI, the ISC hosts and maintains the IASPEI Reference Event List, a bulletin of ground truth events.

- IASPEI

International Association of Seismology and Physics of the Earth Interior, www.iaspei.org.

- International Registry of Seismograph Stations (IR)

Registry of seismographic stations, jointly run by the ISC and the World Data Center for Seismology, Denver (NEIC). The registry provides and maintains unique five-letter codes for stations participating in the international parametric and waveform data exchange.

- ISC Bulletin

The comprehensive bulletin of the seismicity of the Earth stored in the ISC database and accessible through the ISC website. The bulletin contains both natural and anthropogenic events. Currently the ISC Bulletin spans more than 50 years (1960-to date) and it is constantly extended by adding both recent and past data. Eventually the ISC Bulletin will contain all instrumentally recorded events since 1900.

- ISC Governing Council

According to the ISC Working Statutes the Governing Council is the governing body of the ISC, comprising one representative for each ISC Member.

- ISC-located events

A subset of the events selected for ISC review are located by the ISC. The rules for selecting an event for location are described in Section 10.1.3; ISC-located events are denoted by the author ISC.

- ISC Member

An academic or government institute, seismological organisation or company, geological/meteorological survey, station operator, national/international scientific organisation that contribute to the ISC budget by paying membership fees. ISC members have voting rights in the ISC Governing Council.

- ISC-reviewed events

A subset of the events reported to the ISC are selected for ISC analyst review. These events may or may not be located by the ISC. The rules for selecting an event for review are described in Section 10.1.3. Non-reviewed events are explicitly marked in the ISC Bulletin by the comment following the prime hypocentre "Event not reviewed by the ISC".

- ISF

International Seismic Format (www.isc.ac.uk/standards/isf). A standard bulletin format approved by IASPEI. The ISC Bulletin is presented in this format at the ISC website.

- ISS

International Seismological Summary (1918-1963). These bulletins are the predecessors of the ISC Bulletin and represent the major source of instrumental seismological data before the digital era. The ISS contains regionally and teleseismically recorded events from several hundreds of globally distributed stations.

- Network magnitude

The event magnitude reported by an agency or computed by the ISC locator. An agency can report several network magnitudes for the same event and also several values for the same magnitude type. The network magnitude obtained with the ISC locator is defined as the median of station magnitudes of the same magnitude type.

- Phase

A maximum eight-character code for a seismic, infrasonic, or hydroacoustic phase. During the ISC processing, reported phases are mapped to standard IASPEI phase names. Amplitude measurements are identified by specific phase names to facilitate the computation of body-wave and surface-wave magnitudes.

- Prime hypocentre

The preferred hypocentre solution for an event from a list of hypocentres reported by various agencies or calculated by the ISC.

- Reading

Parametric data that are associated to a single event and reported by a single agency from a single station. A reading typically includes one or more phase names, arrival time and/or amplitude/period measurements.

- Report/Data report

All data that are reported to the ISC are parsed and stored in the ISC database. These may include event bulletins, focal mechanisms, moment tensor solutions, macroseismic descriptions and other event comments, as well as phase arrival data that are not associated to events. Every single report sent to the ISC can be traced back in the ISC database via its unique report identifier.

- Shide Circulars

Collections of station reports for large earthquakes occurring in the period 1899-1912. These reports were compiled through the efforts of J. Milne. The reports are mainly for stations of the British Empire equipped with Milne seismographs. After Milne's death, the Shide Circulars were replaced by the Seismological Bulletins of the BAAS.

- Station code

A unique, maximum six-character code for a station. The ISC Bulletin contains data exclusively from stations registered in the International Registry of Seismograph Stations.

12

Acknowledgements

We thank our colleagues at two long-serving seismological observatories in Germany, Collm (CLL) and Berggießhübel (BRG), for accepting our invitation and submitting the articles on the history and operational procedures for this issue of the Summary.

We are also grateful to all the developers of the Generic Mapping Tools (GMT) suite of software (Wessel and Smith, 1998), used extensively here in producing the graphical figures.

Finally, we thank the ISC Member Institutions, Data Contributors, Funding Agencies (including NSF Award EAR-1417970 and USGS Award G15AC00202) and Sponsors for supporting the long-term operation of the ISC.

References

- Adams, R. D., A. A. Hughes, and D. M. McGregor (1982), Analysis procedures at the International Seismological Centre, *Physics of the Earth and Planetary Interiors*, *30*, 85–93.
- Amante, C., and B. W. Eakins (2009), ETOPO1 1 arc-minute global relief model: procedures, data sources and analysis, *NOAA Technical Memorandum NESDIS NGDC-24*, NOAA.
- Balfour, N., R. Baldwin, and A. Bird (2008), Magnitude calculations in Antelope 4.10, *Analysis Group Note of Geological Survey of Canada*, pp. 1–13.
- Bennett, T. J., V. Oancea, B. W. Barker, Y.-L. Kung, M. Bahavar, B. C. Kohl, J. . Murphy, and I. K. Bondár (2010), The nuclear explosion database NEDB: a new database and web site for accessing nuclear explosion source information and waveforms, *Seismological Research Letters*, *81*, doi:10.1785/gssrl.81.1.12.
- Bisztricsany, E. A. (1958), A new method for the determination of the magnitude of earthquakes, *Geofiz. Kozl*, pp. 69–76.
- Bolt, B. A. (1960), The revision of earthquake epicentres, focal depths and origin time using a high-speed computer, *Geophysical Journal of the Royal Astronomical Society*, *3*, 434–440.
- Bondár, I., and K. McLaughlin (2009a), A new ground truth data set for seismic studies, *Seismological Research Letters*, *80*, 465–472.
- Bondár, I., and K. McLaughlin (2009b), Seismic location bias and uncertainty in the presence of correlated and non-Gaussian travel-time errors, *Bulletin of the Seismological Society of America*, *99*, 172–193.
- Bondár, I., and D. Storchak (2011), Improved location procedures at the International Seismological Centre, *Geophysical Journal International*, *186*, 1220–1244.
- Bondár, I., E. R. Engdahl, X. Yang, H. A. A. Ghalib, A. Hofstetter, V. Kirichenko, R. Wagner, I. Gupta, G. Ekström, E. Bergman, H. Israelsson, and K. McLaughlin (2004), Collection of a reference event set for regional and teleseismic location calibration, *Bulletin of the Seismological Society of America*, *94*, 1528–1545.
- Bondár, I., E. Bergman, E. R. Engdahl, B. Kohl, Y.-L. Kung, and K. McLaughlin (2008), A hybrid multiple event location technique to obtain ground truth event locations, *Geophysical Journal International*, *175*, doi:10.1111/j.1365.246X.2008.03,867x.
- Bormann, P., and J. W. Dewey (2012), The new iaspei standards for determining magnitudes from digital data and their relation to classical magnitudes, is 3.3, *New Manual of Seismological Observatory Practice 2 (NMSOP-2)*, P. Bormann (Ed.), pp. 1–44, doi:10.2312/GFZ.NMSOP-2_IS_3.3,10.2312/GFZ.NMSOP-2, <http://nmsop.gfz-postsdam.de>.
- Bormann, P., and J. Saul (2008), The new IASPEI standard broadband magnitude mB, *Seism. Res. Lett*, *79*(5), 698–705.
- Bormann, P., R. Liu, X. Ren, R. Gutdeutsch, D. Kaiser, and S. Castellaro (2007), Chinese national network magnitudes, their relation to NEIC magnitudes and recommendations for new IASPEI magnitude standards, *Bulletin of the Seismological Society of America*, *97*(1B), 114–127, doi:10.1785/012006007835.
- Bormann, P., R. Liu, Z. Xu, R. Ren, and S. Wendt (2009), First application of the new IASPEI teleseismic magnitude standards to data of the China National Seismographic Network, *Bulletin of the Seismological Society of America*, *99*, 1868–1891, doi:10.1785/0120080010.

- Chang, A. C., R. H. Shumway, R. R. Blandford, and B. W. Barker (1983), Two methods to improve location estimates - preliminary results, *Bulletin of the Seismological Society of America*, 73, 281–295.
- Choy, G. L., and J. L. Boatwright (1995), Global patterns of radiated seismic energy and apparent stress, *J. Geophys. Res.*, 100(B9), 18,205–18,228.
- Dziewonski, A. M., and F. Gilbert (1976), The effect of small, aspherical perturbations on travel times and a re-examination of the correction for ellipticity, *Geophysical Journal of the Royal Astronomical Society*, 44, 7–17.
- Dziewonski, A. M., T.-A. Chou, and J. H. Woodhouse (1981), Determination of earthquake source parameters from waveform data for studies of global and regional seismicity, *J. Geophys. Res.*, 86, 2825–2852.
- Engdahl, E. R., and R. H. Gunst (1966), Use of a high speed computer for the preliminary determination of earthquake hypocentres, *Bulletin of the Seismological Society of America*, 56, 325–336.
- Engdahl, E. R., and A. Villaseñor (2002), Global seismicity: 1900–1999, *International Handbook of Earthquake Engineering and Seismology, International Geophysics series*, 81A, 665–690.
- Engdahl, E. R., R. van der Hilst, and R. Buland (1998), Global teleseismic earthquake relocation with improved travel times and procedures for depth determination, *Bulletin of the Seismological Society of America*, 88, 722–743.
- Flinn, E. A., and E. R. Engdahl (1965), Proposed basis for geographical and seismic regionalization, *Reviews of Geophysics*, 3(1), 123–149.
- Flinn, E. A., E. R. Engdahl, and A. R. Hill (1974), Seismic and geographical regionalization, *Bulletin of the Seismological Society of America*, 64, 771–993.
- Gutenberg, B. (1945a), Amplitudes of P, PP and S and magnitude of shallow earthquakes, *Bulletin of the Seismological Society of America*, 35, 57–69.
- Gutenberg, B. (1945b), Magnitude determination of deep-focus earthquakes, *Bulletin of the Seismological Society of America*, 35, 117–130.
- Gutenberg, B. (1945c), Amplitudes of surface waves and magnitudes of shallow earthquakes, *Bulletin of the Seismological Society of America*, 35, 3–12.
- Gutenberg, B., and C. F. Richter (1956), Magnitude and Energy of earthquakes, *Ann. Geof.*, 9, 1–5.
- Hutton, L. K., and D. M. Boore (1987), The ML scale in southern California, *Bulletin of the Seismological Society of America*, 77, 2074–2094.
- IASPEI (2005), Summary of magnitude working group recommendations on standard procedures for determining earthquake magnitudes from digital data, <http://www.iaspei.org/commissions/CSOI.html#wgmm>, http://www.iaspei.org/commissions/CSOI/summary_of_WG_recommendations_2005.pdf.
- IASPEI (2013), Summary of magnitude working group recommendations on standard procedures for determining earthquake magnitudes from digital data, http://www.iaspei.org/commissions/CSOI/Summary_of_WG_recommendations_20130327.pdf.
- IDC (1999), IDC processing of seismic, hydroacoustic and infrasonic data, *IDC Documentation*.
- Jeffreys, H., and K. E. Bullen (1940), *Seismological Tables*, British Association for the Advancement of Science.
- Kanamori, H. (1977), The energy release in great earthquakes, *J. Geophys. Res.*, 82, 2981–2987.
- Kennett, B. L. N. (2006), Non-linear methods for event location in a global context, *Physics of the Earth and Planetary Interiors*, 158, 45–64.
- Kennett, B. L. N., E. R. Engdahl, and R. Buland (1995), Constraints on seismic velocities in the Earth from traveltimes, *Geophysical Journal International*, 122, 108–124.
- Kennett, B. L. N., E. R. Engdahl, and R. Buland (1996), Ellipticity corrections for seismic phases, *Geophysical Journal International*, 127, 40–48.

- Lee, W. H. K., R. Bennet, and K. Meagher (1972), A method of estimating magnitude of local earthquakes from signal duration, *U.S. Geol. Surv.*, Open-File Rep.
- Murphy, J. R., and B. W. Barker (2006), Improved focal-depth determination through automated identification of the seismic depth phases pP and sP, *Bulletin of the Seismological Society of America*, *96*, 1213–1229.
- NMSOP-2 (2012), *New Manual of Seismological Observatory Practice (NMSOP-2)*, IASPEI, GFZ, German Research Centre for Geosciences, Potsdam, doi:10.2312/GFZ.NMSOP-2, <http://nmsop.gfz-potsdam.de>, urn:nbn:de:kobv:b103-NMSOP-2.
- Nuttli, O. W. (1973), Seismic wave attenuation and magnitude relations for eastern North America, *J. Geophys. Res.*, *78*, 876–885.
- Richter, C. F. (1935), An instrumental earthquake magnitude scale, *Bulletin of the Seismological Society of America*, *25*, 1–32.
- Ringdal, F. (1976), Maximum-likelihood estimation of seismic magnitude, *Bulletin of the Seismological Society of America*, *66*(3), 789–802.
- Sambridge, M. (1999), Geophysical inversion with a neighbourhood algorithm, *Geophysical Journal International*, *138*, 479–494.
- Sambridge, M., and B. L. N. Kennett (2001), Seismic event location: non-linear inversion using a neighbourhood algorithm, *Pure and Applied Geophysics*, *158*, 241–257.
- Storchak, D. A., J. Schweitzer, and P. Bormann (2003), The IASPEI standard seismic phases list, *Seismological Research Letters*, *74*(6), 761–772.
- Storchak, D. A., J. Schweitzer, and P. Bormann (2011), Seismic phase names: IASPEI standard, in *Encyclopedia of Solid Earth Geophysics*, edited by H. Gupta, pp. 1162–1173, Springer.
- Tsuboi, C. (1954), Determination of the Gutenberg-Richter's magnitude of earthquakes occurring in and near Japan, *Zisin (J. Seism. Soc. Japan)*, *Ser. II*(7), 185–193.
- Tsuboi, S., K. Abe, K. Takano, and Y. Yamanaka (1995), Rapid determination of Mw from broadband P waveforms, *Bulletin of the Seismological Society of America*, *85*(2), 606–613.
- Uhrhammer, R. A., and E. R. Collins (1990), Synthesis of Wood-Anderson Seismograms from Broadband Digital Records, *Bulletin of the Seismological Society of America*, *80*(3), 702–716.
- Vaněk, J., A. Zapotek, V. Karnik, N. V. Kondorskaya, Y. V. Riznichenko, E. F. Savarensky, S. L. Solov'yov, and N. V. Shebalin (1962), Standardization of magnitude scales, *Izvestiya Akad. SSSR., Ser. Geofiz.*(2), 153–158, pages 108–111 in the English translation.
- Villaseñor, A., and E. R. Engdahl (2005), A digital hypocenter catalog for the International Seismological Summary, *Seismological Research Letters*, *76*, 554–559.
- Villaseñor, A., and E. R. Engdahl (2007), Systematic relocation of early instrumental seismicity: Earthquakes in the International Seismological Summary for 1960–1963, *Bulletin of the Seismological Society of America*, *97*, 1820–1832.
- Woessner, J., and S. Wiemer (2005), Assessing the quality of earthquake catalogues: estimating the magnitude of completeness and its uncertainty, *Bulletin of the Seismological Society of America*, *95*(2), doi:10.1785/012040.007.
- Young, J. B., B. W. Presgrave, H. Aichele, D. A. Wiens, and E. A. Flinn (1996), The Flinn-Engdahl regionalisation scheme: the 1995 revision, *Physics of the Earth and Planetary Interiors*, *96*, 223–297.

GeoSIG has reason to celebrate 2017

Επέτειος Yıldönümü
Anniversaire
Aniversario
Anniversary
25 Jahrestag
Évforduló
Юбилей سالگرد

Swiss manufacturer GeoSIG Ltd provides earthquake, seismic, structural, dynamic and static monitoring and measuring solutions. Day in, day out — year in, year out — their focus is on vibration and earthquake monitoring.

But 2017 is special.

This year marks the 25th anniversary for GeoSIG, which was founded in 1992. Since its establishment, GeoSIG has gone from strength to strength. They have had hundreds of installations worldwide in dam monitoring, NPP, national earthquake monitoring systems, building structural monitoring, special structures, and bridges. They've built up a network of experienced Partners around the globe; and they have a loyal customer base.

Digital Sensor System

- High expandability — up to 15 channels thru 3 analogue and 12 digital inputs
- Easy and low cost installation
- Real-time data conversion and processing
- Reliable Data — for damage detection, decision making and post event evaluation
- Building code compliant (e.g. California, Panama, etc)
- Permanent self-monitoring without affecting its normal operation



GMS nair

- Perfect for weak motion precision recording
- 147dB dynamic range (0.02-20Hz)
- Support for various types of BB seismometers
- Built-in top performance FBA
- Multiple EEW algorithms on board



If It Moves, You'll Know It. Immediately.



For over 40 years REF TEK®, a Trimble brand, has been the trusted partner for seismologists around the globe.

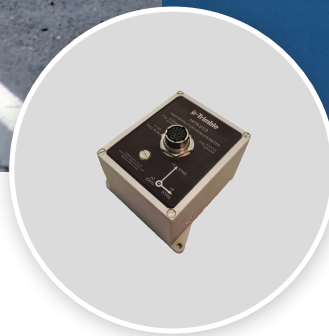
If it shakes, sinks or shifts our reliable sensors and recorders will know about it instantaneously. And you will too, anytime, as sophisticated application software informs you immediately.

Always on the job, offering some peace of mind in an unstable world.



REF TEK 130S-01 High Resolution Seismic Recorder

A compact and lightweight seismic recorder, with IP Communications, ultra-low latency data transmission and removeable data storage. Meets the requirements for earthquake early warning (EEW) systems.



REF TEK 147A Strong Motion Accelerometer

With high sensitivity, large linear range, high resolution and dynamic range the 147A is suitable for free field applications such as microzonation, site response, earthquake monitoring and more.



REF TEK 151B-120 Observer, High Performance Broadband Seismometer

The low self-noise performance makes the Observer an ideal seismometer for seismicity studies in different installation configurations, including observatory and portable, surface and posthole applications.

For more information visit
www.reftek.com

© 2017, Trimble Inc. All rights reserved.

REF TEK
A TRIMBLE BRAND

www.guralp.com

MINIMUS

A REVOLUTION IN MINIATURE

A versatile, compact and low-power 24-bit four channel digitiser with advanced, cloud-based software communications for quick and easy instrument and data management.

The Minimus' feature rich capabilities include simultaneous streaming at multiple sample rates, triggering functionality using NS CAP alert (STA/LTA); and an ultra-low latency mode for early warning applications that can achieve transmission in 40 ms (network dependent).



- > Internal 2 g MEMS accelerometer
- > Compatible with analogue seismic and geophysical sensors
- > Advanced software communications for quick and easy instrument and data management
- > Hot-swappable and dual-redundant microSD storage
- > Choose from GPS, GLONASS or BeiDou precision timing sources
- > Voting capability for networked arrays
- > Bluetooth Android and IOS App for instant sensor installation integrity checking

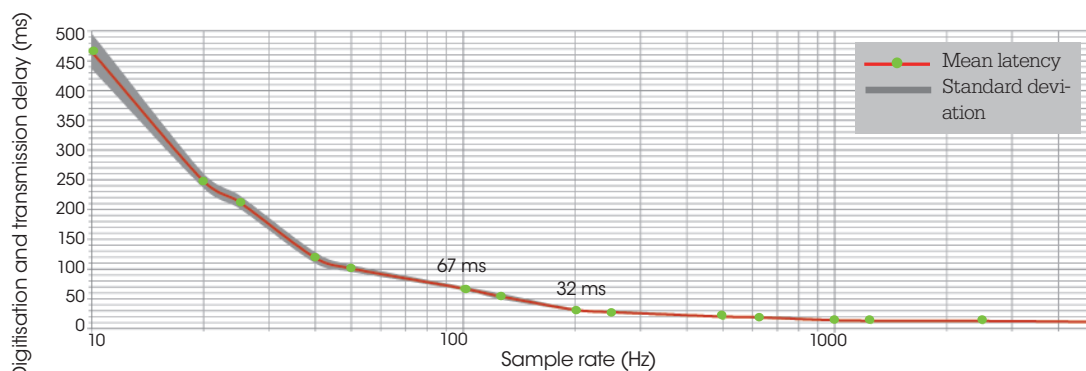
GDI Protocol

RAPID DATA TRANSMISSION FOR EARTHQUAKE EARLY WARNING

GDI uses a flexible packetisation scheme for true, real-time transmission that can deliver waveforms, sample by sample, as they are acquired by the datalogger.

By adapting its transmission to the available communications bandwidth, GDI achieves the fastest possible speed for data flow.

Available on the Güralp Minimus in combination with low-latency causal filtering or, as a free download for further development or integration into existing earthquake early warning networks, visit www.guralp.com for further details.



Measured data delivery times vs. sample rate using a LAN

- > Free-licence source code for incorporation into your EEW network
- > Supported via a plug-in for the CAPS module of SeisCompPro
- > Earthworm module coming soon
- > Rapid data transmission for earthquake early warning systems on all scales
- > Bandwidth-adaptive packetisation scheme drives efficient data flow
- > Responsive sample-by-sample streaming dispatches data instantly
- > Delivers per-channel metadata in SEED format and machine readable State of Health (SoH)
- > Significantly reduced packet headers for higher transmission efficiency

Güralp Systems Limited
Midas House
Calleva Park
Aldermaston
Reading
RG7 8EA
United Kingdom

T +44 118 981 9056
F +44 118 981 9943
E sales@guralp.com

www.guralp.com

Please contact us for more information

E sales@guralp.com

T +44 118 981 9056

WAVES

User-friendly earthquake
waveform analysis software

Download FREE at src.com.au

MiniSEED & more

Spectrogram View

FFT View & Filtering

Convert Velocity,
Displacement &
Acceleration

PGA, PGV & PGD

Estimate Epicentre
and Magnitude

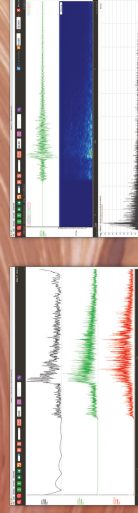
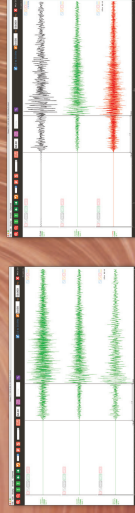
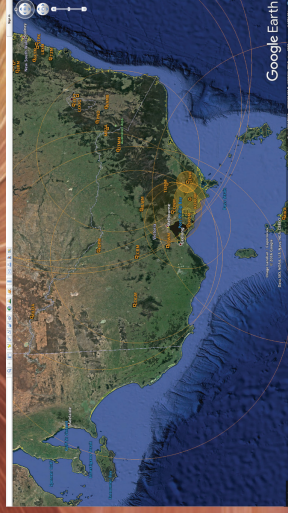
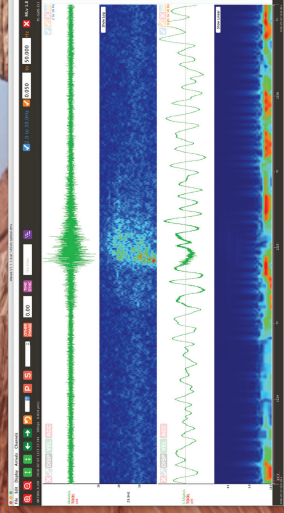
Free to use!

Remove startup
advertisement for
just A\$110

Available for Mac,
Windows & Linux



SEISMOLOGY
RESEARCH
CENTRE



GECKO

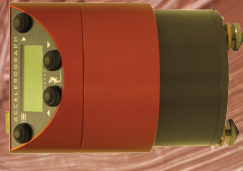


Professional, simple, all-in-one
seismographs & accelerographs



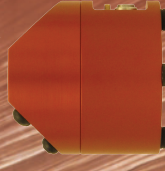
Gecko Prism

30s-80Hz Optical
Broadband Seismograph



Gecko Helix

1Hz to 100Hz
Short Period Seismograph



Gecko SMA-HR

$\pm 2g$ or $\pm 4g$ High Resolution
Triaxial Accelerograph



Gecko Blast

4.5Hz to 140Hz Blast
Monitoring Seismograph



Gecko SMA

Full Scale $\pm 2g$ to $\pm 400g$
Triaxial Accelerograph



Gecko Rugged

3-channel Recorder
IP67 Rated Chassis



Gecko Compact

Low cost fully featured recorder
IP54 for Vaults & Enclosures

src.com.au

